SURFACE CHARACTERIZATION AND ADHESIVE BONDING OF CARBON FIBER-REINFORCED COMPOSITES

by

Joannie W. Chin

Dissertation submitted to the Faculty of the

Virginia Polytechnic Institute and State University

in partial fulfillment of the requirements for the degree of:

DOCTOR OF PHILOSOPHY

in

Materials Engineering Science

APPROVED:

J.P. Wightman, Chairman

D.A. Dillard

J.G. Dillard

R.G. Kander

T.C. Ward

May 1994

Blacksburg, Virginia

SURFACE CHARACTERIZATION AND ADHESIVE BONDING OF CARBON FIBER-REINFORCED COMPOSITES

by

Joannie W. Chin

Committee Chairman: Dr. James P. Wightman

Materials Engineering Science

(ABSTRACT)

The effect of surface pretreatment on the adhesive bonding and bond durability of carbon fiber/epoxy and carbon fiber/bismaleimide matrix composites was studied. Methyl ethyl ketone (MEK) wipe, peel ply, grit blast and gas plasma treatments were the pretreatments of interest. Chemical and physical changes which occurred in the cured composite surfaces following pretreatment were characterized with x-ray photoelectron spectroscopy (XPS), ion scattering spectroscopy (ISS), contact angle analysis, diffuse reflection infrared spectroscopy (DRIFT), profilometry and scanning electron microscopy (SEM). Double lap shear and Boeing wedge configurations were used to evaluate the strength as well as the durability of the composites bonded with an epoxy film adhesive.

Fluoropolymer residues which were found on the composite surfaces were fully removed by grit blasting and oxygen plasma treatments, but not by an MEK wipe. The use of a peel ply prevented fabrication contamination from depositing on the bonding surfaces. In addition to its cleaning effect, oxygen plasma was also capable of incorporating additional polar functionality into the composite surface. The presence of the fluoropolymer contamination on the MEK-wiped surface resulted in low surface energy and wettability, whereas peel ply, grit blast and oxygen plasma improved both the surface energy and the wettability of the composite surfaces. The grit blasted and peel ply surfaces

were observed to have a significant degree of roughness, as measured by profilometry and seen by SEM.

A rubber-toughened epoxy film adhesive was used for the bonding studies. Lap shear strengths were evaluated under ambient conditions as well as at 82°C, both dry and following a 30 day/71°C water exposure. Wedge durability testing was carried out in a dry 75°C oven, 75°C water, 100°C water and aircraft de-icing fluid. Relative to the MEK-wiped controls, lap shear strength as well as hot/wet durability was improved by the peel ply and oxygen plasma treatments for both epoxy and bismaleimide composites. Grit blasting was seen to have some utility for the epoxy composites at room temperature, but was generally observed to be detrimental to strength and durability, particularly in the case of the bismaleimide composites.

In order to separate the effect of surface chemistry from the effect of surface roughness on composite bond strength, a study was carried out in which surface functionality was varied while the topography remained constant. For this purpose, peel ply surfaces, which have a consistent and reproducible degree of roughness, were treated with fluoropolymer compounds and gas plasmas, as well as left untreated. It was found that the removal of fluoropolymer contamination was the main contributor to the observed bond strength improvement following plasma treatment; however, highly functionalized oxygen plasma-treated surfaces showed evidence of improved durability in a hot aqueous environment.

The effect of elapsed time following oxygen plasma treatment of epoxy composites was also studied. XPS atomic concentration, wettability by water and a liquid epoxy resin, and lap shear strengths were plotted as a function of time following removal from the plasma reactor. Changes which occurred in the chemistry and wettability of an oxygen plasma-treated surface had a subsequent negative effect on the lap shear strengths of the bonded specimens.

A study was carried out using model epoxy and bismaleimide compounds in thin film form, for the purpose of studying surface chemistry and interfacial reactions following an oxygen plasma treatment. XPS and infrared reflection-absorption spectroscopy (IR-RAS) were used to probe the reactions which occurred. Close correspondence was found between the XPS and IR-RAS analysis of functional groups incorporated into the surface of the films by the plasma treatment. IR-RAS analysis of the model surfaces following exposure to a neat, liquid epoxy resin revealed that, while adsorption of the liquid epoxy occurred on both plasma-treated and nonplasma-treated surfaces, the oxygen plasma treated surface alone was capable of initiating ring-opening reactions in the epoxy. However, this effect was not observed unless immediate contact was made between the plasma-treated surface and the liquid epoxy resin.

ACKNOWLEDGMENTS

First and foremost, I sincerely thank my research advisor, Dr. James P. Wightman, not only for his excellent scientific guidance, but for his unwavering belief in me and the numerous opportunities which have come my way as a result of his efforts. Throughout my M.S. and Ph.D. work, he has always provided encouragement and allowed me to pursue my own ideas and directions. In addition, "Doc" has always made research exciting and fun with his own irrepressible enthusiasm for science. I can honestly say that I have learned much from him, not only about adhesion, but also about how to enjoy life.

I would also like to thank my committee members - Dr. Dave Dillard, Dr. John Dillard, Dr. Ron Kander and Dr. Tom Ward - with whom I always felt comfortable dropping in and obtaining either academic or research-related assistance. This easy access to technical expertise and interdisciplinary discussion was one of the highlights of my graduate school experience.

Financial support of this project as well as the graduate student fellowships was received from BASF Structural Materials, Inc., the Center for Composite Materials and Structures, and the Adhesive and Sealant Council, Inc. I would like to thank the Center for Adhesive and Sealant Science, not only for research funds, but for its efforts in promoting the study of adhesion in a wide variety of disciplines. Thanks are also extended to the CASS support staff - Virginia Keller, Katy Hatfield and Kim Linkous - for their friendship, cheerful demeanor and helpfulness throughout these years.

A number of individuals provided me with invaluable assistance in carrying out my research. Many thanks to Frank Cromer, who is not only a excellent surface lab manager and teacher, but also a good friend. I would like also to thank Dwayne Rakestraw and Rob Moore for setting up the Instron and Labview® Program for lap shear testing, Mac McCord for the scanning acoustic micrographs, C.C. Kang for showing me how to use the

profilometer, and Chuck Chandler and Danny Reed for helping me cut composites and use the autoclave in the Fab Lab.

Thanks also go out to my fellow group members, both past and present - Francis Webster, Pascal Commercon, Beena Menon, Cheryl Heisey, Holly Grammer, Mojee Cline, Nick Shephard, Hong Zhuang, Shigeo Mori and Hideko Oyama. We have all been through alot together! I sincerely value your friendship as well as assistance in the lab; I hope we will always be able to stay in touch.

I would like to thank my husband, Albert, for his love, understanding and steadfast encouragement through these last five years. Thank you for helping me to believe that I could make it! This degree belongs to you, too. I also thank our son, Matthew Brandon Chin, for being such a cutie and for helping me to keep my perspective. I hope that someday you'll be proud of your mom. Finally, I also thank my parents, Dr. and Mrs. Hsien Chang Wang, and my sisters, Nancy and Amy, for their love, support and prayers throughout graduate school.

DEDICATION:

To Albert and Matthew, my two main men.

"We were built to last
On until forever.
The world is changing fast,
but our love was built to last . . . "

- Tom Petty and the Heartbreakers
Into the Great Wide Open, 1991

TABLE OF CONTENTS

LIST OF FIGURES

LIST OF TABLES

Chapter I: Introduction

In recent years, significant advances have been made in the development and manufacturing of advanced composite materials. Fiber-reinforced polymeric matrix composites, in particular, are unparalleled in terms of specific strength, weight savings and corrosion resistance. These characteristics of composite materials make them suitable for structural applications such as aircraft, automobiles, space and marine vehicles, in which a high degree of performance is required.

In an ideal situation, a composite structure would not contain any joints in its design but would be manufactured as one monolithic entity. In any structure, joints are a source of weakness and/or excess weight, and the process of joining components is less efficient and more expensive than producing the same structure without any joints [1]. However, in actuality, size limitations on structures may be imposed by available materials or the manufacturing process itself, for example, limitations in the size of prepreg lines, presses and autoclaves. Also, certain geometries may be unmoldable or two or more *different* materials may need to be mated together. Therefore, the majority of composite structures are assembled from smaller-scale components which are fabricated separately and then are subsequently joined together.

Two avenues are available for the formation of load-bearing composite joints. Mechanical fastening, which involves the use of screws, pins, rivets and/or bolts, is straightforward in that no adherend surface preparation is required, disassembly can be carried out without incurring significant damage, and joint inspection does not present any abnormal difficulties. This technique is well-established for metal structures. Other metal fastening techniques such as brazing or welding cannot be used on thermosetting composite matrices, due to the intractability of the resin, but may be adapted to thermoplastic composites in the form of fusion welding.

Fiber-reinforced composites, however, lack the ductility of metallic structures and are more sensitive to localized stresses induced by fasteners. In metal structures, the ductility of the metal allows yielding in the vicinity of mechanical fasteners so that stress concentrations can be reduced. In fiber-reinforced composites, holes induced by mechanical fasteners are potential failure sites and can cause delamination, matrix crazing and fiber failure [2]. In addition, holes in fiber-reinforced composites may cut through load-carrying fibers, rendering even the most carefully designed mechanically fastened composite joint to be, at best, only one-half as strong as the laminate itself [3]. All of these factors serve to decrease the structural efficiency of composite structures.

On the other hand, adhesive bonding reduces the weight of a structure, allows for the assembly of dissimilar materials, minimizes stress concentrations by distributing the load over a wide area and is, in general, less costly for large area joints [4]. Adhesive bonding is operative at the molecular level and hence can uniformly distribute bond stress. Structural adhesives are also superior to mechanical fasteners because of their flexibility, toughness and excellent mechanical properties [5]. Improvements in vibration damping and noise reduction can also be realized with the use of adhesive bonds as opposed to mechanical fastening.

A significant recent development in aircraft repair involves the use of prefabricated composite patches and structural adhesives to repair cracks or other such damage in metallic aircraft [6]. This technique is considered to be the most effective and economical method of aircraft repairs in the field. Its success is dependent on the integrity of the bond between the composite patch and the metallic body.

A major challenge to the widespread usage of adhesive bonding techniques in primary composite structures and in field repair work is the lack of understanding of surface preparation techniques and their effect on bond strength as well as on long term bond durability. Adhesive bonds in general must also be resistant to environmental effects

and composite/composite bonds are no exception. Hot/wet environments are particularly deleterious to adhesive bonds, and a key component in bond lifetime has been shown to be proper surface preparation.

Composite surfaces are complex in that they are usually not homogeneous nor smooth and often contain residual contaminants originating from fabrication. Another complicating factor is that composites differ widely in their fiber type and content, resin chemistry and surface finish/texture. A variety of polymers and fibers are used in composite materials; even within the same class of polymer, countless variations in chemistry can exist. Toughening agents and other modifiers also create additional difficulties in analysis.

It is the objective of this work to evaluate the effect of surface pretreatment on the adhesive bonding of fiber-reinforced composite systems. Two thermosetting systems were studied in detail, a rubber-toughened epoxy and a toughened bismaleimide (BMI). Surface analytical techniques were utilized to obtain a more complete understanding of the chemistry and topography of the pretreated composite surfaces, so that those factors which lead to strong, durable composite-to-composite bonds could be identified. The composites were bonded with a structural adhesive for mechanical evaluation under ambient, elevated temperature and elevated temperature/elevated humidity conditions. Results of mechanical testing and determination of failure modes were correlated to information obtained from surface analysis. The specific role of chemical functionality on the composite surface, the existence of interfacial covalent bonds and the aging of plasma-modified surfaces were also addressed. It is expected that the answers uncovered by these studies will lend additional insight into the nature of composite-to-composite bonds.

References

1. "Joining Polymeric Composites, Adhesives" in *International Encyclopedia of Composites*, vol. 2, S.M. Lee, ed., p. 509 (VCH Publishers, New York, 1990).
2. F.L. Matthews in *Joining Fibre-reinforced Plastics*, F.L. Matthews, ed., p. 1 (Elsevier Applied Science Publishers, London, 1987).
3. "Joining, Mechanical Fastening" in *International Encyclopedia of Composites*, vol. 2, S.M. Lee, ed., p. 438 (VCH Publishers, New York, 1990).
4. D.P. Bashford in *Developments in Reinforced Plastics - 5*, p. 205 (Applied Science Publishers, London, 1986).
5. E. Sancaktar, S.C. Schenck and S. Padgilwar, *Ind. Eng. Chem. Prod. Res. Dev.*, **23**, 426 (1984).
6. A.A. Baker, *Composites*, **18(4)**, 293 (1987).

Chapter II: Literature Review

2.1 Composite Materials

Composite materials are defined as those in which two or more distinct components are combined in order to form a material with properties different from those of the individual components [1]. The constituents of a composite remain as distinct phases and are distinguishable on a macroscopic scale. This is an extremely broad definition, which will be narrowed in its scope by considering only those materials which contain a reinforcement phase with a higher modulus than the matrix.

The idea of combining reinforcement and matrix materials of differing properties to create a superior structural material is by no means novel. Wood, for instance, is a naturally occurring composite material, composed of cellulosic reinforcing fibers in a lignin matrix [1]. Man-made composites encompass an enormous variety of materials, dating back to the straw-reinforced mud bricks produced by the Israelites in Biblical times [2].

One phase (or phases) in a composite material is generally referred to as the *reinforcement* and imparts strength and stiffness to the structure; the other phase (or phases), classified as the *matrix*, serves to bind the reinforcement together and assists in load distribution [1]. Advanced composite materials containing continuous fibrous reinforcement are highly anisotropic in their physical properties, possessing their highest strength, stiffness and toughness in the direction of fiber orientation [2]. Modern reinforcement materials include glass, metals, polymers, ceramics and carbon, which can be found in either chopped, continuous or woven forms. The myriad of matrix materials available again includes polymers (both thermoplastic and thermosetting), ceramics, metals and carbon-based materials [3]. The focus in this work and the remainder of this section will be on carbon fiber-reinforced polymeric matrices.

The reinforcement, being the main load-bearing phase of the composite, is on the average 20-150 times stiffer and 50 times stronger than the matrix material [3]. These high strengths and moduli are due to the very small cross-sectional dimensions of fibrous reinforcements, which limit the size and number of flaws which can occur. In order to provide substantive reinforcement, a minimum of 10 volume percent fiber must be present in the composite material. There is a direct relationship between the volume fraction of reinforcing fiber and the stiffness of the composite [1,3]. The orientation of the fibers relative to the direction of the applied stresses also strongly influences the composite strength [4]. Advanced structural composites for high performance applications are actually more accurately described as bonded-fiber materials rather than reinforced plastics, due to the fact that the fiber makes up the majority of the total volume of the system.

Carbon fiber is currently the most widely used type of reinforcing fiber for advanced composite applications. This is attributed to the large-scale manufacturing of carbon fibers which allows them to be produced at reasonable cost and also to the fact they possess excellent mechanical properties [3]. Their tremendous strength and moduli originate from the alignment of covalently bonded basal planes of carbon atoms along the axis of the fiber [2]. Typical tensile strengths and moduli range from 2-5 GPa and 250-500 GPa, respectively [1,2]. Carbon is also an extremely light element with a density of 2.268 g/cm^3 [5]. Carbon fibers also possess excellent resistance to fatigue, corrosion and temperature extremes.

The manufacture of carbon fibers from the controlled pyrolysis of rayon, pitch or poly(acrylonitrile) precursors has been described elsewhere [6,7]. Most processing methods include an initial stabilization treatment which prevents precursor degradation, a thermal treatment which carbonizes the precursor and removes non-carbon elements, and an optional graphitization or high temperature treatment which further improves mechanical properties [5]. Currently, carbon fibers based on poly(acrylonitrile), or PAN, precursors

are the most economical because of higher carbon yields and because they do not require additional graphitization as part of their processing [2].

In addition to binding the reinforcement together in the proper orientation and assisting in load distribution, the matrix phase also provides protection for the reinforcement in hostile environments such as high humidity and corrosive chemicals. Thus, the matrix plays an important role in determining the service conditions and temperature ranges in which the composite can be utilized. By separating the individual fibers in a bundle, the matrix also serves to reduce stress concentrations and prevent crack propagation from one broken fiber to another in the same bundle [1,2].

In terms of mechanical properties, the transverse properties of a unidirectionally reinforced composite are greatly influenced by the mechanical properties of the matrix polymer [1]. Properties such as creep resistance, tensile strength and impact resistance are also a function of the polymer matrix [4]. Also, the matrix polymer provides all of the interlaminar shear strength of the composite [3]. Both thermosetting and thermoplastic polymers are potential candidates for composite matrix resins. Two types of polymer matrices which are commonly used in advanced composite applications, epoxy and bismaleimide, will be discussed in detail in Section 2.2.

Adhesion between the matrix and reinforcement is critical in ensuring the integrity of the fabricated part. The interface in a composite occupies a very large internal surface area and plays an important role in determining composite mechanical properties [5]. Many researchers have studied the interfacial characteristics of carbon-fiber reinforced polymers [8,9]. Because applied loads are transferred to the fibers from the matrix *through* the interface, poor or no adhesion between the fiber and matrix results in poor load distribution and premature failure. On the other hand, the ability of the resin to debond from the fiber ahead of a propagating crack normal to a fiber plays a role in dissipating crack energies. If

no debonding is permitted to occur, the crack energy would then instead be directed into fracturing the fiber [2].

The combination of the appropriate reinforcement and matrix materials leads to the development of high strength and high modulus-to-weight materials. The ability of the matrix to transfer load and dissipate energy can result in composite materials which are stronger than the individual constituent materials involved [4]. The use of these strong but lighter materials results in significant weight savings in structures of up to 30%, compared to the equivalent structure fabricated from metal components [1]. In addition to weight savings, an increase in the structural damping capability of a structure can be realized by the use of polymer matrix composites [10]. From a design point of view, fiber-reinforced composites are more versatile than metals and can be tailored to performance and design requirements [10].

The aerospace and military markets have accounted for the greatest development and usage of carbon fiber-reinforced composite materials, due to the fact that weight is at a premium in these fields and new lightweight materials are continuously sought. Specific components which are fabricated from composite materials include rocket motor cases, nozzles and nose cones in missiles. In aircraft, composite materials are used to produce radomes, rotor blades, fuselages, empennages, wing components and other secondary structure [1,11,12]. The use of composite materials to fabricate primary aircraft structures is still limited, but steadily growing. The FAA certification of the Beech Starship, an all-composite aircraft, is a major step toward use of primary composite structures in the aerospace industry [13].

Space applications for composite materials are also becoming a reality in the development of composite manned space vehicles, satellite components, boosters and planetary probes [4,14]. The proposed space station Freedom will contain trusses fabricated from a toughened epoxy matrix reinforced with an ultra-high modulus carbon

fiber, as are the payload doors on the United State's fleet of space shuttles [10], to name just a few specific examples. The Long Duration Exposure Facility (LDEF) mission which carried experimental composite materials in low earth orbit for close to 6 years yielded valuable information on composite exposure to radiation, micro-meteoroids, vacuum, atomic oxygen, and contamination [15].

After the aerospace industries, additional applications for carbon fiber-reinforced composites are found in the medical fields, where they are used in prosthetic devices and medical equipment. These materials are also found in leisure and sporting goods items such as golf clubs, fishing rods, archery bows and tennis rackets. The electrical properties of carbon fibers are exploited in electronics applications, where they are used to dissipate built-up static charges [5].

The use of composite materials and structures is expected to continue to grow in the coming years. Trends indicate that as new polymers and reinforcement materials with improved processing capability and cost competitiveness are developed, the use of composite materials in both commercial and military markets will increase [12]. By 1999, the market for advanced composites is expected to grow to about 68.4 billion pounds [16].

However, the widespread use of composites may be inhibited by factors such as material cost, initial capital investment, lack of information on performance and reliability as well as fear of risk-taking by manufacturers [11]. There is also concern about the low ductility/toughness and damage tolerance of present-day polymer matrix composites. In the event of an impact, internal delamination could occur and a subsequent drop-off in mechanical properties would result [17,18]. The development of thermoplastic matrix composites is an area which is being heavily researched to address this issue [19].

2.2 High Performance Polymer Matrices

2.2.1 Epoxies

Epoxy resins are the most versatile of all currently available adhesive and composite matrix materials. In advanced composites, it is the most widely used base polymer, possessing a broad range of physical properties and relatively straightforward processing conditions [3]. The desired degree of toughness, mechanical strength, chemical resistance, electrical performance and adhesion in a cured epoxy can be obtained by formulating with the proper types/ratios of curing agents and modifiers, and by varying the structure of the base resin itself [20].

Figure 2.1a shows the synthesis and structure of one common type of epoxy resin. The two main starting materials are epichlorohydrin, an intermediate in the synthesis of glycerin, and bisphenol A, a product of the condensation reaction between acetone and phenol. Epichlorohydrin in excess is reacted with bisphenol A in the presence of sodium hydroxide catalyst to yield a low viscosity, linear material terminated with epoxide groups, known as the diglycidyl ether of bisphenol A (DGEBA) [20]. Another important process used to synthesize DGEBA is the peracid epoxidation of olefins [21].

Further reaction of the liquid DGEBA resin with additional bisphenol A produces higher molecular weight material, as shown in Figure 2.1b. The degree of polymerization **n** which can be attained is a function of the ratio of DGEBA to bisphenol A; greater amounts of bisphenol A yield higher molecular weight, solid products, lesser amounts result in liquid or semi-solid materials [21,22]. The wide range of physical forms available for epoxy resins makes a large number of processing choices possible [20]. Since the repeat unit of the epoxy contains a hydroxyl group, increasing the degree of polymerization also improves adhesion to a variety of substrates [23].

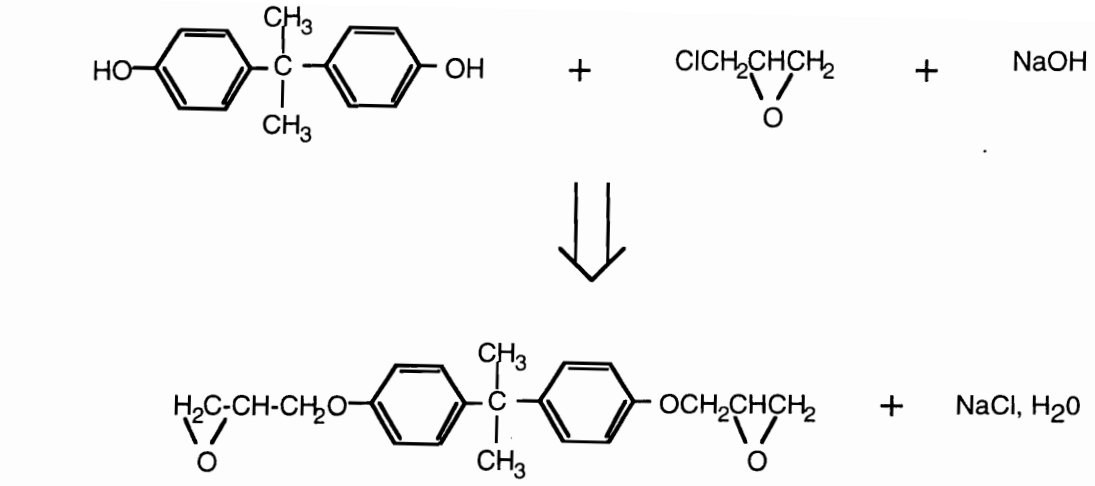

(a)

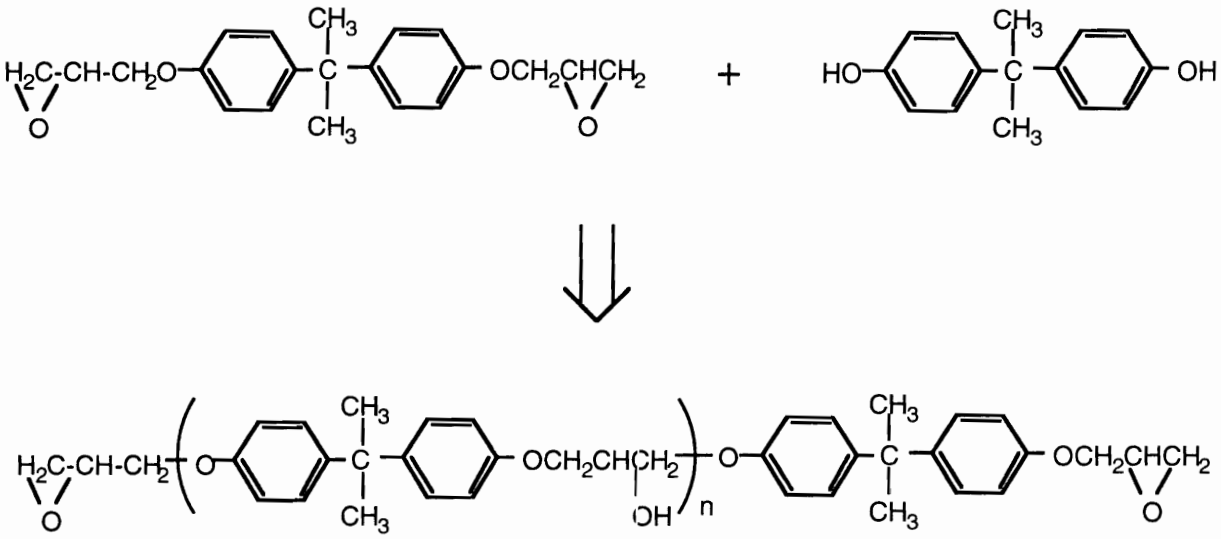

(b)

Figure 2.1: (a) Synthesis of diglycidyl ether of bisphenol A (DGEBA). (b) Chain extension of DGEBA with bisphenol A.

To obtain higher temperature resistance and superior mechanical properties, particularly for use in high performance structural applications, epoxy resins with greater functionality and hence the capability to form higher crosslink density networks are needed. Resins in this category include epoxidized phenol or cresol novolacs, triglycidyl p-amino phenol and tetraglycidylmethylenedianiline. The structures of these resins are shown in Figure 2.2. When formulated with the appropriate curing agents, the cured materials have high T_g's and excellent thermo-oxidative stability [20,24]. Recently, new multifunctional epoxies based on the structure of tetraglycidylmethylenedianiline have been introduced, with claims to further improved hot/wet performance and higher glass transition temperatures [25].

The key to curing epoxy resins is found in the epoxide group, also referred to as an oxirane ring or ethoxylene group. This strained 3-membered ring is highly reactive toward compounds containing active hydrogens such as primary and secondary amines, thiols, carboxylic acids and phenols [21]. To obtain a crosslinked network, these curing agents should be polyfunctional. Hydroxyl-containing compounds such as phenols and alcohols are known to accelerate the epoxy/amine curing reaction [23]. Catalysis with acids or bases leads to homopolymerization of the epoxy resin to a polyether [21]. Because the curing reaction proceeds via a ring-opening pathway, no volatile byproducts are formed and subsequently, shrinkage is low. This is a critical factor in the manufacture of void-free composites.

Cure can proceed at ambient temperature or elevated temperature, depending on the activity of the curing agent or catalyst. In general, room temperature cure, usually involving aliphatic amines and their derivatives, generally results in poor high temperature performance. In some instances, a room temperature curing process can be followed by an elevated temperature post-cure to further boost properties [22]. Higher temperature curing

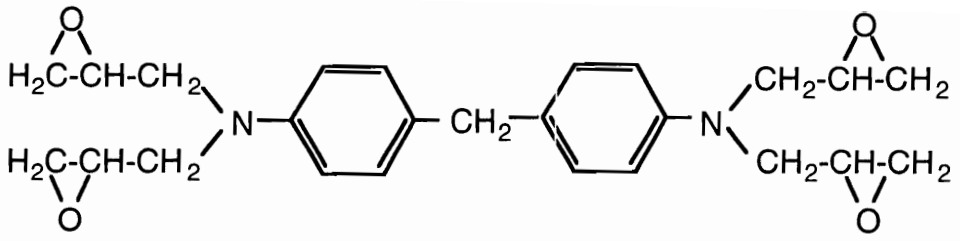

(a)

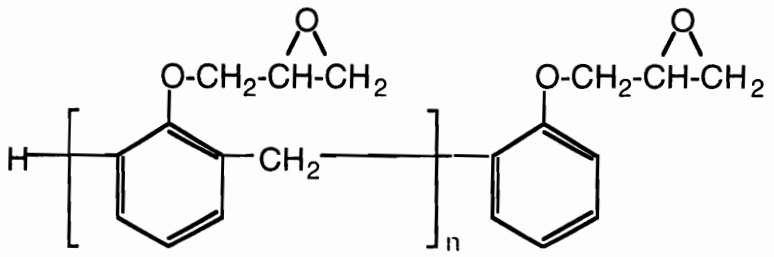

(b)

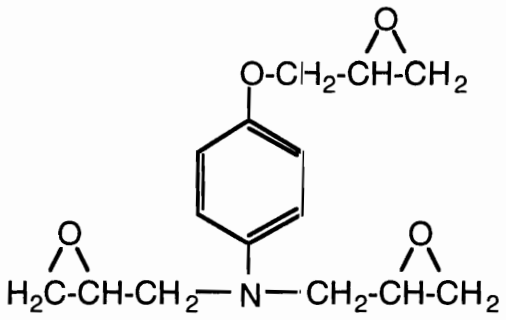

(c)

Figure 2.2: Structures of some representative multifunctional epoxide resins.
(a) tetraglycidylmethylenedianiline (b) glycidyl ether of phenolic novolac (c) triglycidyl p-aminophenol.

cycles are necessary for tertiary amines, aromatic amines, and acid anhydrides, which provide superior high temperature properties. Diaminodiphenylsulfone (DDS), a curing agent which is commonly used in aerospace composites with multifunctional epoxy resins, yields crosslinked systems with T_g's exceeding 200°C [20].

Despite the high thermo-oxidative stabilities, strengths and moduli of the high performance epoxy materials, one major shortcoming which exists is their low toughness or damage tolerance. The high crosslink density which contributes to high T_g and tensile properties also causes these resins to be inherently brittle [26].

A number of approaches to improving the toughness of epoxies have been documented. Initial attempts involved the addition of carboxy-terminated butadiene-acrylonitrile (CTBN) rubber to the epoxy formulation. During cure, the CTBN precipitates to form a system of dispersed rubber particles in the glassy epoxy matrix. This technique does impart improved fracture resistance and ductility to the cured material, but often at the expense of modulus and T_g. Other early work focused on epoxy-nylon and epoxy-urethane blends [27].

Other researchers studied the addition of oligomeric versions of high T_g thermoplastic polymers end-capped with functional groups such as amine and hydroxyl [28]. Thermoplastics which have been tried include polysulfone and polyetherimide [26]. This approach has been shown to improve fracture toughness with minimal effect on thermal properties. A successful variation on this approach involving the formation of an interpenetrating network between an engineering thermoplastic and the epoxy matrix has also been carried out [27]. One drawback to the addition of engineering thermoplastics is that solvent resistance is sometimes compromised. When thermoplastic modifiers are chemically reacted into the epoxy network, superior performance is observed over systems in which the thermoplastic modifiers are only physically blended in [29].

The process of interleafing, defined as the incorporation of layers of a tough material into a composite laminate, has been utilized successfully with epoxy composites. This approach results in high impact strength and superior damage tolerance [27]. The use of elastomer layers arrests interply delamination and subsequently improves the residual compressive strength after impact [30]. Materials which have been used as interleaf resins include thin films of thermoplastic polymers and epoxy films modified with CTBN or urethane rubbers. The latter group of materials undergoes extensive plastic deformation and are speculated to be capable of dissipating energy in the interlaminar regions of the composite [30].

2.2.2 Bismaleimides (BMI)

Bismaleimide (BMI) resins are part of a larger class of polymers known as polyimides, which are derived from carboxylic acid anhydrides and primary diamines, and are characterized by the imide moiety in the polymer backbone [31]. These materials exhibit excellent mechanical properties as well as high thermo-oxidative stability. BMIs are similar to epoxy resins in many aspects, also being excellent matrix materials for advanced composites. They are, however, superior to epoxies in hot/wet properties and thermal stability [3]. Due to moisture absorption effects, epoxies are limited in their maximum hot/wet use temperature to about 120°-170°C [32].

BMI resins differ from conventional polyimide resins in that they are cured through an addition mechanism, as opposed to a cyclo-dehydration reaction which releases water as a byproduct. In general, the use of BMIs in composites involves low molecular weight oligomers which are endcapped with an unsaturated vinyl group. Other addition polyimides containing nadimide, acetylene and benzocyclobutene end-caps have been developed, but will not be discussed in this section [33]. The unsaturated bond in BMI is more reactive than the unsaturated functional groups listed above, due to the fact that it is

directly adjacent to and hence activated by the two imide carbonyls [33]. BMIs are also more "epoxy-like" in their handling characteristics than the other addition polyimides and are thus easier to process.

The general structure of BMI is shown in Figure 2.3. It is prepared by the reaction of maleic anhydride and a primary diamine, which initially yields a bismaleiamic acid. The cyclization of the amic acid to the imide functionality can be accomplished thermally or chemically [34]. The resulting prepolymer or oligomer can be crosslinked into a network through several different pathways. Homopolymerization through the double bonds can proceed via a free radical, thermally-induced mechanism . The maleimide double bond can also undergo what is known as a *Michael Addition*, which is a nucleophilic addition reaction involving nucleophiles such as primary and secondary amines, thiols and phenols [33,35]. Diels-Alder reactions can also occur with dienes, and allylphenols can undergo an "ene" reaction with BMIs. The majority of these reactions take place below 250°C without the evolution of volatile byproducts [36].

As is also the case with epoxies, BMIs are usually formulated with a number of comonomers, reactive diluents, processing additives, toughening agents and catalysts in order to meet the requirements of an advanced composite resin [33]. Due to the high crosslink densities found in the cured networks, BMI composites are also prone to brittleness and low fracture toughness, perhaps to an even greater extent than epoxies [3]. A number of techniques are available to improve BMI mechanical performance in this area. Tailoring the "R" group in the BMI oligomer shown in Figure 2.3 can improve the ductility of the resin if flexible and/or longer linkages are utilized [34]. The development of novel comonomers containing propenyl(phenoxy) and allylphenyl(allylphenol) linkages has been shown to result in improved damage tolerance in BMI composites [33]. Functionalized CTBN rubbers and engineering thermoplastics such as polysulfone, polyetherimide, poly(arylene-ether) and polyhydantoin have been studied [26].

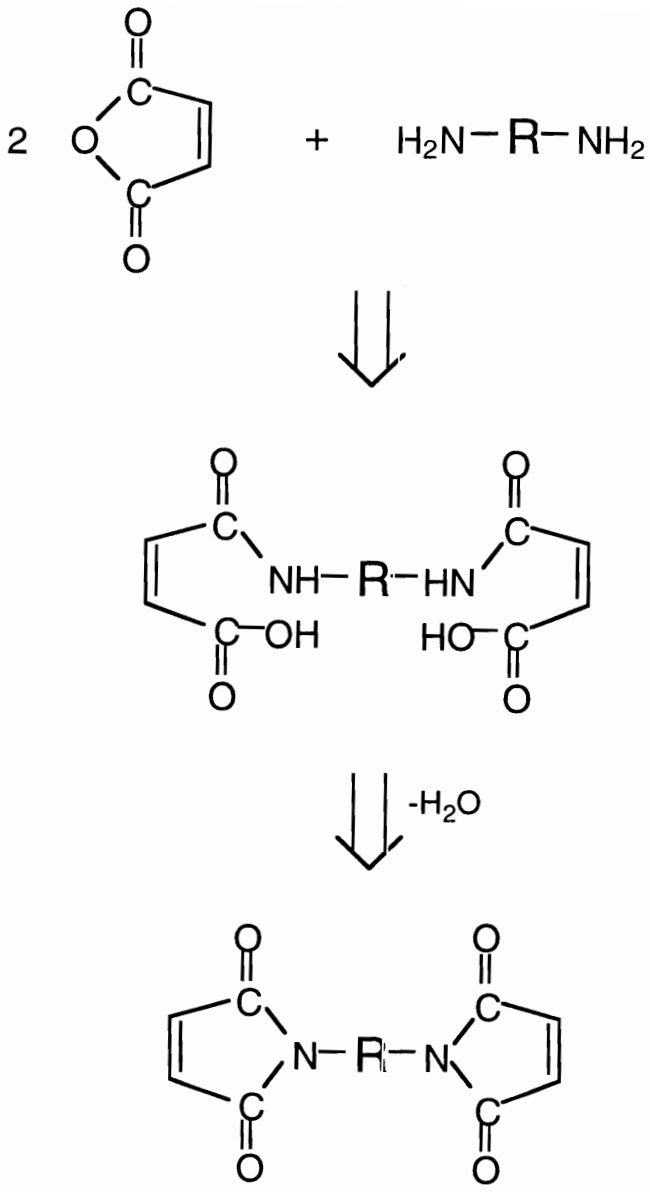

Figure 2.3: Synthesis of bismaleimide resin from maleic anhydride and an aromatic diamine.

2.3 Adhesive Bonding of Composite Materials

2.3.1 Composite Structures

Like any other structural materials, fiber-reinforced composites usually must be joined to create useful structures [37]. For full structural efficiency, the ideal composite structure would be manufactured as one integral, monolithic component. However, limitations in manufacturing technology lead to the presence of joints in composite structures [38,39]. Joining of composites is usually performed to obtain larger physical sizes than can be accommodated by currently available prepreg lines, presses and autoclaves, to create unmoldable geometries, to mate two different materials, and to preserve a degree of freedom [37].

Examples of structures which make use of composite-to-composite bonding include the Airbus Industrie's A310 jetliner tail and the Beech Starship's fuselage. Both of these aircraft are manufactured from large-part assemblies which are manufactured in sections and adhesively bonded together [40]. A thermoplastic composite fighter fuselage developed by Lockheed also utilizes adhesive bonding to join composite components. The use of these bonding techniques successfully eliminated 73% of mechanical fasteners which would have otherwise been required, leading to significant weight savings [41]. The airframe of Bell Helicopter's advanced composite helicopter also makes use of adhesive bonding techniques. In this structure, only 1000 mechanical fasteners are used, compared to the 50,000 which are normally needed for the metal airframe [42].

Other examples of adhesively-bonded composite structures include the McDonnell Douglas AH-64 Apache Horizontal Stabilator [43] and the Westland 30-300 Flight Standard Tailplane [44]. In the sports equipment arena, adhesive bonding was the joining method of choice to attach a composite golf club shaft to the head; the use of an epoxy adhesive ensured that the shaft-to-head connection could withstand a 5500 psi pull test [45].

Composite/composite bonding as well as metal/composite bonding are often involved in the repair of damaged aircraft structures. The need for quick and reliable repair of aircraft has motivated the development of field repair techniques, usually involving the adhesive bonding of pre-cured composite patches using either ambient temperature cure or high temperature cure adhesives [46,47,48]. This technique is considered to be the most effective and economical method for field repair [49]. In order for it to be successfully utilized, good control and understanding of the composite surface pretreatment (for the patch as well as the composite structure) must be present.

2.3.2 Advantages of Adhesive Bonding

Joining of composite components can be accomplished by either mechanical fastening or adhesive bonding, or a combination of both. Mechanical fastening involves the use of rivets, screws and bolts, and is generally not appropriate for fiber-reinforced composites. The mechanical properties of composite materials differ greatly from conventional metals and metal alloys, in that metals can yield to reduce stress concentrations in the vicinity of bolts or rivets, but fiber-reinforced composites cannot. Instead, local debonding between the fibers and matrix resin or intraply/interply splitting may occur instead to locally alleviate the localized stresses [50,51]. Figure 2.4 shows typical failure modes which may occur with mechanically fastened composite joints [52]. It has also been documented that damage zones surrounding fastener holes in composites under fatigue loading may lead to delamination and cracking [53].

In addition, the machining, cutting and drilling of composite materials may lead to additional damage and increased susceptibility to interlaminar shear failure in the composite [37,39]. Mechanically bolted or riveted composite joints rely on an adequate bearing and load transfer capacity of the drilled holes, a requirement which cannot always be met with holes in composite laminates which cut through load-carrying fibers [38]. The end result is

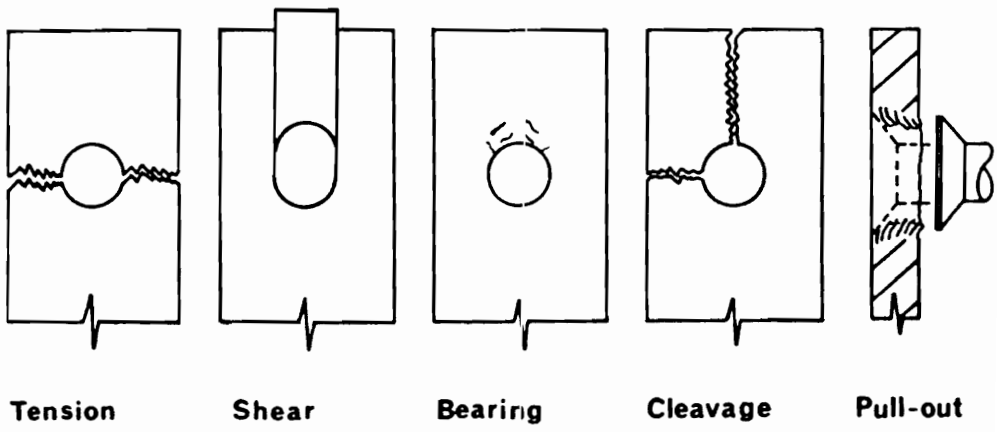

Figure 2.4: Failure modes in mechanically fastened composite joints [52].

that a composite material's full physical property potential is not realized. In the case of thin composite panels (less than 3 mm in thickness), adhesive bonding is generally preferable to mechanical fastening [39].

Another potential problem which is present in mechanically-fastened composite structures involves the galvanic corrosion of carbon fiber-reinforced composites in contact with metallic materials. This type of corrosion can occur when an actively corroding metal is in contact with an electrically conductive composite in the presence of oxygen and an electrolyte solution (salt water, for instance) [54]. Due to the conductivity of the carbon fibers, the exposed ends in a cut panel or drilled hole can serve as electrical contacts in a galvanic cell [2]. As the metal component corrodes, electrons flow into fibers which are in contact with the metal surface. Oxygen undergoes reduction at the fiber surface to form hydroxyl ions, which can proceed to attack the matrix resin. Hydroxyl ion reaction with epoxy resins is typically slow and matrix degradation is not a major problem. However, under some conditions, saponifiable resins such as cyanates, polyimides, bismaleimides and polyesters can react with hydroxides, leading to degradation. In particular, the imide ring in polyimide or bismaleimide resins can undergo hydroxyl-initiated ring-opening reactions [55].

Although this type of corrosion does not commonly occur, its likelihood is increased by the use of metal fasteners to join composite components. Galvanic corrosion is known to occur where salt water can collect, such as in a "leaky" fastener or a butt joint between aluminum and composite sections [55]. The use of adhesive bonding would completely eliminate the possibility of forming a galvanic connection, since exposed fibers in cut panels or drilled holes would not be direct contact with metal components.

The inherent advantage of adhesive bonding is that stresses are distributed, rather than concentrated. Adhesive bonding is also attractive from the standpoint that a reduction in weight can be achieved, smooth external surfaces can be obtained, damping and noise

reduction characteristics are improved, and assembly costs can be reduced. The cost reduction is realized since adhesive bonding is less costly than mechanical fastening on large area bonds [37, 56].

Disadvantages of adhesive bonding are that special adherend surface preparation is required, the effects of thermal cycling and high humidity are not yet well understood and non-destructive inspection is difficult [37]. Also, joint dissassembly and inspection are difficult to carry out without adherend damage. However, the advent of non-destructive evaluation techniques make it possible to determine the quality of adhesively-bonded composite joints.

2.3.3 Adhesives for Composite Bonding

Adhesives which are used to bond composites include polyurethanes [40], polyimides [40,57,58], acrylics [59], phenolics [60], silicones [60] and the industry workhorses, epoxies and toughened epoxies [40,61]. In the aircraft industry where precision placement of adhesives is required, semi-cured or "B-staged" film adhesives, often carried on a scrim or mat, are widely used [58,62,63]. Another common adhesive form is a one or two-component thixotropic paste [60,64]. Co-curing of adhesive and composite prepreg, in which the uncured adhesive and uncured prepreg plies are laid up and consolidated together, is also becoming increasingly popular [40,60].

For thermoplastic composites, many of the same adhesive types are applicable. Thermoplastic polyimides [65] and epoxies, in film and paste form, have been widely used [66,67,68]. Because the polymer matrix in a thermoplastic composite is capable of melting and flowing, dual polymer bonding and co-consolidation techniques can be utilized [67,69]. Ultrasonic welding techniques have also been investigated [70].

As service temperatures of composite materials continue to increase, the heat resistance of adhesives used to join them must also continue to improve. Higher aircraft

speeds will demand that adhesives be resistant to temperatures up to 700°F [40]. Adhesives with a high elongation to failure are preferred so that peel stresses can be minimized [38].

2.4 Surface Pretreatment

2.4.1 General Considerations

Before adhesive bonding can be successfully and reliably applied to composite systems, a number of issues must be studied in detail. As is well-known in the field of metal bonding, composite bonding also recognizes the importance of interface strength and stability. Adhesion of two polymers or of another material to a polymer surface has always been a difficult problem in the utilization of polymeric materials. In comparison to metallic or ceramic substrates, polymers possess lower surface free energies and are not well-wetted by polar compounds, such as adhesives. The surface energies of metals and ceramic materials fall in the range between 500-5000 mJ/m^2, whereas the surface energies of polymeric materials range from approximately 16 to 46 mJ/m^2 [22]. In composite materials, there is usually a thin layer of polymer resin overlaying the top fiber ply; hence the surface characteristics of polymer composites are very similar to those of the matrix resin . Therefore, surface preparation techniques which are successfully used with a given polymer may also be appropriate for that particular polymer containing fiber-reinforcements [71].

The low reactivity of polymer surfaces toward polar materials could be due to the chemical make-up of the polymer, surface contamination from processing aids, low molecular weight species or additives which have diffused to the surface, or all of the above [72]. The surface of a cured composite is particularly complex and always carries the history of the curing process [38]. If it is cured in direct contact with a mold or tool

plate, the surface is almost always contaminated by mold release agents. If laminated with a peel ply, the peeled surface after peel ply removal can also be contaminated by residues of low surface energy from the peel ply fibers. Also, the peeled surface may show pulled-out resin areas, which may lead to inclusions and porosity in the bondline [38].

One type of surface contamination which is universal to almost all polymer composite systems is transfer from fluoropolymer or silicone-based release films. As much as 30% fluorine has been found on composite surfaces after consolidation of the laminate [73]. Parker and Waghorne have characterized the surfaces and evaluated the bondability of composites which were contaminated by fluorine and silicone-based release agents and films [74].

One prerequisite for the formation of a strong bond is that the adhesive wet the surface, a condition which may be prevented by the presence of a substance with a lower critical surface tension lower than that of the adherend [38]. Even a film of contamination only one monolayer thick can greatly reduce adhesion [75]. Hence, surface preparation is extremely critical and is necessary to increase the surface free energy of the substrate and allow wetting to occur, improving the chances for a durable bond to be formed. Surface pretreatment not only serves to remove contamination, but may also increase the surface area for bonding and mechanical interlocking, and/or chemically modify the surface so that additional functionality can be obtained. Care must be taken when carrying out surface pretreatment so that only the chemistry or morphology of a thin surface layer is modified; bulk properties should not be affected [76]. In the following sections, surface pretreatments of specific composite systems will be addressed.

2.4.2 Surface Preparation Techniques

Two of the more commonly utilized pretreatment techniques for composites, abrasion and peel ply, remove the original resin surface and any accompanying

contamination, leaving behind a fresh, slightly roughened surface for bonding [77,78]. It is important that the morphology of the surface be optimum for effective load transfer, i.e. the effective surface area on which the adhesive acts should be as large as possible and allow as much interpenetration of the adhesive as possible to form mechanical anchors [38].

Abrasion of the surface can be accomplished by grit blasting, hand sanding or machine sanding. All three of these techniques tend to be operator-sensitive and not easily reproducible. Abrasion is generally applied until the composite loses its surface gloss and becomes dull and lusterless; it is usually followed by solvent cleaning and drying [71,78]. Grit blasting can be performed with a variety of particulate materials; silicon carbide and aluminum oxide are two of the more commonly used materials. A less commonly used blast treatment, known as "cryoblast", utilizes solid carbon dioxide pellets [76]. This type of treatment has been found to be less damaging to the composite than conventional grits. Grit blasting variables include the grit size, treatment pressure and time, the angle between and the distance from the nozzle to the surface.

Hand sanding and machine sanding is often accomplished with silicon carbide grit-coated paper or Scotch-Brite® pads, either dry or in the presence of a solvent. It has been suggested that abrasion which takes place beneath a layer of reactive primer leads to higher bond strengths than can be obtained by abrasion alone [79]. As in the case of grit blasting, the abraded composite must be vacuumed or rinsed with a solvent to remove residual grit or ablated composite residue, which can lead to reduced joint strengths [44]. Care must also be taken during abrasion not to apply excessively high pressure as to penetrate too deeply into the composite and damage the fiber bundles underlying the surface [38,80].

Peel ply is a layer of fabric which is laid up on the outermost surfaces of the composite and co-cured with it. During cure, the peel ply becomes consolidated into the body of the laminate. This layer is intended to be peeled off prior to bonding and, among

other purposes, serves to protect the surface from contamination [77]. Peel ply materials can be woven glass, nylon, polyester or other synthetic materials. If the peel ply material is used dry, that is, without being impregnated with polymer, a resin-starved surface is produced because the peel ply fabric absorbs some of the matrix resin during cure. When the dry peel ply is pulled off, the top layer of resin on the surface is fractured and removed, leaving behind a rough, fresh surface for bonding. Peel ply fabrics can also be impregnated with resin, creating a polymer-rich surface for bonding.

The surface topography which results from the use of a peel ply is basically the imprint of the fabric weave pattern [76]. Therefore, the filament diameter and thickness of the peel ply, as well as the type of fabric weave, all have an effect on the surface roughness, which in turn determines the bond strengths which can be obtained [76,80]. The regularity of the roughness induced by the use of a peel ply has been speculated to lead to the formation of any bubbles or voids along a plane, thus creating a line of weakness and ultimately a weakened bond [75]. Grit blasting, on the other hand, would create a more random roughness leading to a less uniform placement of voids. In some instances, a release agent is applied to the peel ply to facilitate its removal; it then becomes important to ensure that significant amounts of release agents are not left behind on the bonding surface [81].

Both peel ply and grit blasting increase the surface roughness, a property which usually increases the bondability of a low energy surface to some degree. However, these abrasive treatments are usually insufficient for low energy polymer surfaces and some type of treatment to alter the chemistry of the surface is necessary [78]. Examples of chemical treatments include surface graft polymerization [82], etching in strong acids or bases [76,77,82] and reactive primers [76,82]. Other methods, less commonly utilized, involve treatment with flames [76,83,84] or lasers [71,76,85].

High energy radiation has been shown to be particularly efficient in increasing the surface polarity of polymers. Included in this category are plasma and corona discharge treatments. Plasma treatment is being increasingly used as a surface pretreatment for polymers and composites. It is a clean, environmentally acceptable technique which can result in dramatic changes in surface chemistry, leading to greater surface wettability and polarity [86,87].

A plasma is defined as a partially ionized gas composed of ions, electrons and neutral species. When an organic material is exposed to a radio frequency (RF) plasma, free radicals are initiated in the surface by both chemically active species and ultraviolet/vacuum ultraviolet radiation. These surface radicals may react with gas species and/or adjacent surface free radicals, leading to surface chemistry changes and surface molecular weight changes such as chain scission, crosslinking and/or branching. The specific end-result is dependent on the particular polymer involved and the plasma gas used. Generally speaking, dramatic changes in surface wettability, reactivity and chemical composition are observed after plasma exposure [86,87,88].

Plasma etching can also occur in certain materials via the abstraction of atoms or molecular fragments from the polymer surface, which can then further react to form volatile species which are ultimately removed by the vacuum system. It is generally observed that this type of surface erosion is primarily a property of polymers containing hetero-atoms such as oxygen in the backbone, which can act as active sites for chain scission. This effect is also useful in removal of low molecular weight organic contamination or weakly attached layers on both organic and inorganic surfaces [87].

Although plasmas can be extremely aggressive toward an organic surface, their reactions are limited only to the topmost molecular layers. This allows for selective tailoring of the surface while retaining desired bulk properties. Improvements in surface wettability and increases in surface energy, due to both surface cleaning effects and

increases in the concentration of polar groups, are all factors which may lead to improved adhesion [87]. Thermoplastic composites, in particular, benefit from pre-bonding plasma treatment [67,89,90]. At the present time, plasma treatment is not widely utilized for the treatment of large components for use in structures, due to the fact that large vacuum chambers and pumps are necessary, neither of which is currently economical nor practical [91].

The corona discharge technique is similar to plasma treatment in that it also makes use of a high frequency electrical discharge for surface modification. A high voltage discharge is generated in air between the surface to be treated and a metal electrode. Electrons which are emitted from the electrode collide with air molecules as they travel toward the surface, resulting in electrical breakdown of the air gap. Excited particles, photons, ozone and nitrogen oxide are produced by these collisions [92]. These species eventually encounter the polymer surface, breaking polymer bonds and causing surface free radicals to be formed. Subsequent reactions between these free radicals and components of the ionized air produce a highly oxidized, polar surface. Bond breakage in the surface can also result in the production of short chain oligomers [93].

Corona discharge is well-established for the treatment of polyolefins and has also been extended to the modification of fiber-reinforced composite surfaces [91,94,95]. Surface chemistry changes include the formation of hydroxyl, carboxyl, carbonyl and hydroperoxide functional groups [95,96]. Fluorocarbon residues are also removed by a corona treatment [76]. Like plasma treatments, corona discharge also leads to erosion and texturing of the surface [78]. Both plasma and corona treatments also have a tendency to heat the surfaces being treated and may cause local melting or degradation [76].

An excellent comparison of all the composite surface pretreatment techniques discussed above has been compiled by Marinelli and Lambing [97]. Table 2.1 assesses the technical aspects of grit blasting, priming, chemical etching, peel ply, flame treatment,

Table 2.1: Technical assessment of surface pretreatments for composites [adapted from 97].

Pretreatment	Bond Strength	Dirt, Oil Removal	Surface Oxidation	Surface Roughening	Health and Environment Issues
None	poor/fair	none	none	no	none
Grit Blast	poor long term	good*	very good	extensive	may involve solvent wash
Priming	moderate	fair	poor	no	may contain solvents, chromates
Chemical Etching	moderate	good	very good	moderate	operator safety, chromates
Peel Ply	very good	fair*	minimal	extensive	disposal of used peel plies
Flame	very good	good*	excellent	moderate	minimal
Corona Discharge	moderate to very good	excellent	very good	moderate to high	generates ozone
Gas Plasma	excellent	excellent	very good	moderate to high	minimal

*can also generate contamination

corona discharge and plasma treatment. The manufacturing viability of each pretreatment is evaluated in Table 2.2.

2.4.3 Application to Epoxy Composites

A number of researchers have investigated the effect of surface pretreatment on the adhesion of carbon fiber-reinforced epoxy composites. Crane et al. compared epoxy composites which had undergone SiC hand abrasion, nitric acid etch and nylon and Nomex® peel ply [98]. Comparison of the critical surface free energies of the pretreated composites with the single lap shear bond strengths showed that there was no correlation between wettability and bond strength. Sanding of the composite surfaces resulted in lap shear strengths up to 25% greater than the untreated controls; the use of peel plies did not produce any significant changes in bond strength, and the nitric acid etch resulted in bond strengths almost 50% lower than the control. It was concluded that the peel plies were useful only in that they protected the surface from damage and contamination; it was proposed that the heavy weave pattern which was left behind trapped air in the bondline.

Pocius and Wenz also speculated that the exaggerated roughness of the peel ply surfaces caused air to be trapped in the bondline and also allowed water ingress into the joint [99]. Mechanical abrasion methods were capable of removing substantial amounts of fluorine contamination and were again observed to create the strongest and most durable bonds. The peel ply treated specimens showed rather poor durability in a 160°F/85-100% relative humidity environment. No obvious correlation was found between surface energies and bond strength. In contrast to these results, Matienzo et al. found that peel ply materials did improve lap shear strengths when compared to non-treated control surfaces, as did abrasion with aluminum oxide paper [100].

Abrasion was also found to be a useful pretreatment method by Stone, who observed a direct correlation between the degree of abrasion and double lap shear strengths

Table 2.2: Manufacturing assessment of composite surface pretreatments [adapted from 97].

Pretreatment	Direct Labor Costs	Indirect Labor Costs	Material Costs	Capital Equipment Costs	Processing Limitations
None	none	high	none	none	none
Grit Blast	high	moderate	low	low	low
Priming	high	low	high	low	low to moderate
Chemical Etching	high	low	high	high	moderate to high
Peel Ply	low	moderate	high	low	low
Flame	initially high, then low	low	minimal	low	low
Corona Discharge	initially high, then low	low	minimal	low to moderate	low to moderate
Gas Plasma	moderate	low	minimal	high	moderate to high

of bonded epoxy composites [101]. When the laminates were insufficiently abraded, fluorine was detected on the surface. This was speculated to be the cause of low bond strengths in the case of lightly abraded composites. The point was made that all abrasion treatments should be carefully controlled to achieve complete removal of the contaminated surface without over-abrading to expose the fiber layers.

Parker and Waghorne [102] and Matienzo et al. [100] found that the presence of silicon on an epoxy composite surface originating from silicone mold release agents also resulted in low bond strengths and usually led to interfacial failures. Silicon concentrations of greater than 12% led to significant bond degradation during hot/wet aging. Heavy amounts of either fluorine or silicone contamination were difficult to remove completely and were completely gone only when the entire original top layer of resin was removed. Complete abrasion and removal of surface contaminants caused the locus of failure to be located within the composite itself [102].

Parker and Waghorne also studied pretreated epoxy composite surfaces with optically simulated electron emission (OSEE), a surface analysis technique similar to ultraviolet photoelectron spectroscopy. Surfaces which had not undergone surface pretreatment emitted low OSEE signals, whereas grit blasted and abraded surfaces showed stronger signals. Good correlations were noted between the OSEE signal, contaminant level as measured by XPS and lap shear strength [103]. OSEE was proposed as a viable, nondestructive method for the quality control of composite surfaces prior to bonding.

Corona discharge treatment, mechanical abrasion and acid etching of epoxy composites were carried out by Matz [104]. No significant changes in bond strengths were observed following the corona discharge treatment and the hot/wet durability of the corona-treated samples was quite poor. Mechanical abrasion was the most successful pretreatment in this study, with the highest bond strengths obtained with a medium-heavy Scotchbrite® sanding in the presence of additional abrasive containing quartz and tensides.

Marinelli and Lambing carried out surface pretreatment and adhesion studies on a variety of composite materials, including epoxy reinforced with glass fibers [97]. Contact angle, XPS, SEM and lap shear testing were used to determine the relationship between surface properties and bond strength. Grit blasting, corona discharge and oxygen plasma treatments all served to decrease the water contact angle. A slight increase in ester concentration as measured by XPS was seen for the oxygen plasma-treated surface, with a corresponding decrease in hydrocarbon and carboxylic acid concentrations. Grit blasted surfaces possessed the highest lap shear strengths, followed by oxygen plasma. Corona discharge treated surfaces did not show a significantly increased bond strength beyond that of the as-received control.

A pneumatic adhesion tensile test instrument (PATTI), described in ASTM D4541, double lap shear testing and wedge testing were used by McNamara et al. to evaluate the effect of sanding, grit blasting, acid and base etches, plasma treatment and artificial roughening techniques on epoxy composite bonding [105]. PATTI results of up to 5300 psi were obtained by grit blasting followed by a solvent wipe; chemically etched, plasma-treated and artificially roughened samples lagged behind by 1000-2000 psi. Durability results demonstrated by wedge testing showed very little crack growth for all surface pretreatments.

Seo et al. studied electron beam irradiation of epoxy composites and discovered an increase in surface polarity and wettability following irradiation; however, no bonding experiments were performed [106].

2.4.4 Application to Polyimide/Bismaleimide Composites

To date, there have been virtually no studies performed on the surface pretreatment of fiber-reinforced bismaleimide composites. In one study involving bismaleimide composites, grit blasting and solvent cleaning were the treatments of choice for bonding

prefabricated BMI patches to cracked BMI structures in aircraft [107]. In this process, both the BMI patch and the area around the damaged zone on the aircraft were sanded with a 240 grit abrasive and cleaned with methyl ethyl ketone (MEK). The patch was then bonded to the aircraft with a thermosetting rubber-toughened epoxy. This illustrates the importance of composite bonding in the repair of structures fabricated from composite materials.

A larger volume of work exists on the nadic end-capped LaRC-160 polyimide. In conjunction with NASA-Langley Research Center, Messick et al. analyzed the surface of LaRC-160 composites following various surface pretreatments [108]. Fluorine which was detected on the non-surface treated laminates was postulated to be from release fabrics used during the fabrication process. A Flashblast™ light irradiation process was the most effective method of removing fluorine, whereas chemical treatments such as ethanolic KOH, sulfuric acid/hydrogen peroxide and hydrazine hydrate, were the least effective. Abrasion techniques were observed to be less damaging to the composite surface compared to grit blasting. Critical surface energies correlated directly with the surface fluorine concentration.

In a continuation of the work by Messick et al., DeVilbiss et al. found that the surface fluorine concentration did not significantly affect the initial single lap shear bond strengths of the LaRC-160 composites when bonded with a polyimide adhesive [109]. However, aging of the bonded samples caused the bond strengths to decrease and the locus of failure to shift from cohesive to interfacial failure. XPS depth profiles performed in this study showed the fluorine contamination to be localized to the extreme surface regions of the composite laminate.

Moyer and Wightman studied various mechanical, chemical and plasma treatments on LaRC-160 composites bonded with LaRC-TPI adhesive [110]. Oxygen plasma was found to be the most effective pretreatment method, in that it simultaneously decreased the

fluorine concentration and increased the surface oxygen concentration to yield a more polar, wettable surface. Single lap shear strengths and wedge test durability were improved over non-treated, grit blasted and chemically treated laminates.

Cler conducted a study on the bonding of PMR-15 composite, a thermosetting polyimide, to steel and honeycomb core adherends [58]. The composite laminates were pretreated by grit blasting with 3 μm alumina powder, followed by drying in a circulating air oven. Proprietary primers were also used on the composite surfaces. Bonding was carried out with bismaleimide, polyimide and epoxy/phenolic adhesives in single lap shear and flatwise tensile configurations.

2.5 Mechanical Testing

Testing of adhesively bonded specimens serves as a performance indicator for adhesive evaluation and to evaluate the efficacy of surface pretreatment. While it is relatively straightforward to conduct a test and report the values obtained, care must be taken in the interpretation of the results. This is because each adhesive joint is an assembly of materials, or a *system*, made up of adherends, adhesives, surface layers, and interphase regions [111]. The properties of each of these components are reflected in any mechanical test results obtained. Adhesive joints must also be considered as *structures*, with different stress distributions and behaviors which are dependent upon the particular geometry utilized for bonding. Thus, it is important to understand the limitations and difficulties associated with test geometries selected to evaluate adhesive bond performance.

2.5.1 Lap Shear Tests

Lap shear testing is undoubtedly the most widely used type of mechanical test for adhesive joints, being relatively inexpensive and simple to carry out. These features are

particularly attractive in industrial settings for quality control and inspection purposes. These test methods were developed to evaluate the tensile shear strengths of adhesives as well as to compare adherend surface pretreatments. ASTM specifications which standardize the testing parameters for single lap shear specimens are detailed in D 1002-72 for metal adherends and in D 3163-73 for polymeric substrates. Double lap shear test configurations are described in ASTM D 3528-76. Schematic diagrams of both the double and single overlap configurations are shown in Figures 3.3 and 3.6, respectively, in the Experimental Section.

Although easy to fabricate and test, single lap shear joints present several pitfalls. It is often assumed that all loading is in shear in the plane of the bond, but due to the asymmetry of the joint, tension loading creates a bending moment which results in joint deformation. The result is that the highest stresses are concentrated at the ends of the bond. These maximum shear stresses have been calculated to be as much as six times greater than the measured "average" lap shear strength, calculated by dividing the maximum force needed to debond the specimen by the overlap area. Peel stresses are also concentrated at the bond termini. This type of stress distribution causes most bond failures to occur in a peel or cleavage mode, initiated at the edges of the bond [112].

Bond strength is affected not only by the shear strength of the adhesive, but also by the adhesive and adherend thickness, surface preparation, overlap length, adherend modulus and yield stress, and joint geometry [112,113]. Changing any one of these parameters will affect the measured lap shear strength. Although it is widely used in adhesion research for this purpose, the single lap shear test is a poor way to compare different adhesives. The measured average shear strength is not a material property which is necessarily unique to the adhesive [114]. In addition to these considerations, it is generally difficult to use small test specimens to predict the behavior of large adhesively bonded structures [113].

The single lap shear joint has been the subject of numerous studies to determine the nature of the stress distribution in the bondline. One of the earliest analyses was a linear elastic solution by Volkersen, who modeled the adhesive bond as an infinite number of tiny rivets. This analysis led to the well-known *shear lag* model. Assumptions were made that the adhesive deformed only in shear and that the adherends deformed only in extension. The solution shows that shear strains and stresses in the adhesive layer are at a maximum at each end of the bond for symmetric adherends, as illustrated in Figure 2.5a.

One significant flaw in this model involves not considering the bending moment which originates from non-collinearity of adherends [115]. It is also unrealistic to assume that shear stresses are at a maximum at the very edges of the bondline, because a free surface cannot sustain shear. Instead, it is more likely that the maximum shear stresses occur just inside the bond edges [22].

This bending moment was taken into account by Goland and Reissner, who defined a factor **k**, which is a measure of the degree of bending necessary for the adherends to align themselves with the loading direction. k is equal to 1 for undeformed substrates, but decreases as the load on the joint increases. As the adherends bend during the application of a load, the peel stresses in the system decrease. The main result of this model was that peel stresses in the adhesive were also shown to be at a maximum at the edges of the bond, as shown in Figure 2.5b. It was assumed that both shear and peel stresses are uniform across the adhesive thickness [116].

Allman's analysis [117] took into account bending, shear and normal stresses in the adherends, and also set the shear stress in the adhesive to zero at the ends of the bond. Adams and Peppiatt considered shear stresses in the adhesive layer normal to the loading direction caused by Poisson's ratio effects as well as adherend shear strains [118]. In the analysis of composite joints, these shear strains are particularly important because most fiber-reinforced composite materials have low in-plane shear moduli [115].

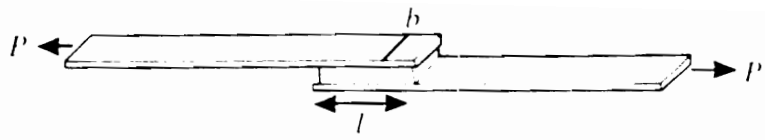

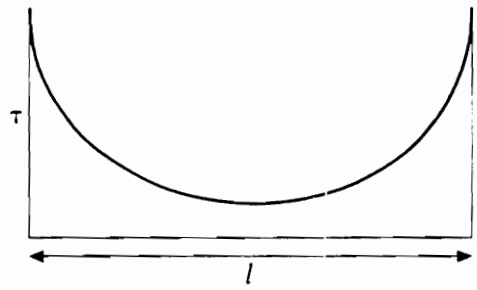

(a)

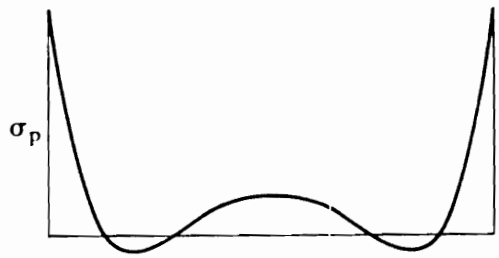

(b)

Figure 2.5: Stresses in single lap shear joints. (a) shear stresses, as calculated by Volkersen, and (b) transverse (peel) stresses calculated by Goland and Reissner [115].

Because present day structural adhesives possess high ductility and hence large strains to failure, modeling the adhesive as an elastic material is not always appropriate. Hart-Smith utilizes a more realistic elastic-plastic model to analyze adhesively bonded lap joints [119]. Finite element methods are also increasingly utilized to model stresses in adhesive joints. The effects of adhesive spew or fillets, singularities, adherend tapering, sharp or rounded corners on the stress distribution, as well as the magnitudes and directions of principal stresses can be readily determined [115].

The double lap shear configuration, which is essentially two single lap joints placed back-to-back, is generally favored over single lap configurations. Its symmetrical construction allows for a collinear application of load; therefore, there are no net bending moments and no joint rotation. As a result, cleavage and peel stresses in the adhesive layer are reduced. For this reason, the Volkersen analysis is more applicable for double lap than for single lap shear joints [22,115]. However, some internal bending does occur in the outer adherends of the double lap specimen, resulting in tensile stresses at the unloaded end of the adhesive layer and compressive stresses at the loaded end [115].

Failure of lap joints can occur cohesively within the adhesive or within the adherend. Failure within the adherend is usually unlikely in the case of metallic adherends but can be quite common in composite joints. If a weak boundary layer is present, lap joints can also fail interfacially [120]. In metal adherends, peel stresses are limited by the adhesive strength, in composite lap joints, peel stresses must be restricted as not to exceed the interlaminar strength of the laminate [119].

2.5.2 Wedge Tests

A major problem with most laboratory mechanical tests is that their results do not correlate with service performance. Lap shear testing as a function of temperature, peel testing as a function of temperature, and exposure of unstressed lap shear joints to various

environments prior to testing have not been able to duplicate in-service conditions. Only when lap-shear specimens are exposed to hostile environments while *under load* do test results approximate in-service failure modes. Hence, a simple test method for loaded specimens in various aggressive environments was desired. This need was the impetus for the development of the wedge test [121].

The wedge test, also known as the Boeing wedge test, crack propagation test, cleavage test, or crack extension test, was initially developed as a method to evaluate aluminum surface pretreatments as related to in-service durability. It has been the primary tool in the optimization of the FPL etch, phosphoric acid anodization, field repair surface treatments, titanium and stainless steel surface treatments and many others [122]. More recently, its use has been extended to other metals, composites and unfilled polymers.

Dimensions of a typical wedge coupon and the wedge itself are given by ASTM D 3762-79; schematic diagrams are shown in Figure 3.4 in the Experimental Section. Other dimensions can be used if the substrate or adhesive materials are costly or difficult to obtain. Ideally, the thickness of the adherends should be large enough so that plastic deformation does not occur [123].

In the standard wedge configuration, two adherend coupons are bonded together with a short unbonded distance at one end into which a wedge is driven. The presence of the wedge puts the adhesive in tension, resulting in the formation of a crack. As shown in Figure 2.6, the length of this initial crack is measured between the point where the wedge taper begins and the crack tip. The specimen is then exposed to the environment of interest, which can be high humidity, heat, thermal shock or salt spray, and the growth of the crack is monitored as a function of time, as depicted in Figure 2.6 [122].

The wedge test is actually a simplified adaptation of the double cantilever beam test, which is a constant load test, rather than a fixed displacement test. Fracture takes place in

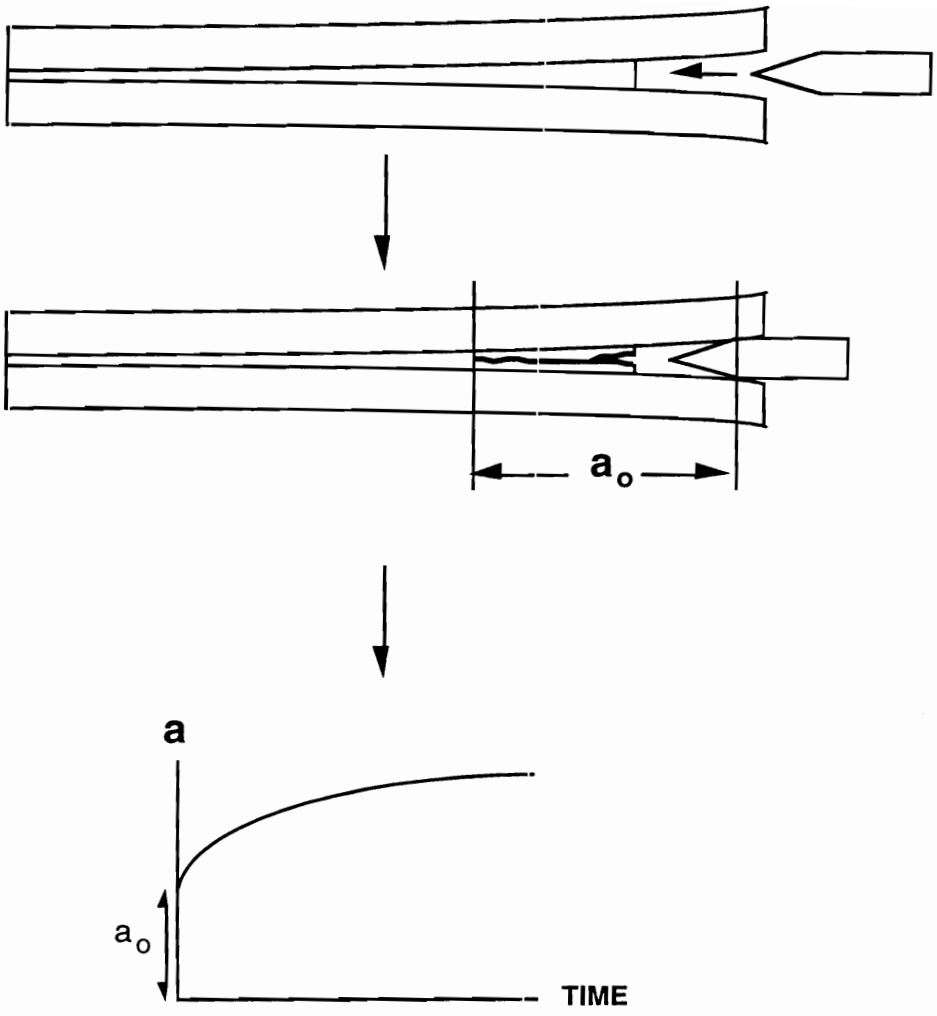

Figure 2.6: Initial crack formation and crack propagation in a Boeing wedge specimen, monitored as a function of time.

mode I, crack opening mode, with no shear components present. The critical strain energy release rate or the fracture energy G_{1c} can be calculated by:

$$G_{1c} = \frac{y^2 E h^3 [3(a + 0.6h)^2 + h^2]}{16[(a + 0.6h)^3 + a^2 h]^2} \quad (2.1)$$

where G_{1c} is the fracture energy, E is the adherend modulus, h is the adherend thickness, a is the crack length, and y the displacement. This expression takes into account bending in the adherends, shear deflection and rotation [123]. The introduction of the wedge results in substrate deformation and the storing of elastic energy in the system. The magnitude of this energy is a function of the stiffness of the adherends, thickness of the wedge, length of the precrack, initial crack length and adhesive toughness. It has been determined that a 1 mm thick wedge corresponds to an applied force of 33 N [124]. As stated above, it is preferred that the adherends do not undergo plastic deformation, which will reduce the stress at the crack tip.

Joints debond when their elastic strain energy release rate G is higher than the adhesive fracture energy. As the crack propagates, this elastic energy is released [122]. Initial fracture results from a sudden increase in the energy of the system when the wedge is inserted, causing a crack to form at high speed. If fracture proceeds in the adhesive, fracture resistance is characteristic of the adhesive; if in the interface, fracture resistance is characteristic of the joint interface [124]. The path followed by a crack depends on the quality of surface pretreatment as well as on the nature of the adhesive [125]. Unstable adhesion results in rapid crack propagation and/or propagation at the interface. Stable adhesion is characterized by propagation within the adhesive and small crack extensions (0-8 mm for bonded aluminum) [126].

It can be seen from Equation 2.1 that the critical strain energy release rate decays as the crack length increases. Equilibrium is reached when the elastic energy remaining in the system is equal to the fracture resistance of the adhesive, the magnitude of which may be

reduced by environmental exposure The equilibrium debond length is often used as a measure of bond quality, in that the durability of the adhesive bond can be correlated to the inverse of the crack length [121,127]. This equilibrium crack length can also be used to calculate the fracture resistance and cleavage strength of the adhesive bond, assuming no plastic yielding has taken place [128].

The deleterious effects of water on adhesion are well-documented, and in the context of the wedge test, the presence of water (liquid or vapor) at the crack tip accelerates crack propagation. Diffusion of moisture through the bondline degrades adhesion by a variety of chemical and physical mechanisms. Depending on the applied load, the actual crack tip may coincide with the advancing weakened bond, or may lag behind [127]. The fracture resistance of the bond decreases and crack extension will proceed until the new value of fracture resistance is met. Thus, the wedge test provides a method to measure the resistance of an adhesive joint to a particular environment [125].

In general, the wedge test possesses numerous advantages in the evaluation of bond durability. It is a simpler and more economical version of the double cantilever beam specimen which combines mode I loading and environmental exposure, resulting in a rigorous durability test. Large numbers of specimens can be tested simultaneously for extended periods of time under a wide variety of conditions [127]. Because the specimens are self-loaded, expensive testing machines or trained personnel are not required. Preparation of the wedge specimens themselves is relatively simple and requires minimal time [126]. The major disadvantage of wedge testing is that is somewhat qualitative in nature and cannot be used quantitatively to distinguish between differing degrees of bond quality [126].

Wedge testing is widely used as a process control tool to check the quality of chemical processing, particularly in adherend surface pretreatment procedures. It is also able to discriminate levels of quality in adhesively bonded parts as well evaluate service

debonds [129]. In general, excellent correlations between in-service performance and wedge test results have been found [121].

2.6 References

1. M. Knight in *Encyclopedia of Physical Science and Technology*, vol. 3, p. 274 (Academic Press, Orlando, 1987).
2. F.P. Gerstle in *Encyclopedia of Polymer Science and Engineering*, vol. 3, p. 776 (Wiley-Interscience, New York, 1986).
3. T.J. Reinhart in *Engineered Materials Handbook*, vol. 1, p. 28 (ASM International, Metals Park, 1987).
4. Composite Materials" in *Kirk-Othmer Encyclopedia of Chemical Technology*, 3rd ed., vol. 5, p. 683 (Wiley-Interscience, New York, 1979).
5. K.K. Chawla, *Composite Materials: Science and Engineering*, p. 19 (Springer-Verlag, New York, 1987).
6. R.J. Diefendorf and E. Tokarsky, *Polym. Eng. Sci.*, **15**(3), 150 (1975).
7. D.M. Riggs, R.J. Shuford and R.W. Lewis in *Handbook of Composite Materials*, G. Lubin, ed., p. 196 (Van Nostrand Reinhold, New York, 1982).
8. L.T. Drzal in *Treatise on Adhesion and Adhesives - 6*, R.L. Patrick, ed., p. 187 (Marcel Dekker, New York, 1989).
9. K. Wolf, R.E. Fornes, J.D. Memory and R.D. Gilbert in *Chemistry and Physics of Carbon*, **18**, P.A. Thrower, ed., p. 93 (Marcel Dekker, New York, 1982).
10. B.R. Noton in *Engineered Materials Handbook*, vol. 1, p. 28 (ASM International, Metals Park, 1987).
11. B.R. Noton, ed., *Composite Materials, vol. 3: Engineering Applications of Composites* (Academic Press, New York, 1974).
12. J.M. Anglin in *Engineered Materials Handbook*, vol. 1, p. 801 (ASM International, Metals Park, 1987).
13. S. Witzler, *Advanced Composites*, p. 59, July/Aug. 1988.
14. V.P. McConnell, *Advanced Composites*, p. 34, Sept./Oct. 1989.
15. *Advanced Materials and Processes*, p. 29, April 1991.

16. A.M. Thayer, *Chemical and Engineering News*, p, 37, July 23, 1990.
17. B. Walter Rosen and N.F. Dow in *Engineered Materials Handbook*, vol. 1, p. 175 (ASM International, Metals Park, 1987).
18. D. Hunston, R. Dehl and W.L. Wu, *Mech. Eng.*, p. 52, March 1986.
19. N. Cogswell in *Materials and Processing - Move into the 90's*, S. Benson, T. Cook, E. Trewin and R.M. Turner, eds. (Elsevier Science Publishers, Amsterdam, 1989).
20. C.A. May in *Engineered Materials Handbook*, vol. 1, p. 66 (ASM International, Metals Park, 1987).
21. H. Lee and K. Neville, *Handbook of Epoxy Resins* (McGraw-Hill, New York, 1967).
22. W.C. Wake, *Adhesion and the Formulation of Adhesives* (Applied Science Publishers, London, 1982).
23. D.T. Behm and J. Gannon in *Engineered Materials Handbook*, vol. 3, p. 94 (ASM International, Metals Park, 1987).
24. R.J. Morgan in *The Role of the Polymeric Matrix in Processing and Structural Properties of Compoiste Materials*, J. Seferis and G. Nicolais, eds., p. 207 (Plenum Press, New York, 1983).
25. J.S. Shim, W. Lee and J. Jang, *Polym. J.*, **23**(7), 903 (1991).
26. R. Bauer, *Proceedings of the ACS Division of Polymeric Materials: Science and Engineering*, **63**, 572 (Fall 1990).
27. R. Drake, *Proceedings of the ACS Division of Polymeric Materials: Science and Engineering*, **63**, 802 (Fall 1990).
28. J.L. Hedrick, I. Yilgor, G.L. Wilkes and J.E. McGrath, *Polym. Bull.*, **13**, 201 (1985).
29. J.A. Cecere and J.E. McGrath, *Polym. Prepr.*, **27**, 299 (1986).
30. S.F. Chen and B.Z. Jang, *Compos. Sci. Technol.*, **41**, 77 (1991).
31. J. Verbicky, Jr. in *Encyclopedia of Polymer Science and Engineering*, 2nd ed., vol. 12, p. 364 (John Wiley and Sons, New York, 1988).
32. M.A. Chaudhari in *Looking Ahead For Materials and Processes*, J. de Bossu, G. Briens and P. Lissac, eds., p. 469 (Elsevier Science Publishers, Amsterdam, 1987).
33. H.D. Stenzenberger, M. Herzog, P. Konig, W. Romer and W. Breitigam, *Proceedings of the 34th International SAMPE Synposium*, 1877 (1989).
34. D. Landman in *Developments in Reinforced Plastics - 5*, G. Pritchard, ed., p. 39

(Elsevier Applied Science Publishers, London, 1986).
35. T. Takekoshi, *Adv. Polym. Sci.*, **94**, p. 2 (Springer-Verlag, Berlin, 1990).
36. D.A. Scola in *Engineered Materials Handbook*, vol. 1, p. 78 (ASM International, Metals Park, 1987).
37. D.P. Bashford in *Developments in Reinforced Plastics - 5*, p. 205 (Applied Science Publishers, London, 1986).
38. R.J. Schliekelmann in *Progress in Science and Engineering of Composites - ICCM-IV*, T. Hayashi, K. Kawanta and S. Umekawa, eds., p. 63 (Tokyo, 1982).
39. F.L. Matthews in *Developments in GRP Technology*, B. Harris, ed., p. 161 (Applied Science Publishers, London, 1983).
40. K.D. Cressy, *Assembly Engineering*, p. 26, April 1990.
41. R.B. Ostrom, S.B. Koch, D.L. Sirz-Safranek, *Proceedings of the 34th International SAMPE Symposium*, 300 (1989).
42. R.G. Anderson, *Proceedings of the 28th National SAMPE Symposium*, 647 (1983).
43. P. Jouin, T. Lee and R. Vitlip, *Proceedings of the 36th International SAMPE Symposium,* 1014 (1991).
44. G.R. Griffiths, W.D. Hillier and J.A.S. Whiting, *Proceedings of the 33rd International SAMPE Symposium*, 308 (1988).
45. P.F. Shafer, *Adhesives Age*, p. 23, October 1993.
46. E.C. Clark and K.D. Cressy, *Proceedings of the 32nd International SAMPE Symposium*, 271 (1987).
47. A.A. Baker, *Composites*, **18**(4), 293 (1987).
48. C.L. Ong and S.B. Shen, *Int. J. Adhes. Adhes.*, **12**(1), 19 (1992).
49. C.L. Ong and S. Shen, *Proceedings of the 34th International SAMPE Symposium*, 1067 (1989).
50. "Joining, Mechanical Fastening" in *International Encyclopedia of Composites*, vol. 2, S.M. Lee, ed., p. 438 (VCH Publishers, New York, 1990).
51. J.W. Renton and J.R. Vinson, *Engineering Fracture Mechanics*, **7**, 41 (1975).
52. F.L. Matthews in *Joining Fibre-reinforced Plastics,* F.L. Matthews, ed., p. 1 (Elsevier Applied Science Publishers, London, 1987).
53. D.S. Saunders, S.C. Galea and G.K. Diermendjian, *Composites*, **24**(4), 309 (1993).

54. L.M. Bates, *Plastics World*, p. 82, August 1991.
55. J. Boyd and S. Speak, *Proceedings of the 37th International SAMPE Symposium*, 1184 (1992).
56. J.R. Vinson, *Polym. Eng. Sci.*, **29**(19), 1325 (1989).
57. D.J. Progar, *J. Adhesion. Sci. Technol.*, **2**(6), 449 (1988).
58. S. Cler, *Proceedings of the 35th International SAMPE Symposium*, 802 (1990).
59. P. K. Guha and J.N. Epel, *Adhesives Age*, p. 31, June 1979.
60. N. Allbee, *Advanced Composites*, p. 42, Nov/Dec. 1989.
61. D.M. Brewis, J. Comyn and J.R. Fowler, *Polymer*, **18**, 76 (1977).
62. "Joining Polymeric Composites, Adhesives" in *International Eneyclopedia of Composites*, vol. 2, S.M. Lee, ed., p. 509 (VCH Publishers, New York, 1990).
63. T.J. Reinhart, Jr. and W.M. Scardino, *Adhesives Age*, p. 23, February 1975.
64. J.W. White, *Adhesives and Sealants Industry*, p. 45, Feb/Mar. 1994.
65. B.A. Stein, W.T. Hodges and J.R. Tyeryar, *J. Aircraft*, **23**(7), 545 (1986).
66. J.W. Powers and W.J. Trzaskos, *Proceedings of the 34th International SAMPE Symposium*, 1987 (1989).
67. P. Davies, W.J. Cantrell, P.Y. Jar, P.E. Bourban, V. Zysman and H.H. Kausch, *Composites*, **22**(6), 425 (1991).
68. A.J. Kinloch, G.K.A. Kodokian and J.F. Watts, *Phil. Trans. R. Soc. Lond. A*, **338**, 83 (1992).
69. A. Benatar and T.G. Gutowski, *SAMPE Q.*, p. 35, October 1986.
70. A. Benatar and T.G. Gutowski, *Proceedings of the 33rd International SAMPE Symposium*, 1787 (1988).
71. J.G. Dillard in *Engineered Materials Handbook*, vol. 3, p. 281 (ASM International, Metals Park, 1987)
72. C.L. Mahoney, *Proceedings of the 34th International SAMPE Symposium,* **34**, 1901 (1989).
73. D.J. D. Moyer and J.P. Wightman, *Surf. Interface Anal.*, **14**, 496 (1989).
74. B.M. Parker and R.M. Waghorne, *Surf. Interface Anal.*, **17**(7), 471 (1991).
75. W.A. Zisman, *Ind. Eng. Chem.*, **55**(10), 19 (1963).
76. J.R.J. Wingfield, *Int. J. Adhes. Adhes.*, **13**(3), 151 (1993).
77. R.F. Wegman, *Surface Preparation Techniques for Adhesive Bonding*, p. 109 (Noyes Publications, New Jersey, 1989).

78. W.A. Dukes and A.J. Kinloch in *Developments in Adhesion - 1*, W.C. Wake, ed. (Applied Science Publishers, London, 1977).
79. C.H. Lerchenthal and M. Brennan, *Polym. Eng. Sci.*, **16**, 760 (1976).
80. T.J. Reinhart in *Engineered Materials Handbook*, vol. 1, p, 681 (ASM International, Metals Park, 1987).
81. A.J. Kinloch in *Handbook of Adhesion*, D.E. Packham, ed., p. 167 (Longman Group UK Ltd., Essex, 1992).
82. "Surface Modification" in *Encyclopedia of Polymer Science and Engineering*, vol. 17, 674 (Wiley-Interscience, New York, 1987).
83. J.G. Dillard, T.F. Cromer, C.E. Burtoff, A.J. Cosentino, R.L. Cline and G.M. MacIver, *J. Adhesion*, **26**, 181 (1988).
84. J.R. Krone, T.P. Murtha and J.A. Stirling, *Proceedings of the 33rd International SAMPE Symposium*, 829 (1988).
85. E. Wurzberg, A. Buchman, E. Zylberstein, Y. Hodengraber and H. Dodiuk, *Int. J. Adhes. Adhes.*, **10**(4), 254 (1990).
86. S.L. Kaplan and P.W. Rose, *Plastics Engineering*, **44(5)**, 77 (1988).
87. E.M. Liston, *J. Adhesion*, **30**, 199 (1989).
88. A.T. Bell and J.R. Hollahan, *Techniques and Applications of Plasma Chemistry* (John Wiley and Sons, New York, 1974).
89. E. Occhiello, M. Morra, G.L. Guerrini and F. Garbassi, *Composites*, **23**(3), 193 (1992).
90. T.H. Yoon and J.E. McGrath, *Proceedings of the 36th International SAMPE Symposium*, 428 (1991).
91. S.-I. Y. Wu, *Proceedings of the 35th International SAMPE Symposium*, 846 (1990).
92. D. Briggs in *Handbook of Adhesion*, D.E. Packham, ed., p. 94 (Longman Group UK Ltd., Essex, 1992).
93. E. Prinz and K.-H Meyer, *Paper, Film and Foil Converters*, p. 49, September 1988.
94. A.J. Kinloch, G.K.A. Kodokian and J.F. Watts, *J. Mater. Sci. Lett.*, **10**, 815 (1991)
95. G.K.A. Kodokian and A.J. Kinloch, *J. Mater. Sci. Lett.*, **7**, 625 (1988).
96. D.F. Lawson, *Rubber Chem. Technol.*, **60**, 102 (1986).
97. J.M. Marinellli and C.L.T. Lambing, *Proceedings of the 38th International SAMPE Symposium*, 1196 (1993).

98. L.W. Crane, C.L. Hamermesh and L. Maus, *SAMPE J.*, **12**(2), 6(1976).
99. A.V. Pocius and R.P. Wenz, *Proceedings of the 30th National SAMPE Symposium,* 1073 (1985).
100. L.J. Matienzo, D.J. Venables, J.D. Fudge and J.J. Velten, *Proceedings of the 30th National SAMPE Symposium,* 303 (1985).
101. W.H. Stone, *Int. J. Adhes. Adhes.*, **5(1)**, 271 (1981).
102. B.M. Parker and R.M. Waghorne, *Composites*, **13**, 280 (1982).
103. B.M. Parker and R.M. Waghorne, *Surf. Interface Anal.*, **17**(7), 471 (1991).
104. Ch. W. Matz, *J. Adhesion,* **22**, 62 (1987).
105. D.K. McNamara, H.M. Hand and C. Arah, *Proceedings for the 6th International Symposium on Structural Adhesives Bonding* (1992).
106. K.S. Seo, R.E. Fornes, R.D. Gilbert and J.D. Memory, *J. Polym. Sci: Part B*, **26**, 245 (1988).
107. R.C. Knight, *Proceedings of the 328h National SAMPE Symposium,* 223 (1983).
108. D.L. Messick, D.J. Progar and J.P. Wightman, *NASA TM 85700*, Oct. 1983.
109. T.A. DeVilbiss, D.L. Messick, D.J. Progar and J.P. Wightman, *Composites*, **16**(3), 207 (1985).
110. D.J. D. Moyer and J.P. Wightman, *Surf. Interface Anal.*, **17**, 457 (1991).
111. D.A. Dillard and D. Lefebvre in *Engineered Materials Handbook*, vol. 3, p. 313 (ASM International, Metals Park, 1987).
112. D.J. Zalucha in *High Performance Adhesive Bonding*, G. DeFrayne, ed., p. 60 (Society of Manufacturing Engineers, Michigan, 1983).
113. G.P. Anderson, S.J. Bennet and K.L. DeVries, *Analysis and Testing of Adhesive Bonds*, chapter 1 (Academic Press, New York, 1977).
114. L.J. Hart-Smith, *Adhesives Age*, April 1987, p. 28.
115. R.D. Adams, *J. Adhesion*, **30**, 219 (1989).
116. M. Goland and E. Reissner, *J. Appl. Mechanics: Trans Am. Socy. Mech. Engineers*, **A66**, 17 (1944).
117. D.J. Allman, *Quart. J. Mechanics and Appl. Math*, **30**, 414 (1977).
118. R.D. Adams and N.A. Peppiatt, *J. Strain Anal.*, **8**, 143 (1973).
119. L.J. Hart-Smith, ASTM STP 749, K.T. Kedward, ed., p. 3 (ASTM, Philadelphia, 1981).
120. E. Sancaktar, S. Schenck and S. Padgilwar, *Ind. Eng. Chem. Prod. Res. Dev.*,

23, 426 (1984).
121. J.A. Marceau, Y. Moji and J.C. McMillian, *Adhesives Age*, October 1977, p. 28.
122. J. A. Marceau and E.W. Thrall in *Adhesive Bonding of Aluminum Alloys*, E.W. Thrall and R.W. Shannon, eds., chapter 10 (Marcel Dekker, New York, 1985).
123. B.M. Parker in *Handbook of Adhesion*, D.E. Packham, ed., p. 504 (Longman Group UK Ltd., Essex, 1992).
124. J. Cognard, *Int. J. Adhes. Adhes.*, **8**, 93 (1988)
125. J. Cognard, *Int. J. Adhes. Adhes.*, **6**, 215 (1986).
126. W. Brockmann in *Engineered Materials Handbook*, vol. 3, p. 663 (ASM International, Metals Park, 1987).
127. D.R. Lefebvre in *Engineered Materials Handbook*, vol. 3, p. 382 (ASM International, Metals Park, 1987).
128. J. Cognard, *J. Adhesion*, **20**, 1 (1986)
129. R.W. Roberts in *Engineered Materials Handbook*, vol. 3, p. 735 (ASM International, Metals Park, 1987).

Chapter III: Experimental

3.1 Materials

Eight and sixteen-ply composite panels of rubber-toughened epoxy (designated 5276) and toughened bismaleimide (designated 5250-4) were fabricated and supplied by BASF Structural Materials, Inc.(Anaheim, CA). The chemical formulations of the composite matrix resins are proprietary. The fiber reinforcement was in the form of a woven fabric manufactured from BASF G30-500 P\W carbon fiber; prepreg plies were laid up so that the warp direction of the fabric in each ply was oriented in the same direction. The rubber-toughened epoxy had a structure which alternated layers of prepreg ply with layers of rubber toughener [1]. The epoxy composite had an average resin content of 42% and an average fiber volume of 57%, while the bismaleimide (BMI) composite had an average resin content of 30% and an average fiber volume of 69%. The 8-ply epoxy composite was approximately 1.5 mm thick (0.06 in.) and the 16-ply laminate was approximately 3 mm (0.13 in.) thick. The 8 and 16-ply BMI laminates are 1.3 mm (0.05 in.) and 2.5 mm (0.1 in.) thick, respectively.

A portion of the composite panels were supplied with a peel ply layer which was co-cured on the outermost surfaces of the composite. The epoxy peel ply fabric was impregnated with an epoxy resin formulation. The BMI peel ply was glass cloth impregnated with a BMI-based resin. The composite panels which were not supplied with a peel ply were fabricated in the conventional manner against fluorinated-ethylene propylene (FEP) films. These latter panels were utilized as controls and for grit blasting and plasma treatment.

The adhesive used for the bonding studies was BASF Metlbond® 1146, a rubber-toughened epoxy film adhesive supplied on a scrim cloth. The thickness of the uncured adhesive film was 0.25 mm (0.01 in.); the cured thickness was approximately 0.10-0.13

mm (0.004-0.005 in.). The T_g of the fully cured adhesive is approximately 137°C [2]. The adhesive film was stored at 0°C and was warmed up to room temperature before removal from the plastic bagging material.

3.2 Surface Pretreatments

As received - Laminates obtained from BASF were simply wiped with methyl ethyl ketone (MEK)and a Kimwipe® tissue, then dried under a stream of nitrogen gas. This step served to remove handling contamination and restore the original, as-processed surface.

Peel ply - Laminates which were supplied with a peel ply layer were kept intact until immediately prior to analyses, at which time a razor blade was used to initiate delamination at the peel ply/composite interface. The peel ply layer was then removed by hand.

Grit blasting - Grit blasting was carried out in an Econoline grit blaster using 150 grit silica at 415 kPa (60 psi) air pressure. Three passes were made with the nozzle at a distance of 15-20 cm (6-8 in.) from the composite panels. Grit blasted samples were then rinsed with MEK and dried under a stream of nitrogen prior to further analysis.

Plasma treatment - Plasma treatments were carried out in a March Instruments Plasmod® unit at a frequency of 13.56 MHz. The plasma reaction chamber and all connecting elements were fabricated entirely from quartz. A perforated aluminum stage was used inside the chamber for holding samples. The plasma power used varied from 10-150 watts, depending on the particular experiment. Gas lines were purged with the gas of interest for 30-60 seconds before use. The plasma chamber was evacuated with a conventional lab vacuum pump to 13-27 Pa (0.1-0.2 torr) before backfilling with the gas of interest to approximately 133 Pa (1 torr), which was then maintained through the duration of the treatment. Oxygen, ammonia and nitrogen gases were utilized to create the plasmas.

All surface analyses were performed within 5 minutes of plasma treatment, to minimize the possibility of surface molecular rearrangement and/or contamination by the atmosphere.

3.3 Characterization of Composite Surfaces

3.3.1 X-ray Photoelectron Spectroscopy (XPS)

XPS, also known as ESCA (Electron Spectroscopy for Chemical Analysis), is ideal for the surface analysis of polymer matrix composites due to its non-destructive nature and its shallow sampling depth. In this work, XPS was used extensively to characterize the chemical changes which occurred in the composite surface as a result of surface pretreatment.

In a typical XPS experiment, the surface of a sample is irradiated with a monoenergetic beam of x-rays, which are absorbed by the atoms in the sample. Each absorption of an x-ray photon may lead to the emission of a photoelectron with a binding energy less than the incident x-ray energy. From a measurement of the kinetic energies of the ejected photoelectrons, the binding energy of an electron from a particular core level can be calculated if the instrument parameters are known [3].

Since the atomic structure of each element in the periodic table is distinct from the others, measurement of binding energies allows the qualitative identification of elements present at the surface. Quantitative information can also be obtained from area intensities of photopeaks along with consideration of the efficiency of x-ray absorption for that particular subshell [4].

XPS is also capable of providing valuable information on oxidation state and molecular bonding through the phenomenon of *chemical shift*. In the analysis of organic materials, the carbon 1s (C1s) level is particularly sensitive to changes in substituent

electronegativity, allowing structural information to be inferred from careful curve-fitting and analyses of peak positions [5].

XPS analysis was performed on a Perkin-Elmer PHI 5400 spectrometer with a Mg K_α achromatic X-ray source (1253.6 eV), operating at 15 keV and 400 watts with an emission current of 30 mA. The spectrometer was calibrated to the $4f_{7/2}$ photopeak of gold and the $2p_{3/2}$ photopeak of copper. Pressure inside the analysis chamber was maintained below 6.6 x 10^{-5} Pa (5 x 10^{-7} torr) during the course of analysis. Samples with dimensions of 1 cm x 1 cm for XPS were cut from the composite panels with a Dremel® rotary power tool equipped with an emery cut-off blade and were mounted onto the spectrometer probe with double-sided tape. Dimensions of the analyzed areas on the samples were typically 1 mm x 3 mm. No neutralization with the electron gun was necessary since only minimal charging effects were present. Between 2-4 samples were analyzed for each surface pretreatment.

For each sample analyzed, a survey scan encompassing the region of 0-1100 eV was first taken. Multiplex scanning of all significant peaks seen in the survey was then carried out. Binding energies for all observed photopeaks were referenced to the value for C-C/C-H hydrocarbon species at 284.6 eV. Atomic concentration calculations and curve-fitting were carried out on an Apollo 3500 computer, using PHI software version 4.0. Atomic concentrations were determined by the following formula:

$$\text{Atomic \% for element X} = \frac{\frac{I_x}{S_x T_x}}{\sum_{i=1}^{n} \frac{I_i}{S_i T_i}} \qquad (3.1)$$

where I is the area of the photopeak, S is the sensitivity factor, T is the total acquisition time for each data point and n is the number of photopeaks considered. Photopeaks of

interest were fitted with Gaussian curves, varying both the peak intensity and position while holding the full width at half maximum (FWHM) at 1.7 ± 0.1 eV.

3.3.2 Ion Scattering Spectroscopy (ISS)

ISS is a surface analysis technique which has sensitivity to the topmost atomic layers in a sample. In ISS analysis, a beam of noble gas ions impinges upon a sample and is scattered inelastically after collision with species in the surface. The inelastically scattered ions are detected and the mass of the surface species is calculated from the following expression:

$$E/E_o = [\cos\theta \pm (A^2 - \sin^2\theta)^{1/2}]^2/(1 + A)^2 \qquad (3.2)$$

where E is the energy of the scattered ions, E_o is the incident ion energy, θ is the scattering angle and $A = M_2/M_1$, where M_1 is the incident ion mass and M_2 is the mass of the surface species [4,6].

In this study, ISS was carried out on the same PHI 5400 spectrometer as described above for XPS. A beam of ^3He ions with a beam voltage of 1.5 kV and an emission current of 25 mA was scattered through an angle of 123°. The beam was rastered over a 1.0 cm x 1.0 cm analysis area while acquiring survey scans from 0.35 to 1.0 E/E_o. In order to avoid sputtering away significant amounts of surface species, acquisition times were limited to 5 minutes or less.

3.3.3 Contact Angle Analysis

The technique of contact angle analysis is an important one in the field of surface science. Through the use of a simple, relatively inexpensive apparatus, the chemistry of the topmost molecular layers of surfaces can be probed and measurements which are made can be correlated directly to surface thermodynamics.

3.3.3.1 Wettability Measurements

By measuring the contact angle of a substance on a surface, the thermodynamic work of adhesion can be calculated from the following expression, known as the Young-Dupre equation:

$$W_A = \gamma_{LV} (1 + \cos \theta) + \pi \qquad (3.3)$$

where γ_{LV} is the surface tension of the probe liquid. π is a term which represents the film pressure and is usually considered to be negligible for low energy surfaces. Generally speaking, if the contact angle is greater than 90°, the liquid is said not to wet the solid. If the contact angle is close to zero, the solid is considered to be wetted. Wetting will usually occur if the surface energy of the substrate is greater than or equal to the surface tension of the probe liquid.

To assess the water wettability of the surface pretreated composites, contact angle analysis was carried out with a Rame-Hart 100-00 115 NRL contact angle goniometer equipped with a camera and video monitor. Drops (5 µl) of deionized distilled water were carefully placed on the substrate with a microliter syringe held in an upright position. The left and right sides of at least 3 to 5 drops were measured and averaged.

A liquid DGEBA epoxy resin, EPON® 830, obtained from Shell Chemical Company (Houston, TX) was used to simulate wetting of the composite surfaces by a molten epoxy adhesive. The chemical structure of EPON® 830 is shown in Figure 2.2, with the average degree of polymerization n between 0 and 1. The epoxide equivalent weight (EEW) and viscosity of EPON® 830 are reported to be 190-198 grams and 170-225 poise, respectively [7]. Maintaining a drop volume between 5-8 µl, EPON® 830 was dispensed onto the composite surfaces and both sides of each drop monitored as a function of time.

To measure the contact angle of an actual epoxy adhesive on the pretreated composite surfaces, Metlbond® 1146 adhesive resin was extracted from the scrim cloth

with MEK, dried and formed into small beads (approximately 2 mm in diameter) which were cured directly onto samples of the pretreated composites. Curing of the beads took place in a standard convection oven at an approximate heat-up rate of 3-4°C/min. followed by a 60 minute hold at 177°C. The contact angles of both sides of the cured beads were measured on a contact angle goniometer. Between 3 and 4 beads were cured and analyzed for each pretreatment.

3.3.3.2 Determination of Composite Surface Energies

In determining the composite surface energies, the effect of surface roughness on the measured contact angle must be accounted for. Wenzel has shown that surface roughness is capable of altering the measured value of the contact angle and warns against confusing the "apparent" or geometric surface area with the *actual* surface area of a solid [8]. If a measured contact angle is less than 90° on a smooth surface, the effect of surface roughening will be to decrease the contact angle; if above 90°, surface roughness will increase the value of the contact angle. A practical method to correct for surface roughness in contact angle measurements was developed by Carre and Schultz [9], who introduced the concept of roughness correction factors.

Composite samples were coated with approximately 50 nm of gold in an Edwards 5150B sputter coater. A sample of Ferrotype (chromium-plated steel photographic plate), obtained from Apollo Metals (Bethlehem, PA), was also coated with gold and served as a reference smooth surface. The contact angles of 5 µl drops of ethylene glycol were measured on the gold-coated composites as well as the gold-coated Ferrotype. A roughness factor R_C, which represents the actual surface area of a sample ratioed to the apparent geometric area, was then calculated via:

$$R_C = \cos \theta_{composite} / \cos \theta_{ferrotype} \qquad (3.4)$$

A number of approaches were utilized to obtain quantitative data on the surface energies of the pretreated composites. One such method is that of Zisman [10] who pioneered the concept of critical surface tension (γ_C). It was found that if a surface is wetted by a series of liquids, such as the n-alkanes, the cosine of the contact angle appeared to be a linear function of the surface tension of the wetting liquid. Extrapolation of the plot to $\cos \theta = 1$ (which corresponds to a wetting angle of zero) yields a corresponding surface tension which can be taken as the critical surface tension γ_C. The critical surface tension is defined as the surface tension of the liquid which will *just* spread on a surface with a zero contact angle.

A non-homologous series of wetting liquids encompassing a wide range of liquid surface tensions was used in this work, including water, glycerol, formamide, methylene iodide, ethylene glycol, 1-bromo-naphthalene, hexadecane, ethanol, and hexane. Both sides of 6-10 drops of each liquid were measured on 2.5 cm x 2.5 cm (1 in. x 1 in.) samples of the pretreated composites, using a Rame-Hart 100-00 115 NRL contact angle goniometer. The volume of each drop was maintained constant at 5 µl. The cosine of the average contact angle for each liquid was plotted versus the surface tension of the liquid, yielding a rectilinear plot with a negative slope which could be extrapolated to $\cos \theta = 1$, thus giving a value for γ_C.

In the case of the high energy oxygen plasma-treated surfaces, all the wetting liquids were observed to spread completely. Thus, in place of the liquids listed above, a series of aqueous sodium hydroxide (NaOH) solutions ranging in concentration from 2.72% w/w to 35.9% w/w were used. These solutions encompassed a range of surface tensions from 74.4 mJ/m^2 to 101.1 mJ/m^2 [11]. The plasma-treated samples were analyzed within 2 minutes of their removal from the plasma reaction chamber. All contact angles were corrected for roughness by multiplying by the appropriate roughness correction factors.

Kaelble 's approach [12] is derived from fundamental relationships involving the work of adhesion. Only dispersion and polar contributions to the surface energy are assumed to be present, and both types of contributions are assumed to be related to their respective work of adhesion through a geometric mean relationship:

$$W_A \text{ (dispersive)} = 2[\gamma_S^D \gamma_L^D]^{1/2} \quad (3.5)$$

$$W_A \text{ (polar)} = 2[\gamma_S^P \gamma_L^P]^{1/2} \quad (3.6)$$

From the expression for the total work of adhesion, which is the sum of the dispersive and polar contributions, the following expression can be derived:

$$W_A / 2[\gamma_L^D]^{1/2} = [\gamma_S^D]^{1/2} + \{\gamma_S^P (\gamma_L^P / \gamma_L^D\}^{1/2} \quad (3.7)$$

A plot of $W_A / 2[\gamma_L^d]^{1/2}$ versus $(\gamma_L^P / \gamma_L^D)^{1/2}$ yields a line with slope $(\gamma_S^P)^{1/2}$, the polar component of the surface free energy, and intercept $(\gamma_S^D)^{1/2}$, the dispersive component of the surface free energy. The same experimental procedure and series of liquids as described above for the Zisman critical surface tension experiment was utilized. The results of the contact angle analysis were plotted according to equation 3.7, and the slopes and intercepts of the plots were obtained via linear regression. Owens and Wendt [13] follow this same approach but measure the contact angles of only two liquids.

Again, due to the extremely high wettability of the plasma-treated surfaces, Kaelble's method could not be used to obtain the components of the surface energy. Instead, a water-in-alkane contact angle experiment, appropriate for use on high energy surfaces was utilized [14]. This technique involves the measurement of water contact angles on a substrate in a non-miscible alkane medium It can be established that for such a system, the following equation for the surface applies:

$$\gamma_W - \gamma_H + \gamma_{HW}\cos\theta_{SW/H} = 2[\gamma_S^D]^{1/2}[(\gamma_W^D)^{1/2} - (\gamma_H)^{1/2}] + I_{SW}^P \quad (3.8)$$

where γ_W is the surface tension of water, γ_H is the surface tension of the alkane, γ_{HW} is the interfacial tension between the water and the alkane, and $\theta_{SW/H}$ is the contact angle of the water on the substrate in the presence of alkane. A plot of $\gamma_W - \gamma_H + \gamma_{HW}\cos\theta_{SW/H}$ versus

$2[(\gamma_W^D)^{1/2} - (\gamma_H)^{1/2}]$ yields a line with a slope of $[\gamma_S^D]^{1/2}$, the dispersive component of the surface energy, and an intercept I_{SW}^P, a quantity which is a function of the polar components of the liquid surface energy and the solid surface energy. In practice, I_{SW}^P can be approximated as $2[\gamma_S^P \gamma_L^P]^{1/2}$. It is also assumed that the water will completely displace the alkane when it contacts the solid surface. In this study, the n-alkanes which were utilized were hexane, octane, decane and hexadecane, all obtained from Aldrich. Deionized distilled water (5 µl drops) were used to contact the surface. As with the NaOH solutions, the composite samples were analyzed within 2 minutes of their removal from the plasma chamber. Three samples were measured in each alkane and their values averaged. The resulting data were plotted according to equation 3.8.

3.3.4 Scanning Electron Microscopy (SEM)

An ISI SX-40 scanning electron microscope was used to analyze the surface topography of the pretreated composite samples as well as the failure surfaces following mechanical testing. Samples were sputter-coated with approximately 30-40 nm of gold to prevent surface charging by the electron beam and mounted onto the sample holder with double-sided tape. The high degree of surface roughness present on both the pretreated composites and the failure surfaces necessitated the use of a sputtered gold layer which is thicker than what is usually utilized. A thin track of silver paint was used to make an electrical connection between the aluminum mount and the gold-coated surface, so that excess surface charge could be dissipated.

SEM was also utilized to determine the degree of polymer penetration into the peel ply-imprinted surfaces. Thermoplastic, amorphous polystyrene with a T_g of 98°C was chosen for this study because it could be removed readily from the peel ply surface following wetting and spreading. As shown in Figure 3.1, polystyrene pellets, pre-flattened on one side, were placed on the composite peel ply surfaces. A glass slide was

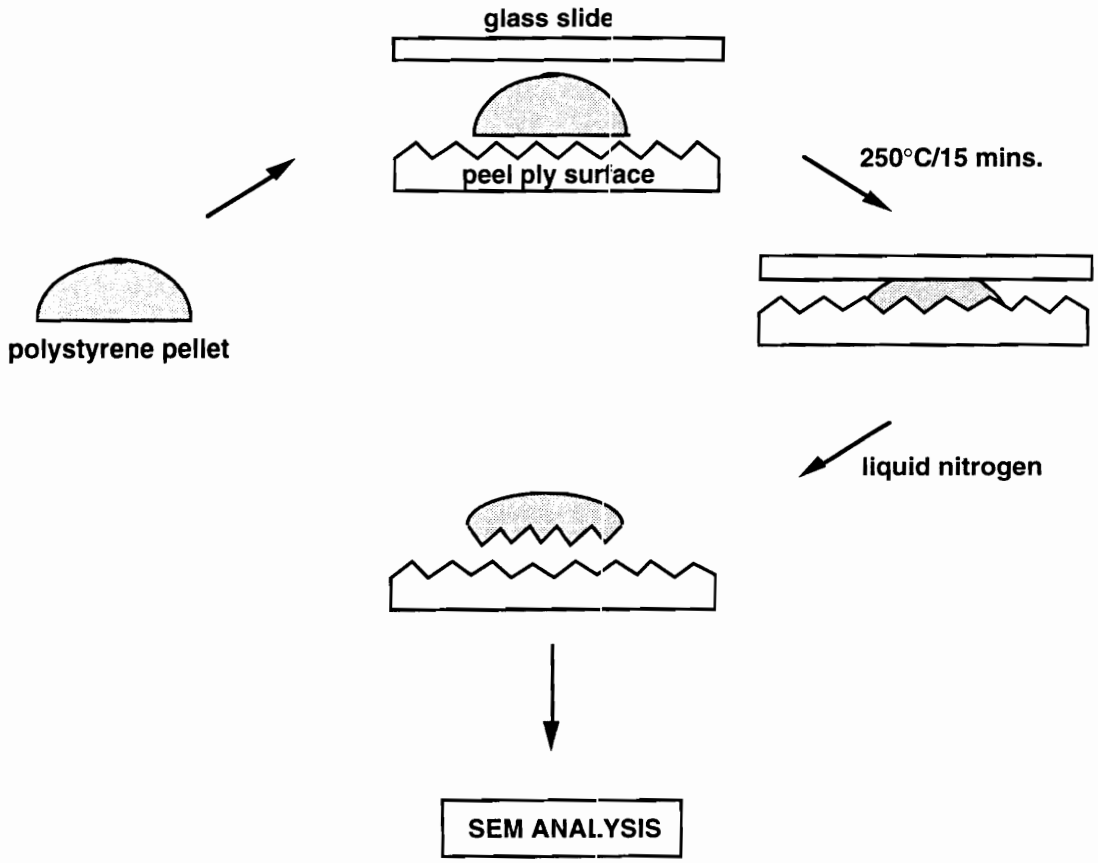

Figure 3.1: Procedure for polystyrene wetting experiments on composite peel ply surfaces.

placed on top of the pellets and the entire assembly was placed in a 225°C oven for 15 minutes. After 15 minutes, the oven was turned off and the samples were cooled to room temperature. At this point, the polystyrene was firmly adhered to the peel ply surface; however, upon contact with liquid nitrogen, the polystyrene spontaneously debonded from the composite. The underside of the polystyrene which had been in contact with the composite surface was examined by SEM using the same procedure described above.

3.3.5 Profilometry

The use of profilometry, defined as the study of the surface texture, provided pictorial information on the surface profiles of the pretreated composites and also quantitative values of surface roughness as given by R_a and R_z. R_a is defined as the average peak-to-center line distance in a surface profile; R_z is the average peak-to-valley distance. A schematic diagram of a profilometer and a typical surface trace are shown in Figure 3.2.

Both Taylor-Hobson Talysurf 4 (Leceister, England) and Perthen Perthometer M3P-M4P (Feinpruf, Germany) profilometers were utilized in this work. Both instruments utilized a diamond stylus with a 2.54 μm (0.0001 in.) tip and a tracking force of 100 mg. All quantitative work was carried out on the Perthometer instrument. Three to four tracings on each pretreated surface were taken and averaged to obtain the reported R_a and R_z values.

3.3.6 Diffuse Reflectance Infrared Spectroscopy (DRIFT)

Although traditionally associated with the analysis of powdered or finely divided samples, diffuse reflectance infrared spectroscopy (DRIFT) has been extended to the surface analysis of polymer films, fibers and coatings [15]. Infrared spectra of carbon fiber-reinforced composite materials have also been obtained by this method [16,17].

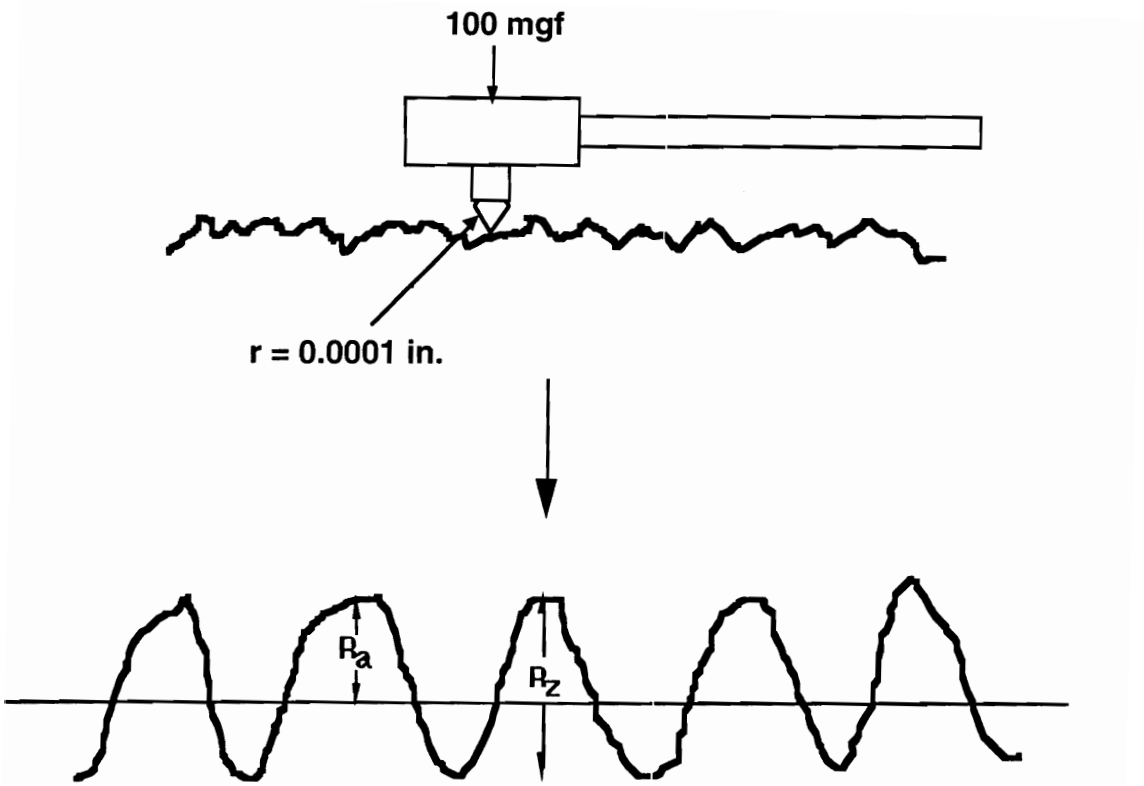

Figure 3.2: Schematic diagram of a profilometer and an example of a surface profile. The quantities R_a and R_Z are defined on the profilometer trace.

Composite samples 1 cm x 1 cm in size were placed directly into a Barnes/Spectra-Tech Collector diffuse reflectance accessory. A Nicolet 810 Fourier transform infrared spectrometer equipped with a mercury cadmium telluride (MCT) detector was used to collect spectral data. 512 scans were taken for each sample at a resolution of 4 cm^{-1}. A polished aluminum mirror served as a background. Each sample was purged in the FTIR bench with dry nitrogen for approximately 1 hour prior to being scanned.

3.4 Bond Fabrication and Testing

3.4.1 Double Lap Shear Testing

Prior to pretreatment, 16-ply and 8-ply laminates were cut into 10.2 cm x 15.2 cm (4 in. x 6 in.) panels, taking care that the warp direction of the carbon fabric reinforcement was always parallel to the 10.2 cm direction. A number of the 16-ply panels were cut into 7.6 cm x 15.2 cm (3 in. x 6 in.) sections for use as filler panels. Cutting of the composites was carried out on a water-cooled diamond-tipped saw. All panels were dried in a 120°C oven for two hours and stored in a desiccator until bonding. Immediately following pretreatment, the samples were assembled in a double lap shear configuration according to the specifications in Boeing Material Specification (BMS) 8-245G, using Metlbond® 1146. This configuration is illustrated in Figure 3.3. Heat resistant tape was used to secure the specimen, and the entire assembly was wrapped in a layer of Teflon®-coated glass fabric as well as a layer of polyester bleeder/breather material.

All the bonded specimens were placed in a vacuum bag within a Thermal Equipment autoclave having an internal diameter of 9 meters and length 15 meters. The cure cycle consisted of a 4°C/min. heat-up to 177°C, with a 90 minute hold at 177°C and 40 psi (276 kPa) pressure, vented. Following bonding, the samples were cut into 2.5 cm (1 in.) wide specimens for testing and dried again at 120°C for 2 hours. Samples for ambient

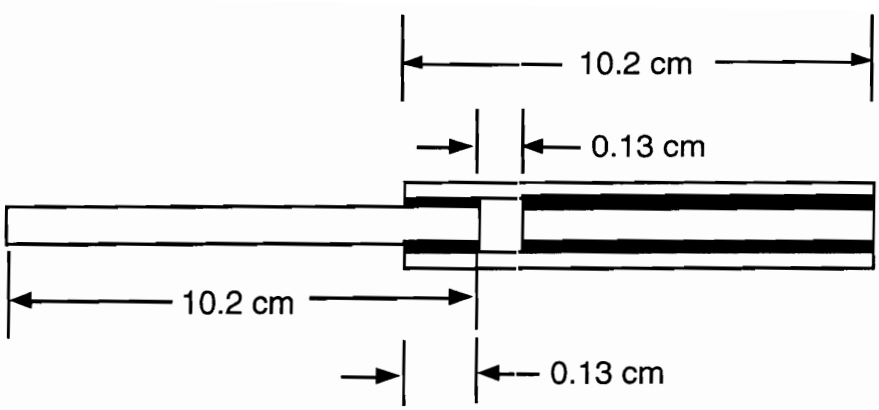

Figure 3.3: Schematic diagram of a double lap shear bond configuration.

temperature testing and 82°C (180°F) testing were stored in a desiccator until testing, samples to be environmentally conditioned were placed in a 71°C (160°F)/100% relative humidity chamber for 30 days.

Tensile testing of the double lap shear joints was carried out on an Instron model 4505 equipped with a 9072 kg (20,000 lb) load cell and interfaced with a Macintosh computer and Labview® program. Due to slippage in the Instron, it was necessary to wrap the top and bottom of each sample with sandpaper prior to insertion into the grips. Specimens were pulled to failure at a cross-head rate of 0.127 cm/min (0.05 in./min.). Peak shear stress was calculated by dividing the maximum breaking load by the bonded area, which had been measured to the nearest 0.008 cm^2 (0.05 in^2). Testing at 82°C (180°F) was carried out in a Thermotron thermal chamber. Samples which had been environmentally conditioned for 30 days were stored in water until testing could be carried out, then wiped dry and inserted into the Instron machine. Percent weight gains were also calculated for the environmentally conditioned specimens.

Examination of the failure surfaces was accomplished by scanning electron microscopy (SEM). The debonded joints were protected with clean aluminum foil and samples were cut from the debonded areas with a hand-held rotary tool.

3.4.2 Wedge Testing

Prior to surface pretreatment, 16-ply laminates were cut into 15.2 cm x 15.2 cm (6.0 in. x 6.0 in.) panels with a water-cooled diamond-tipped saw. Panels were then dried in a 120°C oven for two hours and stored in a desiccator until surface pretreatment could be carried out.

Immediately following pretreatment, the samples were assembled in a wedge configuration according to ASTM D 3762-79 specifications, using Metlbond® 1146 adhesive This configuration is shown in Figure 3.4. Care was taken so that the warp

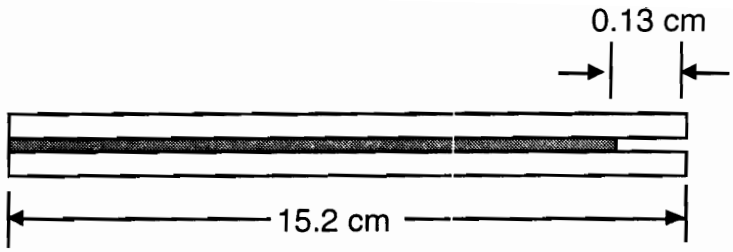

(a)

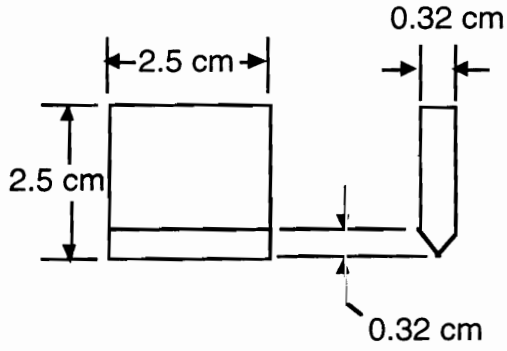

(b)

Figure 3.4: (a) Schematic diagram of the Boeing wedge sample configuration, and (b) Dimensions of stainless steel wedge.

direction of the laminates was consistently placed in the same direction. A 1.3 cm x 15.2 cm (0.5 in. x 6.0 in.) strip of 175 μm (7 mil) thick polytetrafluorethylene film was inserted in one end to form a starter crack. Heat resistant pressure sensitive tape was used to secure the specimen, and the entire assembly was pressed between 6.4 mm (1/4 in.) thick aluminum press plates in a Tetrahedron press. The cure cycle consisted of a 7°C/min. heat-up to 177°C (350°F) under 276 kPa (40 psi) pressure, a 90 minute hold at 276 kPa and 177°C, followed by a cool-down under pressure to room temperature.

Samples were cut into 2.5 cm x 15.2 cm (1.0 in. x 6.0 in.) wide specimens for testing with the warp direction of the laminates parallel to the 15.2 cm (6.0 in.) dimension, and dried again at 120°C for 2 hours. Between 3 and 5 samples were tested for each surface treatment. A 2.54 cm x 2.54 cm x 0.32 cm (1.0 in. x 1.0 in. x 0.125 in.) stainless steel wedge was carefully driven into the open end of each specimen with a hammer to a distance of 1.7 cm. The lengths of initial cracks were measured to the nearest 0.5 mm, from the point on the wedge where the taper begins to the visual end-point of the crack.

Samples were exposed to 75°C dry conditions in a Blue M circulating air oven, 75°C wet conditions in a temperature-controlled water bath, boiling water and aircraft de-icing fluid. De-icing fluid was supplied by Chemicals and Solvents, Inc. (Roanoke, VA) and is qualified to MIL-A-8243D. It is composed of a proprietary mixture of ethylene and propylene glycols. Crack growth was then measured at regular intervals. At the end of the test interval, samples which were still intact were forcibly debonded so that mode of failure could be recorded.

3.4.3 Scanning Acoustic Microscopy (SAM)

Difficulty in the inspection of bonded joints has often been cited as a disadvantage of adhesive bonding. However, increasing progress is being made in the area of non-destructive evaluation techniques, one of which is scanning acoustic microscopy. Acoustic

microscopy utilizes a focused beam of high frequency ultrasound to characterize opaque specimens. Bondline defects and variations can then be detected by fluctuations in the magnitude of reflected ultrasonic energy. An image of the bonded specimen can then be obtained by mechanically scanning the sample and digitally building up the image at each point [18].

Initial experiments involved the use of an Olympus UH-3 scanning acoustic microscope with enhanced image analysis capability to analyze a bonded specimen consisting of two 8-ply epoxy laminates bonded with Metlbond® 1146. A debonded area having dimensions of 5 mm by 30 mm was deliberately induced by inserting a Teflon® spacer directly into the bondline prior to curing. A 20 mm x 15 mm area was scanned at a frequency of 30 MHz.

In a subsequent experiment, the scanning acoustic microscope was used to study 2.5 cm x 2.5 cm (1 in. x 1 in.) specimens constructed from surface pretreated 8-ply epoxy and BMI laminates bonded with Metlbond® 1146. Surface pretreatments utilized were MEK wipe, peel ply, grit blasting and a 5 minute/50 watt oxygen plasma. A 40 mm x 40 mm area was scanned at a frequency of 30 MHz. Areas in which debonding or no bonding was present showed up as bright white spots on a darker, diffuse background.

To calculate the percentage of debonded area, a 1.6 mm (1/16 in.) grid was placed over the micrographs and the number of squares which contained a debonded spot was noted versus the total number of squares contained within the analysis area. Two sets of samples for each epoxy and BMI surface pretreatment were analyzed. One difficulty in carrying out this exercise was that the carbon fiber reinforcement also tended to scatter the ultrasonic waves, causing lighter white spots to appear on the micrograph. The determination of which spots were debonds and which were carbon fibers was critical to the analysis and was left to the discretion of the author.

3.5 Effect of Surface Functionality on Bond Strength and Durability

3.5.1 Surface Functionalization Procedure

Epoxy and BMI laminates supplied with a peel ply overlayer were chosen for this study due to the fact that the surfaces after peel ply removal had a reproducible and consistent profile. In this way, the effect of surface topography could be neglected. Following peel ply removal, 4 different surface chemistries could be generated. One set of samples was treated with MS-122, a fluoropolymer-based mold release agent (Miller-Stephenson Chemical Company, Danbury, CT), which was sprayed onto a Kimwipe® tissue and then rubbed onto the composite surface. A second set was exposed to a 50 watt oxygen plasma for 1 minute and a third set was similarly treated in a 1 min./50 watt ammonia plasma. The fourth and final set of samples was left as-is. Sample set one represented a non-functionalized, fluorine-contaminated surface, set four simulated a situation in which the surface is clean but non-functionalized, and the plasma-treated samples represented surfaces which have been stripped of contamination and additionally functionalized with polar moieties. A schematic diagram of these surfaces is shown in Figure 3.5.

3.5.2 Surface Analysis

Functionalized surfaces were analyzed by XPS using the same conditions described in Section 3.3.1. The contact angles of water, EPON® 830 and Metlbond® 1146 were measured in the same manner as in Section 3.3.3.1

3.5.3 Double Lap Shear Testing

Prior to surface functionalization, peel ply laminates were cut into panels having dimensions of 10.2 cm x 15.2 cm (4.0 in. x 6.0 in.), with the warp direction of the laminates parallel to the 10.2 cm (4.0 in.) direction. The cutting, drying, storage and

Figure 3.5: Schematic representation of functionalized peel ply surfaces.

assembly of the double lap shear joints is the same as described in Section 3.4.1. The surface functionalization of the peel ply surfaces was performed just prior to assembling the joints. Bonding of the double lap shear specimens with Metlbond® 1146 was carried out in a Tetrahedron Press in the same manner as described above for the wedge laminates in Section 3.4.2. Following bonding, the panels were cut into 2.5 cm (1.0 in.) wide specimens for tensile testing and dried for two hours in an oven at 120°C. One set of samples was tested immediately, another set was conditioned in deionized water at 75°C for 15 days prior to testing. Between 4 and 5 samples were tested for each surface treatment and environment.

Tensile testing of the double lap shear joints was carried out on an Instron model 4505 equipped with a 9072 kg (20,000 lb) load cell, and interfaced with a Macintosh computer and Labview® program. Specimens were pulled to failure at a cross-head rate of 0.127 cm/min.(0.05 in./min.). Examination of the failure surfaces was accomplished by scanning electron microscopy (SEM). The debonded joints were protected with clean aluminum foil and samples were cut from the debonded areas with a hand-held rotary tool.

3.6 Surface Aging Effects in Oxygen Plasma-treated Composites

3.6.1 Plasma Treatment and Storage Procedure

This series of experiments characterized the changes in surface chemistry, wettability and bondability which take place during sample storage following oxygen plasma treatment. Only the epoxy composites were utilized in this study. 0.6 cm (0.25 in.) square samples for XPS, 2.5 cm x 2.5 cm (1.0 in. x 1.0 in.) samples for water and EPON® 830 contact angle analysis, and 2.5 cm x 10.2 cm (1.0 in. x 4.0 in.) 16-ply samples for single lap shear testing were cut from the composite panels. Each of the above-mentioned analyses was carried out as a function of time following a 5 min.

treatment with a 50 watt oxygen plasma. While awaiting analysis, samples were stored in sample tins which were wrapped securely with paraffin film and then placed in a desiccator. A different sample was analyzed for each data point.

3.6.2 Surface Analysis

XPS analysis, water and EPON® 830 contact angle measurements were carried out on the plasma-treated composite samples as a function of time. Data were taken immediately after plasma treatment (time = 0), at 2 hours, at 1 and 4 days, and after 1, 2, 3, 7, 10, 14 and 17 weeks. Nonplasma-treated surfaces were also analyzed for comparison purposes.

3.6.3 Single Lap Shear Testing

Single lap shear samples were constructed with Metlbond® 1146 according to ASTM D 3163-73, using a 1.3 cm (0.5 in.) overlap. This configuration is shown in Figure 3.6. Samples were secured with heat-resistant tape and cured in a Tetrahedron press using the same cycle described in Section 3.4.1. Half of the lap shear samples was tested under ambient conditions and the remaining half was placed in a 75°C water bath for 15 days prior to testing. Specimens were pulled to failure on an Instron 4505 at a crosshead speed of 0.127 cm/min. (0.05 in./min.). Between 3 and 5 samples were tested for each storage time.

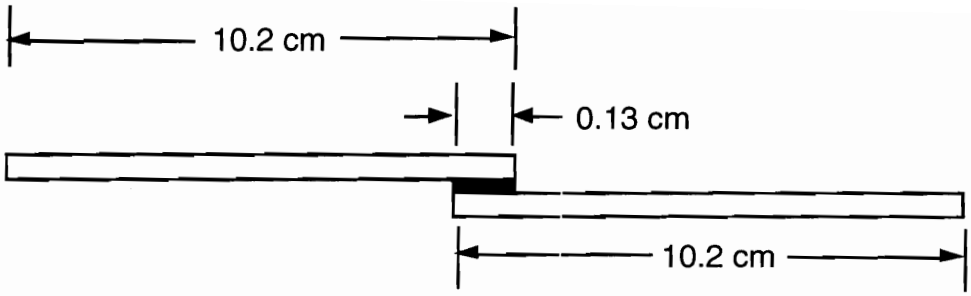

Figure 3.6: Schematic diagram of a single lap shear bond configuration.

3.7 Infrared Reflection Absorption Spectroscopy (IR-RAS)/X-ray Photoelectron Spectroscopy (XPS) Study of Model Composite Surfaces

3.7.1 Materials

To prepare model composite surfaces, thin films were spin-cast from commercially available composite matrix resins. To simulate a high performance epoxy composite, Araldite® MY 720 epoxy resin/HT 976 curing agent system from Ciba Geigy (Hawthorne, New York) was utilized. The structures of MY 720 (N,N,N'N'-tetraglycidyl-4,4'-methylene-bisbenzeneamine, also known as tetraglycidylmethylenedianiline) and HT 976 (4,4'-diaminodiphenylsulfone) are shown in Figure 3.7. This particular epoxy and curing agent combination was one of the earliest high performance epoxy matrix resins developed, possessing good long-term high temperature performance as well as high mechanical strength and chemical resistance [19].

A bismaleimide composite surface was represented by Matrimid® 5292, also from Ciba Geigy. Matrimid® 5292, a two component BMI resin system, is a commonly used starting formulation for many commercial BMI composites and adhesives, with the ability to retain superior mechanical properties at elevated temperature and elevated humidity [20] Matrimid® 5292 part A is a 4,4'-bismaleimidophenylmethane resin and Matrimid® 5292 part B is o,o'-diallyl bisphenol A; chemical structures are shown in Figure 3.8.

3.7.2 Thin Film Preparation

Commercial Ferrotype plates were used as substrates for the thin composite films and were obtained from Apollo Metals (Bethlehem, PA). These plates consist of a 0.5 mm steel base plated with nickel and approximately 80 nm of chromium oxide on the outermost surface. The high reflectivity and high refractive index of the chromium oxide are ideal for reflection absorption infrared spectroscopy.

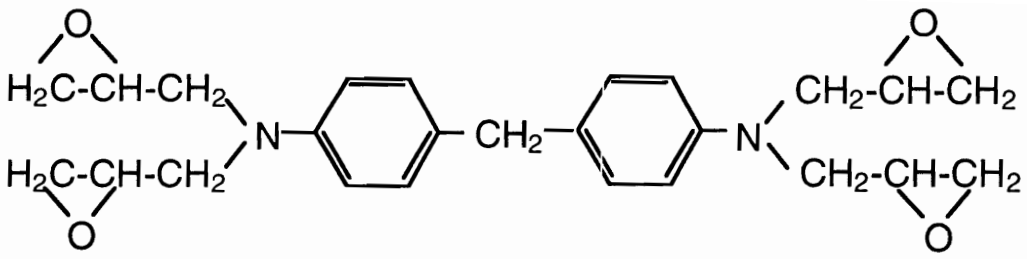

(a)

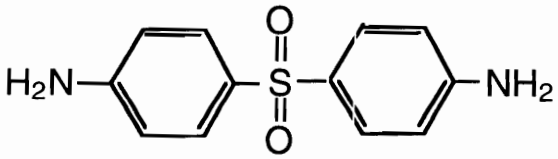

(b)

Figure 3.7: Chemical structures of (a) Araldite® MY 720, N,N,N'N'-tetraglycidyl-4,4'-methylenebisbenzeneamine, and (b) HT976, 4,4'-diaminodiphenylsulfone.

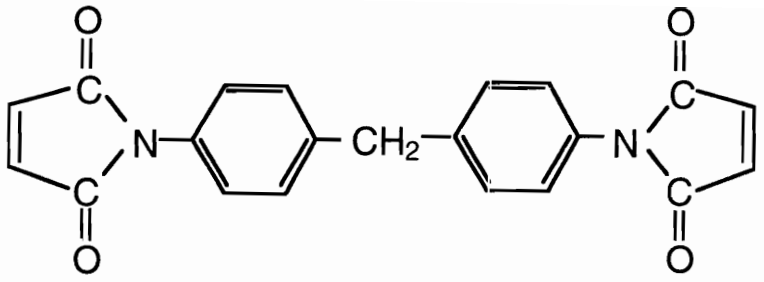

(a)

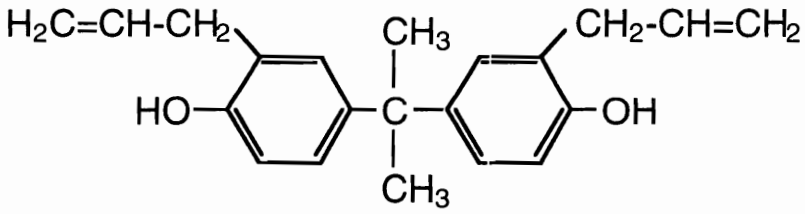

(b)

Figure 3.8: Chemical structures of (a) Matrimid® 5292 Part A, 4,4'-bismaleimido-phenylmethane resin, and (b) Matrimid® 5292 Part B, o,o'-diallyl bisphenol A.

Prior to spin-coating, 3.8 cm x 3.8 cm (1.5 in. x 1.5 in.) Ferrotype plates were cleaned in a 50 watt oxygen plasma for 15 minutes, scrubbed vigorously with deionized water and a Kimwipe® tissue, rinsed in deionized water and dried under a stream of dry nitrogen. This process was then repeated twice. Using a Gaertner L116A dual mode automatic ellipsometer with a 1 mW helium-neon laser light source fixed at an incident angle of 70°, the average refractive index and absorption coefficient of the cleaned chromium substrates were measured to be 3.7 and -4.0, respectively.

To generate dilute solutions of MY 720/HT 976, the manufacturer-recommended mixing ratios for the two components were followed. 100 parts by weight (pbw) of MY 720 were combined with 44 pbw of HT 976 and mixed thoroughly by hand. This mixture was then diluted to a concentration of 1.3% w/w in a solvent mixture consisting of a 2 pbw acetone to 1 pbw methyl ethyl ketone (MEK). Spin-coating was carried out on a custom-built lab spin-coater. Coatings were cured by heating in a forced-air Blue M oven, using a cure cycle consisting of a 30 minute heat-up from room temperature to 200°C and a 90 minute hold at 200°C. When the curing was complete, samples were allowed to cool to room temperature before removal from the oven. Ellipsometric measurements of the film thickness ranged from 40-45 nm.

Matrimid® 5292 solutions were produced by combining 100 pbw of Part A and 85 pbw Part B thoroughly by hand and diluting with 2-methoxyethyl ether (diglyme) to a concentration of 6.8% w/w. Coatings were cured by heating in a forced-air Blue M oven, using a cure cycle consisting of a 30 minute heat-up from room temperature to 200°C and a 60 minute hold at 200°C, followed by a 20 minute heat-up from 200°C-250°C and a 60 minute hold at 250°C. When the curing was complete, samples were allowed to cool to room temperature before removal from the oven. Ellipsometric measurements of the film thickness ranged from 25-27 nm.

Thick films of MY 720, HT 976 and Matrimid® 5292 parts A and B were also spin-cast on Ferrotype plate from acetone solutions in order to obtain structural information about the individual components. Samples were heated in a 100°C oven for 2 hours in order to drive off residual acetone.

3.7.3 XPS Analysis of Plasma-treated Films

6.4 mm (1/4 in.) diameter discs were punched from the coated Ferrotype samples and exposed to a 50 watt oxygen plasma for 30 seconds, taking care to avoid excessive ablation of the thin films. XPS analysis of both the non-exposed and plasma-treated films was carried out according to the procedure described in Section 3.3.1.

3.7.4 IR-RAS Analysis of Plasma-treated Films

Infrared reflection absorption analysis was used to examine the molecular changes in the plasma-treated model composite resins. Although not generally considered to be a surface sensitive analytical technique, IR-RAS is highly suitable for the analysis of thin films on high refractive index substrates [21,22,23]. The strategy which is used involves making the films thin enough so that the surface and near-surface regions constitute a significant percentage of the entire coating thickness. In this way, signals which arise from the near surface layers can be observed in the spectrum of the coating and are not obliterated by the signals originating in the bulk.

Plasma treatment of 3.8 cm x 3.8 cm (1.5 in. x 1.5 in.) spin-coated Ferrotype plates was performed according to the procedure in Section 3.7.3. IR-RAS experiments were performed on a Nicolet 510 Fourier transform infrared spectrometer equipped with a triglycine sulfate (TGS) detector. Reflectance measurements were taken with a Seagull® variable angle reflection accessory from Harrick Scientific Corporation, set at an incidence angle of 75°. A diagram of the Seagull® attachment is shown in Figure 3.9. A zinc

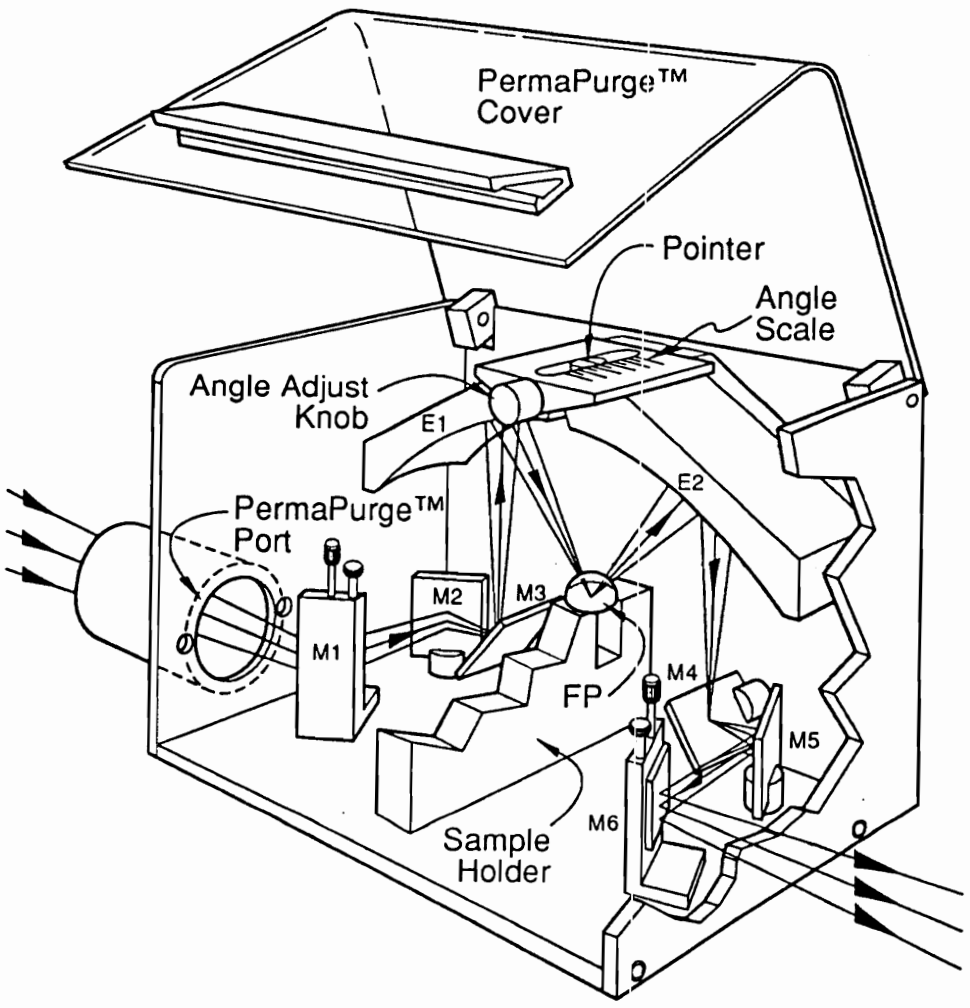

Figure 3.9: Schematic diagram of Harrick Seagull® Variable Angle Reflection Accessory. M's represent flat mirrors, E's represent ellipsoidal mirrors.

selenide polarizer from Spectra-Tech was placed in the optical path of the IR beam to produce parallel (p)-polarized radiation. The spectrometer bench was purged with dry nitrogen for 30-45 minutes between samples. 800 scans were collected and averaged at a resolution of 4 cm^{-1}. A clean, bare Ferrotype plate served as a background. Difference spectra were obtained by subtracting the spectra of non-treated surfaces from the spectra of the plasma-treated surfaces, utilizing Nicolet software for interactive subtraction.

3.7.5 IR-RAS Epoxy Adsorption Studies

Immediately following treatment with a 30 second/50 watt oxygen plasma, polymer-coated Ferrotype plates were immersed in a bath of neat EPON® 830 (no additional crosslinker added). The polymer-coated plates were then heated in the EPON® 830 bath at 180°C for one hour in a convection oven. Following this thermal treatment, excess EPON® 830 was drained from the sample surfaces and the samples then subjected to repeated rinses with methylene chloride solvent in a shaker jar. Six 1 minute rinses were performed, utilizing fresh methylene chloride for each rinse. Following the methylene chloride rinses, sample surfaces were rinsed in a stream of acetone from a wash bottle for approximately 30 seconds, then dried under a stream of nitrogen. Non-plasma-treated samples were also taken through this procedure and served as controls.

IR-RAS analysis was carried out as described above in Section 3.7.4 on the non-treated and plasma-treated surfaces and the plasma-treated surfaces exposed to EPON® 830. Neat EPON® 830 was also analyzed by IR-RAS in order to identify those peaks which were unique to it and which would not be observed in the spectra of MY 720/DDS or Matrimid® 5292.

3.8 References

1. H.G. Recker, V. Alstadt and M. Stangle, *Proceedings of the 37th International SAMPE Symposium*, 493 (1992).
2. BASF Structural Materials Production Information, "Metlbond® 1146."
3. W.M. Riggs and M.J. Parker in *Methods of Surface Analysis*, A.W. Czanderna, ed., p. 103 (Elsevier Scientific Publishing Company, New York, 1975).
4. R. Holm and S. Storp, *Surf. Interface Anal.*, 2(**3**), 96 (1980).
5. D. Briggs in *Practical Surface Analysis by Auger and X-ray Photoelectron Spectroscopy*, D. Briggs and M.P. Seah, eds., p. 359 (John Wiley and Sons, New York, 1983).
6. H. Niehus and R. Spitzl, *Surf. Interface Anal.*, **17**, 287 (1991).
7. Shell EPON® Resins Technical Information
8. R.N. Wenzel, *Ind. Eng. Chem.*, **28(8)**, 988 (1936).
9. A. Carre and J. Schultz, *J. Adhesion*, **15**, 151 (1983).
10. W.A. Zisman, *Ind. Eng. Chem.*, **55**(1), 18 (1963).
11. *Handbook of Chemistry and Physics*, 71st edition, p. 6-102 (CRC Press, Boca Raton, 1991).
12. P.J. Dynes and D.H. Kaelble, *J. Adhesion*, **6**, 195 (1974).
13. D.K. Owens and R.C. Wendt, *J. Appl. Polym. Sci.*, **13**, 1741 (1969).
14. J. Schultz, K. Tsutsumi and J.-B. Donnet, *J. Colloid Interface Sci.*, **59**(2), 273 (1977).
15. M.T. McKenzie, S.R. Culler and J.L. Koenig in *Fourier Transform Infrared Characterization of Polymers*, H. Ishida, ed., p. 377 (Plenum Press, New York, 1987).
16. P.R. Young, B.A. Stein and A.C. Chang, *Proceedings of the 28th National SAMPE Symposium*, 824 (1983).
17. K.C. Cole, A. Pilon, D. Noel, J.J. Hechler, A. Chouliotis and K.C. Overbury, *Appl. Spectrosc.*, **42**(5), 761 (1988).
18. M.G. Somekh in *Handbook of Adhesion*, D.E. Packham, ed., p. 10 (Longman Group UK Ltd. Essex, 1992).
19. Ciba Geigy Araldite® MY 720 Data Sheet.
20. Ciba Geigy Matrimid® 5292 Data Sheet.

21. D.S. Dunn and D.J. McClure, *J. Vac. Sci. Technol.*, **A5(4)**, 1327 (1987).
22. H. Ishida, *Rubber Chem. Technol.*, **60(3)**, 497 (1987).
23. A. Garton, *Infrared Spectroscopy of Polymer Blends, Composites and Surfaces*, p. 87 (Oxford University Press, New York, 1992).

Chapter IV: Results and Discussion

Surface Characterization and Bonding of Toughened Epoxy Composites

The results of surface pretreatment and adhesive bonding of a rubber-toughened, carbon fiber-reinforced epoxy composite are reported in this section. Surface analytical techniques were employed to determine the changes in surface chemistry and topography which resulted from surface pretreatment. The chemical and topographical features of the composite surfaces were in turn correlated to the strengths of bonds made with these materials, as well as to bond durability in various environments.

4.1 Surface Characterization

4.1.1 X-ray Photoelectron Spectroscopy (XPS)

In the study of adhesion, the chemistry of the surface(s) involved is critical in determining the initial level of adhesion and bond durability which can be obtained for a particular system. Surface pretreatment techniques can alter the surface chemistry significantly, particularly in the case of polymeric materials. The chemical composition of the pretreated epoxy composite surfaces was readily obtained by XPS analysis, and is summarized in Table 4.1.

It was observed that the as-received surface, which received only an MEK wipe, contained a significant quantity of fluorine on the surface. This fluorine is attributed to fluoropolymer transfer from the fluorinated-ethylene propylene (FEP) release films used during the composite fabrication process. The presence of residual release materials on fiber-reinforced composite surfaces has also been documented by other workers [1,2]. Moyer and Wightman [3] and Messick et al. [2] have demonstrated that cleaning with sulfuric acid-based chemical agents, hydrazine or ethanolic KOH is not capable of removing fluorine from LaRC-160 laminates. Other work in our lab [unpublished] also

Table 4.1: XPS atomic concentrations of surface pretreated epoxy composites.

	ATOMIC CONCENTRATION (%)						
	C	**O**	**N**	**F**	**S**	**Si**	**Na**
As Received	67.5	14.2	2.2	13.7	0.7	1.4	0.3
Peel Ply	77.3	14.6	7.5	---	0.6	---	---
Grit Blast	73.3	19.0	2.7	---	1.4	3.1	0.5
20 min. Oxygen Plasma	37.2	43.5	5.5	---	5.5	7.0	1.3
20 min. Nitrogen Plasma	54.3	32.8	4.2	0.7	3.7	1.8	2.5
20 min. Ammonia Plasma	71.8	14.2	8.4	0.3	1.6	2.0	1.7

showed that common solvents such as methanol, acetone, methylene chloride and carbon tetrachloride were also not effective in removing fluoropolymer contamination found on LaRC-160 composites.

Carbon and oxygen are expected to be found in an epoxy material; nitrogen and sulfur originate from the curing agent(s) used. The binding energy of the sulfur peaks fell between 167.8 and 168.0 eV, which corresponds to the binding energy for sulfone (O=S=O), which has been documented to be between 167.6-167.8 eV [4,5]. This result suggests the presence of diaminodiphenylsulfone (DDS) in the matrix resin. DDS is a well-known latent curing agent for high performance epoxy formulations [6]. Nitrogen is also contained in the curing agent as well as in the rubber toughener used in the epoxy laminate. Trace amounts of silicon show up in the XPS analysis with binding energies of 102.7-103.6 eV and are thus attributed to silicates or SiO_2. Sodium, another commonly found surface contaminant, is also present in minute quantities.

Laminates which were fabricated with a peel ply layer contained no fluorine, silicon or sodium contaminants on the surface following peel ply removal. Prevention of surface contamination is one of the reasons given for the use of a peel ply layer [7]; thus, this objective appears to be accomplished. The concentration of nitrogen is higher than for the as-received or grit blasted surfaces - this could be due to a different level of curing agent or rubber toughener in the peel ply resin, or it could originate from the peel ply fabric itself. The absence of silicon in the XPS analysis of the composite surface after peel ply removal or the peel ply material itself, and the absence of silicon in energy dispersive x-ray analysis (EDAX) indicates that the peel ply fabric is not glass cloth. Nylon, a nitrogen-containing material, is another commonly used material in peel ply fabric [8].

Grit blasted surfaces were also free from fluorine contamination, since removal of the topmost resin layers from the composite also removed the fluoropolymer residues. A small quantity of silicon found on the surface is attributed to silica grit which was not

removed from the surface. The increase in oxygen concentration is also attributed to the oxygen in SiO_2. Trace amounts of sodium are again observed.

Much more significant changes in surface chemistry are observed in the composite surface following treatment with radio frequency (RF)-generated plasmas. Table 4.1 shows data for 20 minute plasma treatments in oxygen, nitrogen and ammonia. It can be seen that the fluorine contamination is fully removed by oxygen plasma treatment. In fact, it will be shown in a later section that only a 5 minute oxygen plasma treatment is needed to remove all traces of fluoropolymer. In contrast, plasma treatment in nitrogen or ammonia still leave behind trace amounts of fluorine, even after twenty minutes of exposure. For this reason, nitrogen and ammonia plasmas were not pursued further in this study.

Oxygen concentration in the composite surface increases from 14-15% to almost 44% following exposure to oxygen plasma. Nitrogen and sulfur concentrations are also seen to increase. A new nitrogen 1s peak at 401.8 eV is observed in addition to the original peak at 399.8 eV. A 1 eV shift to higher binding energy is also observed for the sulfur peak, which could be indicative of the formation of more oxidized forms of sulfur, such as sulfate [9].

The increase in silicon and sodium could be attributed to surface enrichment, since these elements are not volatile and would not be eroded away in the plasma. Alternatively, silicon deposition on the sample surfaces could result from the action of the high energy oxygen plasma on the walls of the quartz plasma chamber. Sodium, on the other hand, has often been found on carbon fiber tows used to manufacture fiber-reinforced composites.

A study involving the simultaneous oxygen plasma treatment of a variety of polymeric materials is summarized in Table 4.2. The highlighted silicon and sodium values reveal a number of interesting points. It can be seen that while the silicon atomic concentrations fall into a relatively narrow range (between 1 and 5%), the sodium

Table 4.2: XPS atomic concentrations of oxygen plasma-treated polymers.

	ATOMIC CONCENTRATION (%)					
	C	**O**	**N**	**S**	**Si**	**Na**
High Density Polyethylene	72	25	---	---	3	<1
Kapton® Polyimide	59	33	6	---	1	<1
PMR-15 Composite	36	46	5	1	5	7
5276 Epoxy Composite	40	40	9	7	3	<1
5250-4 BMI Composite	53	36	3	---	3	5

concentration varies by as much as an order of magnitude. These findings, along with the fact that sodium is not a component of the quartz plasma chamber, leads to the conclusion that the silicon is deposited on the sample surfaces by the action of the oxygen plasma on the reactor walls. On the other hand, the sodium is most likely present in the bulk of the composite.

An increase in oxygen concentration is also observed for the nitrogen plasma-treated surface, in addition to a small increase in nitrogen. Moyer and Wightman also reported the same results for the nitrogen plasma-treatment of LaRC-160 [3]. Use of an ammonia plasma also results in an increase in nitrogen concentration. The increase in the concentration of nitrogen-containing functional groups in the surface could lead to improved bonding with epoxy-based resins, since the surface itself could behave as a curing agent and form interfacial covalent bonds with the adhesive resin. A study by Webster and Wightman demonstrated that oxygen and ammonia plasma-treated poly(phenylene sulfide) had the capability of curing a one nanometer thick film of EPON® 828 at the surface [10].

An additional level of information which can be obtained from an XPS experiment involves resolving the C1s peak into component peaks, thus yielding information on molecular bonding at the surface. Figure 4.1 shows the curve-fitted C1s photopeaks for the as-received, peel ply, grit blasted and oxygen plasma-treated surfaces.

All the surfaces exhibit a C-C peak at 284.6 eV from the aliphatic and aromatic carbons in the resin. A peak at 286.0-286.2 eV, corresponding to carbon singly bonded to oxygen (C-O) as well as carbon singly bonded to nitrogen (C-N), is also found for all the surface pretreatments. C-O and C-N species are expected to be present in an amine-cured epoxy. Hydroxyl groups which result from the epoxy ring-opening reaction would give rise to a C-O peak; also, this same ring-opening reaction would result in a C-N linkage if the attacking species were an amine.

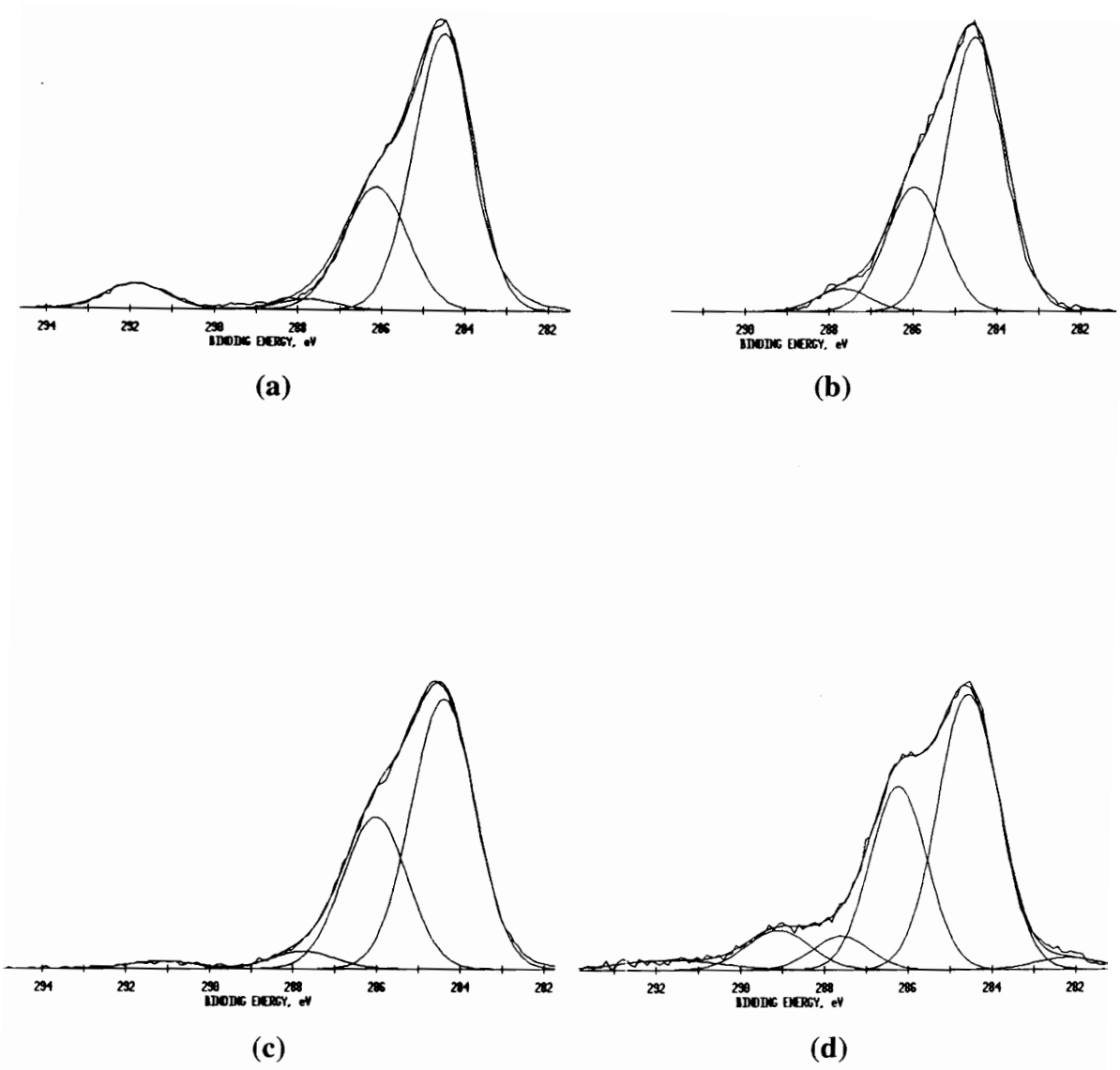

Figure 4.1: Curve-fitted carbon 1s photopeaks from surface pretreated epoxy composites. (a) As received (b) Peel ply (c) Grit blast (d) 5 minute oxygen plasma.

A peak at 287.7 eV, corresponding to a carbonyl (C=O) species, is also found in varying concentrations in all the surfaces. It is the most intense in the peel ply and oxygen plasma-treated surfaces. Shake-up satellites are observed for the grit blasted and oxygen plasma-treated surfaces. These broad, shallow peaks are the result of π - π^* transitions which occur in aromatic materials.

The as-received surface shown in Figure 4.1(a) contains C-C, C-O/C-N and C=O groups as discussed above. However, it also exhibits a C-F linkage at 291.9 eV which is attributed to the fluoropolymer release film residue. The highly electronegative fluorine atom is known to cause a shift in the C1s peak to higher binding energies [11]. No C-F peak is observed for any of the other surfaces, indicating that they are free from fluoropolymer contamination.

The most significant change in photopeak shape is seen with the oxygen plasma-treated surface, shown in Figure 4.1(d). As stated earlier, a 5 minute exposure to oxygen plasma is sufficient to remove all fluorine residues, as shown by the disappearance of the C-F peak originally at 291.9 eV. A new peak to the right of the main C-C peak at 282.5 eV is not present in the C1s photopeak for any other surface. Low binding energy peaks such as this can sometimes be attributed to graphitic carbon species [11]. It is possible that carbon fibers in the surface of the composite have become exposed as a result of the plasma treatment. There is an increase in the concentration of C-O species, as evidenced by the increase in intensity of the peak at 286.0 eV. Although this peak can be assigned to both C-O and C-N species on the basis of binding energy, the much greater increase in oxygen concentration versus the increase in nitrogen concentration indicates that the increase in peak intensity is predominantly caused by additional C-O functionality. A new species found at 289.2 eV is determined to be either carboxylate (O=C-OH) or ester (O=C-OR) species.

An interesting observation was made concerning the nitrogen 1s photopeaks in the epoxy surface as a function of oxygen plasma treatment time at 50 watts. Figure 4.2(a) shows that the original, as-received surface exhibits a single N1s photopeak at 399.8 eV. As seen in Figure 4.2(b), after 1 minute of oxygen plasma treatment, two peaks are seen, with an additional peak at 401.8 eV along with the original peak at 399.8 eV. In Chapter 8 of this dissertation, work with model epoxy formulations confirms that the original nitrogen peak at 399.8 eV can be assigned to the nitrogen in the DDS curing agent. The new peak at 401.8 eV which appears after plasma treatment is a reaction product of plasma exposure, most likely an oxidized amine or a tertiary amine salt.

A study was carried out to determine the length of oxygen plasma exposure time necessary to remove the fluoropolymer contamination and establish a steady-state concentration of oxygen in the surface of the composite. Results of these experiments are shown in Table 4.3. After a 1 minute plasma treatment at 50 watts of power, only traces of fluorine are left. After 5 minutes of treatment, fluorine is completely removed. At the same time, the surface concentration of oxygen is increasing. After only 1 minute of treatment, the oxygen concentration has already increased from approximately 14% to greater than 37%. By 5 minutes, the oxygen concentration has leveled out to approximately 42-43%. Thus, it is seen that no more than 5 minutes of oxygen plasma exposure at 50 watts are necessary to remove surface contamination and build up a steady-state oxygen concentration, demonstrating the speed of the plasma treatment process.

Table 4.4 shows the results of varying oxygen plasma power from 10 to 150 watts, holding exposure time constant at 1 minute. These results show that a 1 minute treatment at 10 or 50 watts is not sufficient to completely remove the fluoropolymer contamination. However, at 100 watts and above, a 1 minute exposure time removes all traces of the fluoropolymer. The oxygen concentration reaches a plateau at 50 watts. This again shows

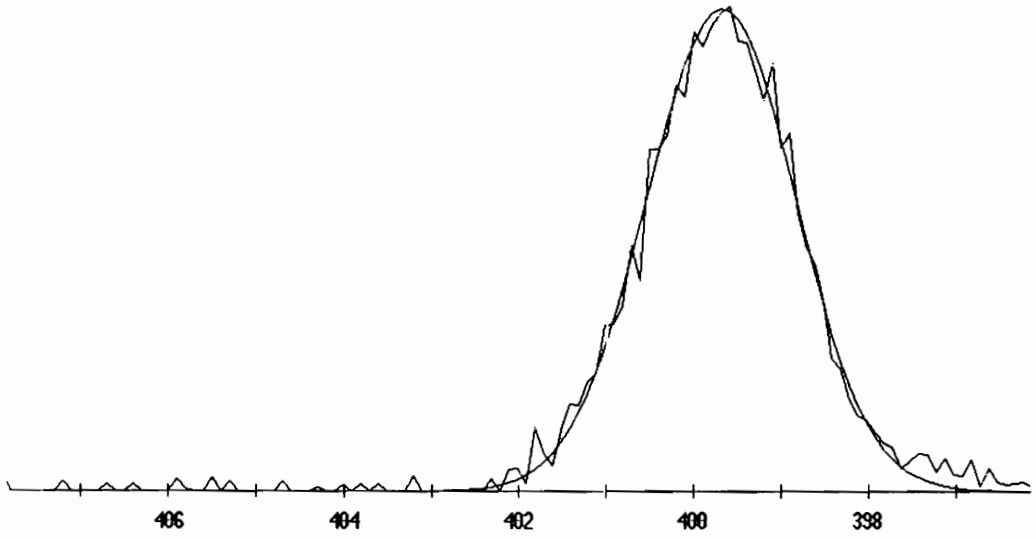

(a)

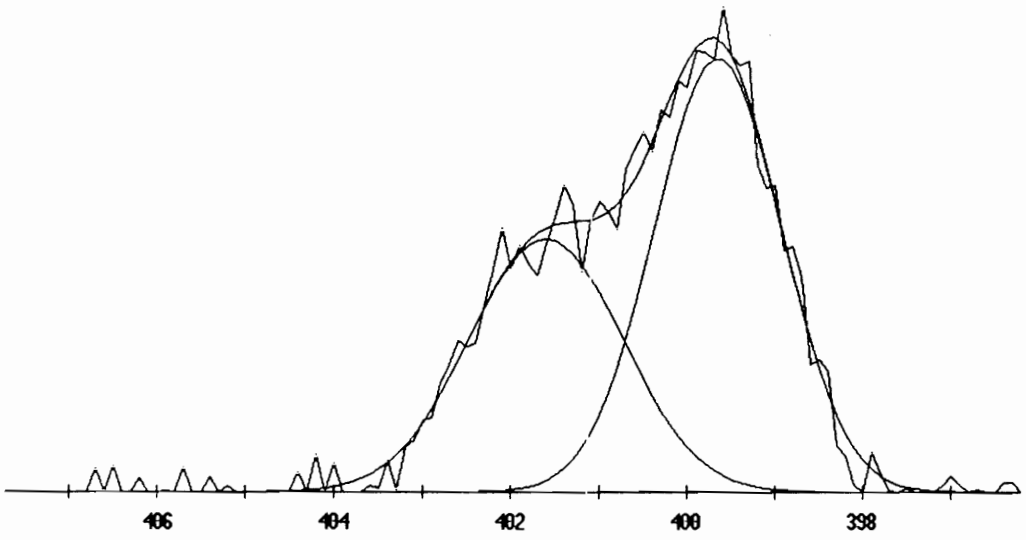

(b)

Figure 4.2: Nitrogen 1s photopeaks from epoxy composites. (a) As received (b) 5 minute oxygen plasma treatment.

Table 4.3: Effect of oxygen plasma treatment time on epoxy surface composition, with plasma power held constant at 50 watts.

	ATOMIC CONCENTRATION (%)						
Time (min.)	**C**	**O**	**N**	**F**	**S**	**Si**	**Na**
1	50.7	37.4	4.4	0.9	3.4	2.1	1.1
5	37.9	43.1	6.9	---	6.4	4.8	0.9
10	40.1	42.1	5.2	---	4.9	6.9	0.8
20	37.2	43.5	5.5	---	5.5	7.0	1.3

Table 4.4: Effect of oxygen plasma power on epoxy surface composition, with plasma treatment time held constant at 1 minute.

	ATOMIC CONCENTRATION (%)						
Power (watts)	**C**	**O**	**N**	**F**	**S**	**Si**	**Na**
10	55.2	32.3	4.1	3.3	2.1	2.2	0.8
50	43.3	40.0	6.8	0.6	5.8	3.2	0.3
100	46.9	39.8	5.2	---	4.8	2.8	0.5
150	46.2	39.9	5.3	---	5.1	2.7	0.8

the rapidity of the plasma process in removing contamination and altering the surface chemistry.

Data from both the treatment time and treatment power studies can be normalized in terms of plasma *energy*. This is calculated by multiplying treatment time in seconds and treatment power in watts to obtain energy in joules. Figure 4.3(a) shows the concentrations of matrix resin elements - carbon, oxygen, nitrogen and sulfur - as a function of plasma energy. Oxygen concentration rises as the plasma energy increases, eventually reaching a plateau value at approximately 6000 J. The carbon concentration decreases correspondingly, while sulfur and nitrogen remain relatively unchanged. Figure 4.3(b) shows the surface contamination of fluorine, silicon and sodium with increasing plasma energy. Fluorine concentration decreases with increasing plasma energy and becomes zero at 6000 J. While the sodium concentration remains constant, the silicon level increases steadily with increasing energy input. This is additional evidence for the deposition of silicon from the plasma chamber itself and also for the presence of sodium within the composite.

4.1.2 Ion Scattering Spectroscopy (ISS)

ISS, which is sensitive to the topmost molecular layer in a surface, is one of the most surface-sensitive techniques available for the analysis of polymer surfaces. It is utilized in this study to provide a comparison to the results obtained by XPS. ISS is not as quantitative as XPS, due to a general lack of knowledge of sensitivity factors for the different elements. Therefore, only qualitative results regarding the presence or absence of various species will be reported. Also, because the analyzer configuration in the instrument utilized for this work used is not optimal for ISS, detection of the lower atomic number elements such as carbon is often poor. ISS spectra of the pretreated epoxy composites are shown in Figure 4.4, showing peak intensity versus the scattered ion energy ratio, E/E_o.

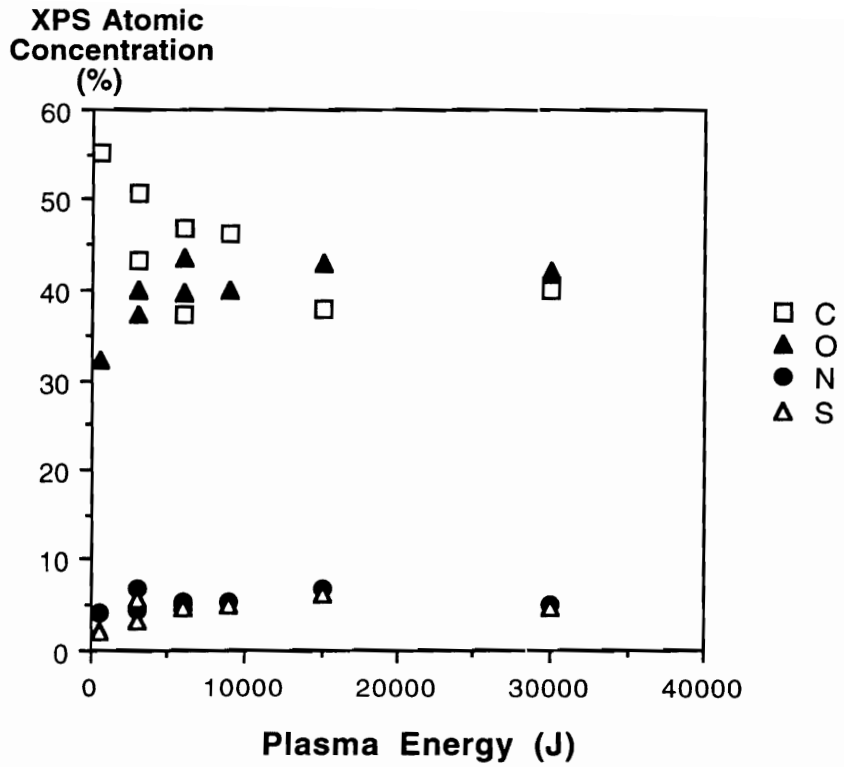

Figure 4.3a: XPS atomic concentrations of epoxy matrix resin elements as a function of total plasma energy.

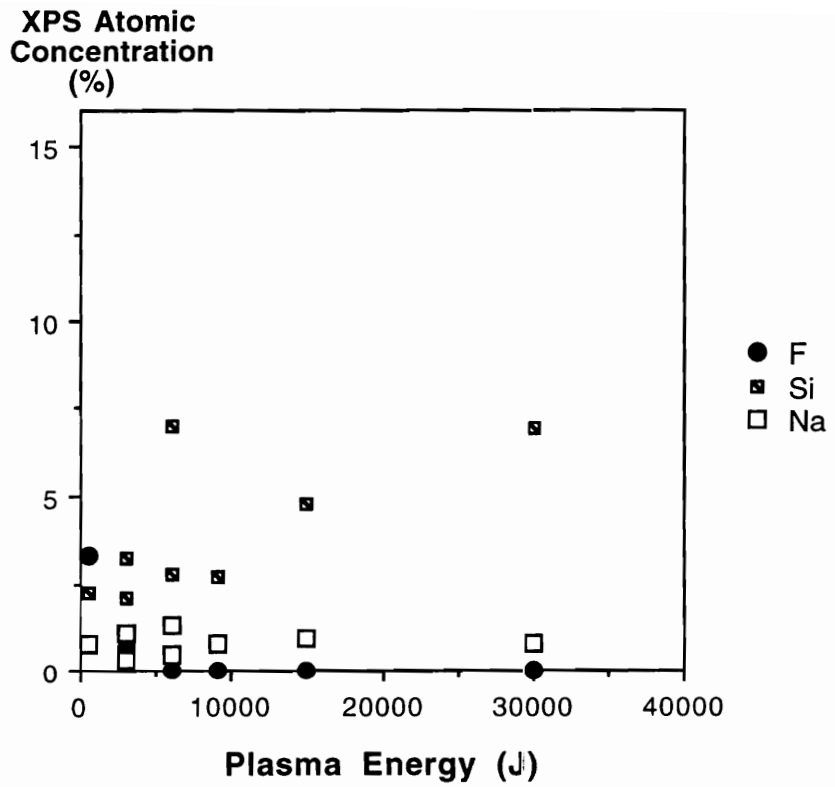

Figure 4.3b: XPS atomic concentrations of epoxy composite surface contaminants as a function of total plasma energy.

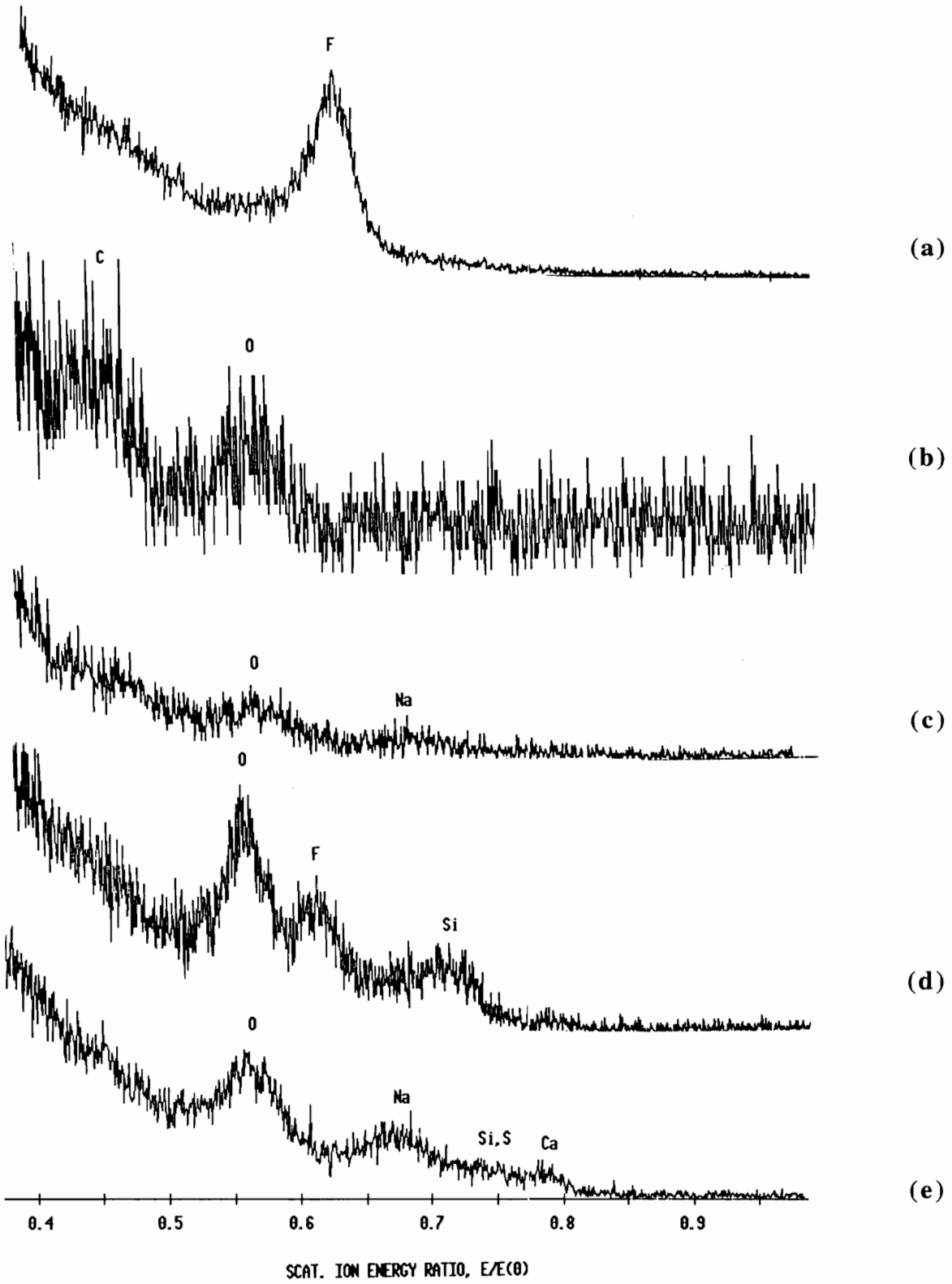

Figure 4.4: ISS spectra of surface pretreated epoxy composites. (a) As received (b) Peel ply (c) Grit blast (d) 1 minute oxygen plasma (e) 5 minute oxygen plasma.

In the spectrum of the as-received surface shown in Figure 4.4(a), the topmost molecular layer of the composite is seen to be primarily composed of fluorine. Carbon, which would be expected to be observed in a fluoropolymer, is not visible for the reasons stated above. Analysis of the original FEP film against which the composites were molded showed an identical spectrum, also containing a single fluorine peak and no carbon. These results complement the XPS results by showing that the as-received composite surface is completely covered by a layer of fluoropolymer. Any adhesive or coating material which would be applied to the composite surface would be in direct contact with this low energy material.

The composite surface after peel ply removal shown in Figure 4.4(b) shows a weak peak for carbon and a stronger one for oxygen. No fluorine or other contaminants are detected in this surface. The grit blasted surface shown in Figure 4.4(c) also shows no fluorine but does show peaks in the oxygen and sodium regions.

Following a 1 minute oxygen plasma treatment at 50 watts of power, both oxygen and fluorine peaks are observed in the ISS spectrum in Figure 4.4(d). XPS results also showed the presence of small amounts of fluorine after a 1 minute/50 watt oxygen plasma treatment. Silicon is also detected at this level of treatment. Following 5 minutes of oxygen plasma treatment, all traces of fluorine are removed, as also observed by XPS, and the oxygen peak is predominant, as seen in Figure 4.4(e). The extreme surface sensitivity of this technique allows the conclusion to be made that fluorine is completely removed even from the topmost surface regions of the composite by a 5 minute/50 watt oxygen plasma treatment. Traces of sodium, silicon, and sulfur are observed in this surface, as was also detected by XPS analysis. Calcium, which was not observed by XPS, is observed in the ISS spectrum.

4.1.3 Contact Angle Analysis

The use of contact angle measurements to determine surface energies is well-known and used by many researchers in the field of adhesion and surface analysis. A myriad of approaches have been developed to obtain the elusive surface energy of a solid material [12,13,14,15,16]. Unfortunately, there is often little or no agreement between the approaches or the results obtained thereof. As stated by Schonhorn et al., there is no universally accepted, direct, non-ambiguous method of measuring polymer surface energies [17]. It is the objective of these experiments to obtain surface energy values for the pretreated composites so that internal comparisons can be made, and differences in wettability and adhesion behavior can be rationalized.

4.1.3.1 Roughness Correction

Prior to calculating the surface free energies of the composite surfaces, it was necessary to determine the effect of the surface roughness on the contact angle. Surface roughness is known to affect the value of the measured contact angle [18]. If the contact angle is less than 90° on a smooth surface, as is the case in this work, roughening the surface will decrease the contact angle. By calculating a roughness correction factor R_C, it becomes possible to factor out the effect of surface roughness by correcting all subsequently measured contact angles by the appropriate R_C. The roughness factors which are obtained can also be correlated to the surface area of the substrate relative to the plane geometric area of the substrate [18]. Thus, the larger the R_C value, the more "finely divided" the surface is.

The roughness factors for the various surface pretreatments were measured relative to a polished chrome steel plate, which has an R_a measured by profilometry of 0.02 μm and an R_z of 0.1 μm. The roughness factor R_C for this reference substrate was taken to be 1.0. Table 4.5 shows the roughness factors for the various surface pretreatments. These

Table 4.5: Roughness correction factors (R_C) for surface pretreated epoxy composites.

	Ethylene Glycol Contact Angle (deg.)	R_C
As Received	43.4 ± 3.4	1.22 ± 0.14
Peel Ply	37.8 ± 3.3	1.32 ± 0.12
Grit Blast	31.8 ± 1.9	1.42 ± 0.06
5 min. Oxygen Plasma	34.8 ± 1.5	1.37 ± 0.05

Referenced to: Gold-coated photographic plate, contact angle = 53.2 ± 3.6

results show that all of the composite surfaces are rougher than the smooth Ferrotype plate, which is an expected result. The grit blasted surface is the roughest of all, having a surface area 42% greater than the smooth Ferrotype plate. The peel ply surface also possess a good deal of surface area. The oxygen plasma-treated surface has a higher roughness than the as-received surface; this could be due to etching of the surface by the plasma at a level which could not be observed by SEM analysis.

4.1.3.2 Surface Energy Analysis

Zisman's approach for determining the critical surface tension and Kaelble's method for determining the polar and dispersive components of the surface free energy, were both utilized in this study. Table 4.6 provides surface tension data for the wetting liquids used in both analyses [19]. These liquids were used in the contact angle analysis of the as-received, grit blasted and peel ply surfaces.

The oxygen plasma-treated surfaces could not be analyzed with this particular series of liquids because of their extremely high wettability. Instead, the critical surface tension of the oxygen plasma-treated surface was determined by using a series of concentrated NaOH solutions in a Zisman-type analysis, the surface tensions of which are listed in Table 4.7 [20]. It was confirmed by SEM that the concentrated NaOH solutions did not degrade the surface during the time of analysis; in addition, the contact angle of these solutions on the surface did not change even after 30 minutes of contact.

The water-in-alkane technique developed by Schultz et al. and described in the Experimental Section was used to obtain the polar and dispersive components of the surface free energy for the oxygen plasma-treated surface. Table 4.8 shows the values of γ_H and γ_{HW} for the 6 alkanes used in the study; values of 72.8, 51.2 and 21.6 mJ/m^2 were utilized for γ_W, γ_W^P and γ_W^D, respectively [21,22]. These values can be inserted into the

Table 4.6: Surface tension data for wetting liquids used in Zisman and Kaelble analyses [19].

Liquid	γ_{LV}	$\gamma_{LV}^{(d)}$	$\gamma_{LV}^{(p)}$
	(mJ/m^2)	(mJ/m^2)	(mJ/m^2)
water	72.8	21.8	51.0
formamide	58.3	32.3	26.0
glycerol	64.0	34.0	30.0
methylene iodide	50.8	48.5	2.3
ethylene glycol	48.3	29.3	19.0
1-bromo-naphthalene	44.6	44.6	0
hexadecane	27.6	27.6	0
ethanol (absolute)	22.4	17.0	5.4
hexane	18.4	18.4	0

Table 4.7: NaOH solution surface tensions [20].

Wt. % NaOH	γ_{LV} (mJ/m^2)
2.72	74.35
5.66	75.85
16.66	83.05
30.56	96.05
35.90	101.05

Table 4.8: Alkane surface and interfacial tension data for water-in-alkane contact angle experiments [21].

ALKANE	γ_H	γ_{HW}
	(mJ/m^2)	(mJ/m^2)
Hexane	18.4	51.3
Octane	21.3	51.2
Nonane	22.9	51.2
Decane	23.4	51.2
Dodecane	25.0	51.3
Hexadecane	27.1	51.5

equations defined in Section 3.3.3.2 to yield straight line plots whose slopes and intercepts provide γ_S^D and γ_S^P, respectively.

Table 4.9 summarizes the surface energies determined by the Zisman, Kaelble and Schultz techniques. The total surface energy, γ_S, is calculated from the sum of the dispersive component γ_S^D and the polar or nondispersive component, γ_S^P.

The surface energy and critical surface tension for the as-received epoxy are approximately equal to literature values for the surface energies of fluorinated polymers, which are usually in the range of 19-21.6 mJ/m^2 [23]. This is consistent with the presence of fluorine detected on the surface of the as-received laminates by both x-ray photoelectron spectroscopy and ion scattering spectroscopy. As discussed previously, this fluorine originates from the fluorinated-ethylene propylene (FEP) release films against which the laminates were consolidated.

The surface energy determined for the epoxy peel ply surface falls close to those obtained for cured epoxy surfaces. Critical surface tensions of 33-46.2 mJ/m^2 have been documented [24,25]. Surface tensions of liquid DGEBA epoxy resins, which are generally considered to be fairly close to the surface energies of their cured counterparts, have been observed to fall between 40.6 and approximately 52 mJ/m^2 [26,27,28]. The surface energies obtained for the grit blasted surfaces are close to those of graphite or carbon surfaces; Dynes and Kaelble reported γ_S values for various graphitic and carbon materials ranging from 37-58 mJ/m^2 [19].

Both γ_C and γ_S obtained for the oxygen plasma-treated surface are significantly higher than that which has been reported for even polar polymers such as poly(amides) or poly(esters). However, it is reasonable to expect that the increase in surface polarity and oxygen concentration plays a large role in increasing the total surface energy. Kinloch et al. have reported that the polar component of the surface energy increases significantly following a corona treatment [29].

Table 4.9: Summary of epoxy composite surface energies (in mJ/m^2).

	$\gamma_s^{(d)}$	$\gamma_s^{(p)}$	γ_s [1]	γ_c [2]
As Received	20.4	4.1	24.5	22.9
Peel Ply	23.9	8.8	32.7	42.8
Grit Blast	29.2	8.8	38.0	50.9
Oxygen Plasma	37.8	33.7	71.5 [3]	88.3 [4]

[1] Obtained via Kaelble's approach, $\gamma_s = \gamma_s^{(d)} + \gamma_s^{(p)}$

[2] Obtained using a Zisman series of non-homologous liquids

[3] Obtained using the 2-liquid method of Carre and Schultz

[4] Obtained utilizing high surface tension NaOH solutions in a Zisman-type analysis

As evident in the data of Table 4.9, discrepancies are observed between the values of γ_C and γ_S obtained for the pretreated composite surfaces. Other researchers have also reported differences between the two values for a given polymer surface [30]; however, it was felt that the differences observed here were too large to be considered insignificant.

Although surface roughness corrections had been made prior to the calculation of surface energy quantities, it was postulated that the roughnesses involved in the peel ply and grit blasted surfaces were too extreme to be corrected for completely, particularly in the case of the channel-like peel ply surface in which a very *regular* pattern of roughness exists. The original derivation by Wenzel to correct for surface profiles in wetting was most likely not intended to apply to this type of surface. Hazlett, in a review of surface roughness and wetting behavior, takes exception to Wenzel's derivation, due to a lack of *texture* specification in defining the roughness ratio [31]. In addition, work performed by Yekta-Fard and Ponter [32], and by Oliver et al.[33] on grooved surfaces, indicates that asymmetric spreading occurs along grooves or channels in a surface (such as are found in the peel ply surface). The contact angle value would then depend on the position at which the measurement is taken.

It was observed experimentally that the discrepancies between the two values characterizing the surface energy seemed to increase in magnitude as the surface roughness of the laminate increased. Figure 4.5 shows a plot of $|\gamma_S - \gamma_C|$, the absolute difference between γ_S and γ_C, plotted against the roughness correction factors R_C listed in Table 4.5. A roughly linear relationship is observed between the magnitude of surface roughness and the difference between the two surface energy values. This supports the speculation that for surfaces with exaggerated roughness patterns, application of commonly used techniques to determine surface energy values may lead to considerable errors.

Good correlation is observed between the surface energy and the total atomic concentration of the polar matrix elements oxygen, nitrogen and sulfur on the composite

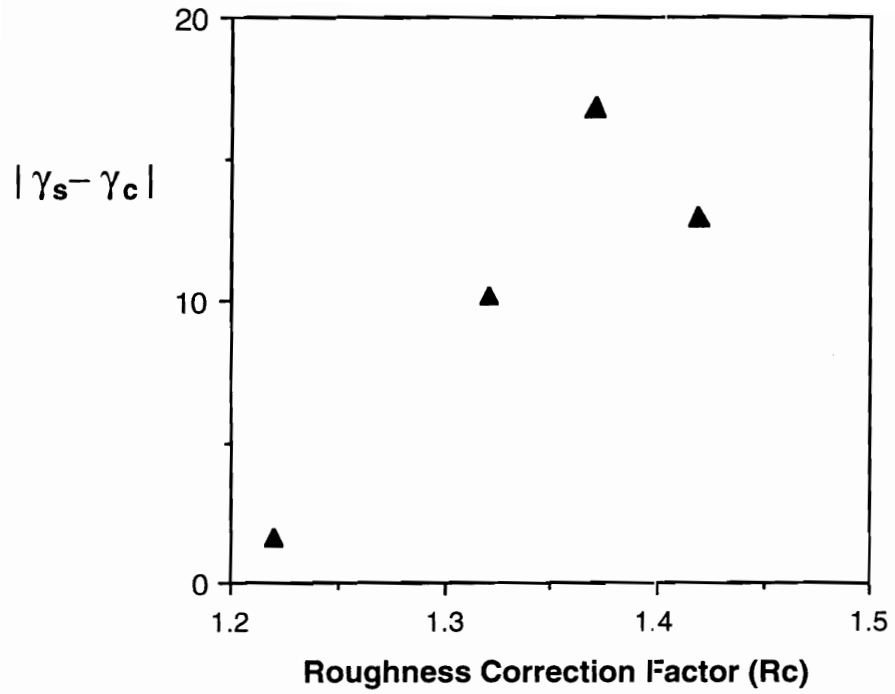

Figure 4.5: Absolute difference between epoxy γ_s and γ_c as a function of surface roughness correction factor, R_C.

surface. Figure 4.6 shows that the total surface energy increases in a linear manner with increasing concentration of oxygen, nitrogen and sulfur. Thus, it appears that higher concentrations of polar elements on the composite surface lead to increased surface energies.

4.1.3.3 Wettability Measurements

The wettability of an adherend surface is of utmost importance in the fabrication of a strong, durable bond. In order for intimate molecular contact to be established at the interface, the adhesive must completely spread over the surface, displacing air and contaminants [34]. This condition is met only when the contact angle of the substance of interest is low or close to zero.

Figure 4.7 shows the values of water contact angles on the pretreated composite surfaces. The as-received surface has a high contact angle due to the presence of the low energy fluoropolymer layer, which is not wetted by water. The contact angles on the peel ply and grit blasted surfaces are shown to be slightly lower, but this is in part due to a surface roughness effect. The absence of fluorine on the peel ply and grit blasted surfaces does not ensure a more hydrophilic surface. A 1 minute, 50 watt oxygen plasma treatment does lower the contact angle significantly, but the trace amounts of fluorine still present prevent the surface from being completely wettable. After 5 minutes of plasma treatment at 50 watts, the contact angle of water is seen to be essentially zero.

Because the actual liquid which will be contacting these pretreated composites is a molten epoxy adhesive, contact angles of EPON® 830 were measured on the composite surfaces. EPON® 830 has a viscosity which is close to the actual minimum viscosity of a BASF epoxy film adhesive during its cure cycle. In comparison to water, EPON® 830 has a higher viscosity and a lower surface tension. It was felt that this was a more realistic probe liquid to assess the wettability of the pretreated surfaces.

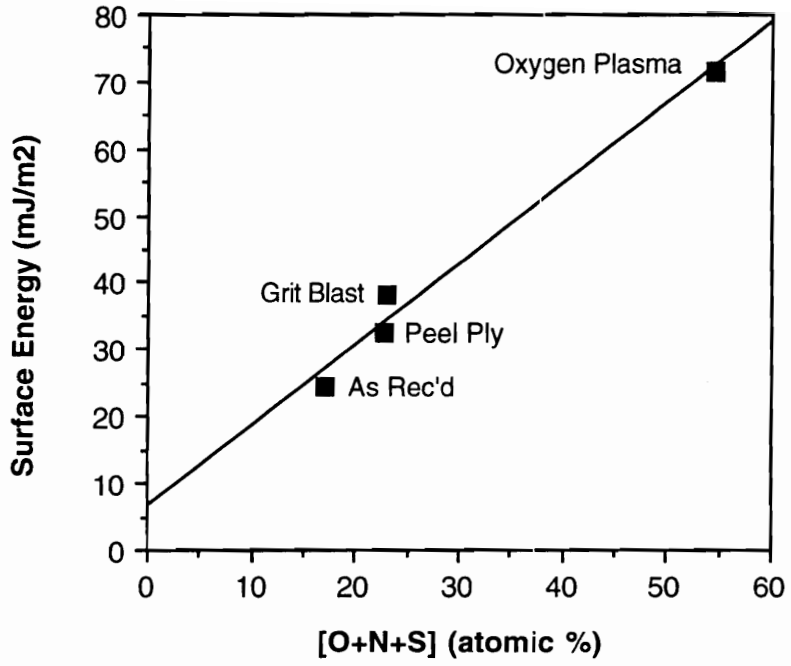

Figure 4.6: Total surface energy γ_s plotted against total XPS atomic concentrations of oxygen, nitrogen and sulfur.

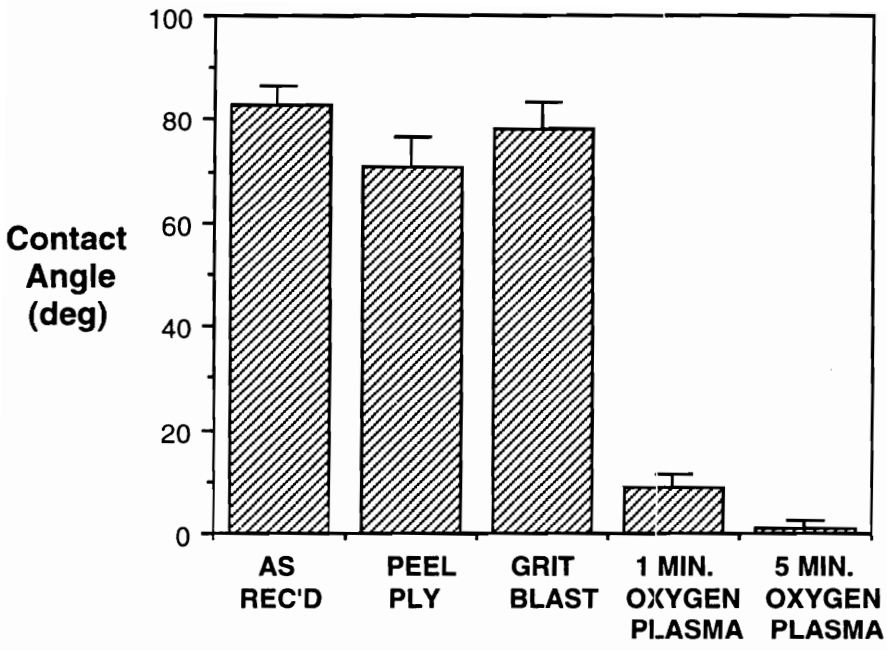

Figure 4.7: Water contact angles on surface pretreated epoxy composites.

It is known that the wetting of polymer surfaces by viscous fluids is different than by low molecular weight liquids. Using horizontal capillaries and slits as models for surface irregularities, Neuman [35] has shown that the average fluid velocity is directly proportional to the cosine of the contact angle and inversely related to the viscosity of the wetting fluid. Schonhorn et al. [36] also found that wetting of surfaces by molten polymers is assisted by capillary forces but retarded by viscous effects. In general, for a polymer melt, the initial contact angle is usually much larger than the equilibrium value [35].

Figure 4.8 shows the EPON® 830 contact angles on the pretreated surfaces as a function of time. The relatively high viscosity of EPON® 830 slows the kinetics of the wetting process and causes the equilibrium contact angle to be reached only after approximately 30-60 minutes. In contrast to the results of the water contact angle analysis, it is observed that while the wettability of EPON® 830 on the as-received, fluorine-contaminated surface is still poor, the wettability behavior of the peel ply, grit blasted and oxygen plasma-treated surfaces is improved. The final equilibrium contact angles as well as the rate of approach to equilibrium are approximately equal for these three pretreatments. The sharp distinction between the oxygen plasma-treated sample and the other two pretreatments as seen in the water contact angle case is not observed. This is due to the fact that all three pretreated surfaces have critical surface tensions higher than that of the liquid epoxy resin, thus ensuring that wetting will occur.

Figure 4.9 shows the final cured contact angles of Metlbond® 1146 on the pretreated epoxy composites. This experiment involves the measuring the contact angle of the actual adhesive resin on a surface, which is more realistic than using a low molecular weight liquid or model compound. As observed in the case of EPON® 830, the Metlbond® 1146 contact angle is high on the as-received surfaces, a consequence of the fluorine contamination. All three pretreatments decreased the contact angle of the cured

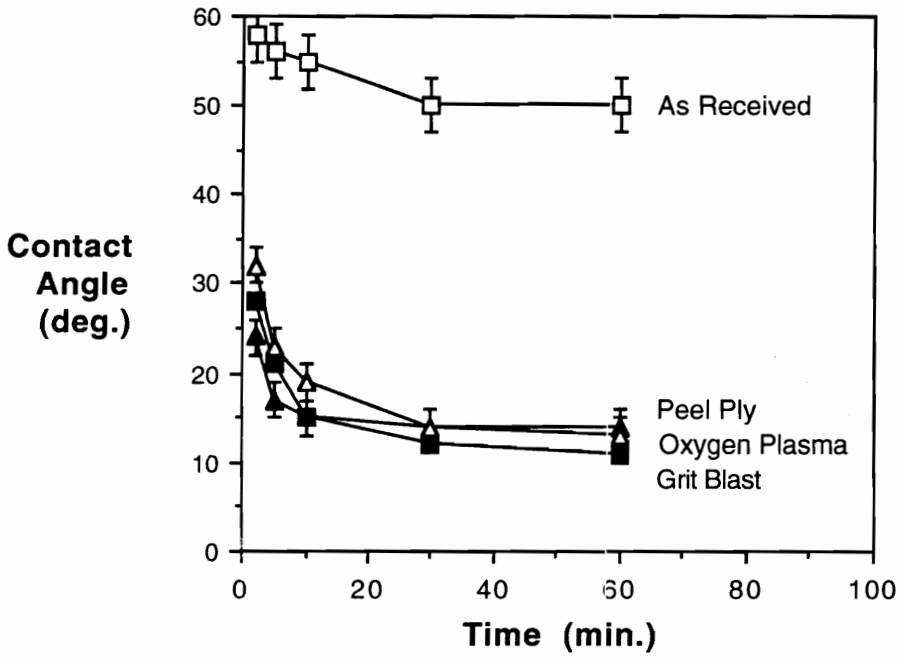

Figure 4.8: EPON® 830 contact angles on surface pretreated epoxy composites, measured as a function of time.

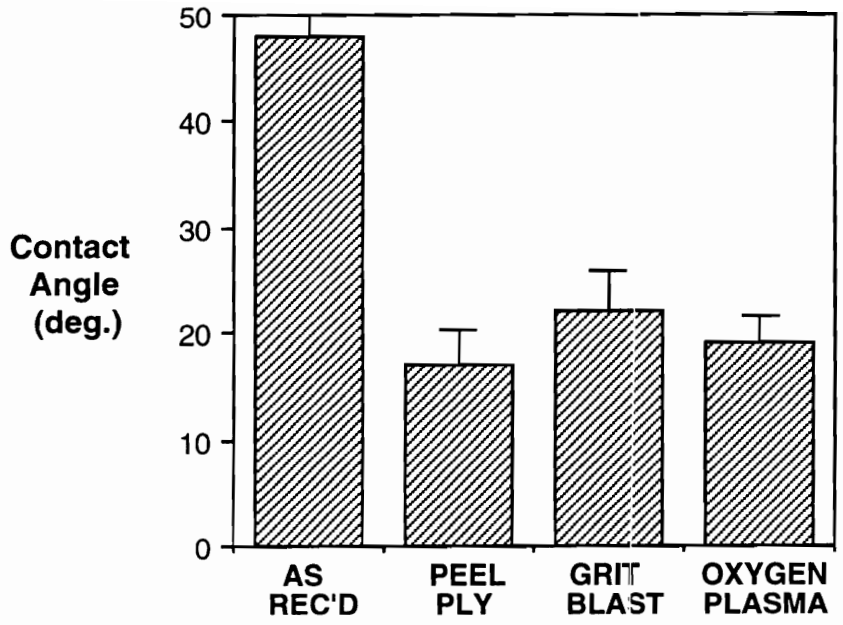

Figure 4.9: Contact angles of cured Metlbond® 1146 resin on pretreated epoxy composites.

epoxy, indicating that the molten epoxy wets the pretreated surfaces more easily, allowing more contact to be made between the adhesive and the surface.

It is interesting to take note of the similarity between the Metlbond® 1146 contact angles and the equilibrium contact angles of EPON® 830, in spite of the rheological differences between the two systems. Both analyses showed a high contact angle for the as-received surface and lower values for the grit blast, peel ply and oxygen plasma pretreatments. However, the final cured contact angles of Metlbond® 1146 were approximately 10-15° higher than the EPON® 830 equilibrium contact angles, most likely due to the fact that the gelation occurs in the Metlbond® 1146 system as cure progresses, unlike the EPON® 830 which maintains a constant low viscosity. Wetting and spreading would be slowed by an increase in the viscosity of the wetting medium, resulting in a higher contact angle.

4.1.4 Profilometry

Surface topography plays an important role in adhesion, due to the fact that the pits, pores or other types of depressions in a surface can provide additional surface for bonding and/or allow mechanical interlocking to take place between substrate and adhesive [37,38]. On the other hand, surface roughness which is too great may allow air to be trapped at the interface, creating stress concentrations in the interphase region of a bond [39]. It is also well-known that the topography of a substrate may also affect the kinetics of wetting; however, this effect may not be as significant when an adhesive is forcibly spread or pressed onto a surface, as is the case in this work [34].

Surface profiles of the pretreated composite surfaces are shown in Figure 4.10. It can be seen that the profiles of the as-received and oxygen plasma-treated surfaces, shown in Figures 4.10(a) and 4.10(d), respectively, have the same visual appearance, indicating that no macroscopic roughness is induced by the plasma treatment. However, the

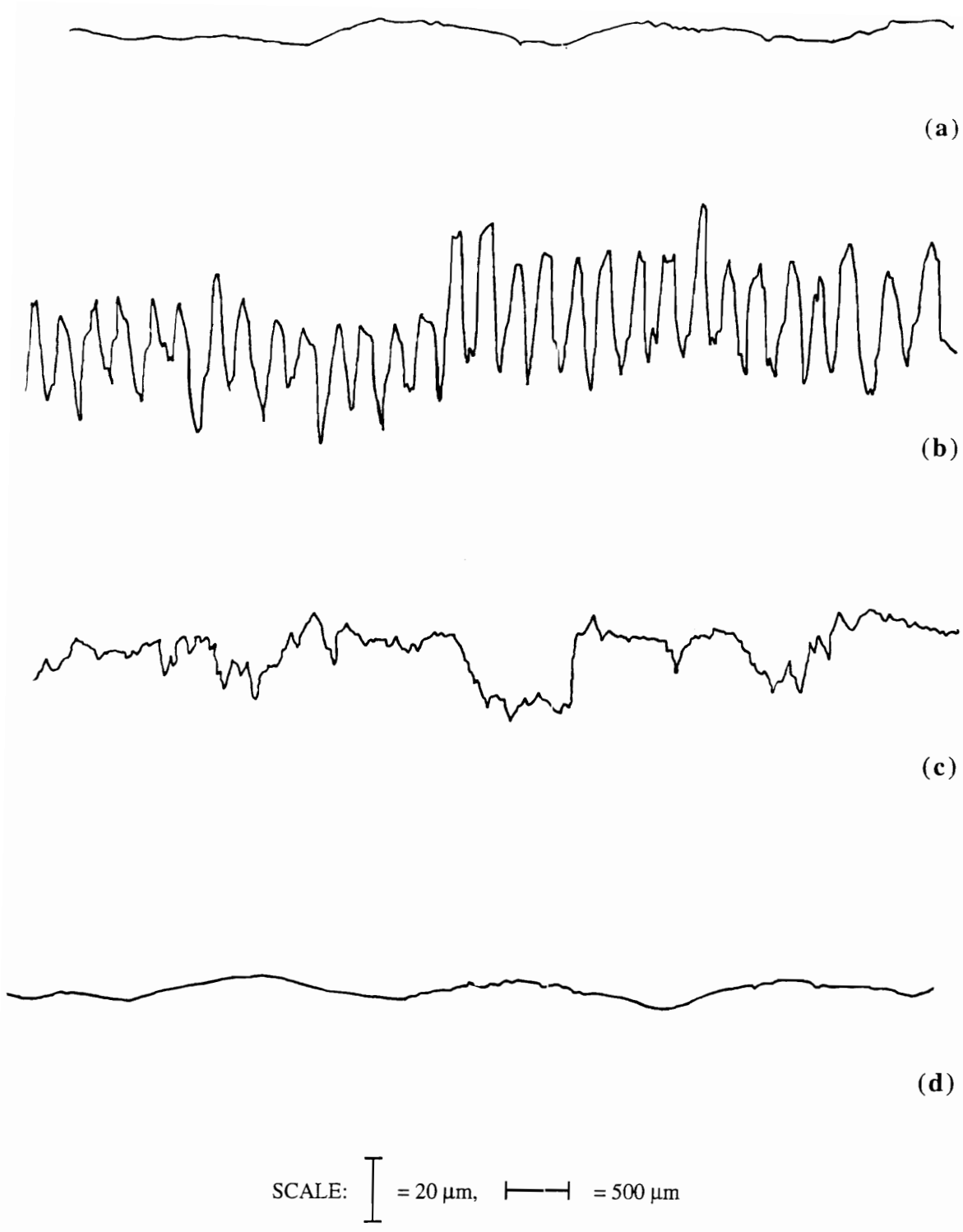

Figure 4.10: Surface profiles of pretreated epoxy composite surfaces. (a) As received (b) Peel ply (c) Grit blast (d) 5 minute oxygen plasma.

calculated surface roughness correction factors (from Section 4.1.3.1) show that there is a difference in surface area between the two surfaces. Because the size of the surface features which can be resolved is limited by the tip radius of the stylus, there may be additional surface textures which cannot be detected with this technique.

The peel ply surface shown in Figure 4.10(b) has a significant profile with a high degree of regularity, which is due to the imprint of the fibers from the peel ply fabric. The grit blasted surface, on the other hand, also shows significant roughness but the peaks and valleys appear in a more random pattern, as seen in Figure 4.10(c).

Surface roughness values (not to be confused with roughness correction factors) calculated from the profilometer traces are listed in Table 4.10. As can be visually ascertained from the traces, the as-received and oxygen plasma-treated surfaces have the lowest R_a and R_z values. The peel ply surface has the highest values of roughness, followed by the grit blasted surface.

4.1.5 Scanning Electron Microscopy (SEM)

The surface topography of the composites has thus far been studied by contact angle measurements and profilometry. SEM also provides an actual view of the surfaces before and after pretreatment. Figure 4.11 shows photomicrographs of as-received, peel ply, grit blasted and oxygen plasma-treated epoxy composite surfaces.

The as-received surface shown in Figure 4.11(a) is relatively smooth, with the exception of randomly-scattered craters and occasional underlying fibers. Due to the concern that the MEK solvent wipe was creating the craters, water, acetone, ethanol and hexane were also tested for their effect on the surface. The appearance of the water-washed surface is completely smooth, but shows contamination from particulate matter from cutting of the sample for analysis. The three other solvents removed the particulates but also produced craters similar to those observed with MEK. It is likely that the rubber toughener

Table 4.10: Epoxy composite surface roughnesses measured by profilometry.

	R_a (microns)	R_z (microns)
As Received	1.3 ± 0.1	6.3 ± 0.9
Peel Ply	11.5 ± 2.4	56.2 ± 8.0
Grit Blast	6.8 ± 2.2	35.3 ± 8.3
5 min. Oxygen Plasma	1.1 ± 0.1	6.8 ± 0.7

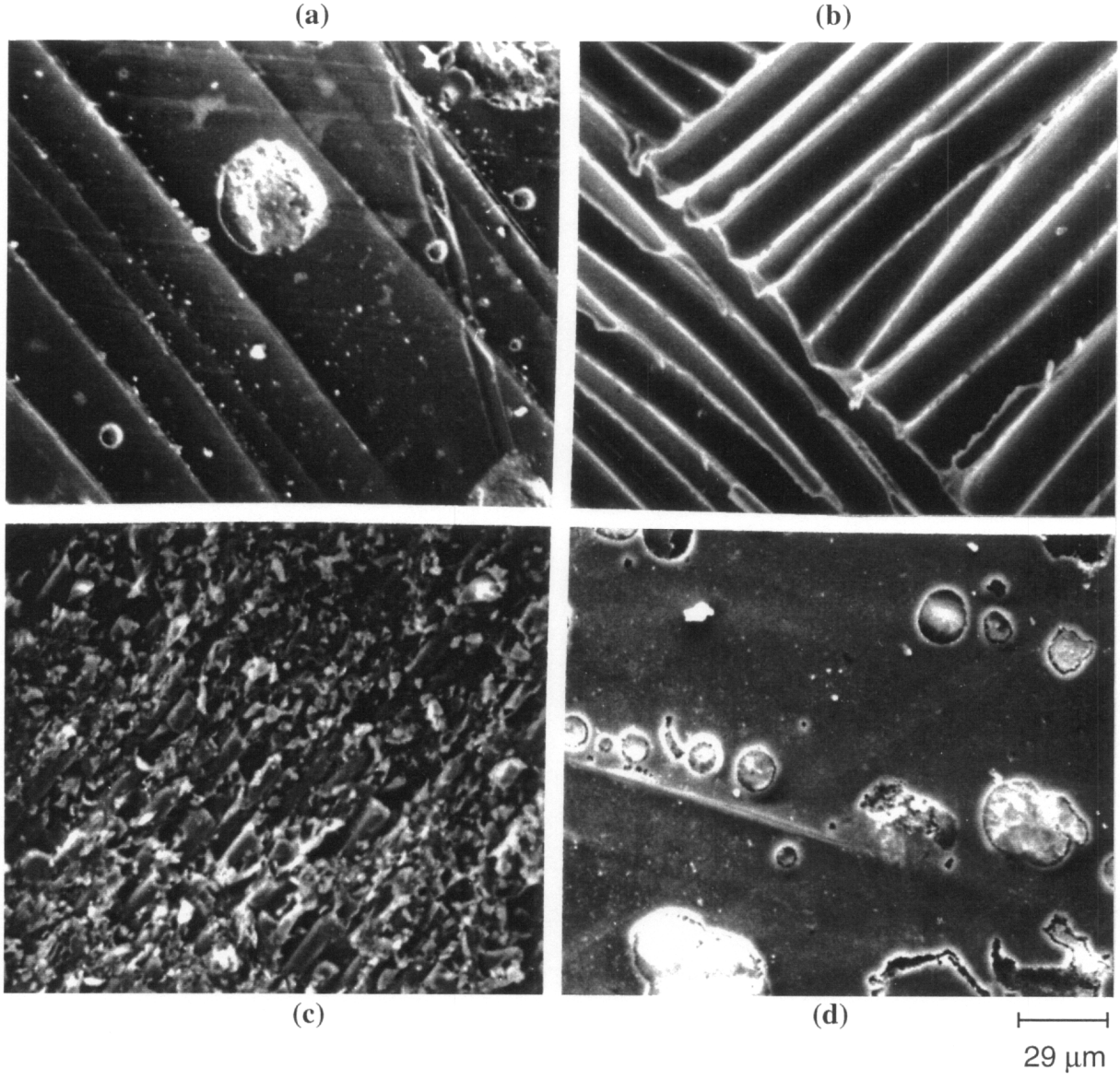

Figure 4.11: SEM photomicrographs of surface pretreated epoxy composites. (a) As received (b) Peel ply (c) Grit blast (d) 5 minute oxygen plasma.

phase is enriched on the composite surface and is not as chemically resistant as the remainder of the matrix, thus being more susceptible to solvent attack.

The composite surface after peel ply removal shown in Figure 4.11(b) clearly shows the imprint left by the peel ply fabric which appears as a pattern of grooves and channels. The peel ply appears to have been removed cleanly and there is no evidence of any resin being stripped from the surface. These grooves and channels may actually facilitate the wetting and spreading of a molten polymer or adhesive. Figure 4.12(b) shows the underside of polystyrene pellet which was pressed against the peel ply surface while above its glass transition temperature. The appearance of the polystyrene pellet is virtually identical to the peel ply fabric which created the original surface topography shown in Figure 4.12(a), indicating that the polystyrene had indeed filled the channels and grooves.

The grit blasted surface shown in Figure 4.11(c) shows a matte, rough appearance with bare and broken fibers plainly visible. Thus, fiber damage by grit blasting is a real possibility, one which may have some implications on the strength of a bonded joint.

The oxygen plasma-treated surface shown in Figure 4.11(d) exhibits a cratered appearance following a 5 minute exposure at 50 watts. Some of the craters appear to show material boiling over from within the composite. The surface of the composite during plasma treatment undergoes a considerable amount of heating. Once a crater is formed by the plasma, non-thermally stable materials - such as the rubber toughener, for instance - may become mobile enough to bubble through the fissures. The area around the craters has a nodular appearance.

The effect of oxygen plasma treatment time on the surface topography is detailed in Figure 4.13. A 1 minute, 50 watt exposure produced very shallow depressions in the surface (no solvent wipe was used in this case). After 5 minutes, the depressions become deeper craters, with some raised blistered areas as described above. At 10 minutes the

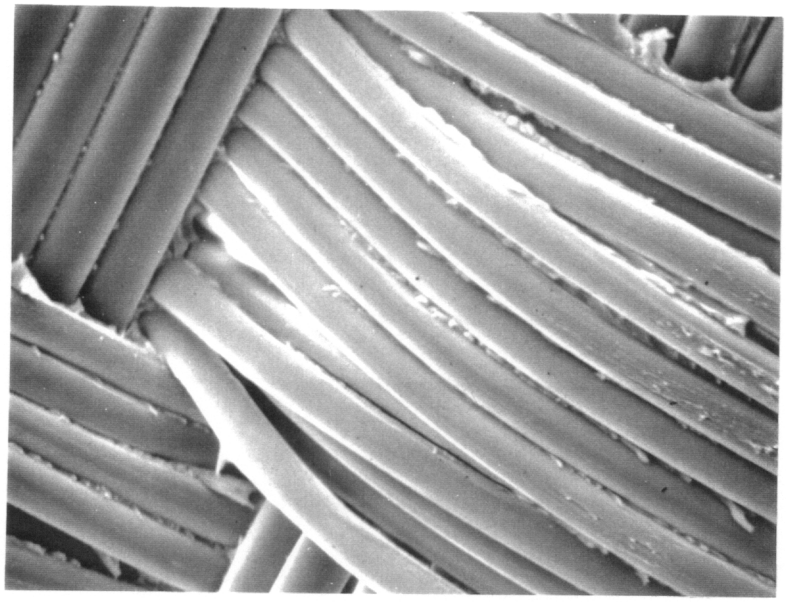

(a)

20 μm

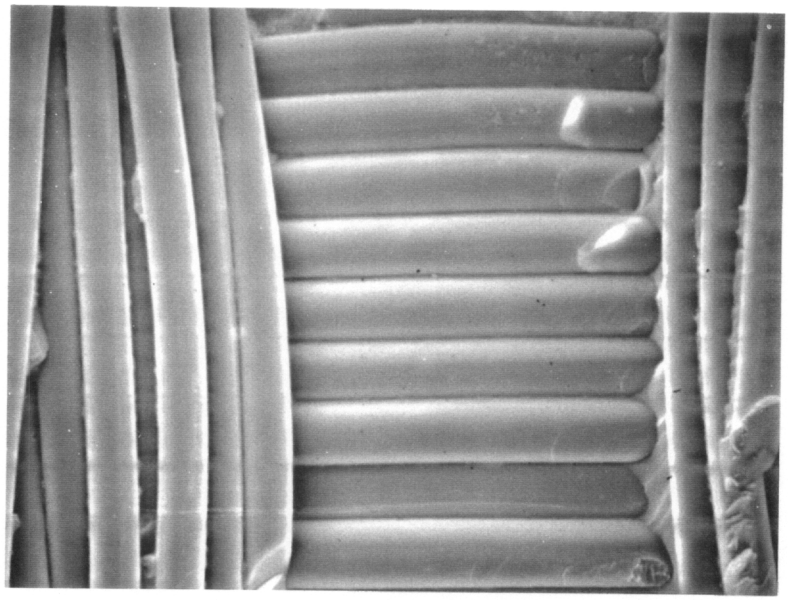

(b)

20 μm

Figure 4.12: SEM photomicrographs of (a) epoxy peel ply fabric, and (b) underside of polystyrene pellet which had melted while in contact with epoxy peel ply surface, illustrating polymer flow into channels and grooves.

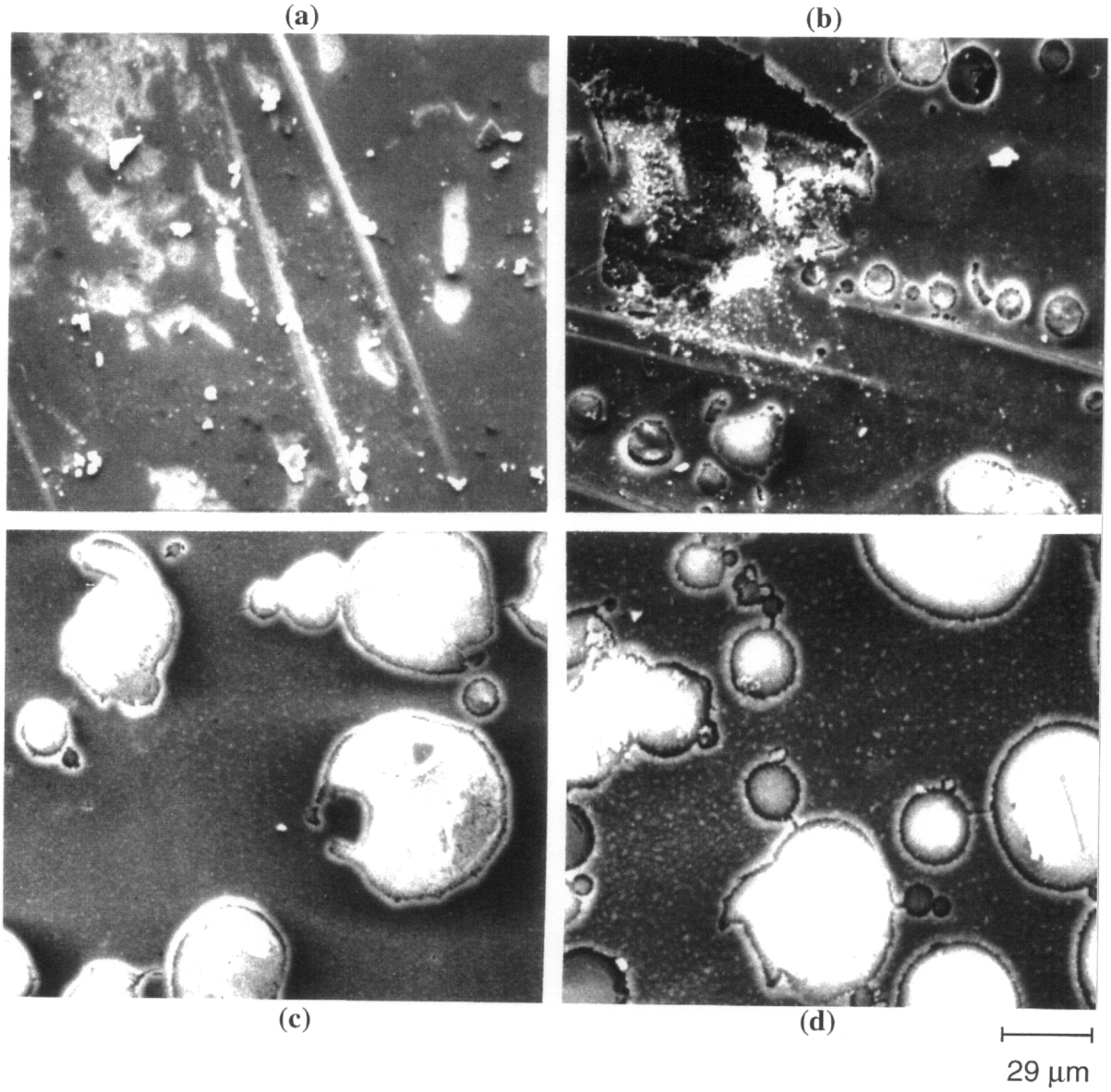

Figure 4.13: SEM photomicrographs of surface pretreated epoxy composites, showing effect of oxygen plasma treatment time. Plasma power was held constant at 50 watts. (a) 1 minute. (b) 5 minutes (c) 10 minutes (d) 20 minutes.

craters have all become raised blisters and a nodular appearance begins to appear in the area between the blisters. At 20 minutes, the raised blisters are still seen and the nodularity increases in prominence between the blistered areas. Again, it is believed that the combination of erosion and heat in a plasma chamber during prolonged exposures has caused some physical changes to occur in the matrix resin, primarily involving the rubber toughener phase.

The effect of varying plasma power at 1 minute treatment time is not as severe. Figure 4.14 shows that there is no change to the surface at 10 watts, 50, 100 and 150 watts. The same shallow abrasions were observed in the 1 minute/50 watt treatment, as noted in Figure 4.13(a).

4.1.6 Diffuse Reflectance Infrared Spectroscopy (DRIFT)

In recent years, DRIFT has become more widely used for the analysis of composite materials. Figure 4.15 shows the DRIFT spectrum of an as-received epoxy composite surface. A sharp, broad peak due to O-H stretching and/or N-H stretching is centered at 3590 cm^{-1}. C-H stretching bands, both aliphatic and aromatic, are prominent at 3070, 2945 and 2860 cm^{-1}. A small peak at 2230 cm^{-1} is assigned to a nitrile absorbance, providing evidence for a nitrile-rubber based toughening agent. Carbonyl stretching is observed at 1785 and 1730 cm^{-1}, the origins of which are unknown. Other significant peaks include an aromatic C=C vibration at 1516 cm^{-1}, C-N bending at 1251 cm^{-1}, and O-H deformation at 1300 and 1324 cm^{-1}.

It was intended to utilize DRIFT to provide molecular information on the pretreated surfaces, in order to complement the atomic information obtained XPS analysis . Although the DRIFT spectrum of the as-received composite surface was relatively straightforward to obtain, it was not successful in revealing changes in the surface composition induced by surface treatment. Carrying out the various surface pretreatments changed the optical

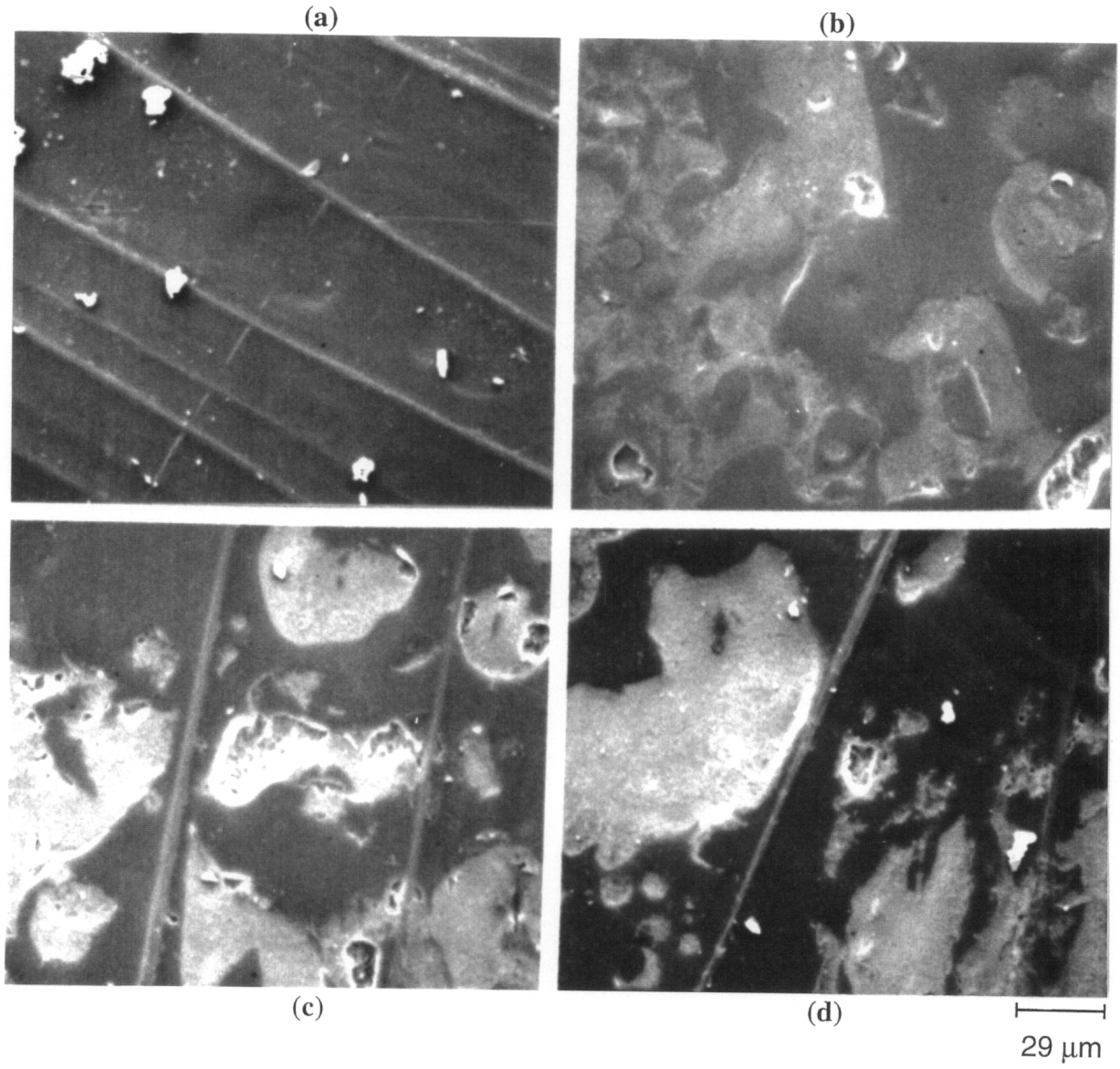

Figure 4.14: SEM photomicrographs showing effect of oxygen plasma power on epoxy composites, treatment time held constant at 1 minute. (a) 10 watts (b) 50 watts (c) 100 watts (d) 150 watts.

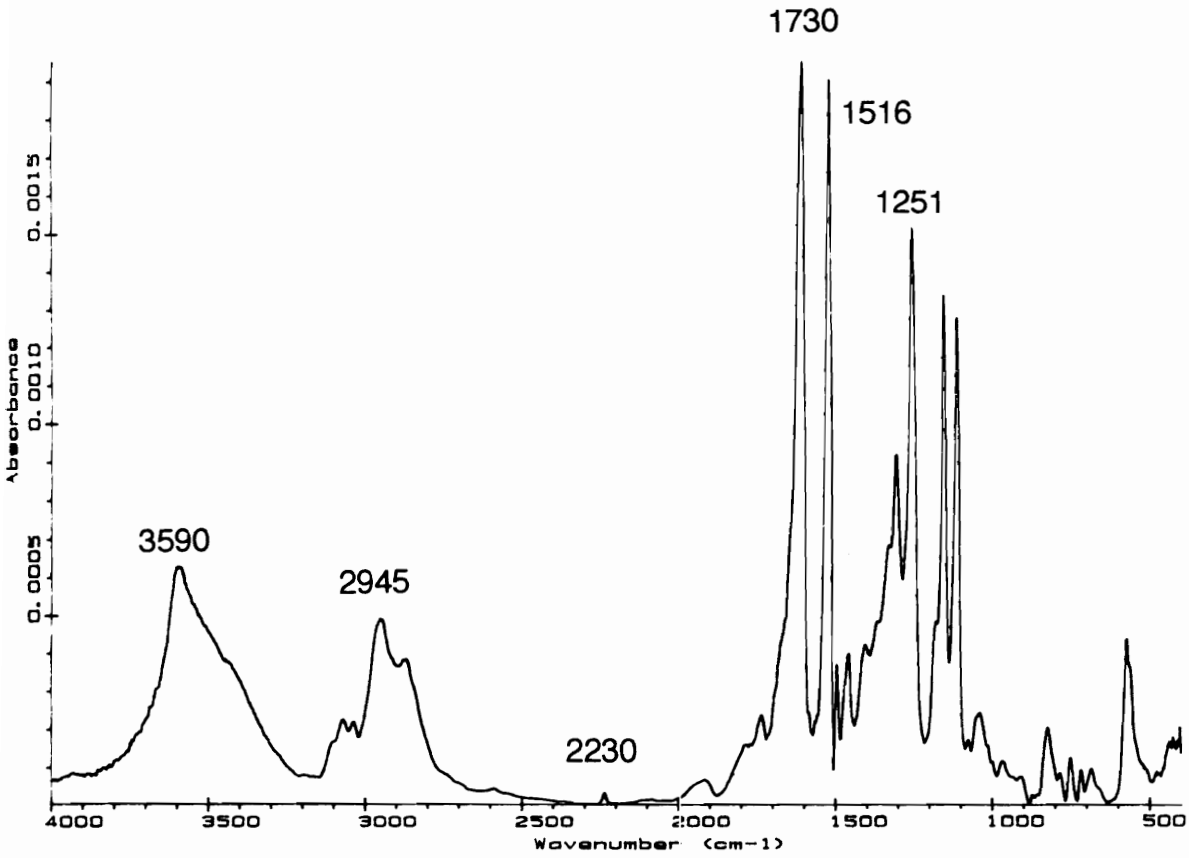

Figure 4.15: DRIFT spectrum of an as-received epoxy composite surface.

properties of the composite surfaces, which often caused spectral distortions and peak shifts to occur. Although an oxygen plasma treatment did not drastically change the condition of the surface, no apparent changes in the surface regions could be detected by this technique.

Although the exact depth of DRIFT sampling is not well-defined, Culler et al. found that peaks from poly (ethylene terephthalate) were visible beneath a 1.5 μm film of poly(vinylidene fluoride) [40]. This is certainly a much greater sampling depth than encountered with either XPS or ISS. Cole et al. also carried out DRIFT analysis of carbon fiber-reinforced epoxy composite and prepreg [41]. They concluded that poor spectral reproducibility and spectral distortion due to front-surface reflection prevented DRIFT from being suitable as a quantitative infrared technique.

4.2 Analysis of Bonded Specimens

4.2.1 Double Lap Shear Testing

The double lap shear strengths of the pretreated epoxy composites bonded with Metlbond® 1146 are summarized in Table 4.11. The ambient temperature results show that the bond strengths of as-received laminates are low, a result which can be directly attributed to the presence of a poorly wetted, fluorine-contaminated surface.

The peel ply pretreatment exhibited the highest lap shear strengths under all testing conditions, followed closely by the oxygen plasma-treated specimens. It had been predicted by other researchers that the roughness of the peel ply surface may entrap air and degrade bond strength and durability [28]; this is evidently not the case in this study. The channels and grooves left behind in the surface following peel ply removal could assist in wetting and spreading of the adhesive by allowing "wicking" to occur. Although the oxygen plasma-treated surface had the highest critical surface tension of all the pretreated

Table 4.11: Double lap shear strengths of surface pretreated epoxy composites bonded with Metlbond® 1146 (in MPa).

Pretreatment	Ambient	82°C Dry	82°C Wet
As Received	12.4 ± 1.7	15.3 ± 2.5	16.9 ± 1.0
Peel Ply	33.6 ± 1.0	20.1 ± 0.4	20.2 ± 2.1
Grit Blast	21.5 ± 2.7	11.4 ± 0.8	11.4 ± 1.3
Oxygen Plasma	30.2 ± 1.2	18.0 ± 2.1	21.8 ± 2.6

composites, the bond strengths which are obtained are not vastly superior to the other pretreatments. Both the oxygen plasma and the peel ply surfaces show good bond durability when tested at elevated temperature and following environmental exposure.

Grit blasting improves the bond strength only at room temperature. The reason for the decrease in bond strength at elevated temperature due to grit blasting is unknown, but is very likely due to the damage induced by the abrasives. Weak boundary layers composed of loosely held broken fibers and matrix resin residue could also contribute to decreased adhesion. Moyer and Wightman reported room temperature single lap shear results for grit blasted LaRC-160 specimens which were lower than the solvent-wiped controls [42].

A general decrease in bond strengths was observed in testing at 82°C (180°F). This could be due to changes in the mechanical properties of either the adherends or the adhesive at elevated temperature, although 82°C does not exceed or even come close to the glass transition temperatures of either the composites or the adhesive. Parker has also documented that joint strengths of composite-to-composite bonds decrease with increasing temperature even below the glass transition temperature [43]. There is relatively little difference in bond strength between the samples tested at 82°C and those tested at 82°C following environmental exposure, an indication that moisture effects are minimal in this adherend/adhesive system.

Table 4.12 shows the amount of moisture absorbed by the lap shear joints during the 30 day exposure to 71°C (160°F)/100% relative humidity conditions. Overall, the relative weight gains of 0.6-0.7% are low, indicating that the particular composite/adhesive combinations studied are not overly susceptible to hot/humid conditions. This observation is consistent with the relative insensitivity of the bond strengths to environmental conditioning. In other work, moisture saturation levels of 0.9-1.98% have been reported for epoxy composites [43,44,45].

Table 4.12: Weight gain in double lap shear joints bonded with Metlbond® 1146, following 30 days in a 71°C/100% RH environment.

Pretreatment	% Change
As Received	+ 0.7
Peel Ply	+ 0.7
Grit Blast	+ 0.6
Oxygen Plasma	+ 0.6

Kinloch and coworkers calculated work of adhesion values for metal/adhesive bonds and found that these values are negative in the presence of water. This implies that spontaneous, interfacial debonding of metal adherends should take place under wet conditions. However, in the case of polymer substrates, the calculated work of adhesion is positive even in the presence of moisture [46]. The surface energy of a polymer is also much less than that of a metal or metal oxide surface, thus there is less of a driving force for water to seek out the interface and initiate interfacial debonding. Thus, interfacial failure in composite bonds under hot/wet conditions is not usually observed for properly prepared surfaces .

Scanning electron microscopy (SEM) analysis of the failure surfaces, summarized in Table 4.13, shows that in addition to failing cohesively in the adhesive, the as-received epoxy joints exhibited a large amount of interfacial failure which was not observed for any other pretreatment. Failure in the peel ply, grit blasted and oxygen plasma-treated specimens was observed to occur cohesively in the adhesive as well as in the laminate; no evidence of interfacial debonding was observed even after environmental conditioning. There was also no significant change in the mode(s) of failure under the various test conditions. This confirms the thermodynamic calculations of Kinloch for composite/composite bonds [46].

4.2.2 Wedge Testing

Figure 4.16 shows the initial crack lengths for the epoxy wedge specimens. An inverse relationship between the initial crack length and the peel strength of a structure has been determined, in that the longer the initial crack, the lower the cleavage or peel strength of the bonded assembly [47]. The as-received specimens show significantly longer initial cracks than any of the surface-pretreated specimens. This result is consistent with the low double lap shear strengths observed with the as-received surfaces. This low cleavage

Table 4.13: SEM analysis of failure modes in epoxy double lap shear joints bonded with Metlbond® 1146.

Pretreatment	Predominant Mode of Failure
As Received	interfacial, adhesive
Peel Ply	adhesive, laminate
Grit Blast	adhesive, laminate
Oxygen Plasma	adhesive, laminate

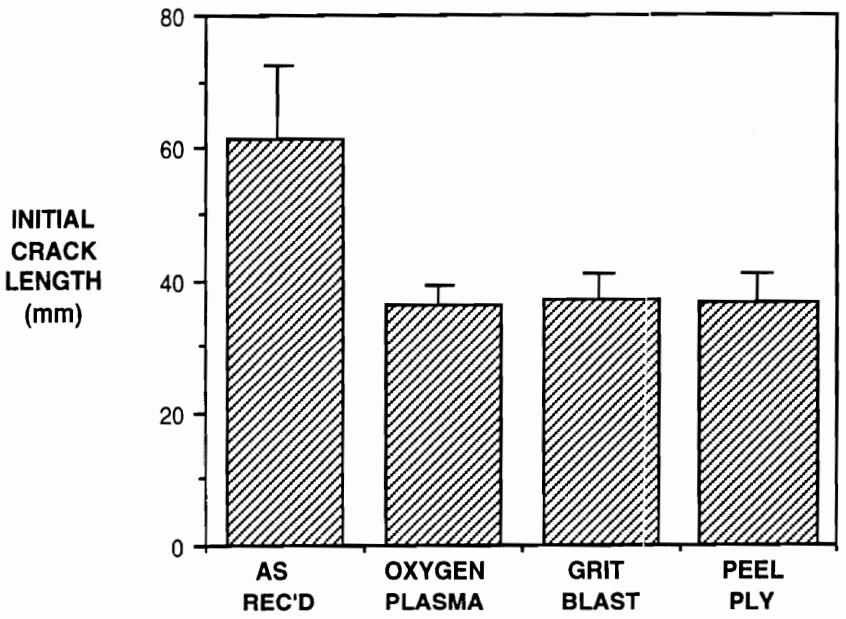

Figure 4.16: Initial crack lengths for surface pretreated epoxy wedge samples bonded with Metlbond® 1146.

strength is again the consequence of the fluoropolymer contamination transferred to the laminate surface during the processing cycle. No significant differences are seen between the initial crack lengths of the oxygen plasma, grit blast or peel ply wedge specimens.

Crack growth for samples in a dry 75°C environment is shown in Figure 4.17. Under this testing condition, no significant crack growth is observed. For each surface pretreatment, the crack only grows an additional 2-4 mm before reaching a plateau value. Testing was carried out beyond 1000 hours with no observations of continued crack growth. These studies in a 75°C environment show that epoxy laminates have good durability at elevated temperature when bonded with Metlbond® 1146. Although the as-received epoxy surface exhibited a large initial crack, it does not propagate at a high rate during 75°C exposure.

The situation changes when the testing is carried out in a 75°C wet environment. Crack growth trends for the epoxy wedge samples are shown in Figure 4.18. The as-received samples show slow crack propagation as previously observed in the 75°C (dry) environment, then take a large jump after 300 hours. It is now also observed that the grit blasted samples show an increased crack growth rate relative to the oxygen plasma and peel ply samples. This is consistent with the 180°F wet double lap shear results in which the as-received and grit blasted samples show poorer hot/wet bond performance when compared with the oxygen plasma and grit blasted samples. It can be concluded that the combined effect of temperature and moisture is much more damaging to these adhesively-bonded composites than temperature alone. This is, of course, a widely-held conclusion in adhesion science.

Another interesting point to note is that, although the crack growths were accelerated in the hot/wet environment, the absolute values of crack extension are quite small when compared to adhesively bonded metal systems, in which even adequate surface preparations may yield high crack growth. This observation may be explained utilizing the

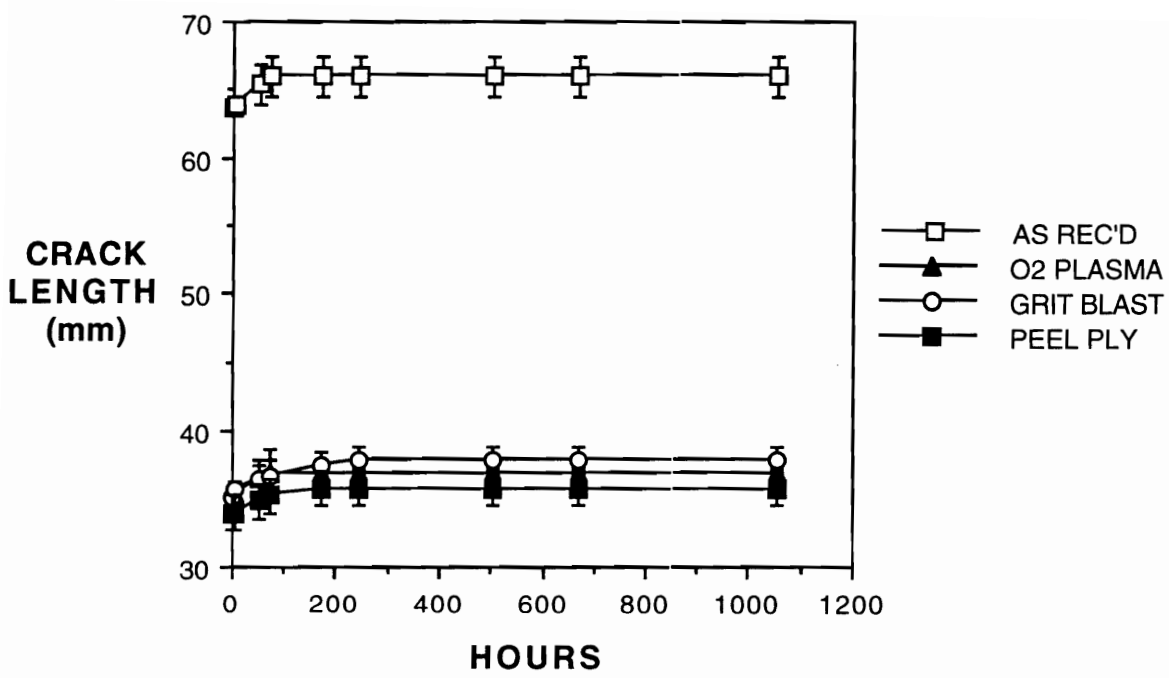

Figure 4.17: Crack growth in surface pretreated epoxy wedge samples bonded with Metlbond® 1146, monitored as a function of time at 75°C.

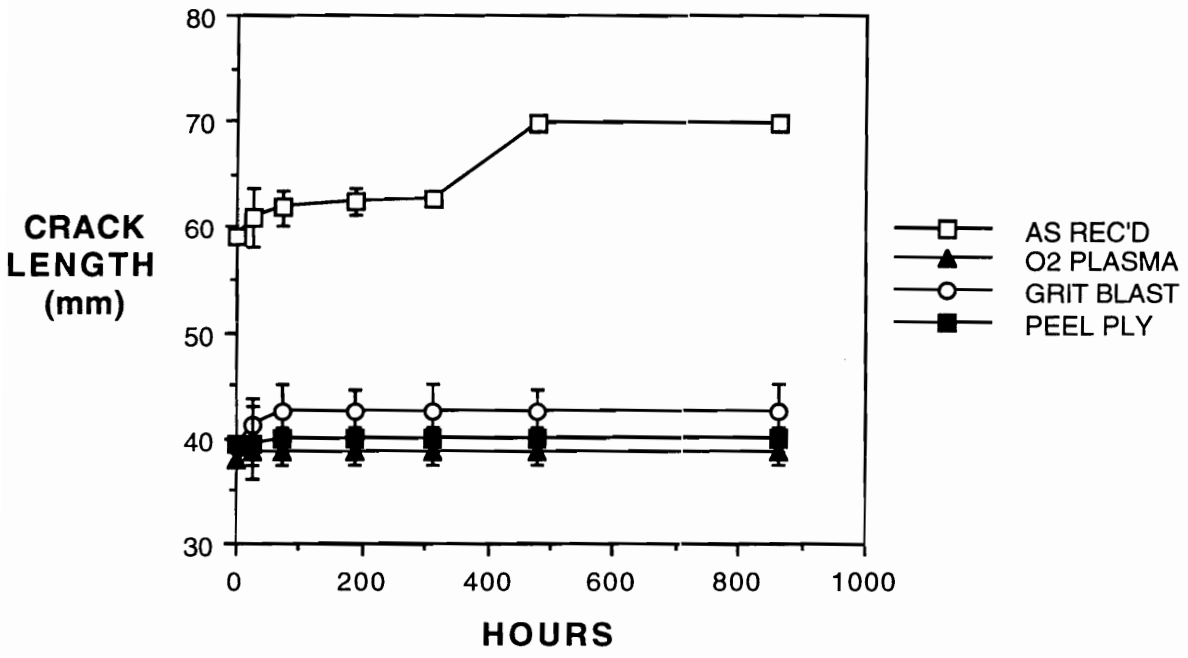

Figure 4.18: Crack growth in surface pretreated epoxy wedge samples bonded with Metlbond® 1146, monitored as a function of time in 75°C water.

thermodynamic reasoning established by Kinloch, which rationalized the difference in hot/wet behavior between metal and composite adherends [46].

Because the wedge specimens which were immersed in 75°C water had not completely debonded, they were next exposed to boiling water. Figure 4.19 shows crack propagation for these samples. Rapid crack growth is evident for these samples, with grit blasting standing out as the least durable surface treatment. Oxygen plasma and peel ply fall close together in their growth curves. The as-received specimens show minimal crack growth, but this is due to the fact that the initial cracks at the beginning of the test were so large that very little stored elastic energy remained in the joints to promote further crack growth.

Boiling water is seen to be a very harsh environment for composite bonds, in which all samples showed large crack extensions. As reported earlier, a 75°C dry environment did not promote any additional crack growth beyond the initial crack regardless of surface pretreatment, whereas 75°C water was capable of differentiating between the durable bonds resulting from peel ply and oxygen plasma treatments and less durable bonds formed by bonding as-received and grit blasted surfaces.

De-icing fluid was initially anticipated to be a corrosive environment which would be encountered by composite materials in aircraft applications. However, the effect of de-icing fluid on the composite joints was minimal. No crack growth was observed for any pretreatment even after 1750 hours of immersion. It is concluded that the combination of organic compounds present in aircraft de-icing fluid is not detrimental to these epoxy composite joints at room temperature.

Table 4.14 summarizes the modes of failure for the epoxy wedge specimens. The as-received wedges showed 100% interfacial failure between the composite surface and the adhesive, whereas all other pretreatments exhibited varying degrees of cohesive failure in the adhesive and the laminate. This result points out the detrimental effect of surface

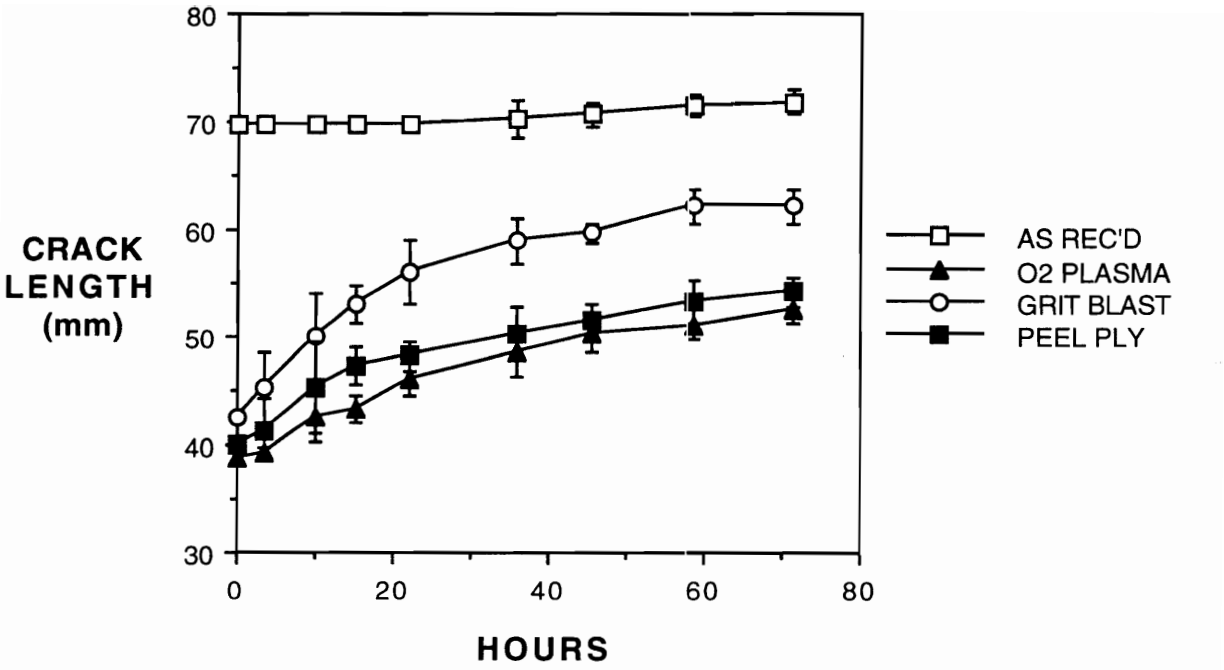

Figure 4.19: Crack growth in surface pretreated epoxy wedge samples bonded with Metlbond® 1146, monitored as a function of time in 100°C water.

Table 4.14: Predominant modes of failure for surface pretreated epoxy wedge samples, bonded with Metlbond® 1146.

Pretreatment	Initial Crack	75°C Dry	75°C Wet	100°C Wet
As Received	I	I	I	I
Oxygen Plasma	50% A, 50% L	20% A, 80% L	A	A
Grit Blast	50% A, 50% L	20% A, 80% L	A	A
Peel Ply	40% A, 60% L	50% A, 50% L	A	A

I = interfacial between adhesive and composite; A = cohesive in adhesive; L = cohesive in laminate

contamination on bond performance and is also consistent with the prediction that well-prepared composite/composite bonds should not fail interfacially even under hot/wet conditions.

4.2.3 Scanning Acoustic Microscopy (SAM)

Scanning Acoustic Microscopy (SAM) is a technique which shows great promise for the nondestructive evaluation of adhesively bonded samples. The SAM technique utilizes a focused beam of high frequency ultrasonic waves to analyze the sample, resulting in a map which reflects the variation in acoustic reflectivity arising from voids and differing material densities. SAM has already been shown to be successful in locating flaws within composite materials and within bondlines of metals bonded to other metals [48]. The objective of this series of experiments was to determine if debonded regions could be detected in 8-ply epoxy laminates bonded with Metlbond® 1146.

A composite joint composed of two 8-ply epoxy samples bonded with Metlbond® 1146 was first analyzed by SAM to determine if a deliberately induced debond could be detected. Analysis of this sample, shown in Figure 4.20, revealed that this artificial flaw was clearly visible through an 8-ply composite sandwich. Bright white regions in the micrographs are indicative of a debonded or unbonded area, whereas fuzzier, lighter white areas are due to reflection from the carbon fiber reinforcement.

Figure 4.21 shows SAM micrographs of surface pretreated epoxy bonds. A number of bright white debonded areas are evident in each joint, which stand out above the diffuse scattering from the fibers. Figure 4.22 shows the percentage of the total analyzed area which is debonded. Both the peel ply and grit blasted surfaces show a larger percent debond relative to the as-received and oxygen plasma-treated surfaces. This result correlates well with the more pronounced surface topography observed for grit blasted and peel ply surfaces (see Table 4.10).

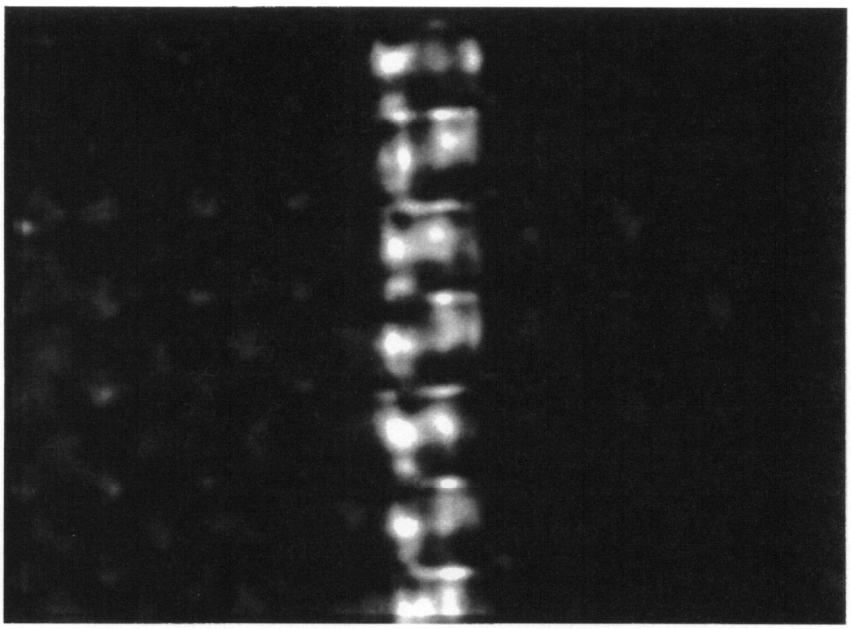

Figure 4.20: Scanning acoustic micrograph of a deliberately induced bondline flaw in two 8-ply epoxy composites bonded with Metlbond® 1146.

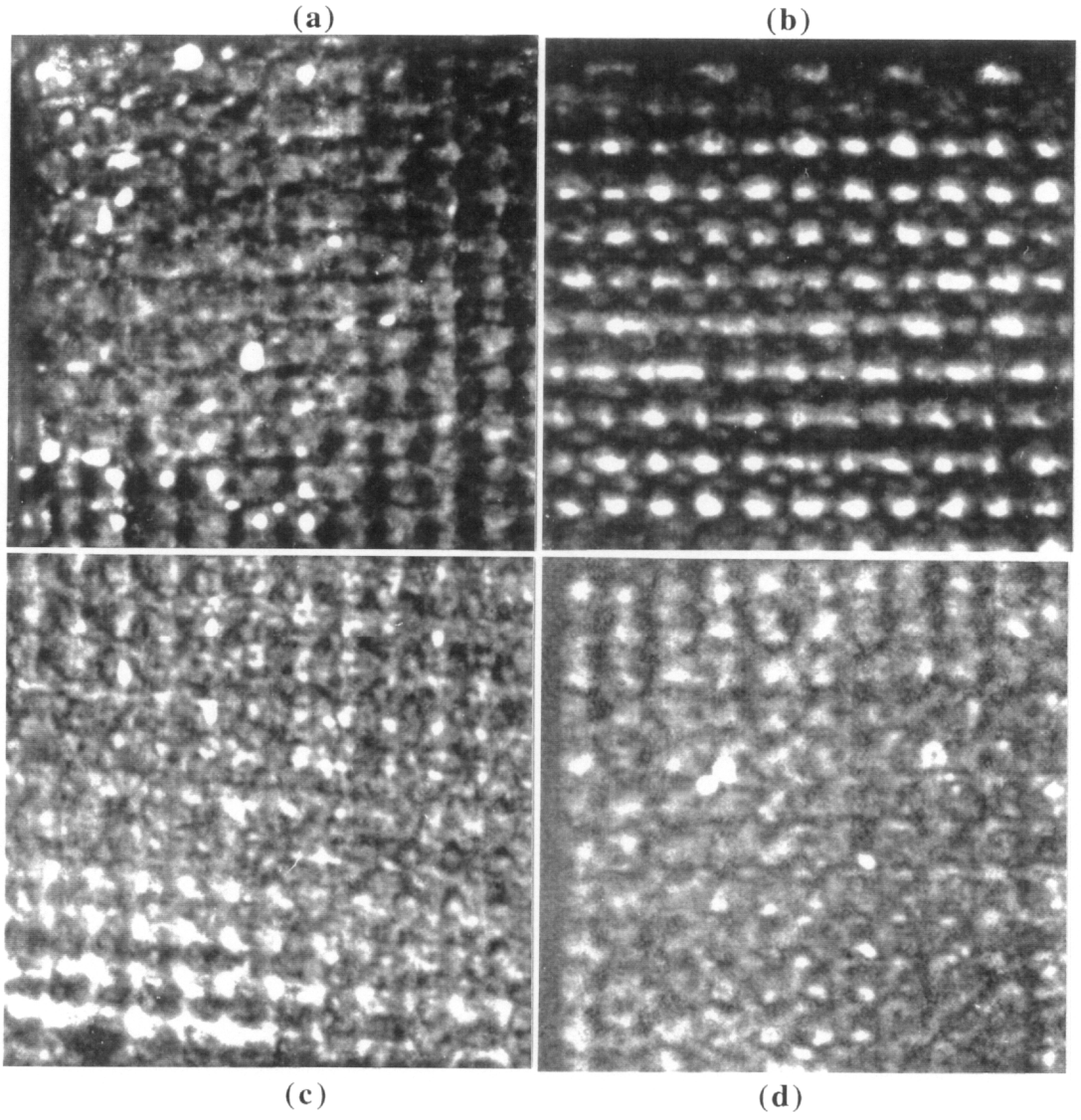

Figure 4.21: Acoustic micrographs of surface pretreated 8-ply epoxy composites bonded with Metlbond® 1146. (a) As received (b) Peel ply (c) Grit blast (d) Oxygen plasma.

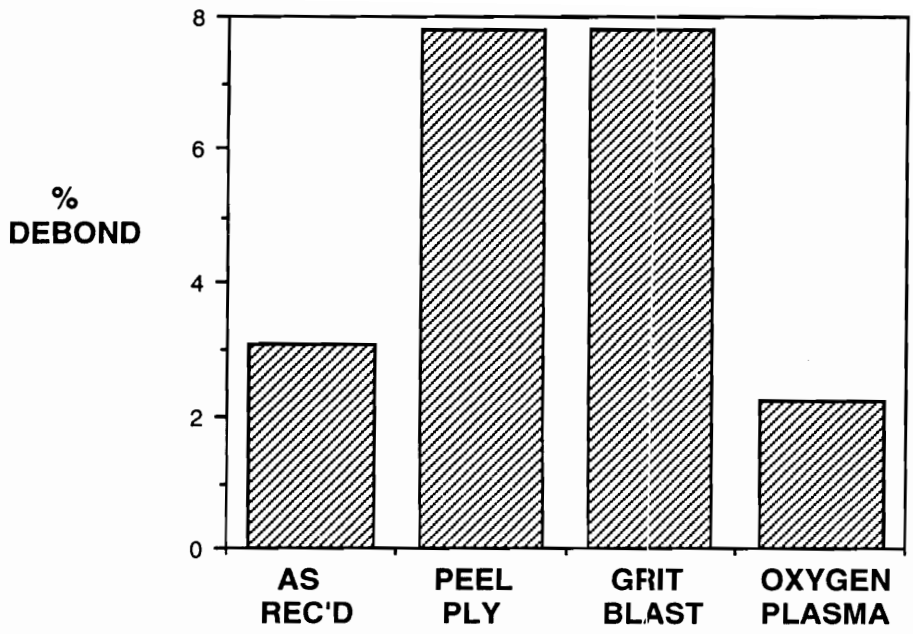

Figure 4.22: Percentage of debonded area in epoxy composites bonded with Metlbond® 1146, calculated from scanning acoustic micrographs.

4.3 Conclusions

Significant changes in the chemistry and topography of the epoxy composites were observed following surface preparation by grit blasting, plasma treatment and peel ply. A MEK solvent wipe was determined to have negligible effect on surface chemistry and the removal of processing contamination. Grit blasting and oxygen plasma treatment were successful in removing fluoropolymer release film residues, while the use of a peel ply prevented the initial fluoropolymer contamination from occurring. Oxygen plasma treatment also provided additional benefit in increasing the oxygen concentration in the composite, thus ensuring a highly polar and wettable surface for bonding. The surface energies of the grit blasted, oxygen plasma-treated and peel ply surfaces were increased relative to the as-received control, due to the absence of the fluoropolymer contamination. Although the oxygen plasma-treated surface had the highest surface energy, it was not wetted to any greater extent by epoxy resin than the peel ply or grit blasted surface.

The roughness of the peel ply and grit blasted surfaces was significantly greater than those of the as-received and oxygen plasma-treated surfaces. Initial bond strengths were not adversely affected by this degree of roughness. However, the surface damage induced by the grit blast treatment was extensive and is postulated to decrease the hot/wet durability of the grit blasted double lap shear and wedge samples. Surface contamination was shown to have a detrimental effect on both lap shear strength and wedge durability. Oxygen plasma and peel ply surface treatments, although yielding dissimilar surface chemistries and topographies, were found to provide excellent initial strength as well as resistance to hot/wet environments.

4.4 References

1. B.M. Parker and R.M. Waghorne, *Composites*, **13**, 28 (1982).
2. D.L. Messick, D.J. Progar and J.P. Wightman, *NASA Technical Memorandum 85700*, October 1983.
3. D.J.D. Moyer and J.P. Wightman, *Surf. Interface Anal.*, **14**, 492 (1989).
4. C.U. Ko and J.P. Wightman, *J. Adhesion*, **24**, 93 (1987).
5. G. Beamson and D. Briggs, *High Resolution XPS of Organic Polymers* (John Wiley and Sons, Chichester, 1992).
6. D.T. Behm and J. Gannon in *Engineered Materials Handbook*, vol. 3, p. 94 (ASM International, Metals Park, 1990).
7. L.W. Crane, C.L. Hamermesh and L. Maus, *SAMPE J.*, **12**(2), 6 (1976).
8. W.A. Dukes and A.J. Kinloch in *Developments in Adhesion - 1*, W.C. Wake, ed., p. 251 (Applied Science Publishers, London, 1977).
9. C. D. Wagner, W.M. Riggs, L.E. Davis, J.F. Moulder and G.E. Muilenberg, *Handbook of Photoelectron Spectroscopy* (Perkin-Elmer Corporation, Eden Prairie, 1979).
10. H.F. Webster and J.P. Wightman, *J. Adhesion Sci. Technol.*, **5**(1), 93 (1991).
11. D. Briggs in *Practical Surface Analysis by Auger and X-ray Photoelectron Spectroscopy*, D. Briggs and M.P. Seah, eds., p. 359 (John Wiley and Sons, London, 1983).
12. W.A. Zisman in *Advances in Chemistry*, **43**, F.M. Fowkes, ed., chap. 1 (American Chemical Society, Washington D.C., 1964).
13. S. Wu, *J. Colloid Interface Sci.*, **71**(3), 605 (1979).
14. R.J. Good, *J. Adhesion Sci. Technol.*, **6**(12), 1269 (1992).
15. J. Vial and A. Carre, *Int. J. Adhes. Adhes.*, **11**(3), 140 (1991).
16. T. Hata, Y. Kitazaki and T. Saito, *J. Adhesion*, **21**, 177 (1987).
17. H. Schonhorn, H.L. Frisch and G.L. Gaines, *Polym. Eng. Sci.*, **17**(7), 440 (1977).
18. R.N. Wenzel, *Ind. Eng. Chem.*, **28**(8), 988 (1936).
19. P.J. Dynes and D.H. Kaelble, *J. Adhesion*, **6**, 195 (1974).
20. *Handbook of Chemistry and Physics*, 71st Edition, D.R. Lide, ed., p. **6**-102 (CRC Press, Boca Raton, 1991).

21. J. Schultz, K. Tsutsumi and J.-B. Donnet, *J. Colloid Interface Sci.*, **59**(2), 272 (1977).
22. A. Carre and J. Schultz, *J. Adhesion*, **15**, 151 (1983).
23. D. H. Kaelble, *Physical Chemistry of Adhesion* (Wiley-Interscience, New York, 1971).
24. D.H. Kaelble in *Epoxy Resins: Chemistry and Technology*, C.A. May and Y. Tanaka, eds., p. 331 (Marcel Dekker, New York, 1973).
25. W. Gutowski, *Int. J. Adhes. Adhes.*, **7**(4), 189 (1987).
26. Y. L. Hsieh, M. Wu and D. Andres, *J. Colloid Interface Sci.*, **144**(1), 127 (1991).
27. Shell EPON® Resin Structural Reference Manual.
28. A.V. Pocius and R.P. Wenz, *Proceedings of the 30th National SAMPE Symposium*, 1073 (1985).
29. A. J. Kinloch, G. K. A. Kodokian and J. F. Watts, *J. Mater. Sci. Lett.*, **10**, 815 (1991).
30. D.K. Owens and R.C. Wendt, *J. Appl. Polym. Sci.*, **13**, 1741 (1969).
31. R.D. Hazlett, *J. Adhesion Sci. Technol.*, **6**(6), 625 (1992).
32. M. Yekta-Fard and A.B. Ponter, *J. Adhesion Sci. Technol.*, **6**(2), 253 (1992).
33. J.F. Oliver, C. Huh and S.G. Mason, *J. Adhesion*, **8**, 223 (1977).
34. A.J. Kinloch, *J. Mater. Sci.*, **15**, 2141 (1980).
35. K. Neuman, *J. Colloid Interface Sci.*, **26**, 209 (1968).
36. J. Schonhorn, H.L. Frisch and T.K. Kwei, *J. Appl. Phys.*, **37**(13), 4067 (1966).
37. D.E. Packham in *Adhesion Aspects of Polymeric Coatings*, K.L. Mittal, ed. (Plenum Press, New York, 1983).
38. D.J. Arrowsmith, *Trans. Inst. Met. Finish.*, **48**, 88 (1970).
39. W.A. Zisman, *Ind. Eng. Chem.*, **55**(10), 19 (1963).
40. S.R. Culler, M.T. McKenzie, L.J. Fina, H. Ishida and J.L. Koenig, *Appl. Spectrosc.*, **36**(6), 791 (1984).
41. K.C. Cole, A. Pilon, D. Noel, J.-J. Hechler, A. Chouliotis and K.C. Overbury, *Appl. Spectrosc.*, **42**(5), 761 (1988).
42. D.J.D. Moyer and J.P. Wightman, *Surf. Interface Anal.*, **17**, 457 (1991).
43. B.M. Parker, *Compos. Struct.*, **6**, 123 (1986).
44. A.C. Loos and G.S. Springer in *Environmental Effects on Composite Materials*, G. S. Springer, ed., chap. 4 (Technomie Publishing Co., 1981).

45. R.L Schulte and R.J. DeIasi, *IEEE Trans. on Nuclear Sci.*, **NS-28**(2), 1841 (1981).
46. A.J. Kinloch in *Polymer Surfaces and Interfaces,* W.J. Feast and H.S. Munro, eds. (John Wiley and Sons, New York, 1987).
47. J. Cognard, *J. Adhesion,* **20**, 1 (1986).
48. M.H. McCord and J.C. Duke, Jr., *Proceedings of the 15th Annual Meeting of the Adhesion Society*, 1992, p. 71.

Chapter V: Results and Discussion

Surface Characterization and Bonding of Toughened Bismaleimide Composites

The results of surface pretreatment and adhesive bonding of a rubber-toughened, carbon fiber-reinforced bismaleimide (BMI) composite are reported in this section. As also carried out in Chapter IV for the toughened epoxy composites, surface analytical techniques were employed to determine the changes in surface chemistry and topography which resulted from surface pretreatment. The chemical and topographical features of the composite surfaces were in turn correlated to the strengths of bonds made with these materials, as well as to bond durability in various environments.

5.1 Surface Characterization

5.1.1 X-ray Photoelectron Spectroscopy (XPS)

In the study of adhesion, the chemistry of the surface(s) involved is critical in determining the initial level of adhesion and bond durability which can be obtained for a particular system. Surface pretreatment techniques can alter the surface chemistry significantly, particularly in the case of polymeric materials. The chemical composition of the pretreated BMI composite surfaces was readily obtained by XPS analysis, and is summarized in Table 5.1.

As was observed for the epoxy composite, the as-received BMI surface contained about 12% fluorine on the surface. This is approximately the same level of contamination as was observed for the epoxy laminates. Carbon, oxygen and nitrogen are elements expected to be found in a bismaleimide resin. The binding energy of the N1s photopeak at 400.4 eV is consistent with that of imide functionality [1]. Sulfur which is present may

Table 5.1: XPS atomic concentrations of surface pretreated BMI composites.

	ATOMIC CONCENTRATION (%)						
	C	**O**	**N**	**F**	**S**	**Si**	**Na**
As Received	63.9	17.5	2.6	12.4	0.3	2.9	0.4
Peel Ply	74.0	16.0	9.6	---	---	0.4	---
Grit Blast	78.4	16.4	2.8	---	0.1	1.7	0.6
20 min. Oxygen Plasma	55.6	33.8	3.3	---	0.5	4.5	1.3
20 min. Nitrogen Plasma	57.2	32.2	4.6	0.8	3.4	0.4	1.4
20 min. Ammonia Plasma	61.9	21.1	9.3	1.3	4.4	0.7	1.3

originate from the toughening agent, a comonomer or some other additive. Trace amounts of sodium and silicon in the form of silicates are also observed.

Laminates which were fabricated with a peel ply layer contained no fluorine or sodium contamination on the surface following peel ply removal. Prevention of surface contamination is one of the reasons given for the use of a peel ply layer [2]; thus, this objective appears to be accomplished. The concentration of nitrogen is higher than for the as-received or grit blasted surfaces - this could be due to a different level of comonomer or toughener in the peel ply resin. Silicon which was found in the composite surface after peel ply removal had a binding energy of 103.0 eV and is thus attributed to SiO_2. Analysis of the underside of the removed peel ply layer also showed high concentrations of inorganic silicon (10-12%) and smaller quantities of calcium (2-3%), indicating that the peel ply fabric is a glass cloth.

Grit blasting is an effective method of fluoropolymer removal, completely eliminating all traces of fluorine from the surface. Residual sulfur, silicon and sodium contamination were found on the grit blasted surface. Silicon and sodium are attributed to silica grit which was not fully removed from the surface.

Significant changes in surface chemistry are observed in the composite surface following treatment with radio frequency (RF)-generated plasmas. Table 5.1 shows the results of 20 minute plasma treatments in oxygen, nitrogen and ammonia. It can be seen that the fluorine contamination is fully removed by oxygen plasma treatment. In fact, it will be shown in a later section that only a 5 minute oxygen plasma treatment is needed to remove all traces of fluoropolymer. Oxygen concentration in the composite surface increases from approximately 18% to almost 34% following exposure to oxygen plasma.

The use of nitrogen plasma also produced an increase in the oxygen concentration, but did not increase the nitrogen concentration significantly. Also, even after 20 minutes of treatment in a nitrogen plasma, traces of fluorine are still detected on the surface. Ammonia

plasma, on the other hand, increased the nitrogen concentration from approximately 3% to 9%. The oxygen concentration is also slightly increased by the ammonia plasma treatment. The binding energy of the N1s photopeak is observed to shift from its original position at 400.4 eV to 399.5 eV following ammonia plasma exposure. This phenomenon has been previously observed in the ammonia plasma treatment of LaRC-TPI, a thermoplastic polyimide, and is attributed to the formation of amides from the original imide groups [3]. Due to the fact that traces of fluorine are still detected on the surface even after a 20 minute treatment, neither nitrogen nor ammonia plasma treatments were investigated further.

Curve-fitted C1s photopeaks for the surface pretreated BMI laminates are shown in Figure 5.1. All four surfaces show a hydrocarbon C-C peak at 284.6 eV, a C-O peak (from the BMI backbone, toughening agents or other additives) and/or a C-N peak (from the imide C-N linkage) at 286.0 eV and an imide carbonyl peak (O=C-N) at 288.4 eV. Aromatic π - π^* shake-up satellites are also observed for the peel ply and grit blasted surfaces at 290.2-291.4 eV. The satellite peak in the as-received surface in Figure 5.1(a) is obscured by the C-F peak from the fluoropolymer contamination at 291.8 eV.

Figure 5.1(d) shows the dramatic change in photopeak shape following treatment with oxygen plasma. There is an increase in the intensity of the C-O/C-N peak at 286.0 eV and the imide peak at 288.4 eV. Two new peaks can be resolved from the photopeak envelope at 287.4 eV and 290.3 eV, corresponding to carbonyl (C=O) and carbonate ($O=C(-O)_2$) species. Again, it can be seen that the increase in the surface oxygen concentration following oxygen plasma exposure is attributed to the formation of oxygen-containing functional groups.

Table 5.2 shows the effect of oxygen plasma treatment time at 50 watts of power. It is seen that a 1 minute treatment removes all but approximately 2% of the surface fluorine. After 5 minutes of treatment at 50 watts, fluorine is no longer detected. The oxygen concentration reaches a plateau value around 5 minutes. The effect of plasma

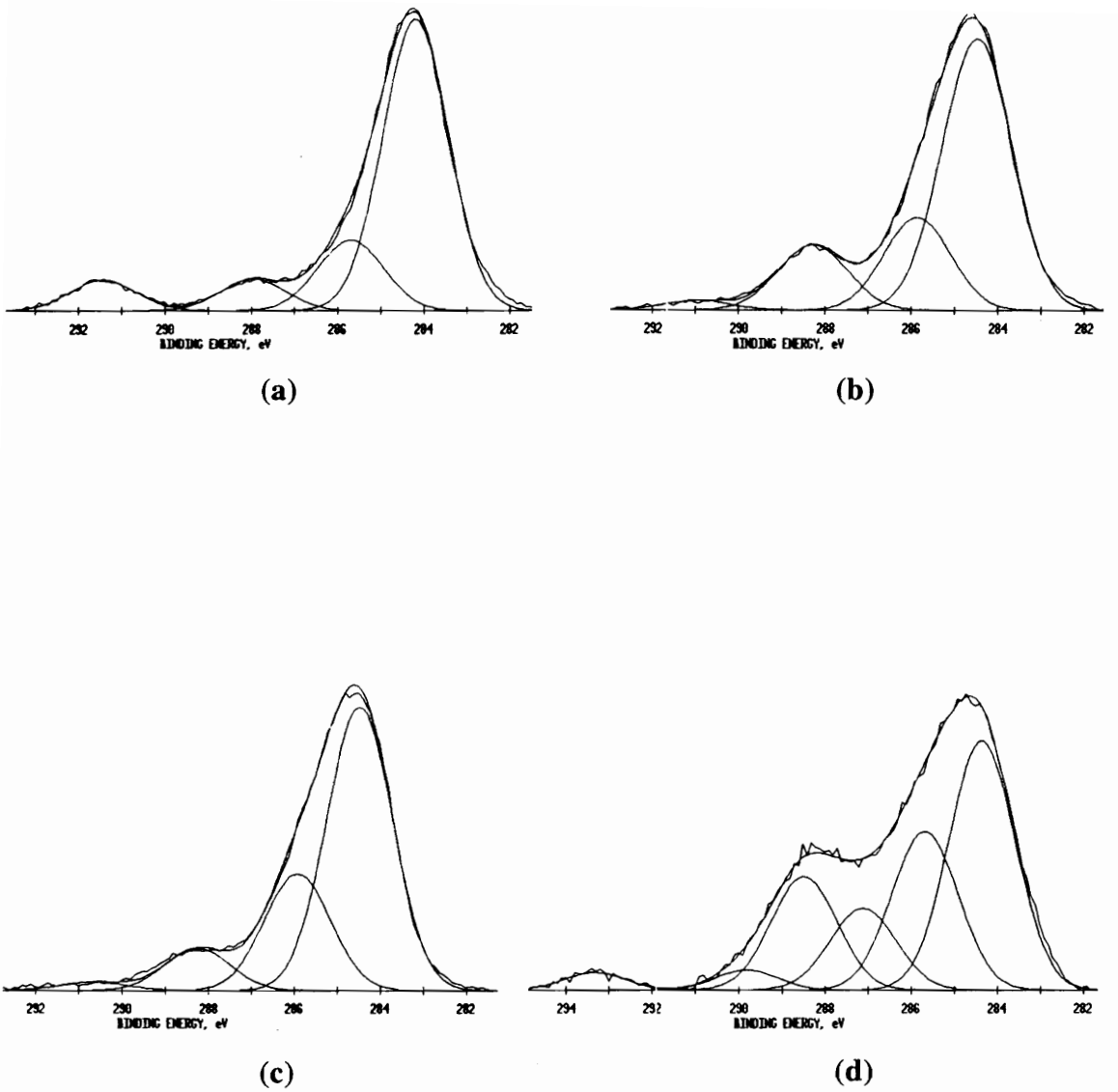

Figure 5.1: Curve-fitted carbon 1s photopeaks from surface pretreated BMI composites. (a) As received (b) Peel ply (c) Grit blast (d) 5 minute oxygen plasma.

Table 5.2: Effect of oxygen plasma treatment time on BMI surface composition, with plasma power held constant at 50 watts.

	ATOMIC CONCENTRATION (%)						
Time (min.)	**C**	**O**	**N**	**F**	**S**	**Si**	**Na**
1	50.7	36.7	4.2	2.1	0.5	4.5	1.2
5	50.0	38.8	3.3	---	0.7	6.2	1.0
10	49.6	39.3	3.6	---	0.7	5.3	1.5
20	47.4	41.9	2.6	---	0.3	4.3	3.5

power is detailed in Table 5.3. 1 minute at either 10 or 50 watts of plasma power is not long enough to remove fluorine. However, a 1 minute treatment at 100 watts of power and above is capable of removing all fluorine and establishing a steady-state concentration of oxygen.

Figure 5.2a shows data from the plasma power and plasma exposure time experiments normalized in terms of plasma energy. Carbon concentration decreases and levels out around 6000 J as plasma energy increases, whereas the oxygen concentration increases and also levels out around 6000 J. The nitrogen concentration is seen to remain relatively constant. Figure 5.2b shows the decrease in fluorine concentration and the increases in silicon concentration with increasing plasma energy. Little change is observed for the concentration of sodium on the composite surface. These results are similar to those observed for the oxygen plasma treatment of epoxy composites.

5.1.2 Ion Scattering Spectroscopy (ISS)

ISS, which is sensitive to the topmost molecular layer in a surface, is one of the most surface-sensitive techniques available for the analysis of polymer surfaces. It is utilized in this study to provide a comparison to the results obtained by XPS. ISS is not as quantitative as XPS, due to a general lack of knowledge of sensitivity factors for the different elements. Therefore, only qualitative results regarding the presence or absence of various species will be reported. Also, because the analyzer configuration in the instrument utilized for this work used is not optimal for ISS, detection of the lower atomic number elements such as carbon is often poor. ISS spectra of the pretreated BMI composites are shown in Figure 5.3, showing peak intensity versus the scattered ion energy ratio, E/E_o.

ISS spectra which are obtained for the surface pretreated BMI composites are similar to those of the pretreated epoxy laminates. As shown in Figure 5.3(a), the spectra of the as-received sample exhibits only a single fluorine peak, indicative of fluoropolymer

Table 5.3: Effect of oxygen plasma power on BMI surface composition, with plasma treatment time held constant at 1 minute.

	ATOMIC CONCENTRATION (%)						
Power (watts)	**C**	**O**	**N**	**F**	**S**	**Si**	**Na**
10	60.0	32.0	4.1	0.7	1.8	0.4	1.0
50	56.7	35.1	4.4	0.4	0.5	1.9	1.0
100	54.2	37.1	4.4	---	0.4	2.5	1.4
150	58.1	32.9	4.8	---	0.6	1.6	2.0

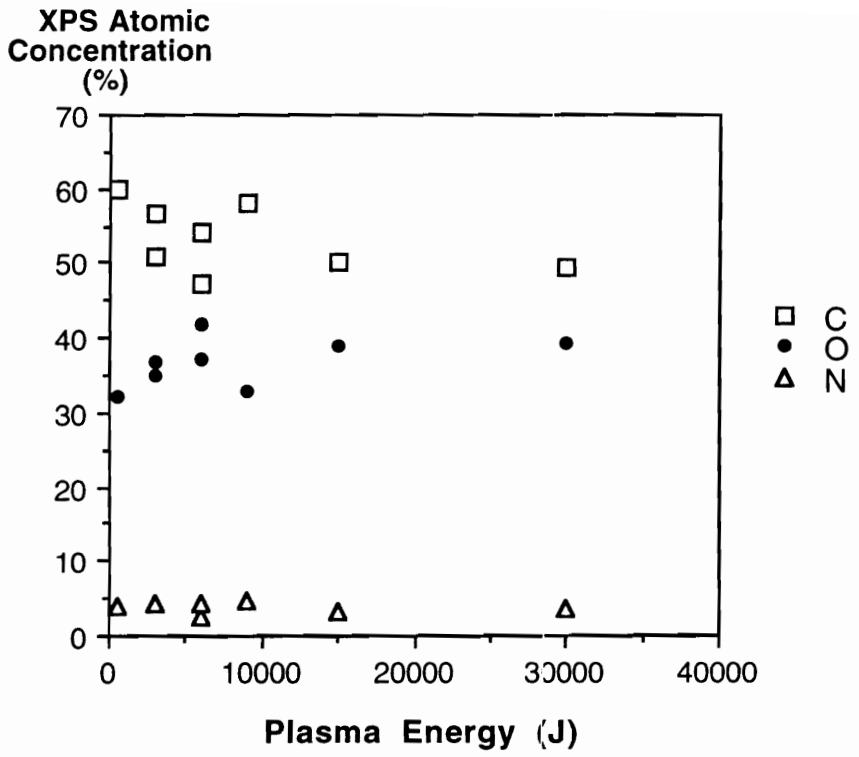

Figure 5.2a: XPS atomic concentrations of BMI matrix resin elements as a function of total plasma energy.

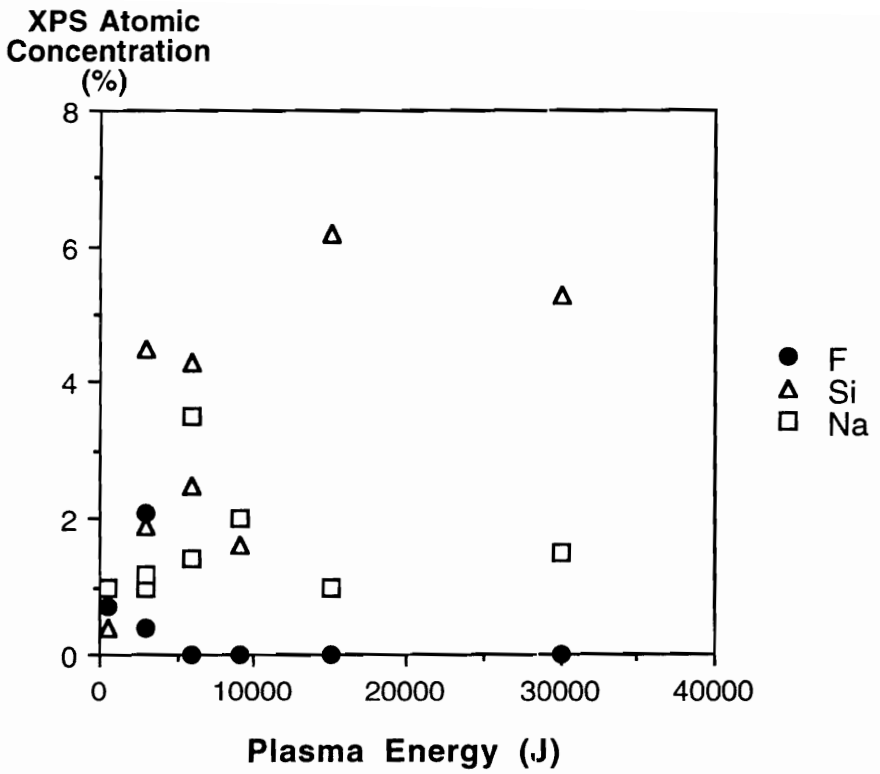

Figure 5.2b: XPS atomic concentrations of BMI composite surface contaminants as a function of total plasma energy.

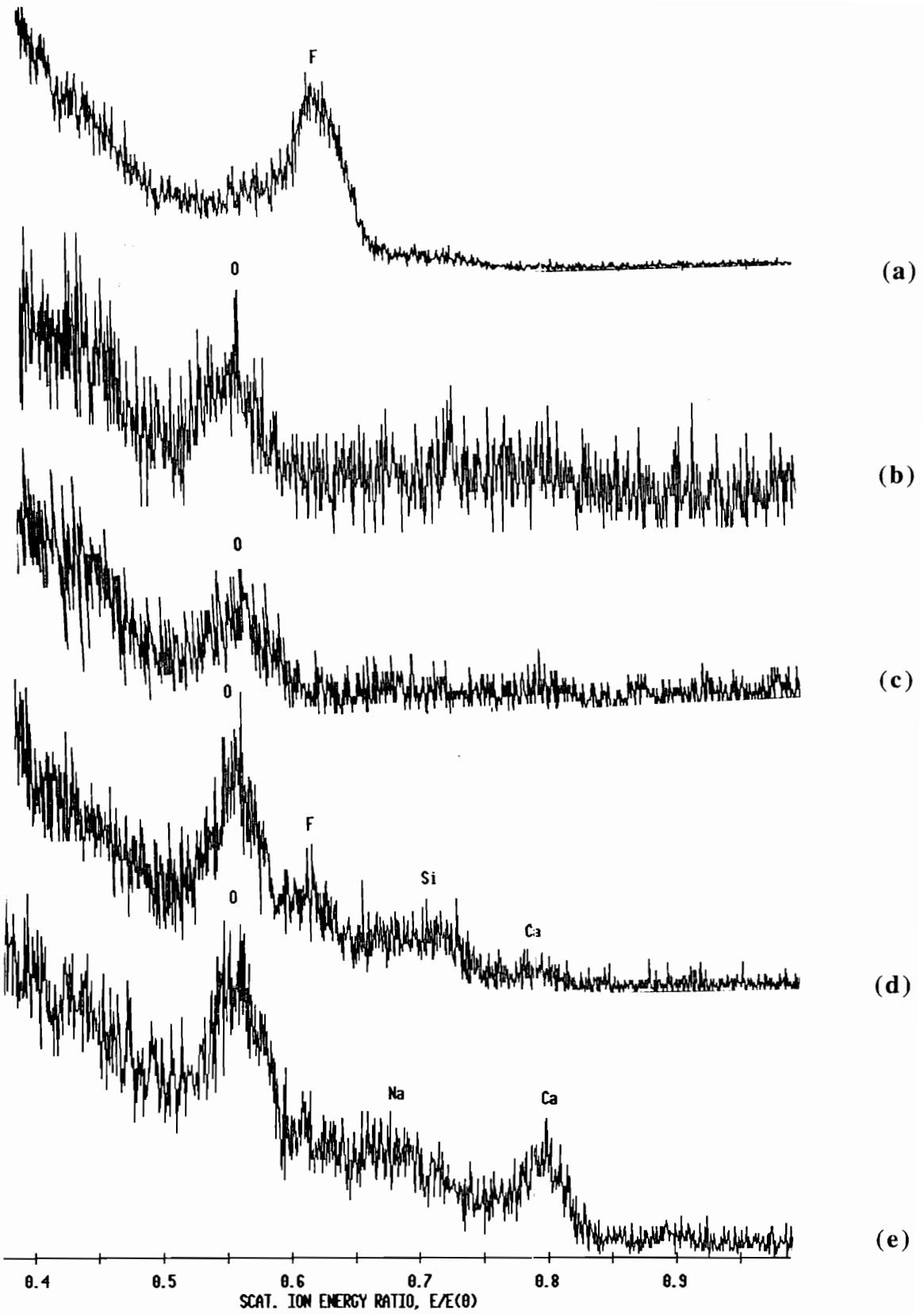

Figure 5.3: ISS spectra of surface pretreated BMI composites. (a) As received (b) Peel ply (c) Grit blast (d) 1 minute oxygen plasma (e) 5 minute oxygen plasma.

transfer from the composite release films. No fluorine is detected on either the peel ply or grit blasted surface, shown in Figures 5.3(b) and 5.3(c) respectively. Instead, a single oxygen peak is observed. As seen by XPS, 1 minute of oxygen plasma treatment at 50 watts of power leaves behind some fluorine residue but increases the oxygen concentration; the ISS spectrum in Figure 5.3(d) shows both an enhanced oxygen peak as well as a residual fluorine peak. Finally, Figure 5.3(e) shows the completely removal of surface fluorine. Both Figure 5.3(d) and 5.3(e) indicate the presence of silicon, sodium and calcium.

Although it is difficult to extract quantitative data from these ISS experiments, they are valuable tools in analyzing the extreme topmost atomic layers of a surface and serve to complement the chemical composition information obtained by XPS.

5.1.3 Contact Angle Analysis

The use of contact angle measurements to determine surface energies is well-known and used by many researchers in the field of adhesion and surface analysis. A myriad of approaches have been developed to obtain the elusive surface energy of a solid material [4,5,6,7,8]. Unfortunately, there is often little or no agreement between the approaches or the results obtained thereof. As stated by Schonhorn et al., there is no universally accepted, direct, non-ambiguous method of measuring polymer surface energies [9]. It is the objective of these experiments to obtain surface energy values for the pretreated composites so that internal comparisons can be made, and differences in wettability and adhesion behavior can be rationalized.

5.1.3.1 Roughness Correction

Prior to calculating the surface free energies of the composite surfaces, it was necessary to determine the effect of the surface roughness on the contact angle. The

roughness factors for the various surface pretreatments were measured relative to a polished chrome steel plate, which has an R_a measured by profilometry of 0.02 μm and an R_z of 0.1 μm. The roughness factor R_C for this reference substrate was taken to be 1.0.

Roughness correction factors for the BMI composite surfaces are shown in Table 5.4. It is observed, as is expected, that all 4 pretreated surfaces have a greater surface area than the smooth Ferrotype plate used as a reference. The peel ply surface is the roughest surface, followed by the grit blasted surface, the oxygen plasma-treated surface and the as-received surface, in descending order of roughness. Again, it is observed that the plasma treatment may be inducing some microporosity which is changing the effective surface area relative to the as-received surface.

5.1.3.2 Surface Energy Analysis

Zisman's approach for determining the critical surface tension, Kaelble's method for determing the polar and dispersive components of the surface free energy, and the Schultz water-in-alkane analysis for high energy surfaces, all described in detail in the Experimental Section, were utilized in this study.

Table 5.5 summarizes the surface energies determined by the Zisman, Kaelble and Schultz methods. The total surface energy, γ_S, is calculated from the sum of the dispersive component γ_S^D and the polar or nondispersive component, γ_S^P. The surface energy and critical surface tension for the as-received BMI are approximately equal to literature values for the surface energies of fluorinated polymers, which are usually in the range of 19-21.6 mJ/m^2 [10]. This is consistent with the presence of fluorine detected on the surface of the as-received laminates by both x-ray photoelectron spectroscopy and ion scattering spectroscopy. As discussed previously, this fluorine originates from the fluorinated-ethylene propylene (FEP) release films against which the laminates were consolidated.

Table 5.4: Roughness correction factors (R_C) for surface pretreated BMI composites.

	Ethylene Glycol Contact Angle (deg.)	R_C
As Received	51.9 ± 1.7	1.03 ± 0.08
Peel Ply	20.0 ± 3.0	1.57 ± 0.06
Grit Blast	37.0 ± 3.9	1.33 ± 0.14
5 min. Oxygen Plasma	43.5 ± 3.1	1.21 ± 0.12

Referenced to: Gold-coated photographic plate, contact angle = 53.2 ± 3.6

Table 5.5: Summary of BMI composite surface energies (in mJ/m^2).

	$\gamma_s^{(d)}$	$\gamma_s^{(p)}$	γ_s [1]	γ_c [2]
As Received	25.0	6.3	31.3	26.1
Peel Ply	20.1	19.9	40.0	57.5
Grit Blast	30.8	8.3	39.1	49.8
Oxygen Plasma	36.4	42.3	78.7 [3]	90.3 [4]

[1] Obtained via Kaelble's approach, $\gamma_s = \gamma_s^{(d)} + \gamma_s^{(p)}$

[2] Obtained using a Zisman series of non-homologous liquids

[3] Obtained using the 2-liquid method of Carre and Schultz

[4] Obtained utilizing high surface tension NaOH solutions in a Zisman-type analysis

The unusually high energy of the BMI peel ply surface is a bit suspect, and may be due to an incomplete subtraction of the surface roughness effect. The surface energies obtained for the grit blasted surfaces are close to those of graphite or carbon surfaces; Dynes and Kaelble reported γ_S values for various graphitic and carbon materials ranging from 37-58 mJ/m^2 [11].

Both γ_C and γ_S obtained for the oxygen plasma-treated surface are significantly higher than that which has been reported for even polar polymers such as poly(amides) or poly(esters). However, it is reasonable to expect that the increase in surface polarity and oxygen concentration plays a large role in increasing the total surface energy. Kinloch et al. have reported that the polar component of the surface energy increases significantly following a corona treatment [12].

As evident in the data of Table 5.5, discrepancies are observed between the values of γ_C and γ_S obtained for the pretreated composite surfaces. Other researchers have reported differences between the two values for a given polymer surface [13]; however, it was felt that the differences observed here were too large to be considered insignificant. Although surface roughness corrections had been made prior to the calculation of surface energy quantities, it was postulated that the roughnesses involved in the peel ply and grit blasted surfaces were too extreme to be corrected for completely, particularly in the case of the channel-like peel ply surface in which a very *regular* pattern of roughness exists.

It was observed for the BMI composites, as was also pointed out for epoxy composites in Section 4.1.3.2, that the discrepancies between the two values characterizing the surface energy seemed to increase in magnitude as the surface roughness of the laminate increased. Figure 5.4 shows a plot of $|\gamma_S - \gamma_C|$, the absolute difference between γ_S and γ_C, plotted against the roughness correction factors R_C listed in Table 5.4. A linear relationship is observed between the magnitude of surface roughness and the difference between the two surface energy values. This supports the speculation that for surfaces with

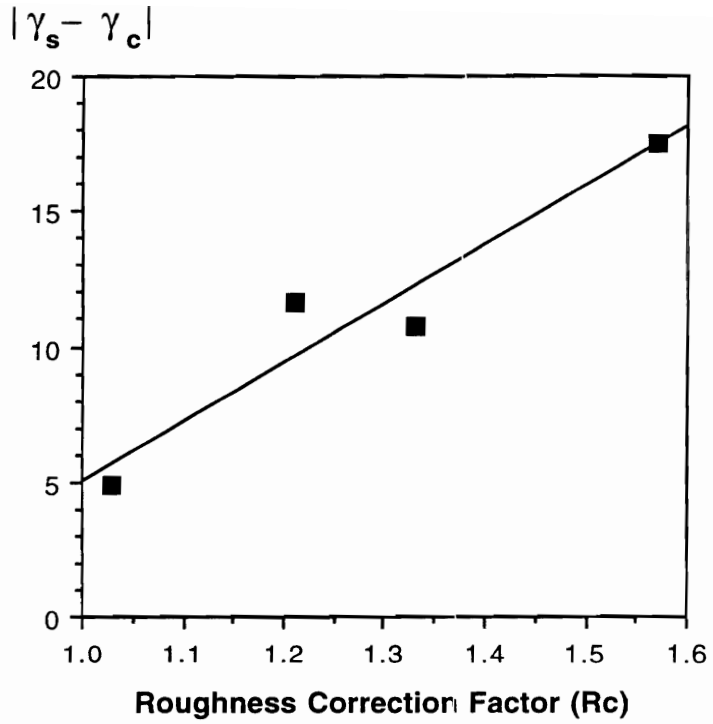

Figure 5.4: Absolute difference between BMI γ_s and γ_c as a function of surface roughness correction factor, R_C.

exaggerated roughness patterns, application of commonly used techniques to determine surface energy values may lead to considerable errors.

Good correlation is observed between the surface energy and the total atomic concentration of the polar matrix elements oxygen and nitrogen on the composite surface. Figure 5.5 shows that the total surface energy increases in a linear manner with increasing concentration of oxygen and nitrogen. Thus, it appears that higher concentrations of polar elements on the composite surface lead to increased surface energies.

5.1.3.3 Wettability Measurements

The wettability of an adherend surface is of utmost importance in the fabrication of a strong, durable bond. In order for intimate molecular contact to be established at the interface, the adhesive must completely spread over the surface, displacing air and contaminants [14]. This condition is met only when the contact angle of the substance of interest is low or close to zero.

Water contact angle data for the pretreated BMI surfaces is shown in Figure 5.6. This analysis shows that the peel ply and grit blasted surfaces exhibit a lower contact angle than the non-wettable, fluorine contaminated as-received surface, and that the 1 minute and 5 minute oxygen plasma treatments reduce the contact angle significantly. The slightly higher value of the 1 minute oxygen plasma-treated surface is attributed to the small quantities of fluorine still present on the surface, as shown by both XPS and ISS.

Because the actual liquid which will be contacting these pretreated composites is a molten epoxy adhesive, it was of interest to measure the contact angles of EPON® 830 on the pretreated composite surfaces. EPON® 830 has a viscosity which is close to the actual minimum viscosity of a BASF epoxy film adhesive during its cure cycle. In comparison to water, EPON® 830 has a higher viscosity and a lower surface tension, and was felt to be a more realistic probe liquid to assess the wettability of the pretreated surfaces.

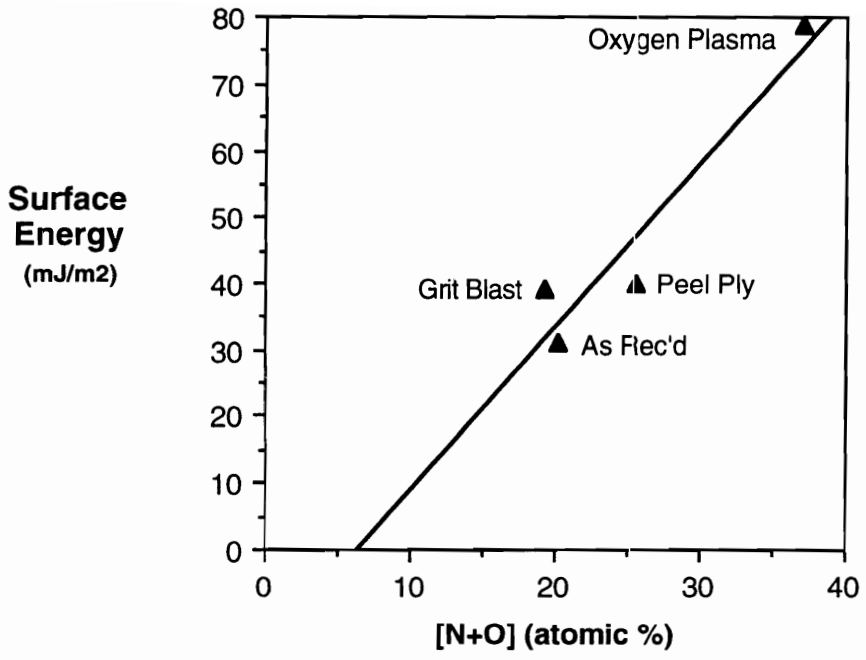

Figure 5.5: Total surface energy γ_s plotted against total XPS atomic concentrations of oxygen and nitrogen.

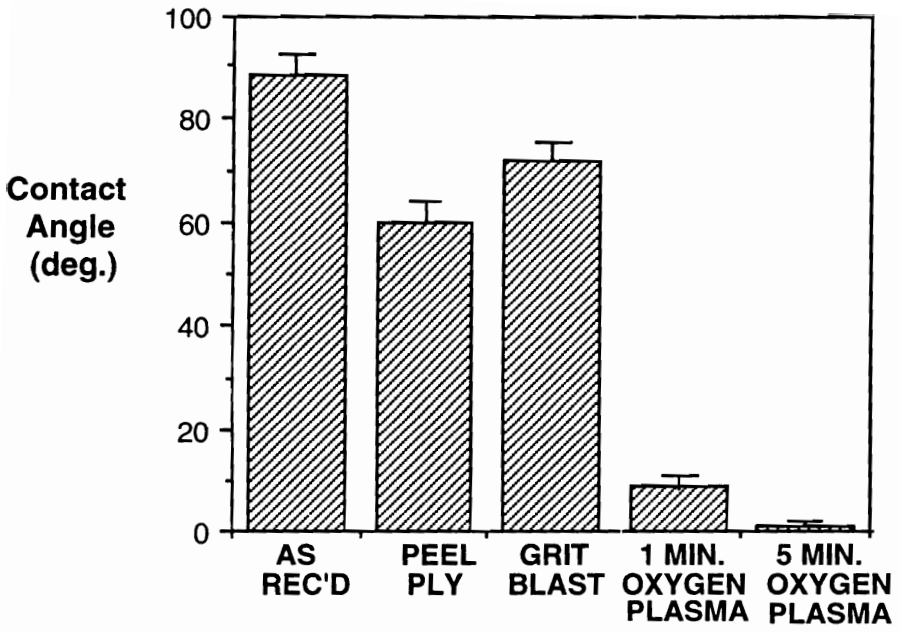

Figure 5.6: Water contact angles on surface pretreated BMI composites.

Turning now to the results of EPON® 830 contact angle analysis shown in Figure 5.7, it is seen that there is now a large difference in the wettability of the as-received surface as compared to the wettability of the oxygen plasma-treated, grit blasted and peel ply surfaces. The latter group of surfaces exhibit very similar wettability behavior when EPON® 830 is used, in contrast to the differences observed in water wettability. This is because the critical surface tension of the as-received surface is lower than both the surface tensions of water and EPON® 830, while the grit blasted and peel ply surfaces have critical surface tensions which fall in between the surface tensions of water and EPON® 830. The oxygen plasma-treated surface alone has a critical surface tension higher than both that of water and EPON® 830, thus it is wetted well by both liquids.

Figure 5.8 shows the final cured contact angles of Metlbond® 1146 on the pretreated BMI composites. This experiment involves the measuring the contact angle of the actual adhesive resin on a surface, which is more realistic than using a low molecular weight liquid or model compound. As observed in the case of EPON® 830, the Metlbond® 1146 contact angle is high on the as-received surfaces, a consequence of the fluorine contamination. All three pretreatments decreased the contact angle of the cured epoxy, indicating that the molten epoxy wet the pretreated surfaces more easily, allowing more contact to be made between the adhesive and the surface.

5.1.4 Profilometry

Surface topography plays an important role in adhesion, due to the fact that the pits, pores or other types of depressions in a surface can provide additional surface for bonding and/or allow mechanical interlocking to take place between substrate and adhesive [15,16]. On the other hand, surface roughness which is too great may allow air to be trapped at the interface, creating stress concentrations in the interphase region of a bond [17]. It is also well-known that the topography of a substrate may also affect the kinetics of wetting;

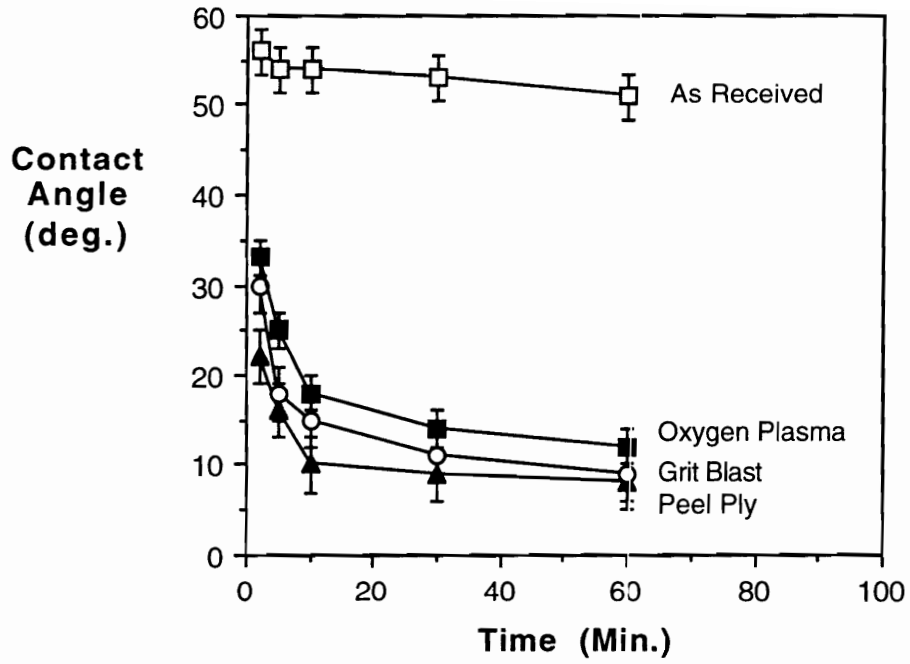

Figure 5.7: EPON® 830 contact angles on surface pretreated BMI composites, measured as a function of time.

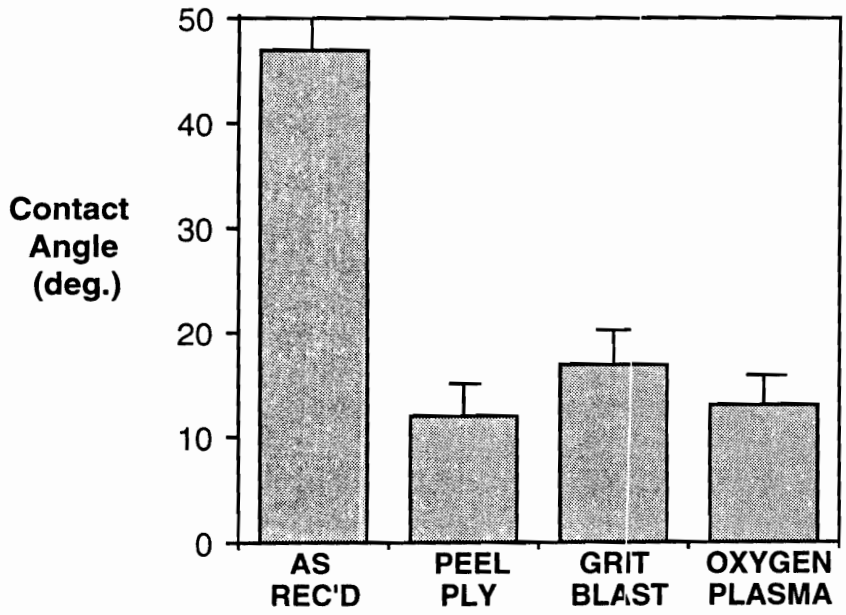

Figure 5.8: Contact angles of cured Metlbond® 1146 resin on pretreated BMI composites.

however, this effect may not be as significant when an adhesive is forcibly spread or pressed onto a surface, as is the case in this work [14].

Profilometer traces for the pretreated surfaces are shown in Figure 5.9. The high fiber content of the BMI laminates causes the fiber bundles from the carbon fiber fabric to be quite visible in the surface. This is evident in the regular, sinusoidal surface profile shown in Figure 5.9(a) for the as-received surface. The peel ply surface profile shown in Figure 5.9(b) is extremely jagged and rough, with peaks occurring in a regular pattern. Figure 5.9(c) shows the grit blasted surface to also possess a great deal of roughness, but unlike the peel ply surface, the peaks occur more randomly. The oxygen plasma-treated surface shown in Figure 5.9(d) is very similar to the as-received surface, but appears to have lost some of the smooth sinusoidal appearance seen in 5.9(a). This may be attributed to an erosion of the surface by the plasma treatment.

Table 5.6 shows the values of R_a and R_z for the pretreated surfaces. As can be deduced from the profilometry traces, the roughest surface is the peel ply surface, followed by the grit blasted surface, the oxygen plasma-treated surface and the as-received surface, in descending order of roughness. This is also the same sequence of roughness as shown by the roughness correction factors (R_C) determined by contact angle analysis.

5.1.5 Scanning Electron Microscopy (SEM)

The surface topography of the composites has thus far been studied by contact angle measurements and profilometry. SEM also provides an actual view of the surfaces before and after pretreatment. Figure 5.10 shows photomicrographs of as-received, peel ply, grit blasted and oxygen plasma-treated BMI composite surfaces.

Figure 5.10(a) shows the fiber bundles which are clearly visible in the surface of the as-received laminate. The resin itself is smooth and relatively featureless at this level of magnification. The composite surface after peel ply removal shown in Figure 5.10(b)

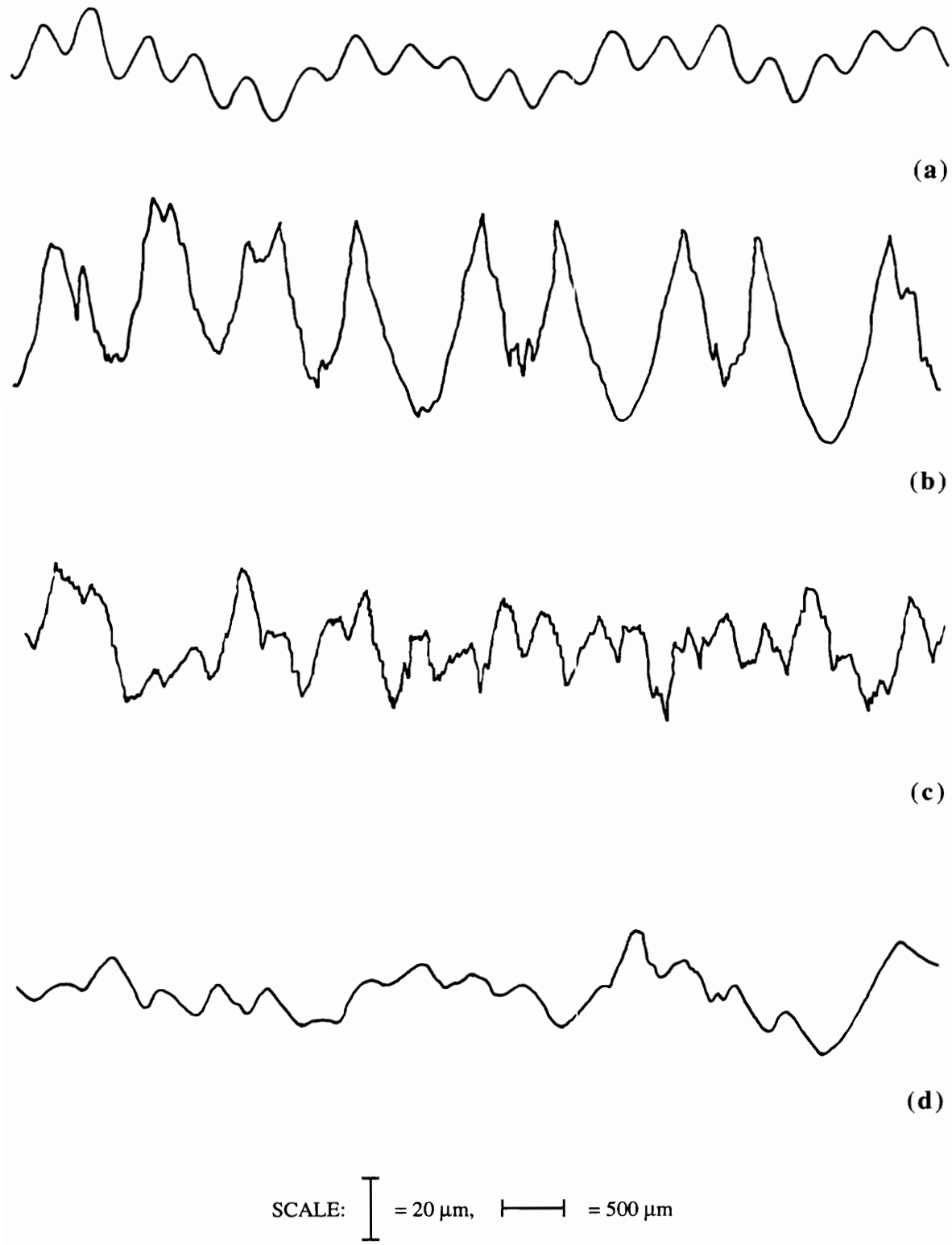

Figure 5.9: Surface profiles of pretreated BMI composite surfaces. (a) As received (b) Peel ply (c) Grit blast (d) 5 minute oxygen plasma.

Table 5.6: BMI composite surface roughnesses measured by profilometry.

	R_a (microns)	R_z (microns)
As Received	4.9 ± 0.2	23.6 ± 2.3
Peel Ply	18.7 ± 2.1	75.6 ± 9.0
Grit Blast	8.3 ± 2.9	45.3 ± 8.3
5 min. Oxygen Plasma	5.6 ± 0.7	29.6 ± 3.8

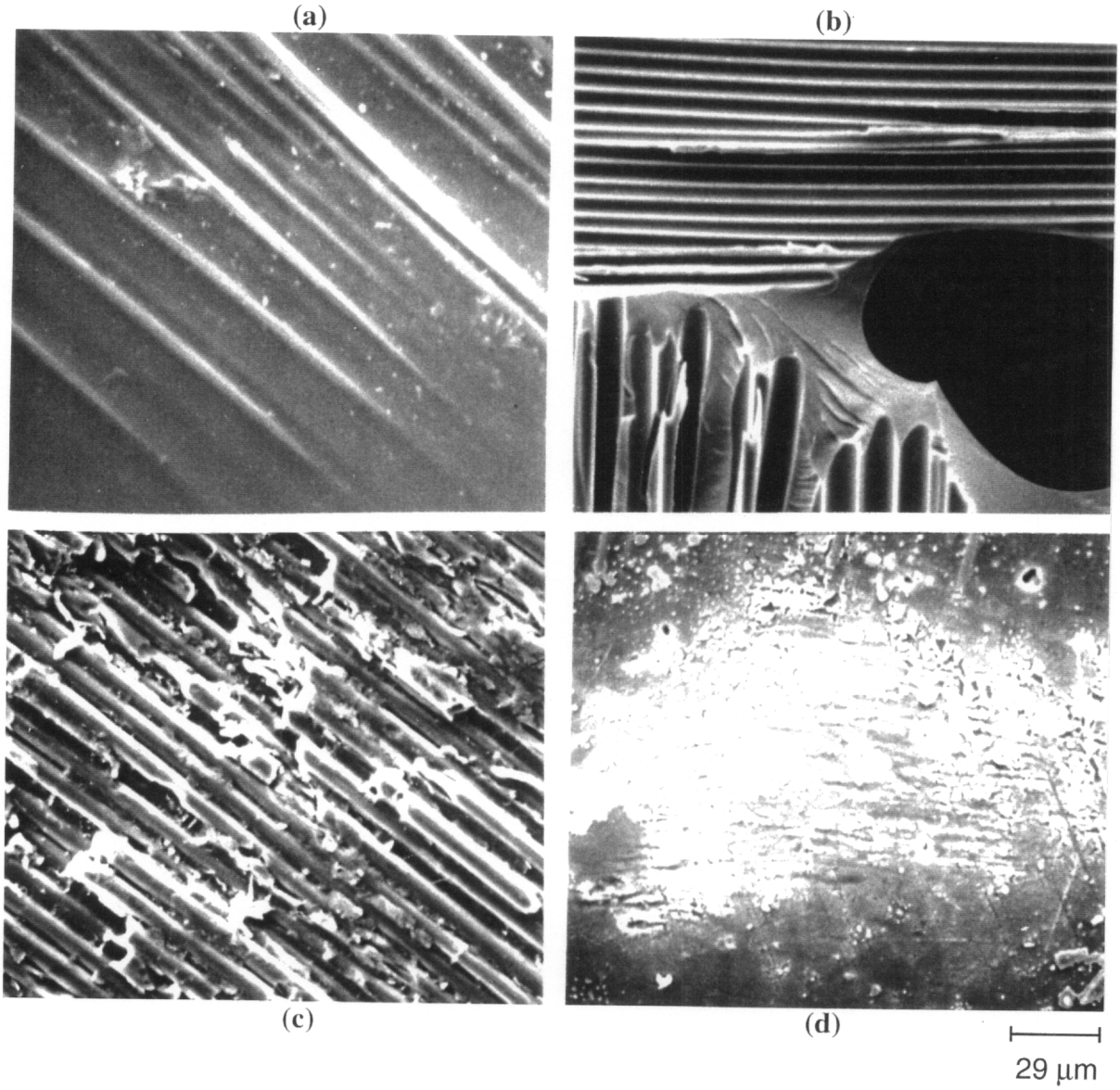

Figure 5.10: SEM photomicrographs of surface pretreated BMI composites. (a) As received (b) Peel ply (c) Grit blast (d) 5 minute oxygen plasma.

clearly shows the imprint left by the peel ply fabric and appears as a pattern of grooves and channels. These grooves and channels may actually facilitate the wetting and spreading of a molten polymer or adhesive. The peel ply appears to have been removed cleanly but the presence of craters indicates that resin fracture and removal has occurred in the surface as a result of peel ply stripping. This was confirmed by SEM analysis of the corresponding peel ply underside, which showed resin globs which matched exactly with the voids in the laminate surface. The grit blasted surface in Figure 5.10(c) shows a significant quantity of bare, exposed fibers, some of which appear to be broken off along their length. Figure 5.10(d) shows abraded patches which resulted from oxygen plasma treatment.

To illustrate the flow of molten adhesive into the surface grooves created by the peel ply fabric, polystyrene pellets were heated above their T_g while in contact with the peel ply surface. Figure 5.11(b) shows the underside of polystyrene pellet which was pressed against the peel ply surface while above its glass transition temperature. The appearance of the polystyrene pellet is virtually identical to the peel ply fabric which created the original surface topography shown in Figure 5.11(a), indicating that the polystyrene had indeed filled the channels and grooves.

Figure 5.12 documents the effect of oxygen plasma exposure time. Not much change is observed at 1 minute of plasma treatment at 50 watts. As the treatment time increases to 5 minutes, shallow abraded patches similar to those shown in Figure 5.10(d) between to appear between fiber bundles. At 10 minutes, the abraded patches begin to increase in prominence. After 20 minutes of treatment, the entire area of resin between fiber bundles appears to have been etched away entirely.

Figure 5.13 shows the effect of oxygen plasma power. No significant changes are seen to occur at 1 minute/10 watts of treatment. At 50, 100 and 150 watts, abraded patches become visible. However, there is really no change in the degree of abrasion as a function

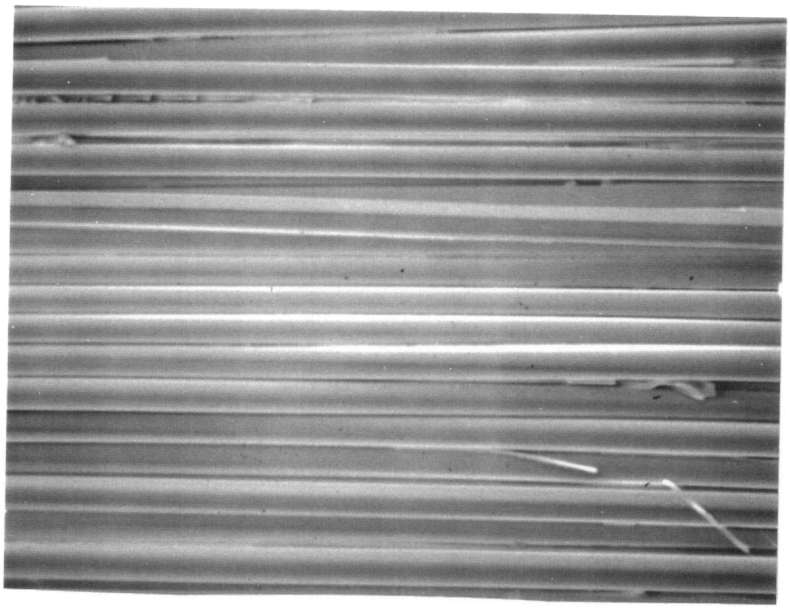

(a)

20 μm

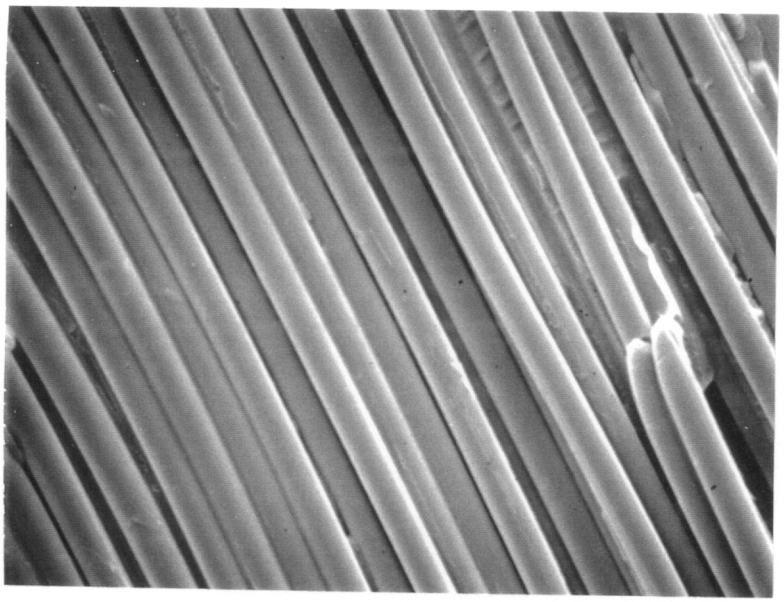

(b)

20 μm

Figure 5.11: SEM photomicrographs of (a) BMI peel ply fabric, and (b) underside of polystyrene pellet which had melted while in contact with BMI peel ply surface, illustrating polymer flow into channels and grooves.

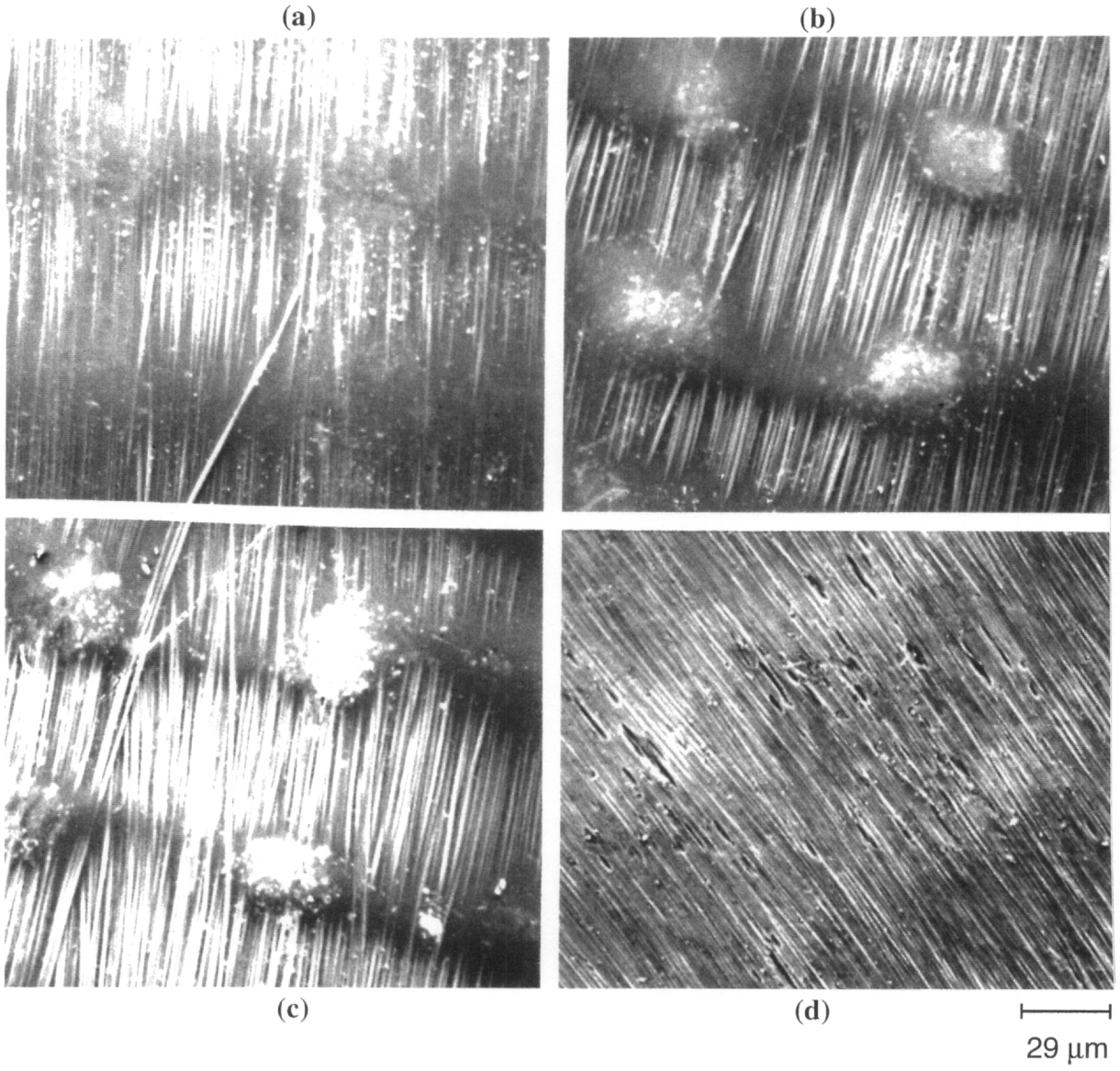

Figure 5.12: SEM photomicrographs of surface pretreated BMI composites, showing effect of oxygen plasma treatment time. Plasma power was held constant at 50 watts. (a) 1 minute. (b) 5 minutes (c) 10 minutes (d) 20 minutes.

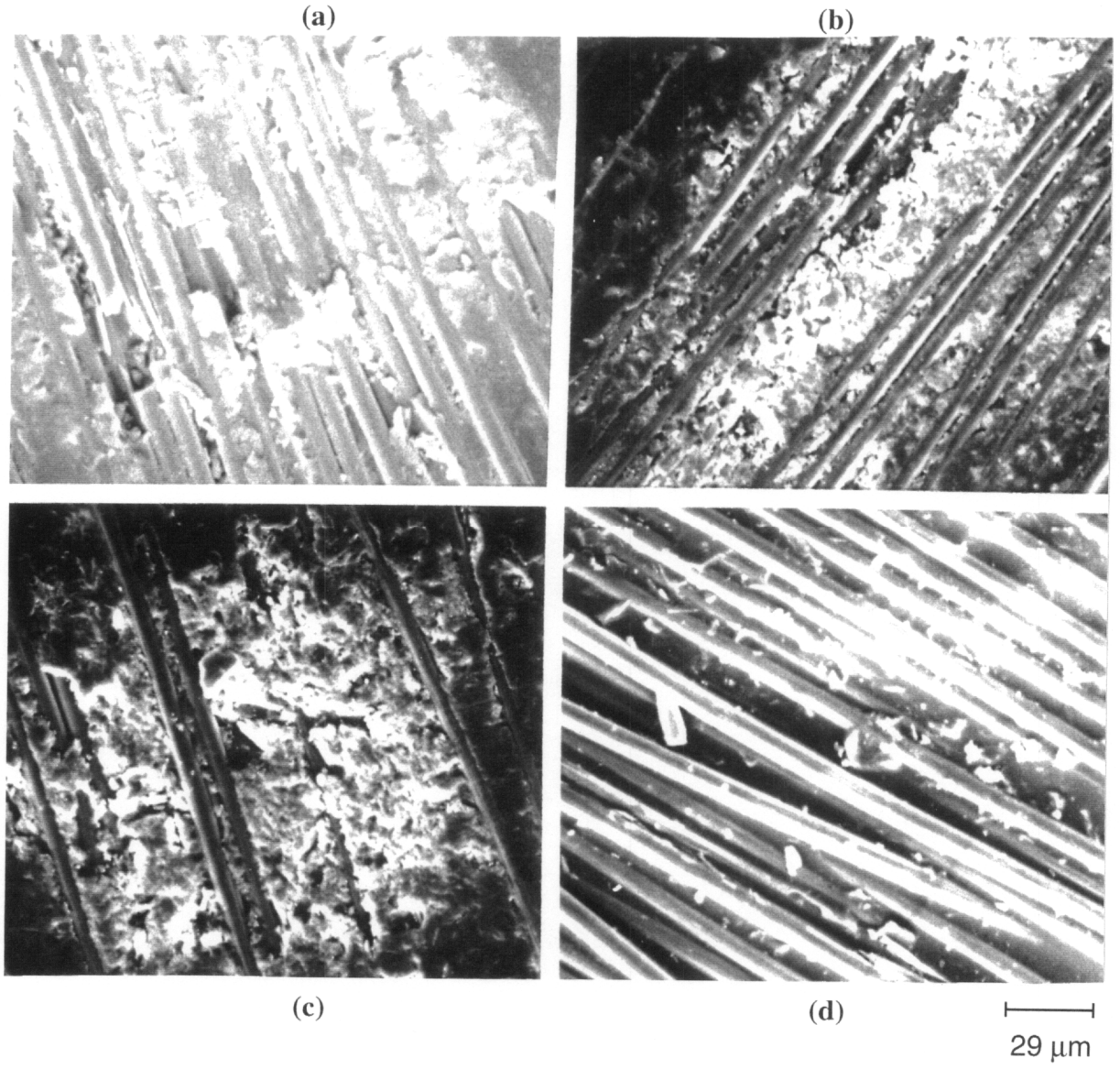

Figure 5.13: SEM photomicrographs showing effect of oxygen plasma power on BMI composites, treatment time held constant at 1 minute. (a) 10 watts (b) 50 watts (c) 100 watts (d) 150 watts.

of increasing power at the exposure times utilized. It might be expected that increasing the treatment time would better differentiate between the power levels utilized.

5.1.6 Diffuse Reflectance Infrared Spectroscopy (DRIFT)

In recent years, DRIFT has become more widely used for the analysis of composite materials. Figure 5.14 shows the DRIFT spectrum of an as-received BMI composite surface. An O-H stretching peak is seen at 3500 cm^{-1}, C-H stretching is evident at 2960 and 2935 cm^{-1}. Interestingly, these C-H vibrations are characteristic of *aliphatic* compounds. Imide carbonyl stretching is observed at 1787 and 1732 cm^{-1}, with C-N or C-O stretching peaks present at 1270 cm^{-1}.

It was intended to utilize DRIFT to provide molecular information on the pretreated surfaces, in order to complement the atomic information obtained XPS analysis . Although the DRIFT spectrum of the as-received composite surface was relatively straightforward to obtain, it was not successful in revealing changes in the surface composition induced by surface treatment. Carrying out the various surface pretreatments changed the optical properties of the composite surfaces, which often caused spectral distortions and peak shifts to occur. Although an oxygen plasma treatment did not drastically change the optical appearance of the surface, no apparent changes in the surface regions could be detected by this technique.

Although the exact depth of DRIFT sampling is not well-defined, Culler et al. found that peaks from poly (ethylene terephthalate) were visible beneath a 1.5 μm film of poly(vinylidene fluoride) [18]. This is certainly a much deeper sampling depth than encountered with either XPS or ISS. Cole et al. carried out DRIFT analysis of carbon fiber-reinforced epoxy composite and prepreg [19]. They concluded that poor spectral reproducibility and spectral distortion due to front-surface reflection prevented DRIFT from being suitable as a quantitative infrared technique.

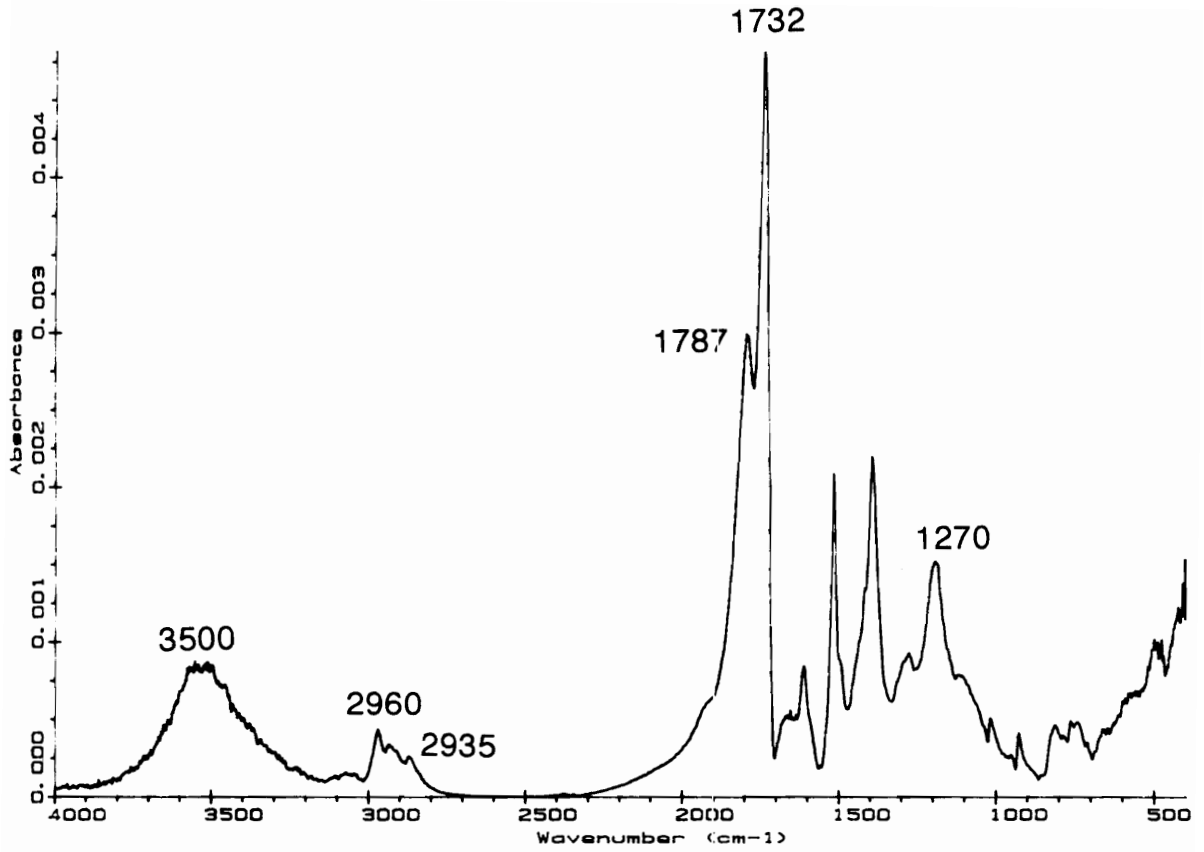

Figure 5.14: DRIFT spectrum of an as-received BMI composite surface.

5.2 Analysis of Bonded Specimens

5.2.1 Double Lap Shear Testing

The double lap shear strengths of the pretreated BMI composites bonded with Metlbond® 1146 are summarized in Table 5.7. The ambient temperature results show that the bond strengths of the as-received laminates are low, a result which can be directly attributed to the presence of a poorly wetted, fluorine-contaminated surface.

The peel ply pretreatment exhibited the highest lap shear strengths under all testing conditions, followed closely by the oxygen plasma-treated specimens. It had been predicted by other researchers that the roughness of the peel ply surface may entrap air and degrade bond strength and durability [20]; this is evidently not the case in this study. The channels and grooves left behind in the surface following peel ply removal could assist in wetting and spreading of the adhesive by allowing "wicking" to occur. Although the oxygen plasma-treated surface had the highest critical surface tension of all the pretreated composites, the bond strengths which are obtained are not vastly superior to the other pretreatments. Oxygen plasma and the peel ply treatments show the highest two bond strengths when tested at elevated temperature and following environmental exposure.

For the BMI composite under all three testing conditions, grit blasting was observed to decrease bond strengths, even below the level of the as-received controls. The reason for the decrease in bond strength due to grit blasting is yet unknown, but could be due to the damage in the composite surfaces produced by the abrasive grit used. Weak boundary layers composed of loosely held broken fibers and matrix resin residue could also contribute to decreased adhesion. Moyer and Wightman reported room temperature single lap shear results for grit blasted LaRC-160 specimens which were lower than the solvent-wiped controls [21].

A decrease in bond strengths was observed for all surface pretreatments in testing at 82°C. This could be due to changes in the mechanical properties of either the adherends or

Table 5.7: Double lap shear strengths of surface pretreated BMI composites bonded with Metlbond® 1146 (in MPa).

Pretreatment	Ambient	82°C Dry	82°C Wet
As Received	14.6 ± 2.1	9.3 ± 0.5	7.0 ± 1.0
Peel Ply	21.8 ± 0.4	11.2 ± 1.2	9.6 ± 1.8
Grit Blast	10.9 ± 0.3	7.0 ± 0.5	6.0 ± 0.5
Oxygen Plasma	19.8 ± 0.3	10.7 ± 0.9	7.7 ± 1.2

the adhesive at elevated temperature, although 82°C does not exceed or even come close to the glass transition temperatures of either the BMI composite or the adhesive. Parker has also documented that joint strengths of composite-to-composite bonds decrease with increasing temperature even below the glass transition temperature [22]. A decrease in bond strength is observed between the samples tested at 82°C and those tested at 82°C following environmental exposure, an indication that moisture can be detrimental to bond strength in this system.

Table 5.8 shows the amount of moisture absorbed by the lap shear joints during the 30 day exposure to 71°C (160°F)/100% relative humidity conditions. Overall, the relative weight gains of 0.6-1.5% are low, indicating that the particular composite/adhesive combinations studied are not overly susceptible to water ingress.

Scanning electron microscopy (SEM) analysis of the failure surfaces, summarized in Table 5.9, shows that in addition to failing cohesively in the adhesive and in the laminate, the as-received BMI joints exhibited a large amount of interfacial failure which was not observed for any other pretreatment. Failure in the peel ply, grit blasted and oxygen plasma-treated specimens was observed to occur cohesively in the adhesive as well as in the laminate; no evidence of interfacial debonding was observed even after environmental conditioning. There was also no significant change in the mode(s) of failure under the various test conditions.

Kinloch and coworkers calculated work of adhesion values for metal/adhesive bonds and found that these values are negative in the presence of water. This implies that spontaneous, interfacial debonding of metal adherends should take place under wet conditions. However, in the case of polymer substrates, the calculated work of adhesion is positive even in the presence of moisture [23]. The surface energy of a polymer is also much less than that of a metal or metal oxide surface, thus there is less of a driving force for water to seek out the interface and initiate interfacial debonding. Thus, interfacial

Table 5.8: Weight gain in double lap shear joints bonded with Metlbond® 1146, following 30 days in a 71°C/100% RH environment.

Pretreatment	**% Change**
As Received	+ 0.8
Peel Ply	+ 0.6
Grit Blast	+ 1.5
Oxygen Plasma	+ 1.0

Table 5.9: SEM analysis of failure modes in BMI double lap shear joints bonded with Metlbond® 1146.

Pretreatment	Predominant Mode of Failure
As Received	interfacial, adhesive, laminate
Peel Ply	adhesive, laminate
Grit Blast	adhesive, laminate
Oxygen Plasma	adhesive, laminate

failure in composite bonds under hot/wet conditions is not usually observed for properly prepared surfaces .

5.2.2 Wedge Testing

Figure 5.15 shows the initial crack lengths for the BMI wedge specimens. The initial cracks for the BMI laminates bonded with Metlbond® 1146, shown in Figure 5.15, reveal that the difference in average crack length between the as-received surface and the other pretreated samples is only on the order of 3-4 mm, compared to the greater than 20 mm difference observed with the epoxy laminates. These small differences re not statistically significant in light of the magnitude of the standard deviations involved, which are on the order of 3-5 mm. This insensitivity could be due to the fact that the surface energy of the as-received BMI laminate is not as low as would be expected for a fluorine-contaminated surface, and may be more forgiving toward an adhesive. As also observed for the epoxy laminates, there are no significant differences between the initial crack lengths for the oxygen plasma, grit blast and peel ply samples.

Crack growth for samples in a dry 75°C environment is shown in Figure 5.16. Under this testing condition, no significant crack growth is observed. For each surface pretreatment, the crack only grows an additional 2-4 mm before reaching a plateau value. Testing was carried out beyond 1000 hours with no observations of continued crack growth. These studies in a 75°C environment show that BMI laminates have good durability at elevated temperature when bonded with Metlbond® 1146.

The situation changes when the testing is carried out in a 75°C wet environment, as shown in Figure 5.17. The as-received samples show a large increase in crack length as a function of exposure time, and the grit blasted surface also shows greater crack extension when compared to the oxygen plasma and peel ply samples. It can be concluded that the combined effect of temperature and moisture is much more damaging to these adhesively

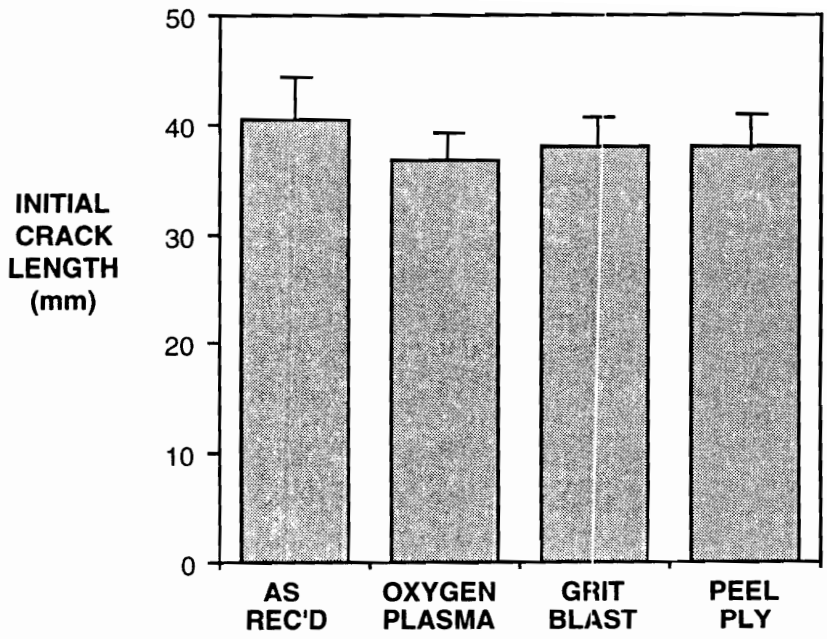

Figure 5.15: Initial crack lengths for surface pretreated BMI wedge samples bonded with Metlbond® 1146.

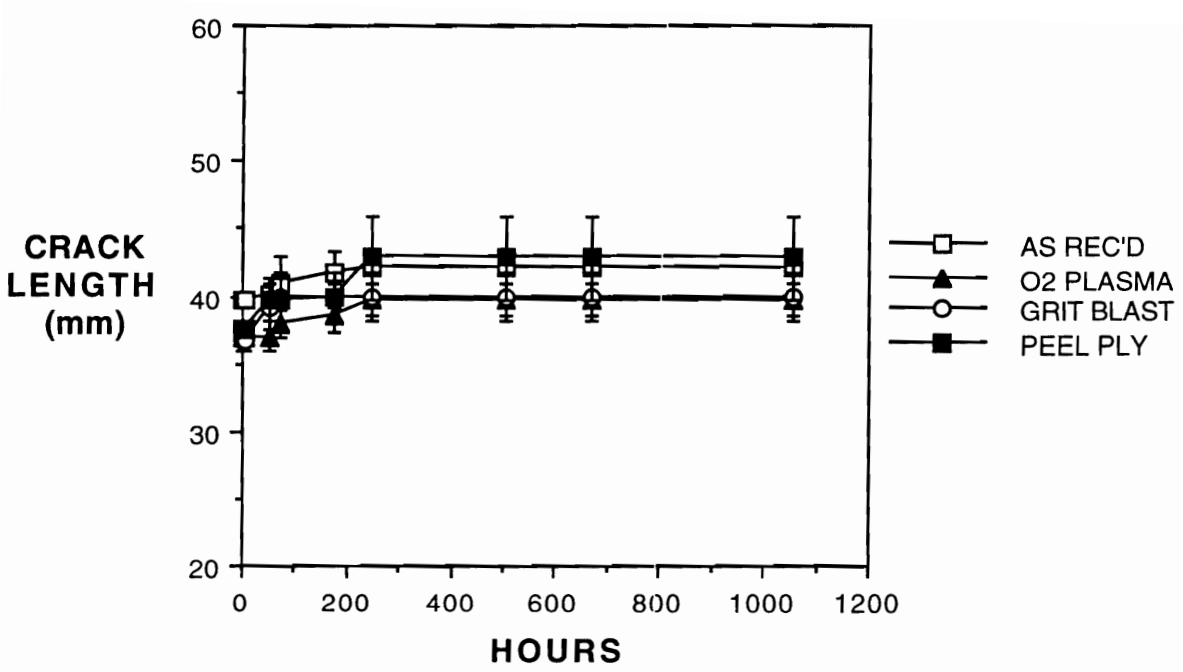

Figure 5.16: Crack growth in surface pretreated BMI wedge samples bonded with Metlbond® 1146 , monitored as a function of time at 75°C.

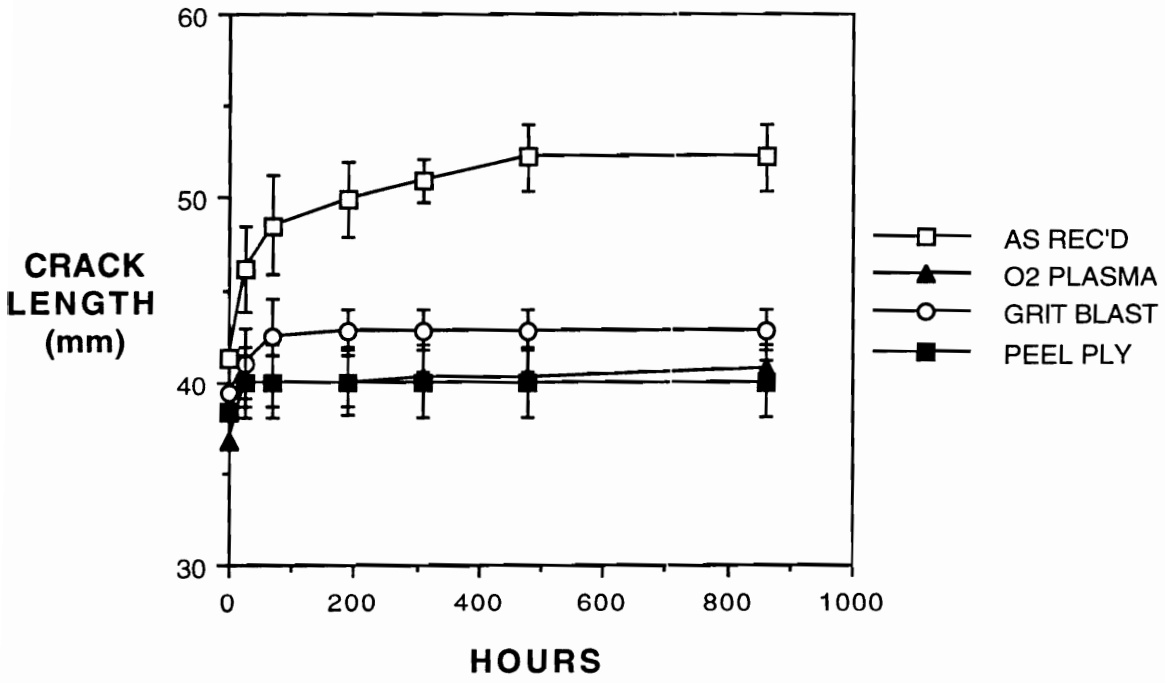

Figure 5.17: Crack growth in surface pretreated BMI wedge samples bonded with Metlbond® 1146, monitored as a function of time in 75°C water.

bonded composites than temperature alone. This is, of course, a widely-held conclusion in adhesion science.

Figure 5.18 shows crack propagation for BMI wedge specimens in boiling water. Cracks in the as-received BMI wedges grew rapidly and the entire joint debonded prior to the end of the test. The remaining surface treatments also exhibited significant crack growth; grit blasting was not seen here to be particularly detrimental to crack durability. Boiling water is seen to be a very harsh environment for composite bonds, in which all samples showed large crack extensions. As reported earlier, a 75°C dry environment did not promote any additional crack growth beyond the initial crack regardless of surface pretreatment, whereas 75°C water was capable of differentiating between the durable bonds resulting from peel ply and oxygen plasma treatments and less durable bonds formed by bonding as-received and grit blasted surfaces.

Immersion of the wedge specimens in aircraft de-icing fluid is illustrated in Figure 5.19. This environment was initially anticipated to be a corrosive one which would be encountered by composite materials in aircraft applications. However, the effect of de-icing fluid on the composite joints was minimal. For the BMI composites, only the as-received specimens exhibited additional crack growth beyond the initial crack, which was on the order of 10 mm after 1750 hours. It is therefore concluded that the combination of organic compounds present in aircraft de-icing fluid is not particularly detrimental to properly prepared composite bonds at room temperature.

Table 5.10 summarizes the modes of failure for the BMI wedge specimens. The as-received samples showed predominantly interfacial failure between the composite surface and the adhesive, whereas all other pretreatments exhibited varying degrees of cohesive failure in the adhesive and the laminate. This result points out the detrimental effect of surface contamination on bond performance and is also consistent with the

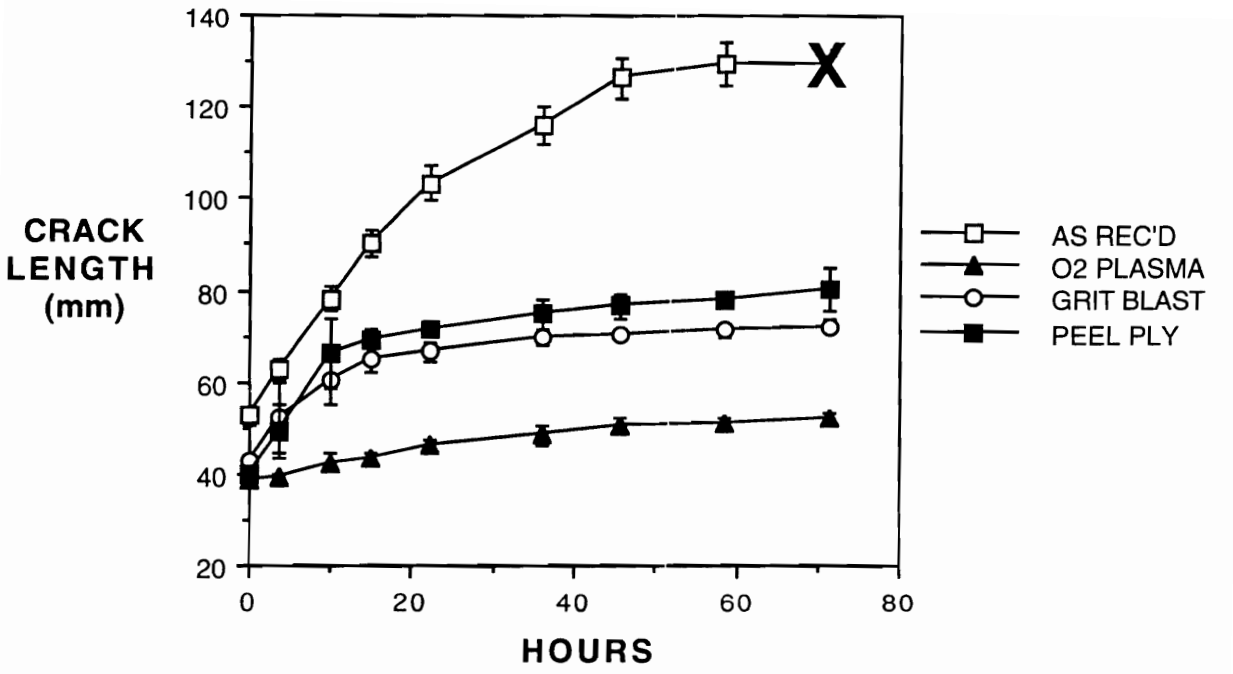

Figure 5.18: Crack growth in surface pretreated BMI wedge samples bonded with Metlbond® 1146, monitored as a function of time in 100°C water (**X** - indicates complete debonding).

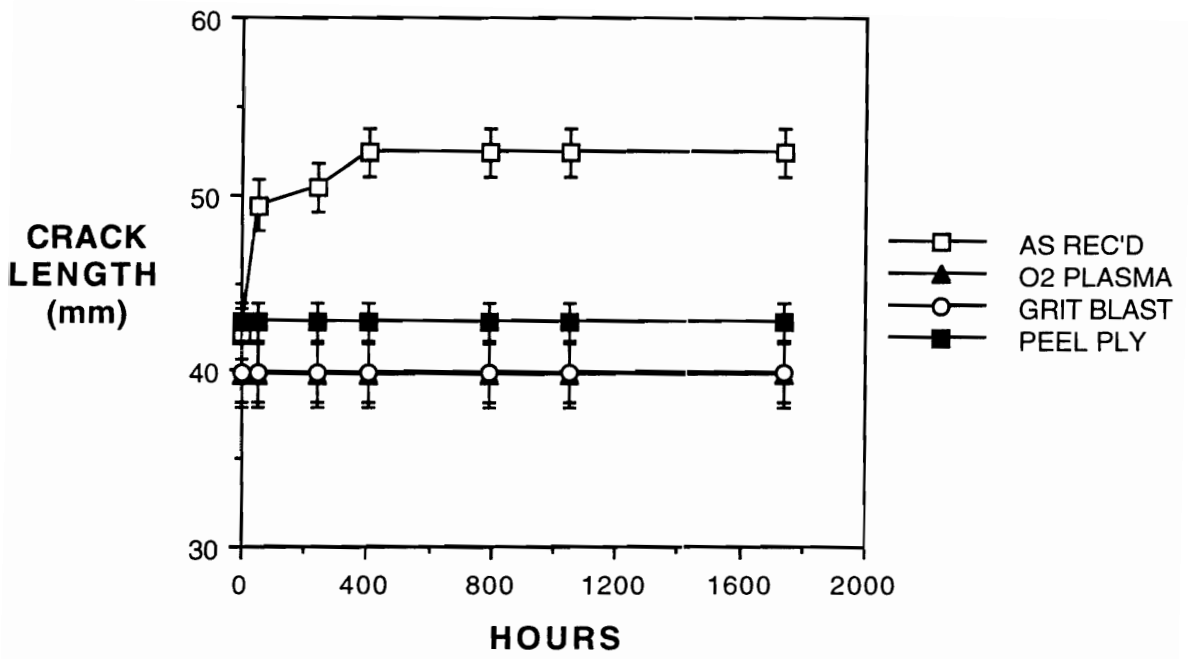

Figure 5.19: Crack growth in surface pretreated BMI wedge samples bonded with Metlbond® 1146, monitored as a function of time in aircraft de-icing fluid.

Table 5.10: Predominant modes of failure for surface pretreated BMI wedge samples, bonded with Metlbond® 1146.

Pretreatment	Initial Crack	75°C Dry	75°C Wet	100°C Wet	De-icing Fluid
As Received	50% I, 50% L	I	I	I	I
Oxygen Plasma	L	L	A	A	---
Grit Blast	L	L	A	A	---
Peel Ply	50% A, 50% L	L	A	A	---

I = interfacial between adhesive and composite; A = cohesive in adhesive; L = cohesive in laminate

prediction that well-prepared composite/composite bonds should not fail interfacially even under hot/wet conditions.

5.2.3 Scanning Acoustic Microscopy (SAM)

Scanning Acoustic Microscopy (SAM) is a technique which shows great promise for the nondestructive evaluation of adhesively bonded samples. The SAM technique utilizes a focused beam of high frequency ultrasonic waves to analyze the sample, resulting in a map which reflects the variation in acoustic reflectivity arising from voids and differing material densities. SAM has already been shown to be successful in locating flaws within composite materials and within bondlines of metals bonded to other metals [24]. The objective of this series of experiments was to determine if debonded regions could be detected in 8-ply BMI laminates bonded with Metlbond® 1146.

Figure 5.20 shows SAM micrographs of surface pretreated BMI bonds. A number of bright white debonded areas are observed in each micrograph, which stand out above the diffuse scattering from the fibers. Figure 5.21 shows the percentage of the total analyzed area which is debonded. For the BMI composite, the grit blasted surface shows a higher level of debonding relative to the other pretreatments. The oxygen plasma surface also showing a slightly higher percent debonding, the reason for this being unclear. It is significant, however, that the grit blast surface treatment shows greater debonded areas and has also been observed to result in poorer initial strength and bond durability.

5.3 Conclusions

Significant changes in the chemistry and topography of the BMI composites were observed following surface preparation by grit blasting, plasma treatment and peel ply. A MEK solvent wipe was determined to have negligible effect on surface chemistry and the

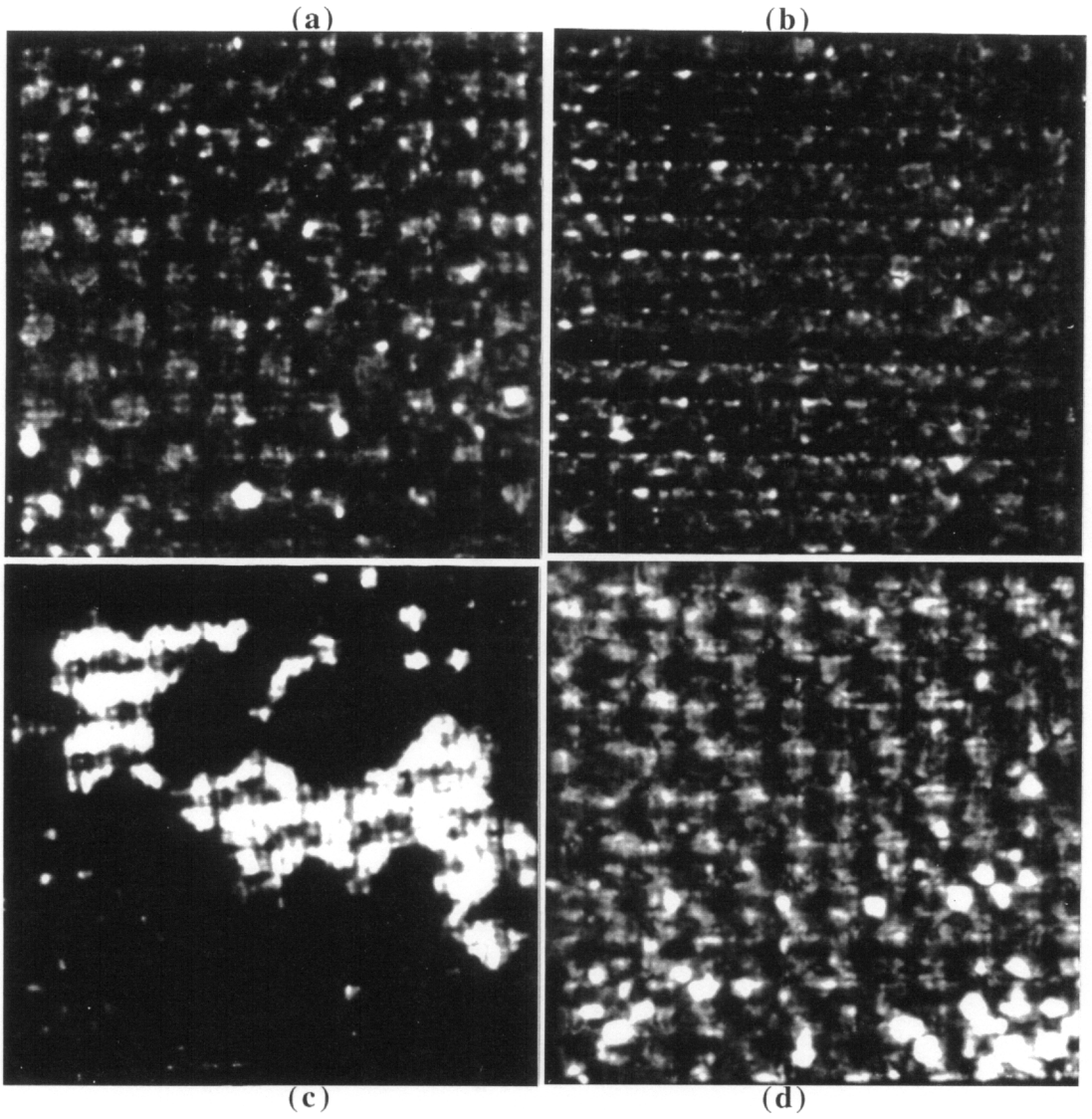

Figure 5.20: Acoustic micrographs of surface pretreated 8-ply BMI composites bonded with Metlbond® 1146. (a) As received (b) Peel ply (c) Grit blast (d) Oxygen plasma.

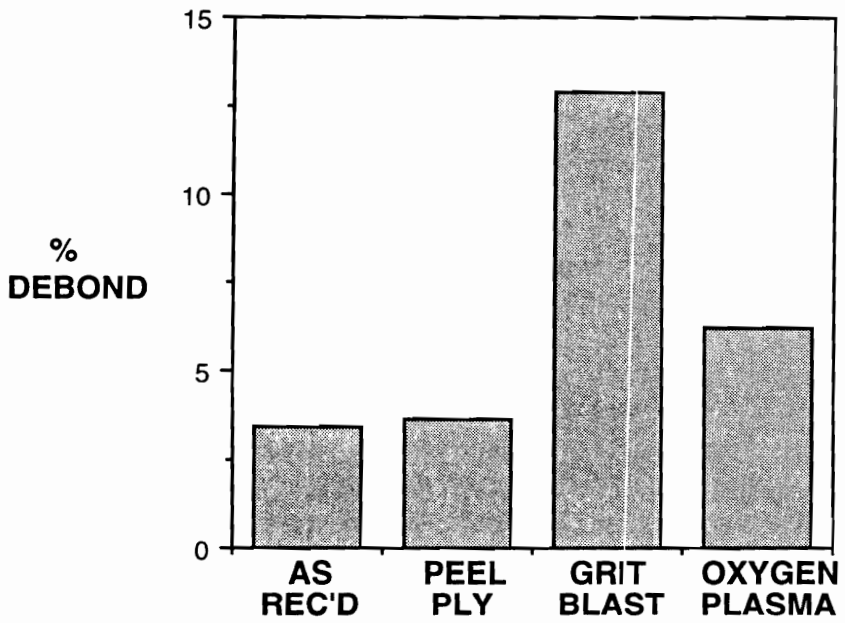

Figure 5.21: Percentage of debonded area in BMI composites bonded with Metlbond® 1146, calculated from scanning acoustic micrographs.

removal of processing contamination. Grit blasting and oxygen plasma treatment were successful in removing fluoropolymer release film residues, while the use of a peel ply prevented the fluoropolymer initial contamination from occurring. Oxygen plasma treatment also provided additional benefit in increasing the oxygen concentration in the composite, thus ensuring a highly polar and wettable surface for bonding. The surface energies of the grit blasted, oxygen plasma-treated and peel ply surfaces were increased relative to the as-received control, due to the absence of the fluoropolymer contamination. Although the oxygen plasma-treated surface had the highest surface energy, it was not wetted to any greater extent by epoxy resin than the peel ply or grit blasted surface.

The roughness of the peel ply and grit blasted surfaces was significantly greater than those of the as-received and oxygen plasma-treated surfaces. Initial bond strengths were not adversely affected by this roughness in the peel ply surface. However, the surface damage induced by the grit blast treatment was extensive and is postulated to decrease the initial bond strength as well as hot/wet durability. Surface contamination had a detrimental effect on both lap shear strength and wedge durability. Oxygen plasma-treated and peel ply surfaces, although dissimilar in surface chemistry and topography, were found to yield good initial strength as well as resistance to hot/wet environments.

5.4 References

1. H.J. Leary and D.S. Campbell, *Surf. Interface Anal.*, **1**(3), 75 (1979).
2. L.W. Crane, C.L. Hamermesh and L. Maus, *SAMPE J.*, **12**(2), 6 (1976).
3. J.W. Chin and J.P. Wightman, *J. Adhesion*, **36**, 25 (1991).
4. W.A. Zisman in *Advances in Chemistry,* **43**, F.M. Fowkes, ed., chap. 1 (American Chemical Society, Washington D.C., 1964).
5. S. Wu, *J. Colloid Interface Sci.*, **71**(3), 605 (1979).
6. R.J. Good, *J. Adhesion Sci. Technol.*, **6**(12), 1269 (1992).

7. J. Vial and A. Carre, *Int. J. Adhes. Adhes.*, **11**(3), 140 (1991).
8. T. Hata, Y. Kitazaki and T. Saito, *J. Adhesion*, **21**, 177 (1987).
9. H. Schonhorn, H.L. Frisch and G.L. Gaines, *Polym. Eng. Sci.*, **17**(7), 440 (1977).
10. D. H. Kaelble, *Physical Chemistry of Adhesion* (Wiley-Interscience, New York, 1971).
11. P.J. Dynes and D.H. Kaelble, *J. Adhesion*, **6**, 195 (1974).
12. A. J. Kinloch, G. K. A. Kodokian and J. F. Watts, *J. Mater. Sci. Lett.*, **10**, 815 (1991).
13. D.K. Owens and R.C. Wendt, *J. Appl. Polym. Sci.*, **13**, 1741 (1969).
14. A.J. Kinloch, *J. Mater. Sci.*, **15**, 2141 (1980).
15. D.E. Packham in *Adhesion Aspects of Polymeric Coatings*, K.L. Mittal, ed. (Plenum Press, New York, 1983).
16. D.J. Arrowsmith, *Trans. Inst. Met. Finish.*, **48**, 88 (1970).
17. W.A. Zisman, *Ind. Eng. Chem.*, **55**(10), 19 (1963).
18. S.R. Culler, M.T. McKenzie, L.J. Fina, H. Ishida and J.L. Koenig, *Appl. Spectrosc.*, **36**(6), 791 (1984).
19. K.C. Cole, A. Pilon, D. Noel, J.-J. Hechler, A. Chouliotis and K.C. Overbury, *Appl. Spectrosc.*, **42**(5), 761 (1988).
20. A.V. Pocius and R.P. Wenz, *Proceedings of the 30th National SAMPE Symposium,* 1073 (1985).
21. D.J.D. Moyer and J.P. Wightman, *Surf. Interface Anal.*, **17**, 457 (1991).
22. B.M. Parker, *Compos. Struct.*, **6**, 123 (1986) .
23. A.J. Kinloch in *Polymer Surfaces and Interfaces,* W.J. Feast and H.S. Munro, eds. (John Wiley and Sons, New York, 1987).
24. M.H. McCord and J.C. Duke, Jr., *Proceedings of the 15th Annual Meeting of the Adhesion Society*, 1992, p. 71.

Chapter VI: Results and Discussion

Effect of Surface Functionality on Bond Strength and Durability

In describing the phenomenon of adhesion, mechanical interlocking and molecular interactions are often cited as possible mechanisms for achieving a strong bond. It is relatively simple to conceptualize the penetration of an adhesive into a roughened surface containing interstitial spaces; envisioning interactions between chemical moieties on surfaces and in adhesives is not as straightforward. The use of gas plasma treatments in this work allowed a variety of surface chemistries to be obtained without any significant change in surface topography. Therefore, the focus of this section is concerned with the effect of surface chemical functionality on adhesive bond strength and durability.

One objective in this study was to separate the cleaning versus the chemical functionalization effects of gas plasma treatment. As discussed in Sections 4.1.1 and 5.1.1, oxygen plasma simultaneously removed fluorocpolymer contamination and increased the oxygen concentration in both epoxy and BMI composites, thus making it difficult to ascertain which effect was responsible for the observed improvement in lap shear strength and wedge durability. The second objective was to determine if additional surface chemical functionality served any beneficial purpose when coupled with a strong mechanical interlocking mechanism as is present in the peel ply surfaces.

To carry out these objectives, it was desired to obtain surfaces with distinctly different chemical functionalities while maintaining the same surface topography. These studies were carried out on the peel ply surfaces, which represented model surfaces free of extraneous contamination and possessing a controlled, regular level of roughness. As described in detail in Section 3.5.1 of the Experimental chapter, Figure 3.5 shows how the original peel ply surface can be transformed into one with a different surface chemistry. It

is expected that these studies will reveal the effect of surface chemistry on initial bond strength as well as bond durability.

6.1 Surface Analysis

X-ray photoelectron spectroscopy (XPS) analysis was carried out on the functionalized surfaces to establish the surface chemistries which were present. Tables 6.1 and 6.2 show the XPS results for both the functionalized epoxy and BMI laminates. As would be expected, the fluorinated peel ply shows a large concentration of fluorine on the surface. Most of the original surface is masked by the mold release agent, as evidenced by the very low nitrogen concentrations on both the epoxy and BMI surfaces. The oxygen plasma-treated epoxy surface shows a more than two-fold increase in oxygen concentration relative to the original peel ply surface. The ammonia plasma-treated epoxy actually shows a decrease in oxygen concentration, and only a small increase in the concentration of nitrogen. Similar XPS results were observed for the functionalized BMI peel ply surfaces.

The wettability of the functionalized surfaces was assessed by various probe liquids. The results of water contact angle analysis are shown in Figures 6.1 and 6.2, with similar results being observed for both epoxy and BMI surfaces. The expected high contact angle, greater than 90°, is observed for the fluorinated surfaces. The original epoxy and BMI peel ply surfaces show a lower water contact angle, but are not characterized as hydrophilic surfaces. Following a 5 minute oxygen plasma, the contact angle of water on the peel ply surfaces is essentially zero, indicating complete wettability. A 5 minute ammonia plasma-treated surface exhibits a lower contact angle than the original and fluorinated surfaces, but is not nearly as wettable as the oxygen plasma-treated surface. These results show that the increase in surface energy and wettability resulting from plasma treatment is predominantly due to the chemical functionalization effect of plasma and that the removal of fluorine plays a more minor role in the energy increase.

Table 6.1: XPS atomic concentrations of functionalized epoxy peel ply surfaces.

	ATOMIC CONCENTRATION (%)						
	C	**O**	**N**	**F**	**S**	**Si**	**Na**
Original Peel Ply	77.3	14.6	7.5	---	0.6	---	---
Fluorinated	28.9	1.6	1.4	68.3	---	---	---
5 min. Oxygen Plasma	48.4	37.8	8.1	---	4.0	1.7	---
5 min. Ammonia Plasma	81.1	8.9	8.9	---	0.7	---	0.4

Table 6.2: XPS atomic concentrations of functionalized BMI peel ply surfaces.

	ATOMIC CONCENTRATION (%)							
	C	**O**	**N**	**F**	**S**	**Si**	**Na**	**Ca**
Original Peel Ply	74.0	16.0	9.6	---	---	0.4	---	---
Fluorinated	29.8	0.7	1.0	68.5	---	---	---	---
5 min. Oxygen Plasma	60.9	29.5	7.4	---	0.3	0.5	0.8	0.6
5 min. Ammonia Plasma	75.6	12.0	9.2	---	0.4	0.9	1.0	0.9

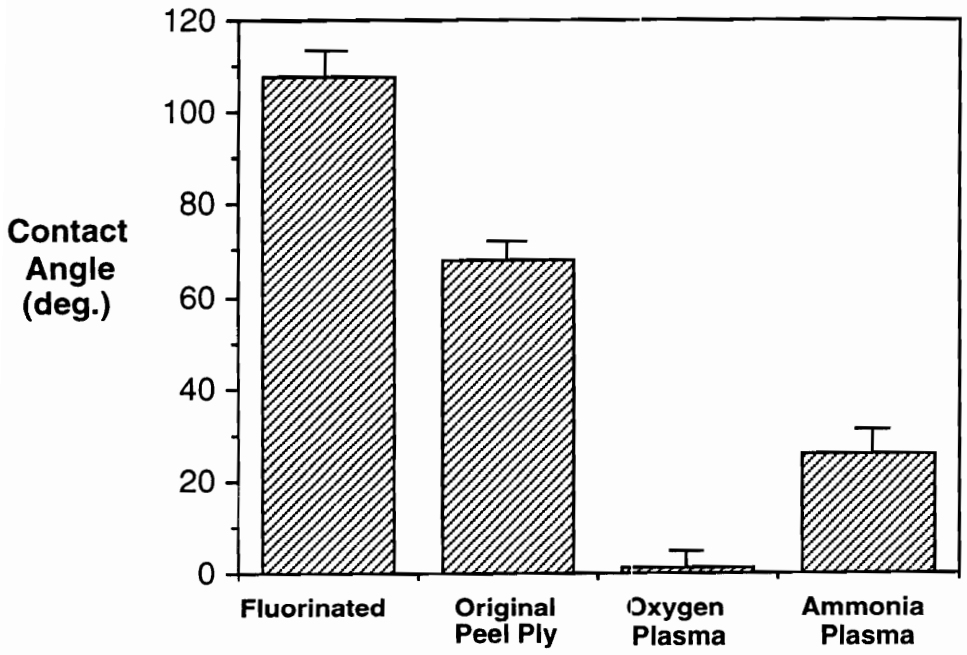

Figure 6.1: Water contact angles on functionalized epoxy peel ply surfaces.

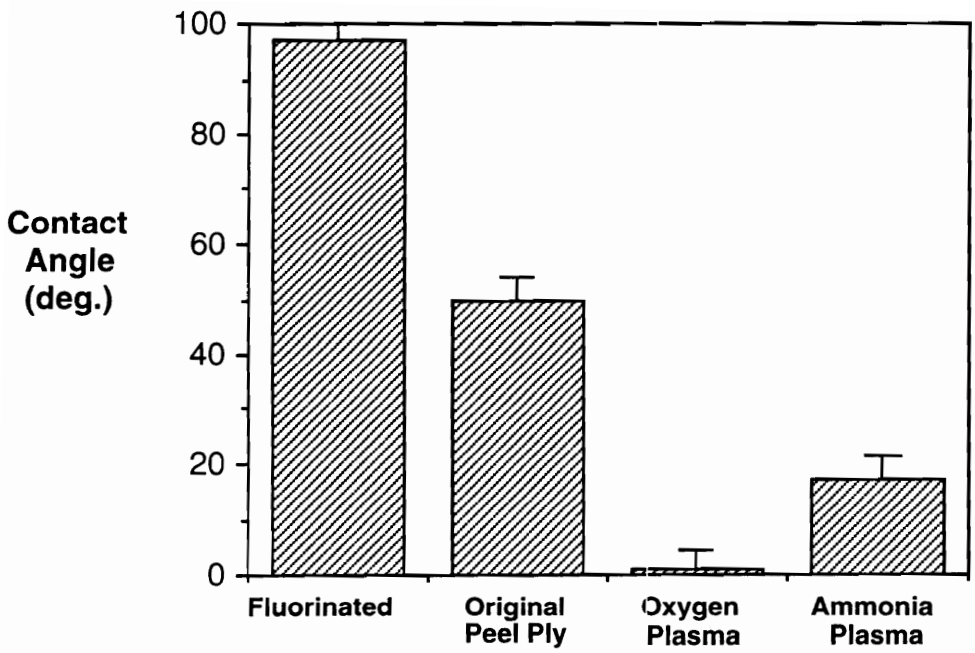

Figure 6.2: Water contact angles on functionalized BMI peel ply surfaces.

Turning now to EPON® 830 as the probe liquid, it is observed that wetting of the functionalized surfaces by an epoxy differs from the wettability of water, as was also observed in the analysis of the pretreated composite surfaces discussed in Sections 4.1.3.3 and 5.1.3.3. Figure 6.3 shows the epoxy contact angles on the functionalized epoxy peel ply surfaces. The fluorinated surface shows very little affinity for the liquid epoxy. The oxygen plasma-treated surface shows a slight improvement in wettability relative to the original surface. The most interesting observation is that the ammonia plasma-treated surface actually displays poorer wettability than the original peel ply, although it was observed to have a higher affinity for water than the original peel ply surface. In fact, very little spreading of the epoxy resin was noted on the ammonia plasma-treated epoxy peel ply surface. Because the surface energy of this surface was observed to increase in the water contact angle experiments, it is postulated that this non-spreading of epoxy on the ammonia plasma-treated surface may be due to chemical reaction at the interface, causing the layer of liquid epoxy resin directly adjacent to the plasma-treated surface to become immobilized.

The contact angles of EPON® 830 on the functionalized BMI peel ply surfaces, shown in Figure 6.4, differ from those observed for the epoxy surfaces. The fluorinated surface again exhibits low wettability, but now the original peel ply surface, the ammonia plasma-treated surface and the oxygen plasma-treated surface are all wetted equally well by the liquid epoxy. The curiously low wettability of the liquid epoxy on the ammonia plasma-treated epoxy surface is not observed in the case of the ammonia plasma-treated BMI. It is suspected that the action of ammonia plasma on the BMI surface produces amide functionality, as observed with other polyimides [1]. Amides are not known to be extremely reactive toward epoxy resins. On the other hand, exposure of the epoxy composite surface to ammonia plasma may result in amine formation, which would be quite amenable to reaction with epoxy.

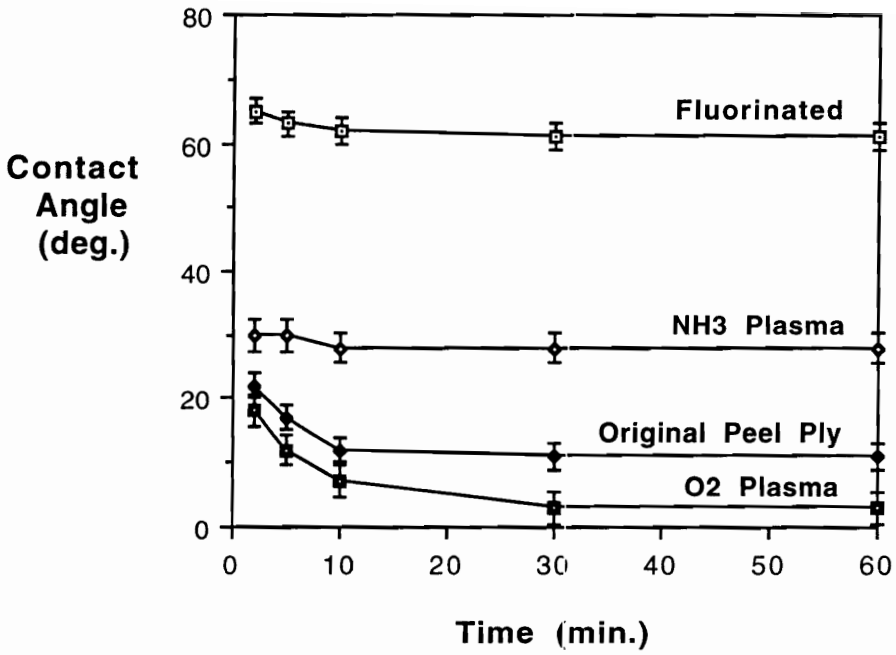

Figure 6.3: EPON® 830 contact angles on functionalized epoxy peel ply surfaces, measured as a function of time.

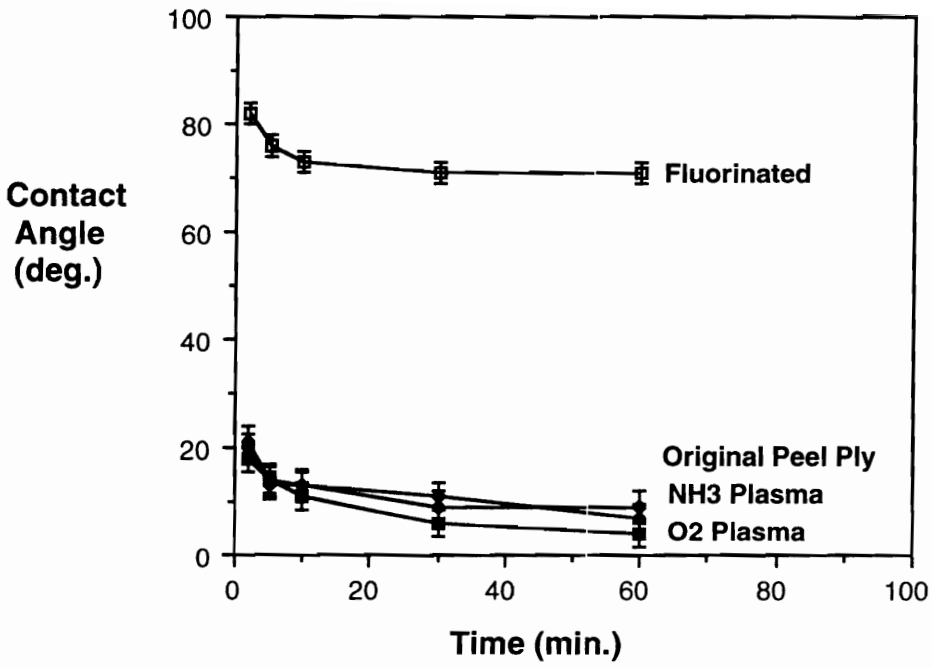

Figure 6.4: EPON® 830 contact angles on functionalized BMI peel ply surfaces, measured as a function of time.

Contact angle studies with Metlbond® 1146 resin were carried out to complement the analyses already completed with water and EPON® 830. Results are shown in Figures 6.5 and 6.6. For both the epoxy and BMI laminates, the contact angle of Metlbond® 1146 on the fluorinated surface is quite high, indicating poor wettability. This is an expected result in light of the high surface fluorine concentration following the fluorination treatment. The as-received surface is wetted to the same degree as the oxygen plasma and ammonia plasma-treated surfaces, a result consistent with the EPON® 830 contact angle results for the functionalized BMI peel ply surfaces, but not consistent with the results for the functionalized epoxy peel ply surfaces.

It had been observed earlier that the contact angle of EPON® 830 on the ammonia plasma-treated epoxy peel ply was observed to be significantly higher than on the original epoxy peel ply . This was an unusual result because water contact angle analysis showed the ammonia plasma-treated surface to have higher surface energy than the original surface. It was then postulated that perhaps amine functional groups were created on the epoxy surface as a result of ammonia plasma exposure. These functional groups could then react with the liquid epoxy, thus immobilizing it and preventing further wetting. The reason why the Metlbond® 1146 resin does not exhibit similar results could be due to the fact that not only is this resin already B-staged and thus has a lower concentration of reactive diglycidyl ether groups, but there is also a competition for these groups between the surface of the functionalized peel ply and the crosslinking agent within the bulk of the adhesive itself. Therefore, any specific interaction of the surface functional groups with the adhesive would be minimal.

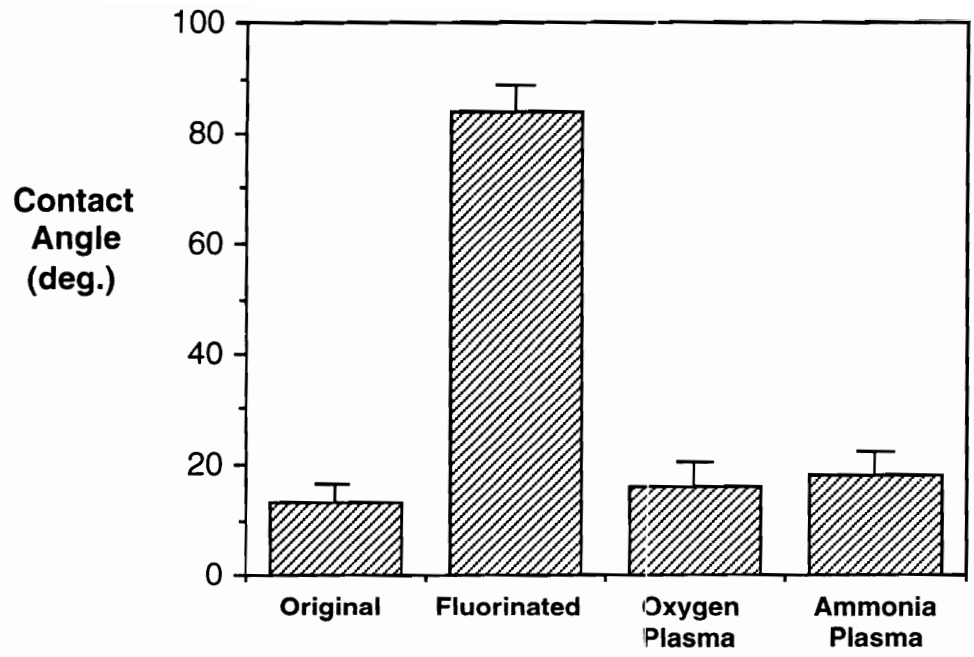

Figure 6.5: Metlbond® 1146 contact angles on functionalized epoxy peel ply surfaces.

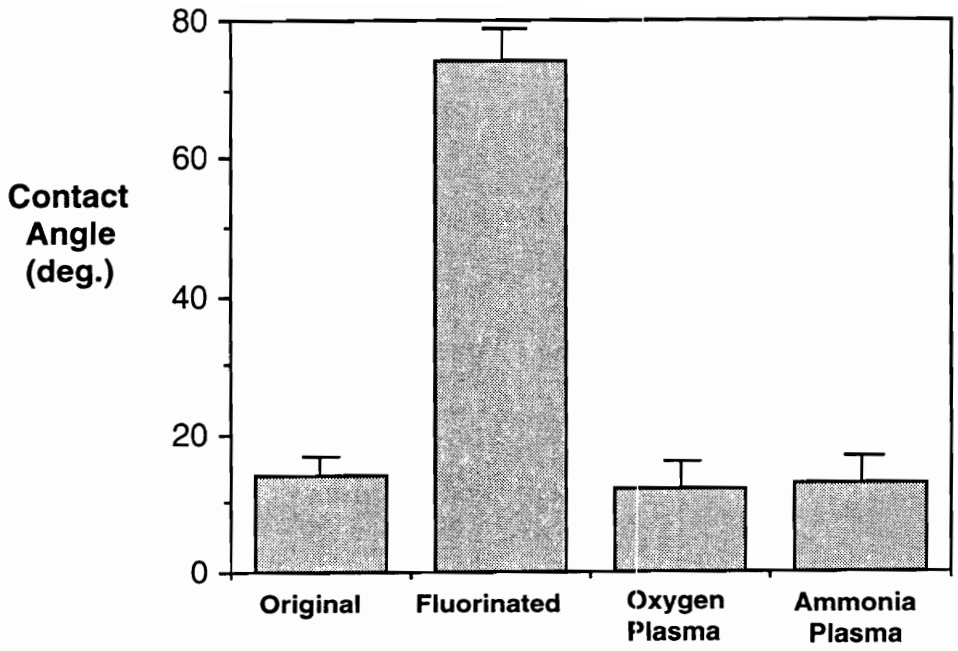

Figure 6.6: Metlbond® 1146 contact angles on functionalized BMI peel ply surfaces.

6.2 Double Lap Shear Testing

Double lap shear testing of the functionalized peel ply samples was performed on samples which had no prior conditioning and samples which had been immersed in a aqueous 75°C environment for 15 days. Results for the samples which had not undergone environmental conditioning are shown in Figures 6.7 and 6.8, for epoxy and BMI composites, respectively In the case of the BMI laminates, only oxygen plasma functionalization was performed, due both to limited material and to the fact that no unusual surface effects were observed with the ammonia plasma-treated BMI peel ply.

It is shown for both the epoxy and the BMI samples, that the fluorinated surfaces have low lap shear strengths relative to the original and plasma-treated samples. This is an expected result. In comparing the fluorinated surfaces to the original peel ply, a situation which simulates fluorine "removal" without subsequent chemical functionalization, the observed increase in lap shear strength is significant and parallels that which was observed in the original double lap shear testing of oxygen plasma-treated surfaces.

The more interesting result in both cases is that plasma treatment does *not* increase the lap shear strength beyond that of the original peel ply. It is seen that when comparing the original peel ply samples with the plasma-treated materials, no significant changes in lap shear strength are observed. These results definitively show that the mechanism of adhesion improvement is only the removal of release film contamination, and not due to any interactions resulting from plasma treatment. Additional chemical functionality does not appear to provide any benefit in terms of *initial bond strength.*

Figures 6.9 and 6.10 show double lap shear strengths of samples which had been conditioned in 75°C water for 15 days. Again, a large relative increase is seen between the fluorinated and original peel ply samples, but no improvements are observed for the plasma-treated surfaces relative to the original peel ply. However, the data contained in Table 6.3 show an interesting trend. This table shows the percent change in lap shear

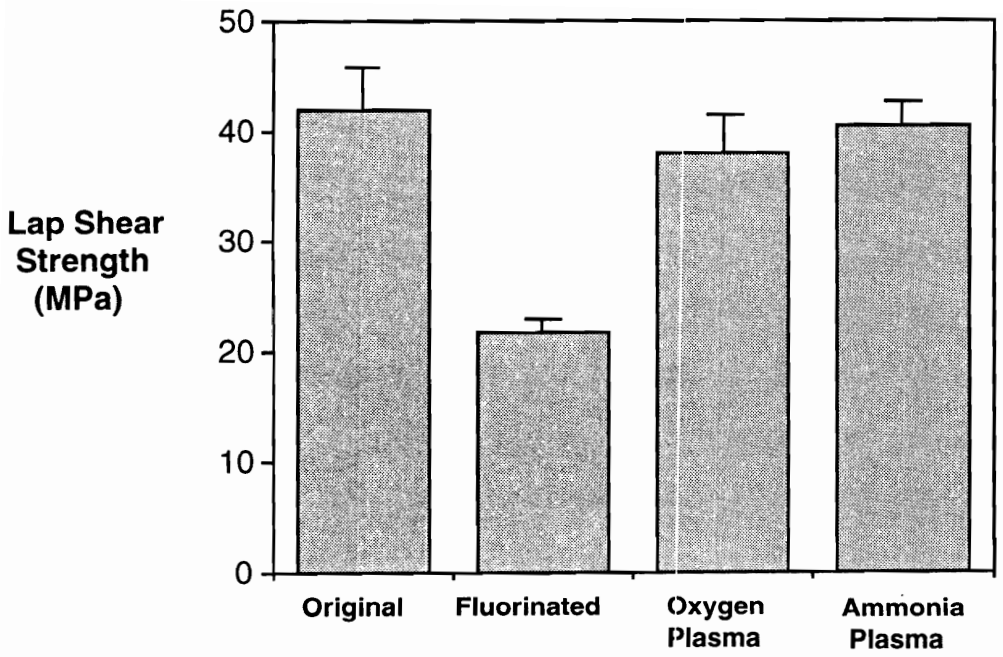

Figure 6.7: Double lap shear strengths of functionalized epoxy peel ply samples bonded with Metlbond® 1146, no pre-conditioning.

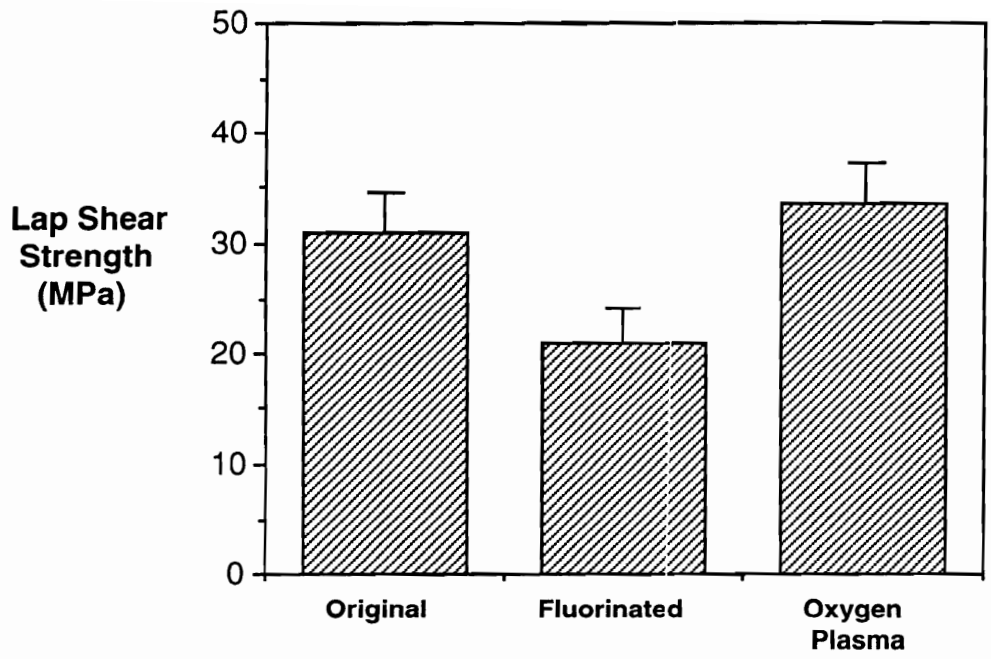

Figure 6.8: Double lap shear strengths of functionalized BMI peel ply samples bonded with Metlbond® 1146, no pre-conditioning.

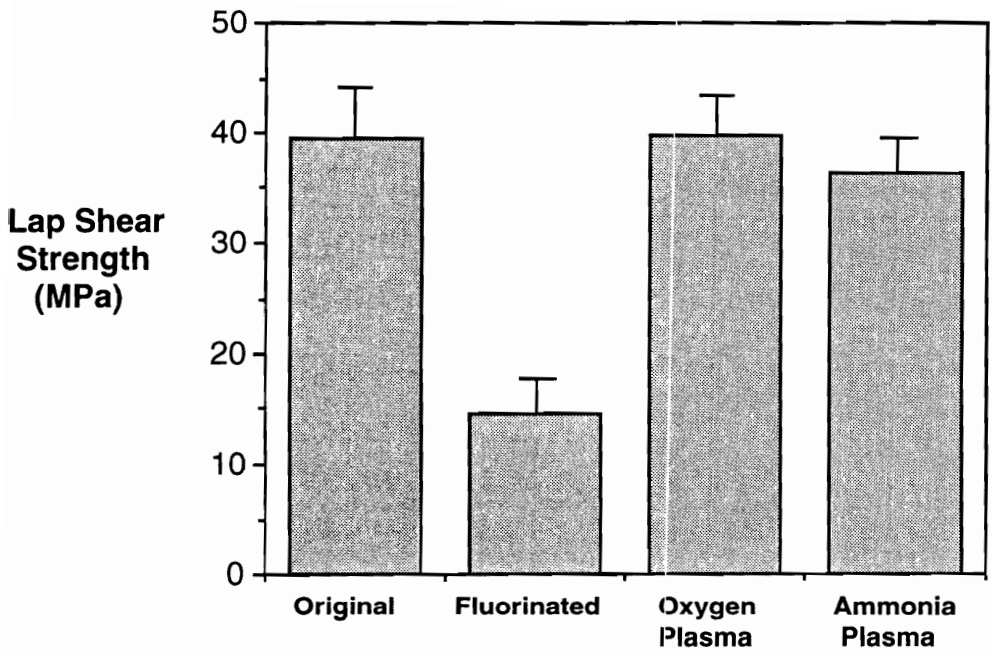

Figure 6.9: Double lap shear strengths of functionalized epoxy peel ply samples bonded with Metlbond® 1146, following a 15 day immersion in 75°C water.

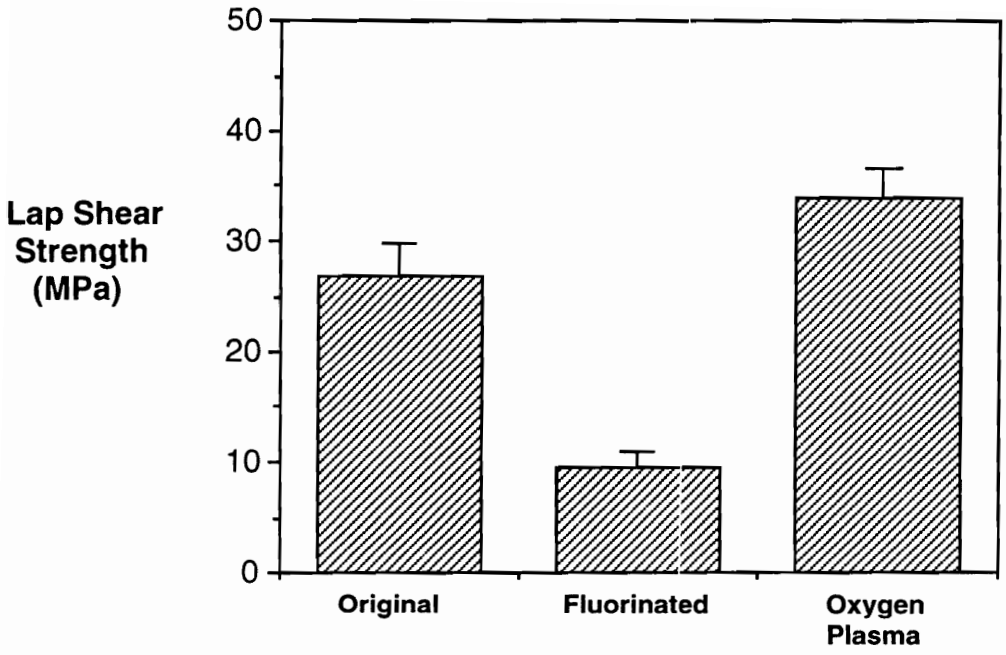

Figure 6.10: Double lap shear strengths of functionalized BMI peel ply samples bonded with Metlbond® 1146, following a 15 day immersion in 75°C water.

Table 6.3: Percent change in lap shear strengths for functionalized epoxy and BMI peel ply samples bonded with Metlbond® 1146, following 15 day/75°C water immersion.

	PERCENT CHANGE	
	Epoxy	**Bismaleimide**
Original	-6.0	-12.4
Fluorinated	-32.4	-55.0
Oxygen Plasma	+4.2	+0.6
Ammonia Plasma	-9.9	---

strength between the unconditioned and the conditioned samples. It is observed that the fluorinated samples exhibited the greatest loss in strength following a hot/wet exposure. Smaller losses in strength are also observed for the original peel ply surface as well as the ammonia plasma-treated epoxy. It is significant that only the oxygen plasma-treated samples did not exhibit any drop in lap shear strength.

These results imply that, while the oxygen plasma did not demonstrate any apparent benefit in improving initial bond strengths, some improvement in hot/wet durability may be realized by this surface pretreatment. Other researchers have also suggested that chemical functionality or interfacial reactions may not necessarily provide additional intrinsic adhesion, but could give improved chemical or hydrothermal resistance [2,3]. At the present time, there is still a lack of evidence on the presence and reactivity of surface functional groups, their potential for interfacial reaction, and the effect of said reaction on adhesion and bond durability.

It should also be noted that the durability of the oxygen plasma-treated peel ply samples is better than that which is demonstrated by the oxygen plasma-treated samples discussed in Sections 4.2.1 and 5.2.1. This could be due to the fact that a synergistic effect results from the combination of mechanical interlocking and surface functional groups, giving rise to a high degree of intrinsic adhesion. Wake has suggested that the magnitude of joint strength which can be achieved is the product of mechanical interlocking effects as well as surface free energy components [4]:

Strength = (constant) x (mechanical component) x (surface free energy components)

Thus, for maximum bond strength, the adherend should have a high degree of surface roughness as well as a high energy surface. These two conditions are met for the functionalized peel ply materials, which could serve to explain the increased durability observed in a hot/wet environment.

The modes of failure for the double lap shear samples, as determined by SEM, are summarized in Tables 6.4 and 6.5. The fluorinated samples exhibited 100% interfacial failure in all cases. The original peel ply samples showed a combination of adhesive and laminate failure, with the epoxy laminates exhibiting a small degree of interfacial failure. A slightly greater degree of cohesive failure was observed for the oxygen plasma-treated surfaces. No obvious differences in failure mode were observed between the unconditioned and environmentally conditioned samples. The fact that the mode of failure was not observed to change significantly with changes in surface pretreatment or conditioning environment is puzzling. The implication here may be that the strength-controlling factors are not necessarily interfacial in nature.

6.3 Conclusions

It has been demonstrated that the removal of fluorine contamination from epoxy and BMI composite surfaces yields significant improvements in initial lap shear strength. The lap shear strength increases due to oxygen plasma treatment documented in Sections 4.2.1 and 5.2.1 are concluded to result from this surface cleaning effect. Incorporation of additional chemical functionality in the composite surface does not provide further increases in bond strength, when compared to a clean but non-functionalized surface. Conversely, the removal of fluorine contamination did not result in increased surface energies, a result which is only achieved by plasma treatment.

Although no improvements in initial strength were observed, oxygen plasma-treated surfaces exhibited excellent durability when conditioned in a hot/wet environment prior to testing, being the only samples which did not lose significant bond strength. Polar functional groups resulting from plasma treatment could be interacting in some manner with the functional groups in the adhesive to impart higher water resistance. However, this

Table 6.4: Modes of failure for functionalized epoxy and BMI peel ply lap shear samples, bonded with Metlbond® 1146, no pre-conditioning.

	Epoxy	Bismaleimide
Original	A,L,I	A,L
Fluorinated	I	I
Oxygen Plasma	A,L	A,L
Ammonia Plasma	A,L	---

A = Adhesive L = Laminate I = Interfacial

Table 6.5: Modes of failure for functionalized epoxy and BMI peel ply lap shear samples, bonded with Metlbond® 1146, following 15 day conditioning in 75°C water.

	Epoxy	Bismaleimide
Original	A,L	A,L
Fluorinated	I	I
Oxygen Plasma	A,L	A,L
Ammonia Plasma	A,L	---

A = Adhesive L = Laminate I = Interfacial

interaction is apparently not sufficient to significantly increase initial bond strength. Chapter VIII describes a study involving model composite surfaces and provides insight into the type of interactions which may be occurring between the plasma-treated substrate and a model adhesive.

6.4 References

1. J.W. Chin and J.P. Wightman, *J. Adhesion*, **36**, 25 (1991).
2. W.A. Zisman, *Ind. Eng. Chem.*, **55**(10), 19 (1963).
3. A.J. Kinloch, *J. Mater. Sci. Lett.*, **15**, 2141 (1980).
4. W.C. Wake, *Adhesion and the Formulation of Adhesives*, p. 69 (Applied Science Publishers, London, 1976).

Chapter VII. Results and Discussion

Surface Aging Effects in Oxygen Plasma-treated Composites

In order for plasma treatment to become a viable industrial surface pretreatment technique, the stability or "shelf life" of the plasma treated surface must be established. This knowledge will help to determine whether a particular adhesive or coating material must be applied immediately after treatment for maximum performance, or whether parts can be stored for some length of time before further processing. This section discusses changes which occur in the surface chemistry and wettability of oxygen plasma-treated epoxy composites as a function of time following plasma treatment. These findings were correlated to single lap shear strengths of bonds which were fabricated from samples which had been stored for varying amounts of time following plasma treatment. It is anticipated that surface aging effects will be observed and will have a subsequent effect on bond strength and durability.

7.1 Surface Analysis

XPS analysis of the plasma-treated epoxy composites was carried out to characterize changes in surface chemistry as a function of storage time. Figure 7.1 shows the atomic concentrations of the primary elements found in the epoxy matrix resin - carbon, oxygen, nitrogen, and sulfur - over a period of almost 3000 hours (about 17 weeks). It was seen that while the concentrations of nitrogen and sulfur change only slightly over time, carbon concentration increases from its value immediately following plasma treatment of 33% to more than 62%. There is a simultaneous decrease in oxygen concentration from 47% to 28%.

Figure 7.2 shows changes in the curve-fitted C1s photopeak as a function of time. Peaks at 286.3, 288.0 and 289.3 eV, which are associated with polar functional groups,

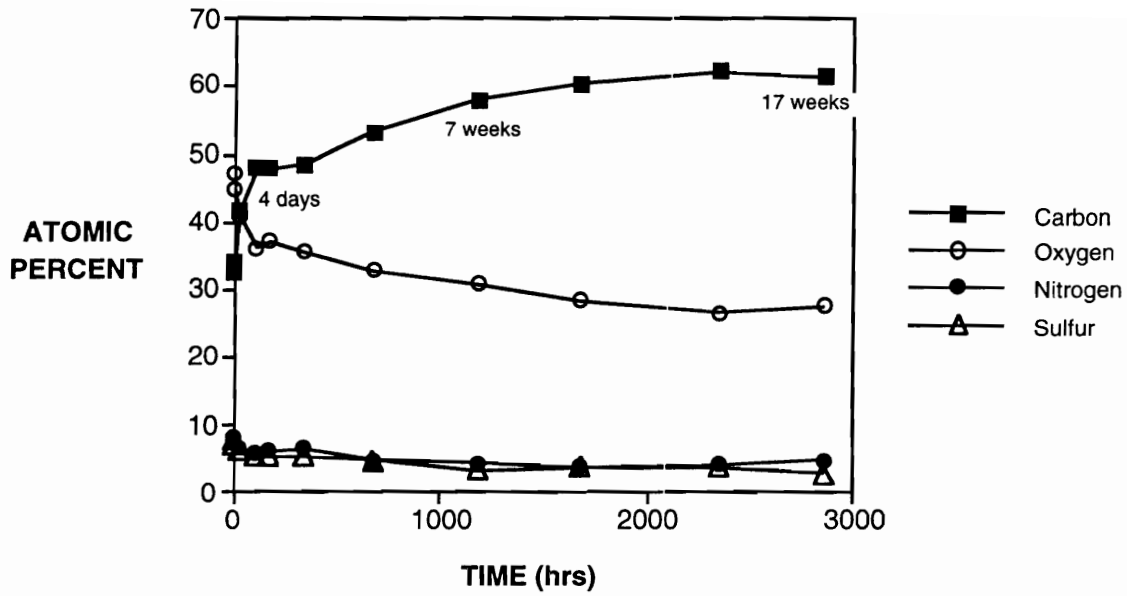

Figure 7.1: XPS atomic concentrations of oxygen plasma-treated epoxy composites as a function of storage time after plasma treatment.

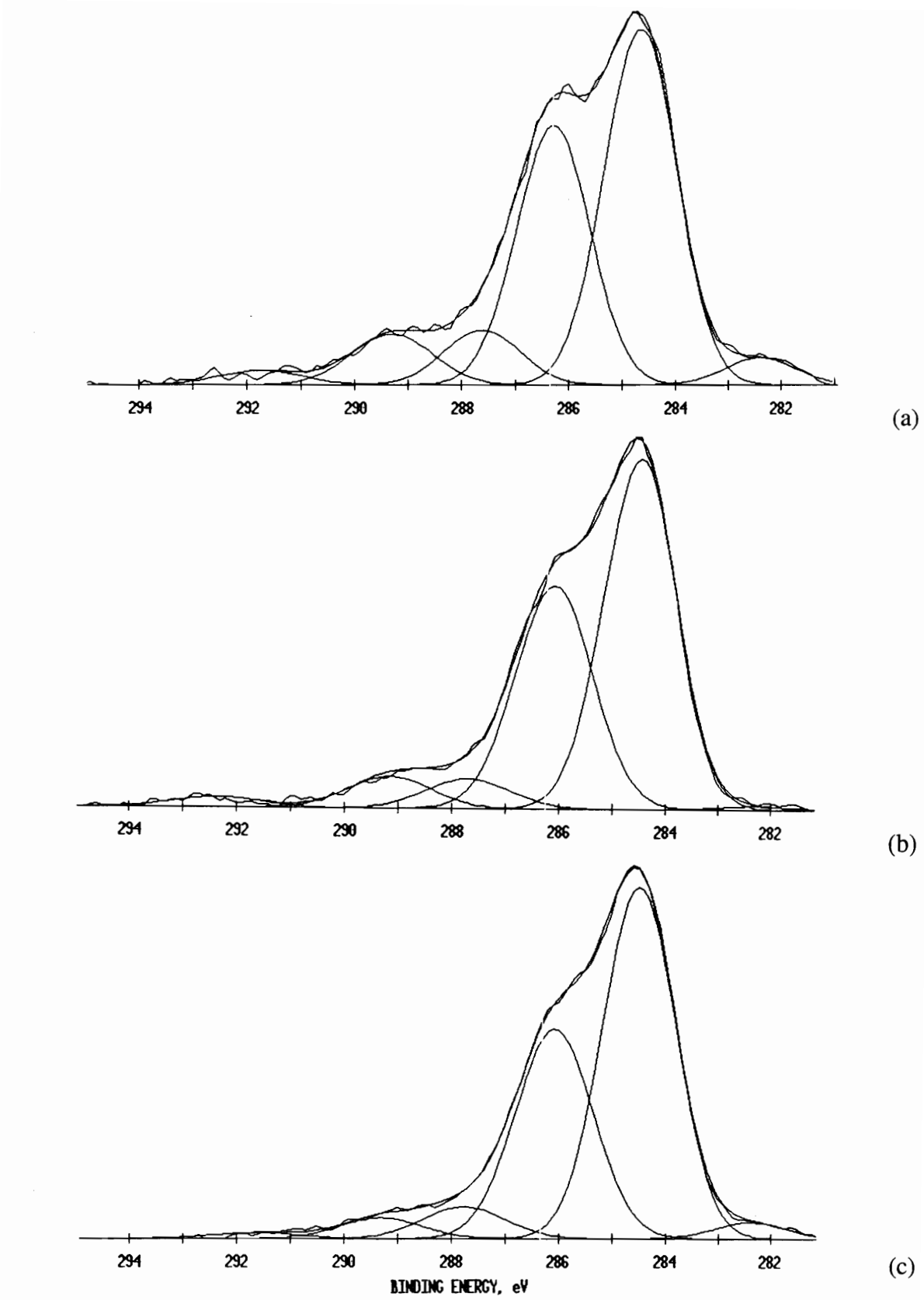

Figure 7.2: Curve-fitted carbon 1s photopeaks for samples stored after plasma treatment. (a) 0 hours (b) 1 day (c) 1 week.

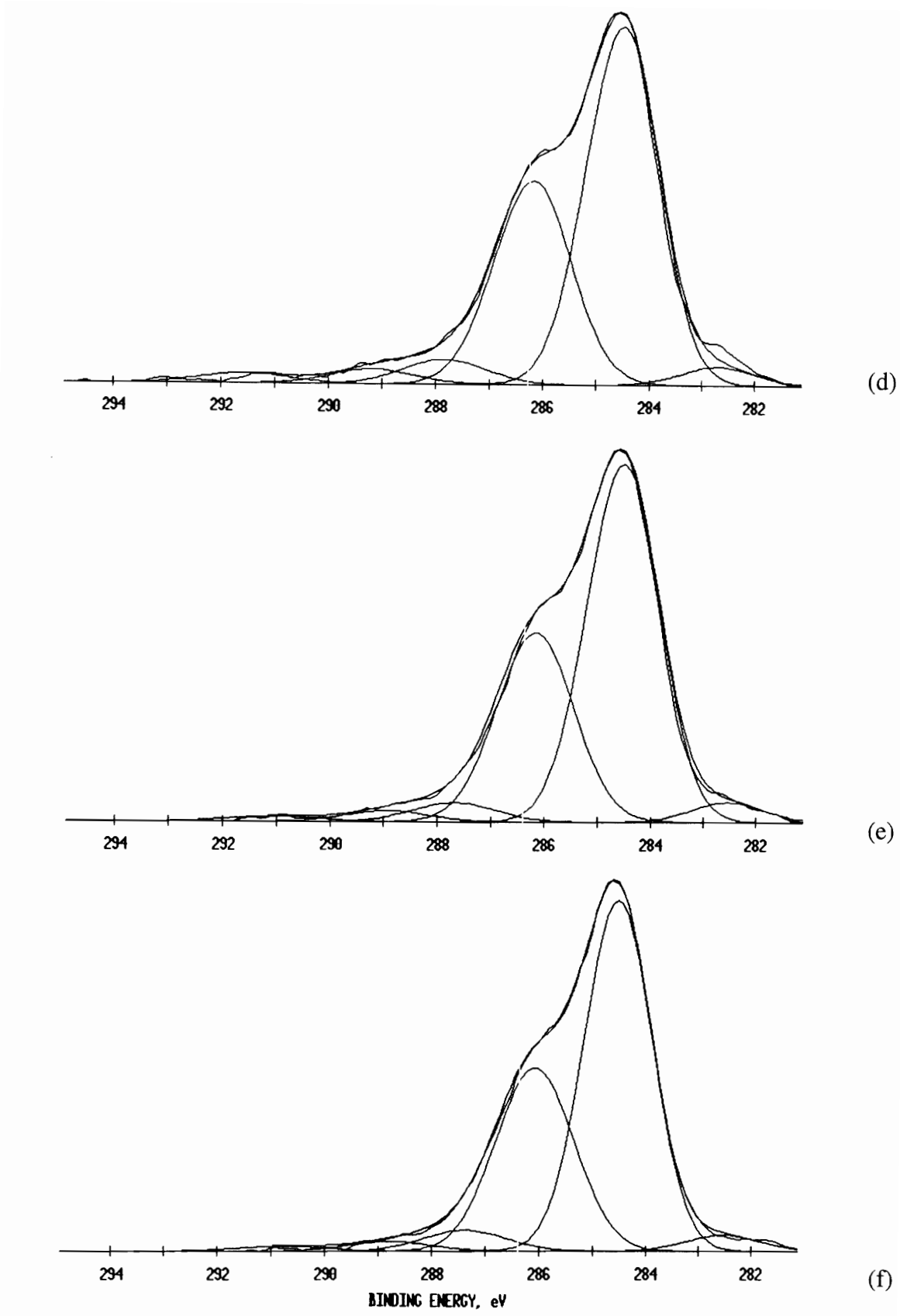

Figure 7.2 (continued): Curve-fitted carbon 1s photopeaks for samples stored after plasma treatment. (d) 3 weeks (e) 7 weeks (f) 17 weeks.

diminish in intensity as time progresses. Although the O1s photopeak at 532.5 eV shown in Figure 7.3 is difficult to curve-fit due to its symmetry, changes can still be observed in the overall peak shape. Immediately after plasma treatment, the oxygen peak is skewed toward lower binding energy; as storage time increases, the peak is seen to become more symmetric.

Changes are also observed for the N1s photopeak, shown in Figure 7.4. The two components of the photopeak, at 399.7 and 401.8 eV, change in relative intensity as storage time increases. The peak at 399.7 eV increases at the expense of the 401.8 eV peak. Work with model epoxy systems, discussed in detail in Chapter VIII, has shown that the peak at 399.7 eV is the original amine nitrogen and that the peak at 401.8 eV, tentatively identified as oxidized nitrogen moieties, results from oxygen plasma treatment. Thus, it is interesting to observe that the original amine nitrogen concentration is increasing over that of plasma-treated amine. This appears to indicate that some migration or diffusion of components into or out of the plasma-treated layer is occurring.

Figure 7.5 shows the ratio of the two nonpolar carbon peaks at 282.4 eV (graphitic carbon) and 284.6 eV (hydrocarbon) to the polar peaks at 286.3, 288.0 and 289.3 eV. This ratio increases over time and levels out around 8-10 weeks, again confirming the tendency of the surface to move toward lower polarity.

Water wettability of the surface as a function of time is summarized in Figure 7.6. The water contact angle increases rapidly during the first 4 weeks and then levels out at approximately 44°. It does not appear that the original contact angle on the untreated surface of greater than 80° would be reached. Although the surface energy appears to be decreasing, it does not completely revert to its original state. This is because fluoropolymer residue which originally caused the surface to be non-wettable was removed by plasma exposure, which is a non-reversible process.

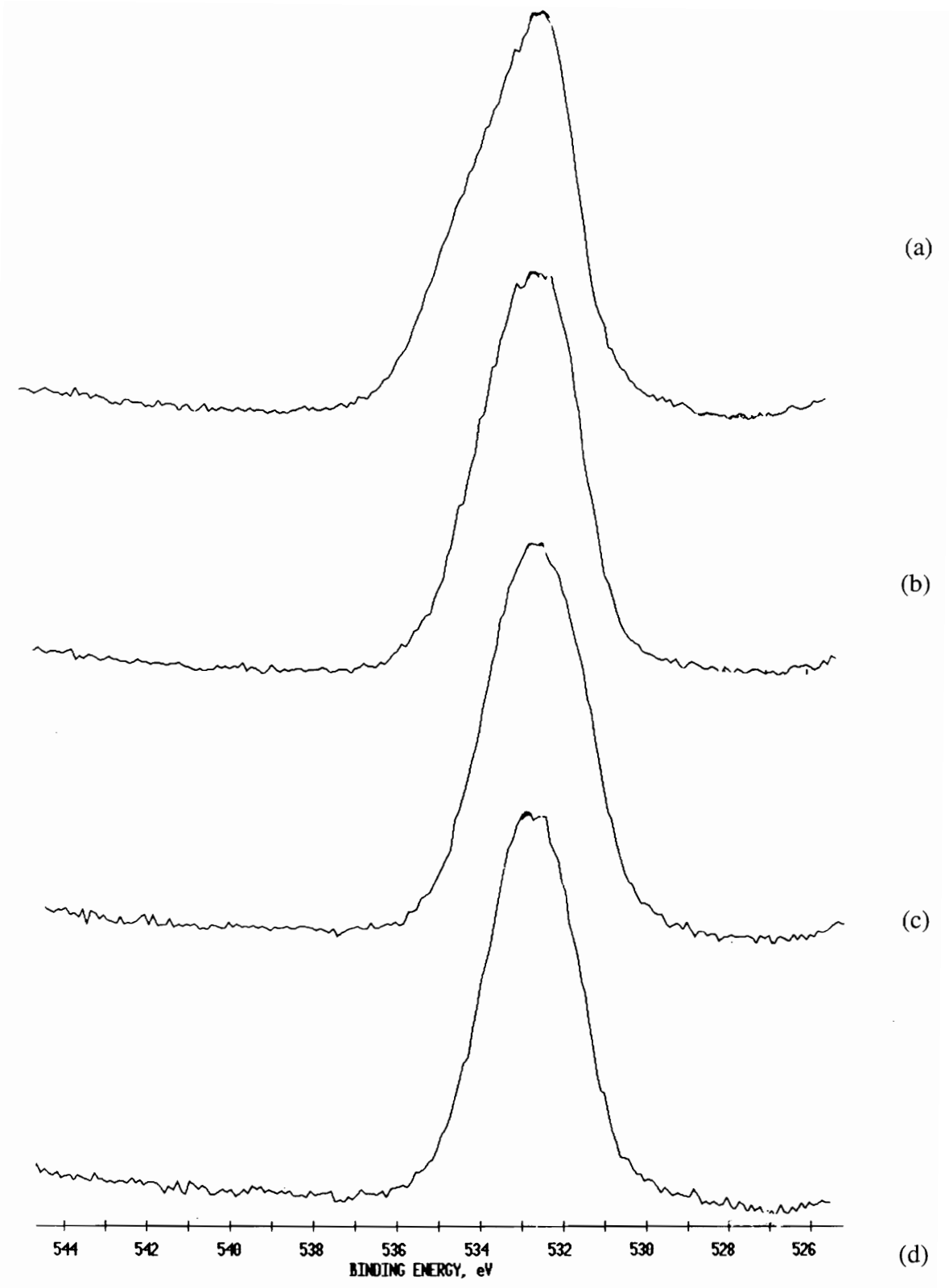

Figure 7.3: Oxygen 1s photopeaks for samples stored following oxygen plasma treatment. (a) 0 hours (b) 1 day (c) 7 weeks (d) 17 weeks.

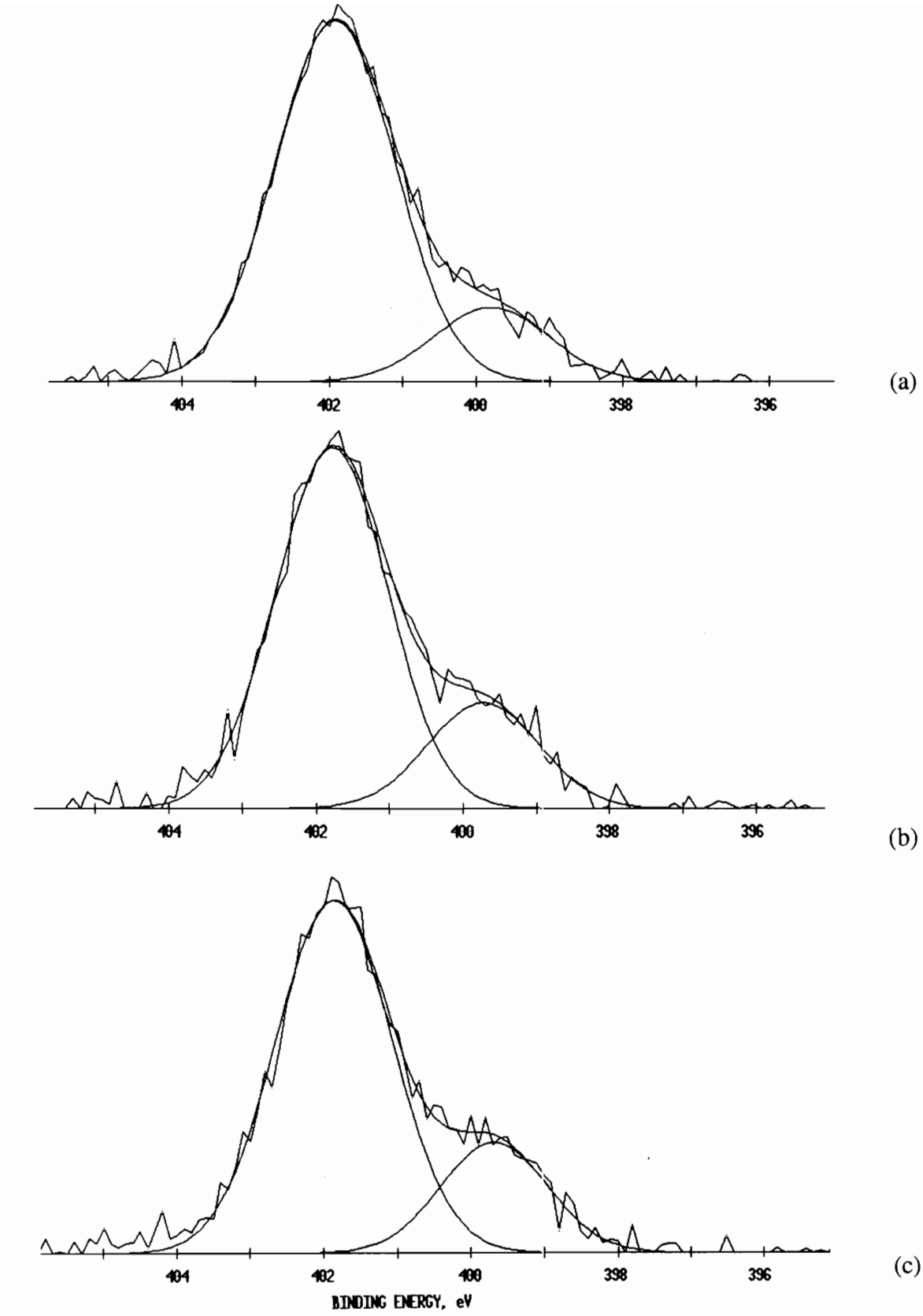

Figure 7.4: Curve-fitted nitrogen 1s photopeaks for samples stored after plasma treatment. (a) 0 hours (b) 1 day (c) 1 week.

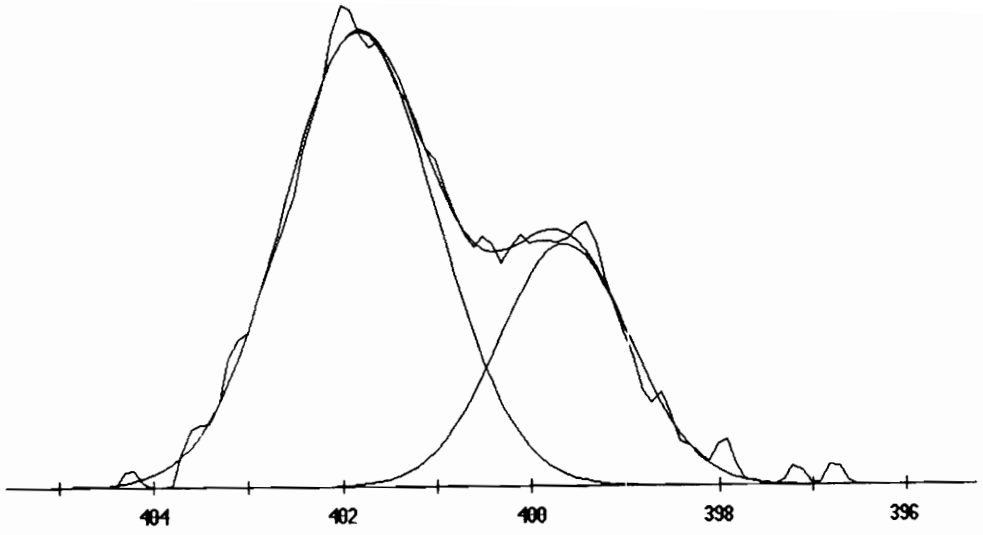

(d)

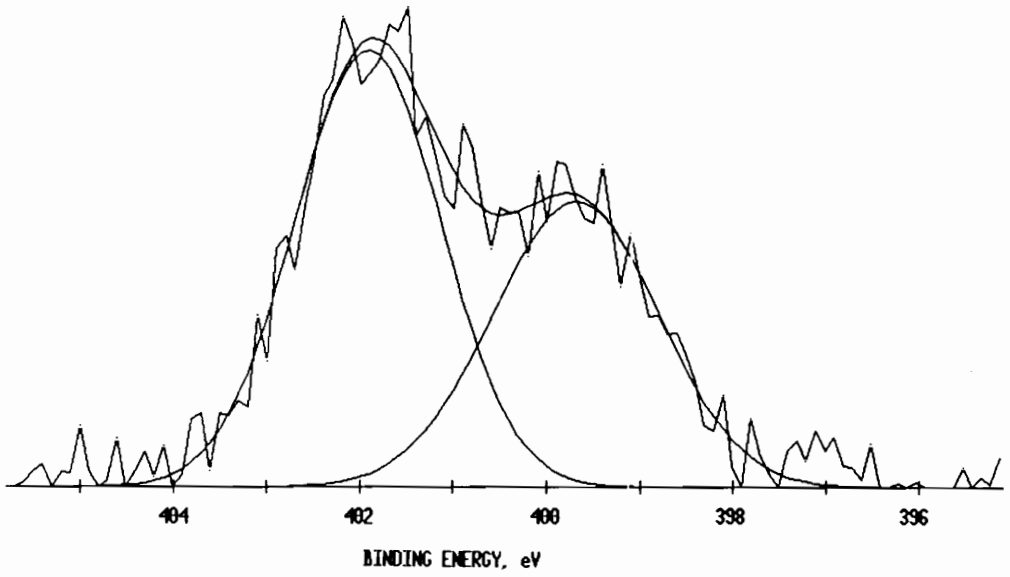

(e)

Figure 7.4 (continued): Curve-fitted nitrogen 1s photopeaks for samples stored after plasma treatment. (d) 7 weeks (e) 17 weeks.

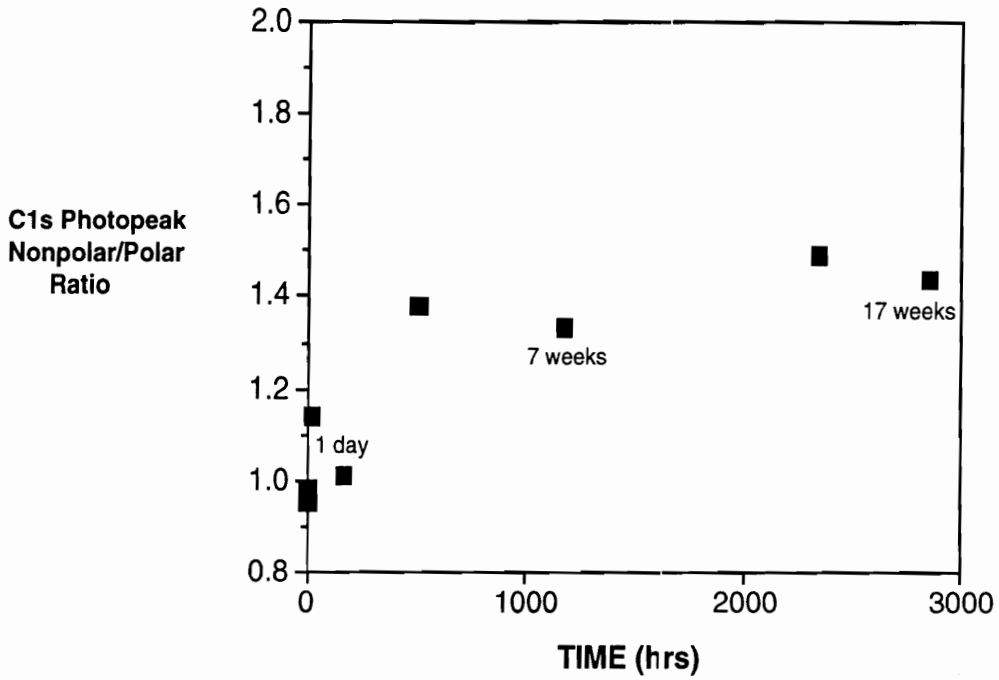

Figure 7.5: Ratio of nonpolar to polar groups in the epoxy composite C1s photopeak, plotted as a function of storage time after oxygen plasma treatment.

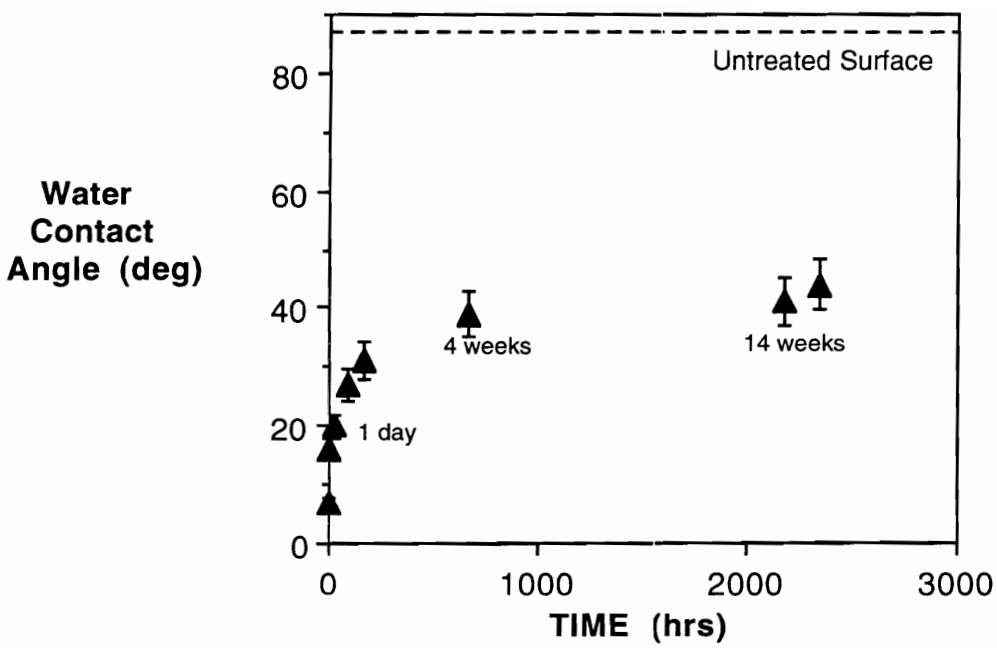

Figure 7.6: Water contact angles on oxygen plasma-treated epoxy composite surfaces, monitored as a function of storage time after plasma treatment.

EPON® 830 contact angles, shown in Figure 7.7, exhibit minimal change over the 17 week storage period and show no tendency to revert to the original, nonplasma-treated value. Since the composite is being bonded with an epoxy resin-based adhesive, the EPON® 830 wettability data is important in showing that although the surface chemistry and water wettability of the plasma-treated composites may have changed over time, the wetting of the surface by an epoxy resin does not change significantly. This implies that the surface energy of the plasma-treated composite surfaces decreases from greater than 72 mJ/m^2 (the surface tension of water) to somewhat less than 40-50 mJ/m^2 (the approximate surface tension of EPON® 830) following plasma treatment.

7.2 Single Lap Shear Testing

Figure 7.8 shows lap shear strengths of samples tested without environmental conditioning. A decrease in lap shear strength occurs as a function of time. Bond strengths drop from about 27 MPa for samples bonded immediately after plasma treatment to approximately 13-22 MPa after storage. A best fit line drawn through the data, taking into account the error bars, shows a negative slope. Alternatively, it may be interpreted that the lap shear strength drops quickly in the first 24 hours, then reaches a plateau. In any case, it appears that the changes in surface chemistry and wettability do have a detrimental effect on bond performance.

Results of lap shear testing performed after exposure to 75°C water for 15 days are shown in Figure 7.9. This data also shows a decrease in lap shear strength with storage time, particularly within the first 24 hours. The relative percentage decrease in lap shear strength is calculated and displayed in Figure 7.10. Although there is a great deal of scatter in the data, a computer-generated best fit line shows a slight positive slope, indicating that bond durability also decreases as storage time after plasma treatment increases. Taken

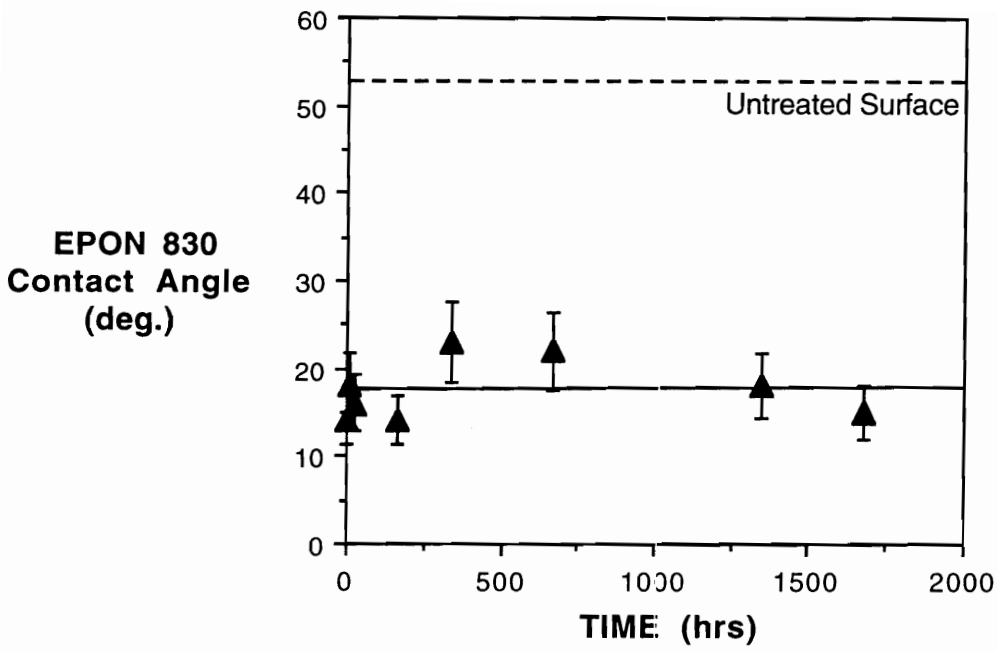

Figure 7.7: EPON® 830 contact angles on oxygen plasma-treated epoxy composite surfaces, monitored as a function of storage time after plasma treatment.

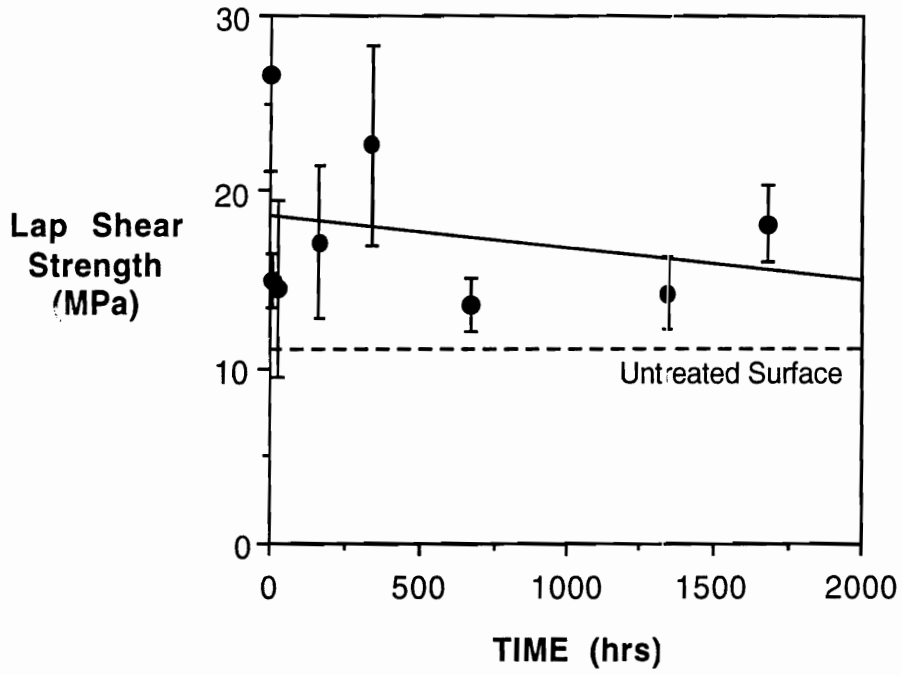

Figure 7.8: Ambient single lap shear strengths of oxygen plasma-treated epoxy laminates, tested as a function of storage time between plasma treatment and bond fabrication.

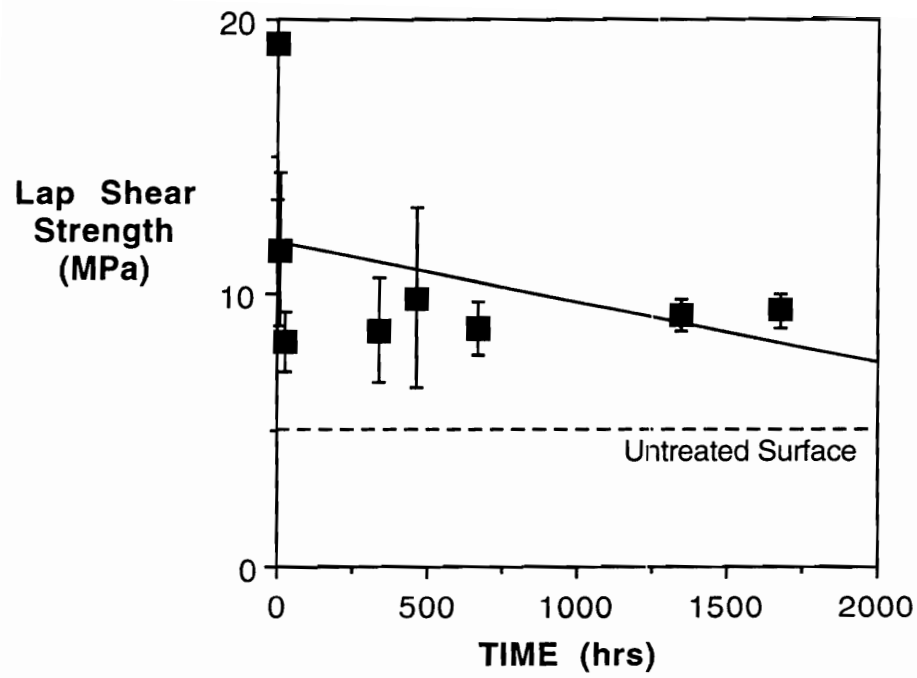

Figure 7.9: Single lap shear strengths of oxygen plasma-treated epoxy laminates immersed in 75°C water for 15 days, tested as a function of storage time between plasma treatment and bond fabrication.

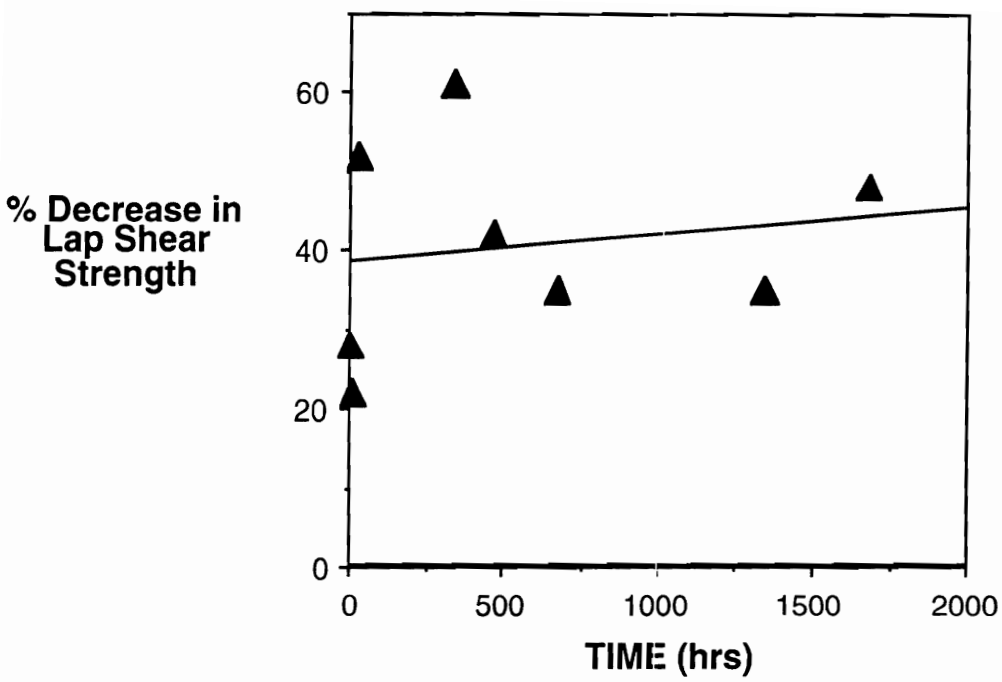

Figure 7.10: Percent decrease in lap shear strengths of oxygen plasma-treated epoxy composites after exposure to 75°C water for 15 days, monitored as a function of time between plasma treatment and bond fabrication.

together, the lap shear test results lead to the conclusion that bond strength and durability decrease as the length of time between surface activation and adhesive bonding increases. The main mode of failure in both the as-processed and environmentally exposed samples was a combination of adhesive and laminate failure.

The results of the EPON® 830 contact angle analysis have shown that wettability of the surface by an epoxy resin does not change significantly as a function of time, thus the main factor in determining bond strength and durability must be the presence of surface functional groups. Figure 7.11 shows lap shear strengths plotted as a function of oxygen concentration. A possible positive trend is seen in this data, suggesting that there may be a correlation between bond strength and the concentration of oxygen-containing functional groups on the surface. However, the magnitude of the error bars involved make it difficult to arrive at a definitive conclusion.

Other workers who have studied the phenomenon of surface aging have also observed similar trends in contact angle and surface composition following plasma or corona discharge treatment. Garbassi et al. reported increases in the contact angle of water on plasma-treated polypropylene. It was observed that the contact angles increased at a faster rate when the storage temperature was elevated, indicating that some type of molecular motion is responsible for the change in surface wettability [1]. Researchers at 3M compared the plasma aging of two polymers, polypropylene and poly(ethylene terephthalate), and found that the differing polarities of the two bulk polymers resulted in different aging behaviors. In nonpolar polypropylene, there is little tendency for diffusion or migration to take place in the polar overlayer, whereas in the polar poly(ethylene terephthalate) there is more potential for interaction between the polar bulk and the polar modified surface [2,3]. In the adhesive bonding of PEEK/carbon fiber composites, Davies et al. found that lap shear strengths dropped from >30 MPa to 11-12 MPa after a period of 10 days [4].

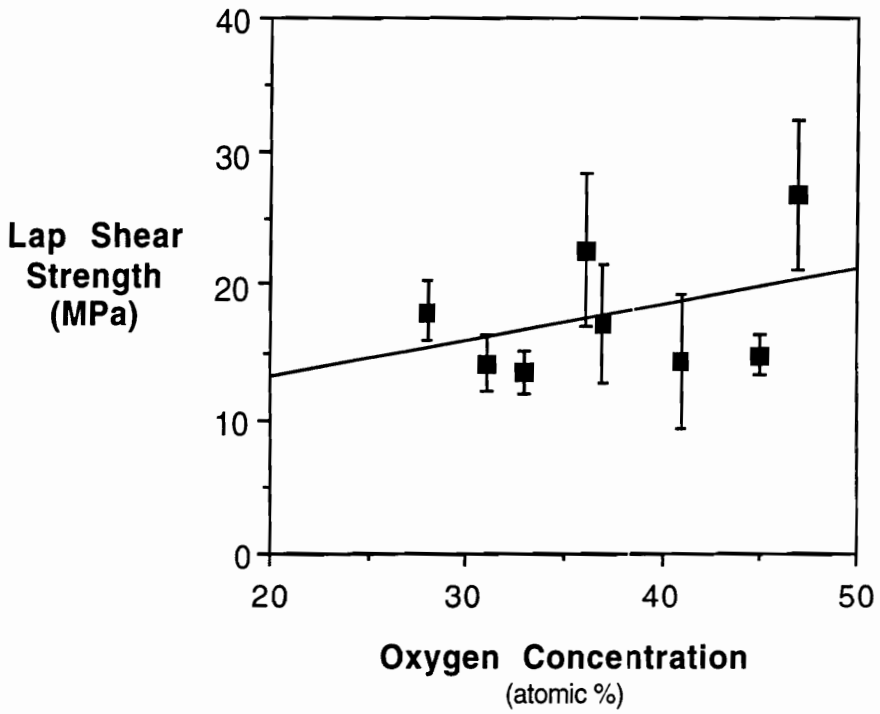

Figure 7.11: Single lap shear strengths of oxygen plasma-treated epoxy laminates versus XPS oxygen atomic concentration.

It may be possible to stabilize the plasma-treated surface by optimizing storage conditions. For instance, storing treated adherends at a lower temperature to decrease molecular mobility may prevent significant changes from occurring. Another option could involve storing samples in an inert atmosphere such as nitrogen or argon. Occhiello et al. showed that plasma aging could be overcome if the treated surface is interfaced with a high energy medium, such as water. They postulated that the surface will rearrange itself to minimize interfacial energy, thus if the surface is in contact with low energy air, a lower surface free energy will result [5].

7.3 Conclusions

Plasma aging effects were observed in the oxygen plasma-treated epoxy composites. Both the surface energy assessed by contact angle analysis and the polarity of the surface analyzed by XPS decreased as the length of time after plasma treatment increased. In turn, these changes in the nature of the surface decreased bond strength and durability as measured by lap shear testing. The largest drop in bond strength was observed to occur within the first day. This behavior may necessitate special handling of the modified surfaces in order to obtain optimum adhesion when immediate bonding of the pretreated surfaces is not possible. In general, the maximum adhesion and durability was obtained when bonding took place immediately following plasma exposure.

7.4 References

1. F. Garbassi, M. Morra, E. Occhiello, L. Barino and R. Scordamaglia, *Surf. Interface Anal.*, **14**, 585 (1989).
2. J.M. Strobel, M. Strobel, C.S. Lyons, C. Dunatov and S.J. Perron, *J. Adhesion Sci. Technol.*, **5(2)**, 119 (1991).
3. M. Strobel, C.S. Lyons, J.M. Strobel and R.S. Kapaun, *J. Adhesion Sci. Technol.*, **6(4)**, 429 (1992).
4. P. Davies, C. Courty, N. Xanthopoulos and H.J. Mathieu, *J. Mater. Sci. Lett.*, **10**, 335 (1991).
5. E. Occhiello, M. Morra, G. Morini, F. Garbassi and P. Humphrey, *J. Appl. Polym. Sci.*, **42**, 551 (1991).

Chapter VIII: Results and Discussion

Infrared Reflection Absorption Spectroscopy (IR-RAS)/X-ray Photoelectron Spectroscopy (XPS) Study of Model Composite Surfaces

The objective of the research described in this section was to study the changes in oxygen plasma-treated composite surfaces by using model compounds with known structures and stoichiometries. As described in detail in the Experimental Section, a tetrafunctional epoxy and diaminodiphenylsulfone (DDS) system was chosen to represent an epoxy composite matrix resin, and a commercial two-component bismaleimide simulated a bismaleimide composite. Infrared reflection absorption spectroscopy (IR-RAS) and x-ray photoelectron spectroscopy (XPS) analysis of thin films made from these materials enabled molecular information on the plasma-treated surfaces to be obtained, as well as provided insight into the mechanism of interaction between the plasma-treated surfaces and adhesives.

8.1 Epoxy Model Surfaces

8.1.1 IR-RAS Analysis of Components and Cured Films

Prior to the analysis of the plasma-treated surfaces, infrared analysis of the components which make up the model epoxy film was carried out. Figure 8.1(a) shows the IR-RAS spectrum of Araldite® MY 720, a tetrafunctional epoxy resin, spin-coated on a chrome steel substrate from a 1.3% w/w solution in acetone and MEK. Prominent bands corresponding to aromatic ring vibrations are seen at 1615 and 1520 cm^{-1}. C-N stretching modes are observed at 1337 and 1386 cm^{-1}. Peaks at 1258 and 1237 cm^{-1} correspond to symmetric stretching of the unopened epoxide ring. The characteristic asymmetric stretching vibrations of the epoxide ring appear at 908 and 845 cm^{-1}.

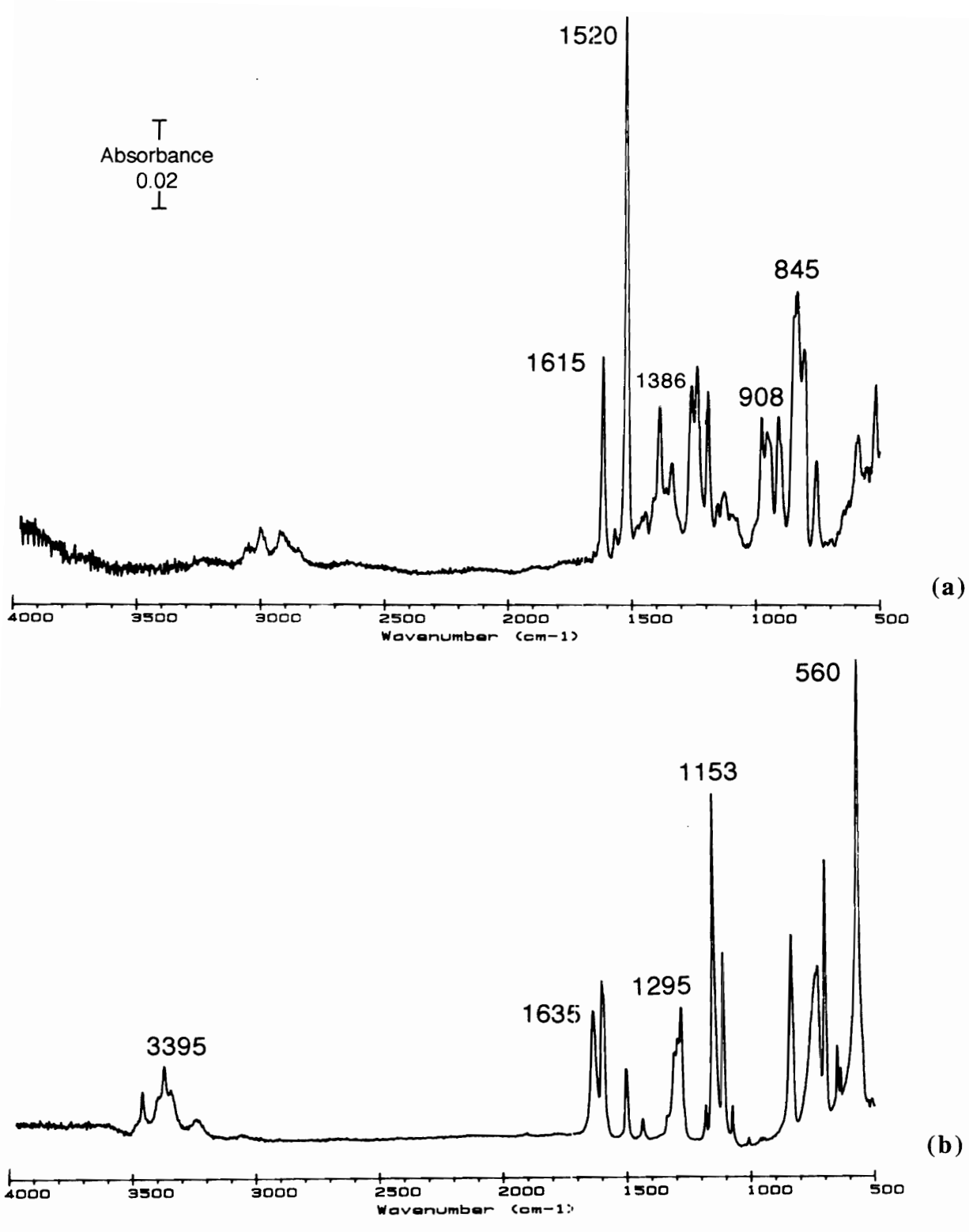

Figure 8.1: (a) IR-RAS spectrum of Araldite® MY 720 tetrafunctional epoxy resin, and (b) IR-RAS spectrum of HT 976 diaminodiphenylsulfone crosslinking agent.

The IR-RAS spectrum of the diaminodiphenylsulfone (DDS) crosslinker, HT 976, is shown in Figure 8.1(b). Bands of importance include the aromatic N-H stretching modes at 3395 and 3367 cm^{-1}, and the corresponding N-H bend for primary aromatic amines at 1635 cm^{-1}. Vibrations corresponding to the sulfone group are the O=S=O asymmetric stretching modes at 1338, 1307 and 1295 cm^{-1}. C-N stretching bands also fall in this region. The sulfone symmetric stretching mode and scissors deformation are seen at 1153 and 560 cm^{-1}, respectively.

Curing of the tetrafunctional epoxy and the amine curing agent to form a crosslinked network involves the reaction of the primary amine hydrogens with the epoxide rings. Each reaction of an amine hydrogen with an epoxide ring results in ring-opening and the evolution of a secondary hydroxyl group. Homopolymerization of the epoxide resin to form a polyether structure is also a possibility [1].

In the spectrum of the cured MY 720/HT 976 film shown in Figure 8.2, no bands are observed at 845, 908, 1258 or 1237 cm^{-1}, indicating that the epoxide ring has undergone reaction with the DDS crosslinker. The sulfone symmetric stretch at 1153 cm^{-1} is evident in the spectrum; however, bands corresponding to the N-H stretching modes as well as the primary amine bending at 3395, 3367 and 1635 cm^{-1} are no longer observed. This also confirms the reaction of the crosslinker with the tetrafunctional epoxy, a process which results in the consumption of amine hydrogens as well as epoxide rings. An increase is seen in the breadth of the peak at 1307 cm^{-1}, previously assigned to either C-N stretching or asymmetric O=S=O stretching in DDS. This may be indicative of O-H bending in the hydroxyl groups which are a product of the epoxy ring opening reaction.

8.1.2 Oxygen Plasma Treatment of Cured Films

Both XPS and IR-RAS were used to study the changes which occur in the surface of oxygen plasma-treated MY 720/HT 976 thin films. Table 8.1 shows the theoretical

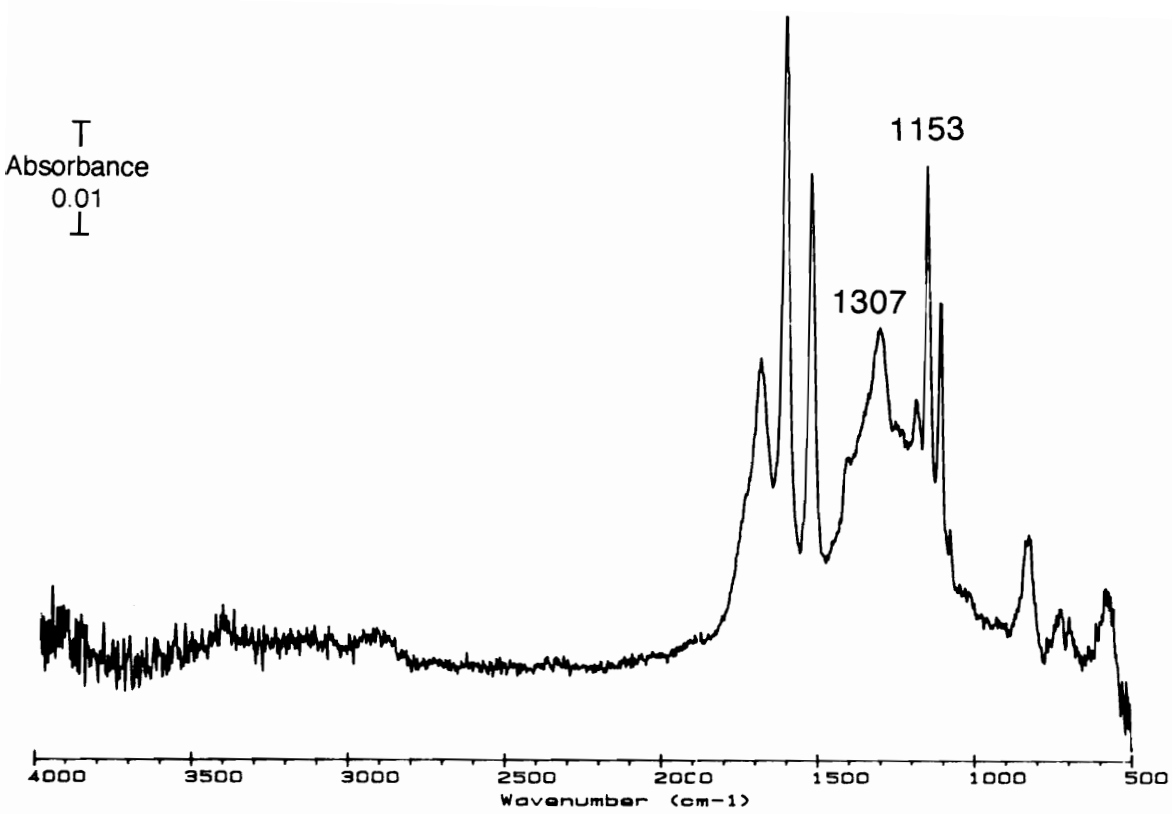

Figure 8.2: IR-RAS spectrum of a cured MY 720/HT 976 film.

Table 8.1: Theoretical and XPS atomic compositions of unmodified and oxygen plasma-treated MY 720/HT 976 films.

	Surface Composition (atomic %)		
	Theoretical	**Unmodified**	**Oxygen Plasma**
Carbon	77	76	53
Oxygen	13	16	35
Nitrogen	8	7	8
Sulfur	2	1	4

atomic concentration of a formulation composed of 100 pbw of MY 720 and 44 pbw HT 976, compared to the measured XPS atomic concentrations of a cured, unmodified MY 720/HT 976 film and a cured film treated in oxygen plasma. Good agreement is observed between the theoretical and actual atomic concentrations for the unmodified surface. The excess oxygen which is found on the unmodified film surfaces may originate from residual solvent used to spin-coat the films. Following oxygen plasma exposure, the atomic concentrations of oxygen and sulfur are seen to increase.

Curve-fitting of the carbon 1s photopeaks was carried out and is depicted in Figure 8.3. In the unmodified surface of Figure 8.3(a), peaks at 284.6, 286.0, 287.5 and 289.0 eV can be fitted to the main peak envelope. These peaks are usually assigned to C-C/C-H hydrocarbon species, C-O/C-N, C=O and O-C=O functionality, respectively [2]. The presence of C-O moieties can be accounted for in the epoxide rings from the MY 720 and C-N linkages in both the MY 720 and HT 976.

A few anomalies are present in the XPS curve fit analysis of the cured MY 720/HT 976 films. XPS analysis of poly(ether sulfone) by Beamson and Briggs showed that the carbons directly adjacent to the sulfone group exhibit a binding energy shift of approximately +0.6 eV relative to hydrocarbon species at 284.6 eV; however, no peaks could be fitted to the MY 720/HT 976 C1s photopeak at this binding energy [3]. In addition, there are no C=O or O-C=O groups in either the epoxy resin or the crosslinker, as can be ascertained by the chemical structures of these two materials. There are also no carbonyl stretches observed in the IR-RAS spectrum of the cured MY 720/HT 976 films. It is possible that surface oxidation may have occurred during the high temperature cure cycle, resulting in the formation of various oxidized carbon species, detectable by XPS but not by IR-RAS.

Figure 8.3(b) shows the curve-fitted carbon 1s photopeak for the oxygen plasma-treated surface. Peaks at 286.0, 287.5 and 289.0 eV have increased in intensity, indicative

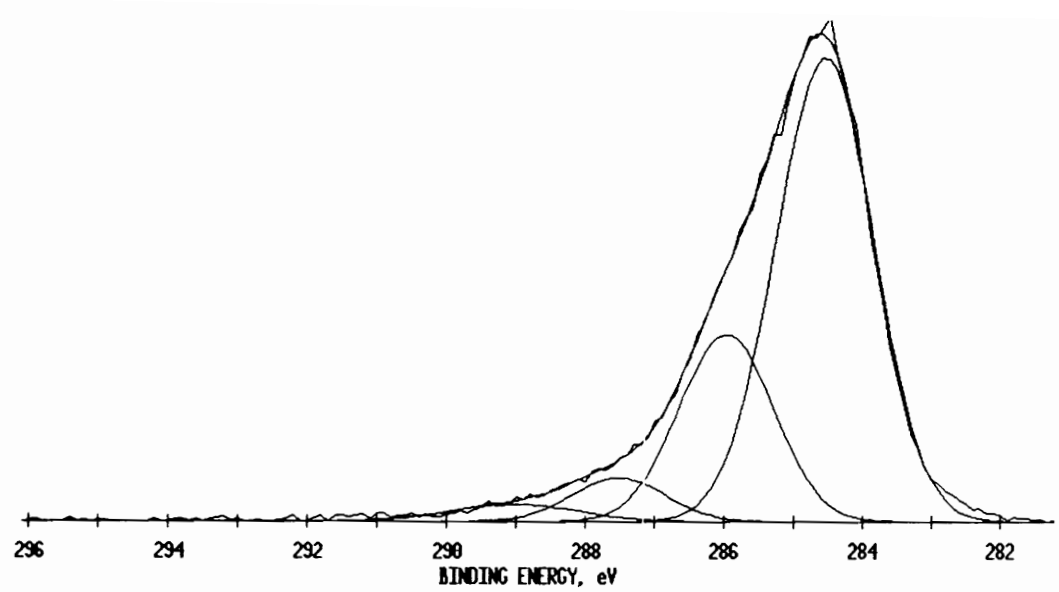

(a)

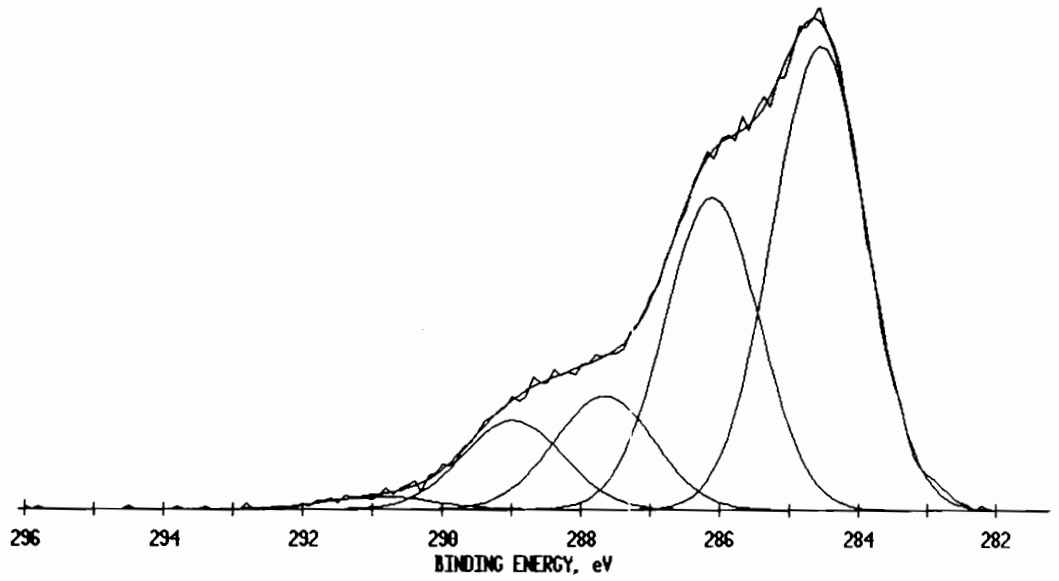

(b)

Figure 8.3: Curve-fitted XPS carbon 1s photopeaks for (a) unmodified, and (b) oxygen plasma-treated MY 720/HT 976 films.

of an increase in the surface concentration of hydroxyl, carbonyl and carboxylate/ester species as a result of plasma treatment. A new peak is also observed at 291.0 eV. It is not clear whether this is a peak corresponding to a new oxygen-containing functional group, such as carbonate, or a π -->π^* shake-up satellite.

Changes are also observed in the nitrogen 1s photopeak shown in Figure 8.4. In the unmodified surface, a single nitrogen peak is observed at approximately 399.7 eV, corresponding to amine nitrogens in both the epoxy resin and crosslinker [3]. Following plasma exposure, a peak is observed at 401.8 eV is observed in addition to the original one at 399.7 eV. This finding is identical to the results observed for the oxygen plasma-treated epoxy composite surfaces discussed in Section 4.1.1. The peak at 401.8 eV could be due to some type of oxidized nitrogen species [4]. A nitrogen 1s binding energy of 401.8 eV has been reported for $N_2H_6SO_4$ [4], and nitrogen in the tertiary amine salt $-N(CH_3)_3^+$ has been observed to exhibit a binding energy of 401.74 eV [3].

No significant changes were observed in the shape or location of the oxygen 1s photopeak. Following oxygen plasma treatment, the sulfur 2p photopeak was observed to shift from its original position at 167.7 eV to 168.6 eV. This shift to higher binding energy is indicative of the transformation of the original sulfone sulfur to a more oxidized form of sulfur, such as sulfate [4].

Infrared analysis of the plasma-modified epoxy surface served to complement the molecular information obtained from curve-fitting the XPS photopeaks. Figure 8.5 shows the IR-RAS difference spectrum obtained by subtracting the spectrum of the unmodified surface from the spectrum of the oxygen plasma-treated surface. Peaks are observed in the difference spectrum at 1770, 1438 and 1205 cm^{-1}. The peak at 1770 cm^{-1} can be assigned to C=O stretching in ester or carboxylic acid species [5]. This assignment is consistent with the increase in the XPS peak at 289.0 eV. The peak at 1205 cm^{-1} is identified as a C-O stretch [6], which corresponds with the increased intensity of the XPS photopeak at

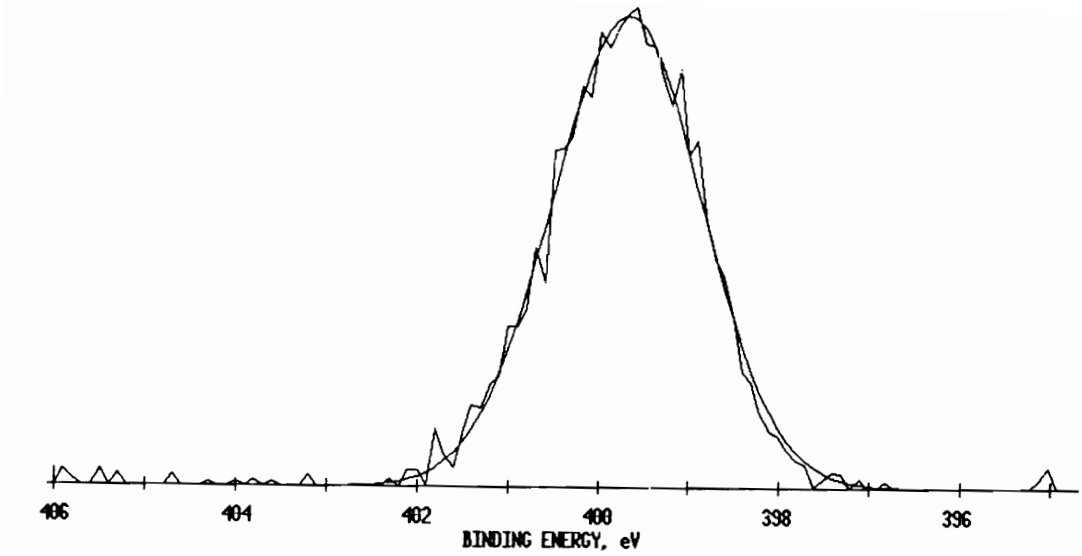

(a)

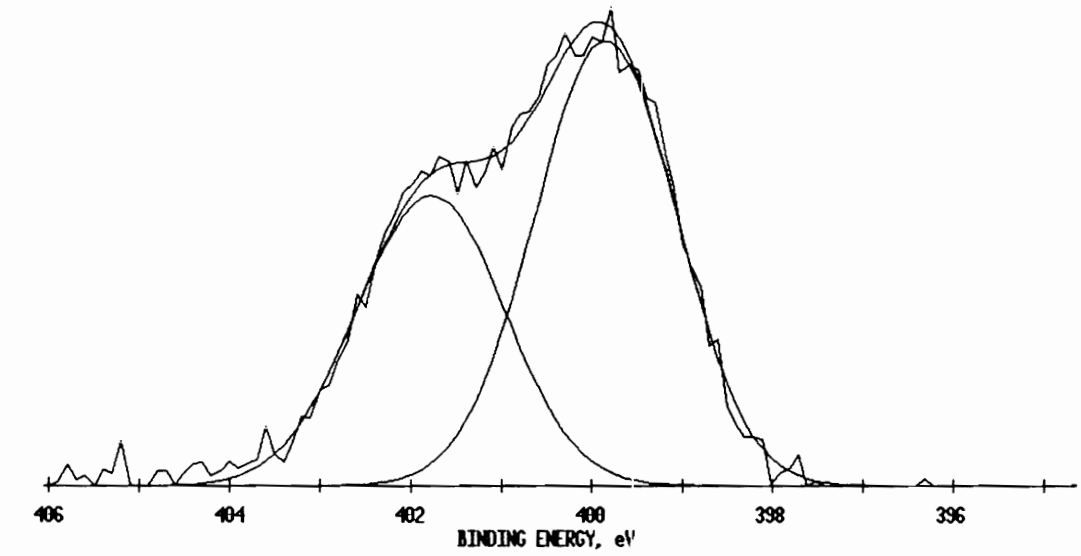

(b)

Figure 8.4: Curve-fitted XPS nitrogen 1s photopeak for (a) unmodified, and (b) oxygen plasma-treated MY 720/HT 976 films.

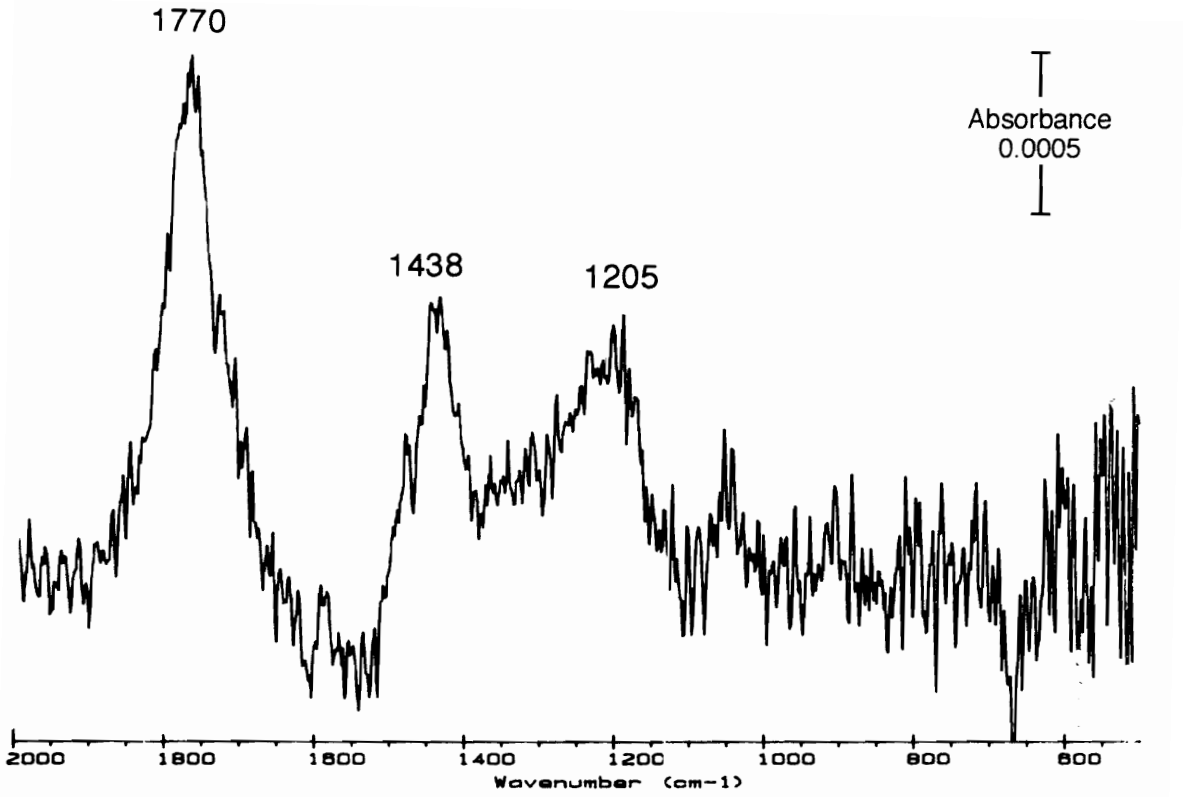

Figure 8.5: IR-RAS difference spectrum of oxygen plasma-modified MY 720/HT 976.

286.0 eV. The peak at 1438 cm^{-1} can be tentatively assigned to either a ketonic methyl or methylene C-H bend or an O-H bend [5]. In general, it can be seen that the XPS and IR-RAS results are in agreement with each other in terms of the surface functional groups identified following oxygen plasma exposure.

Other researchers have reported similar results for oxygen plasma-modified surfaces. Dunn and McClure studied oxygen sputter-etched poly(ethylene terephthalate) by IR-RAS, and observed new bands at 1740 and 1200 cm^{-1}, which provided evidence for the presence of esters, aldehydes and/or carboxylic acids [7]. Webster and Wightman carried out IR-RAS analysis on oxygen plasma-treated poly (phenylene sulfide) and also found subtraction peaks corresponding to C=O and C-O vibrational modes [8]. Work published by Chin and Wightman on oxygen plasma-treated LaRC-TPI, a thermoplastic polyimide, documented the presence of IR-RAS peaks at 1770, 1390 and 1205 cm^{-1}. These peaks were assigned to carboxylic acid or ester C=O and C-O stretching [9].

8.1.3 EPON® 830 Adsorption Studies

To determine potential interactions of the plasma-treated surface with adhesives, the plasma-treated MY 720/HT 976 surfaces were immersed in liquid EPON® 830 after a 30 second, 50 watt oxygen plasma treatment. It was hypothesized that following solvent rinsing of the immersed surfaces to remove physisorbed EPON® 830, a residual thin layer of more tightly bound or chemisorbed material would remain and should be detected by IR-RAS analysis. A similar study was carried out by Webster and Wightman, using plasma-treated poly(phenylene sulfide) as a substrate for EPON® 828 adsorption [8].

It was necessary to first carry out the IR-RAS analysis on neat EPON® 830 films so that infrared bands unique to this DGEBA epoxy could be identified and used to determine if adsorption had taken place on the plasma-treated model epoxy surfaces. The IR-RAS spectrum of EPON® 830 is shown in Figure 8.6. Bands of significance include

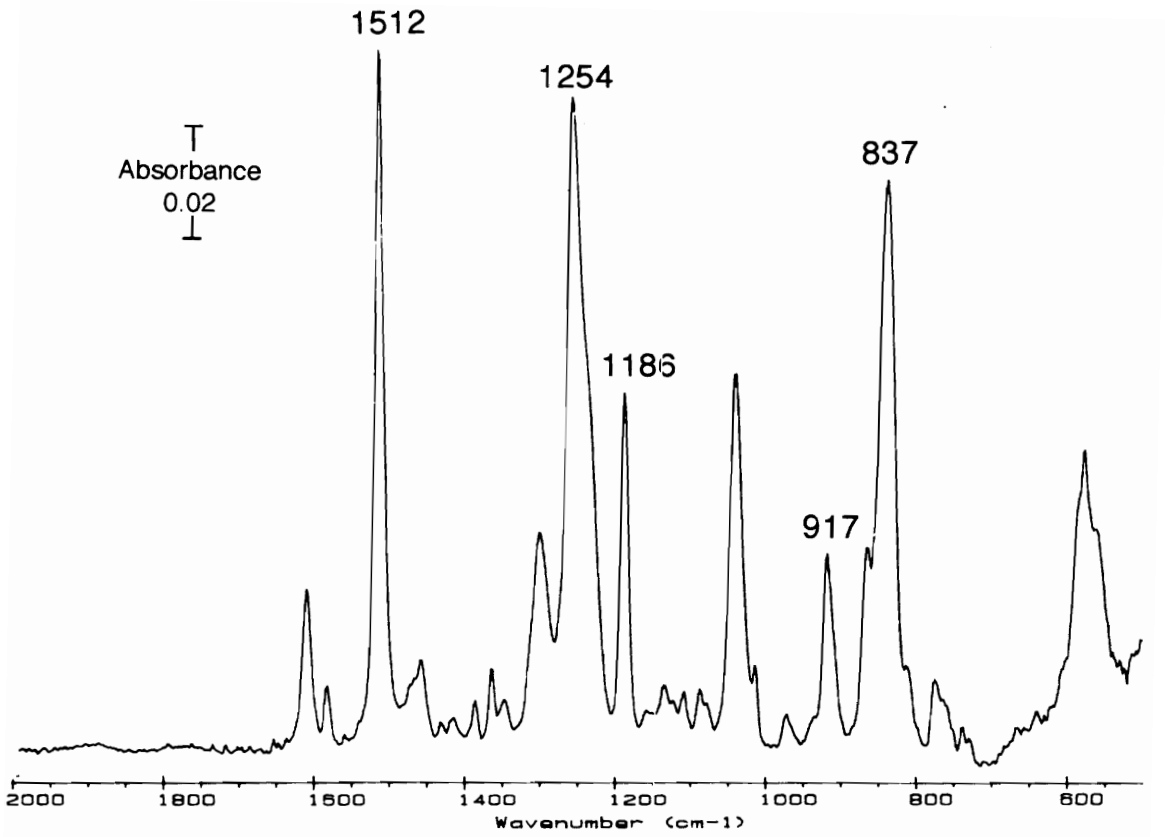

Figure 8.6: IR-RAS spectrum of EPON® 830.

an aromatic C-C stretch at 1512 cm^{-1}, aryl C-O stretch and C-O-C symmetric deformation at 1254 cm^{-1}, in-plane C-H bend and aryl-C-aryl stretch at 1186 cm^{-1}, and an out-of-plane, para-disubstituted benzene bending mode at 837 cm^{-1}. Bands which correspond to the unopened epoxide ring are found at 864 and 917 cm^{-1}. The 837 cm^{-1} peak is also assigned to the epoxide ring by a number of researchers [1,5].

Figure 8.7(a) shows the IR-RAS spectrum of a nonplasma-treated MY 720/HT 976 film following epoxy immersion and solvent rinsing. When compared to the original spectrum of MY 720/HT 976 (see Figure 8.2), a number of changes are evident. New peaks are observed at 1254 and 917 cm^{-1}, corresponding to EPON® 830 C-O-C stretching as well as epoxide ring vibrations. There are also increases in the intensities of peaks at 1519 and 1186 cm^{-1}, which are present in the EPON® 830 spectrum as well as in the spectrum of unmodified MY 720/HT 976 prior to EPON® 830 immersion.

These changes observed in the MY 720/HT 976 spectrum following immersion in an epoxy bath confirm that adsorption of EPON® 830 has occurred on the surface of the MY 720/HT 976 film. However, the presence of the epoxide ring vibration at 917 cm^{-1} indicates that no reaction has taken place between the MY 720/HT 976 surface and the EPON® 830, because the epoxide rings remain unopened and intact.

When the procedure is repeated using an oxygen plasma-treated MY 720/HT 976 substrate, the IR-RAS spectrum shown in Figure 8.7(b) results. This spectrum is virtually identical to the one shown in Figure 8.7(a) for the nonplasma-treated surface. Once again, the presence of the epoxy ring vibration at 917 cm^{-1} originating from the EPON® 830 indicates that no reaction has occurred between the surface and the neat epoxy resin. These preliminary results appear to indicate that the plasma-treated surface is not capable of initiating a reaction with an epoxy resin.

However, the experiment was repeated with one important change made to the procedure. The original method involved obtaining the IR-RAS spectrum of the plasma

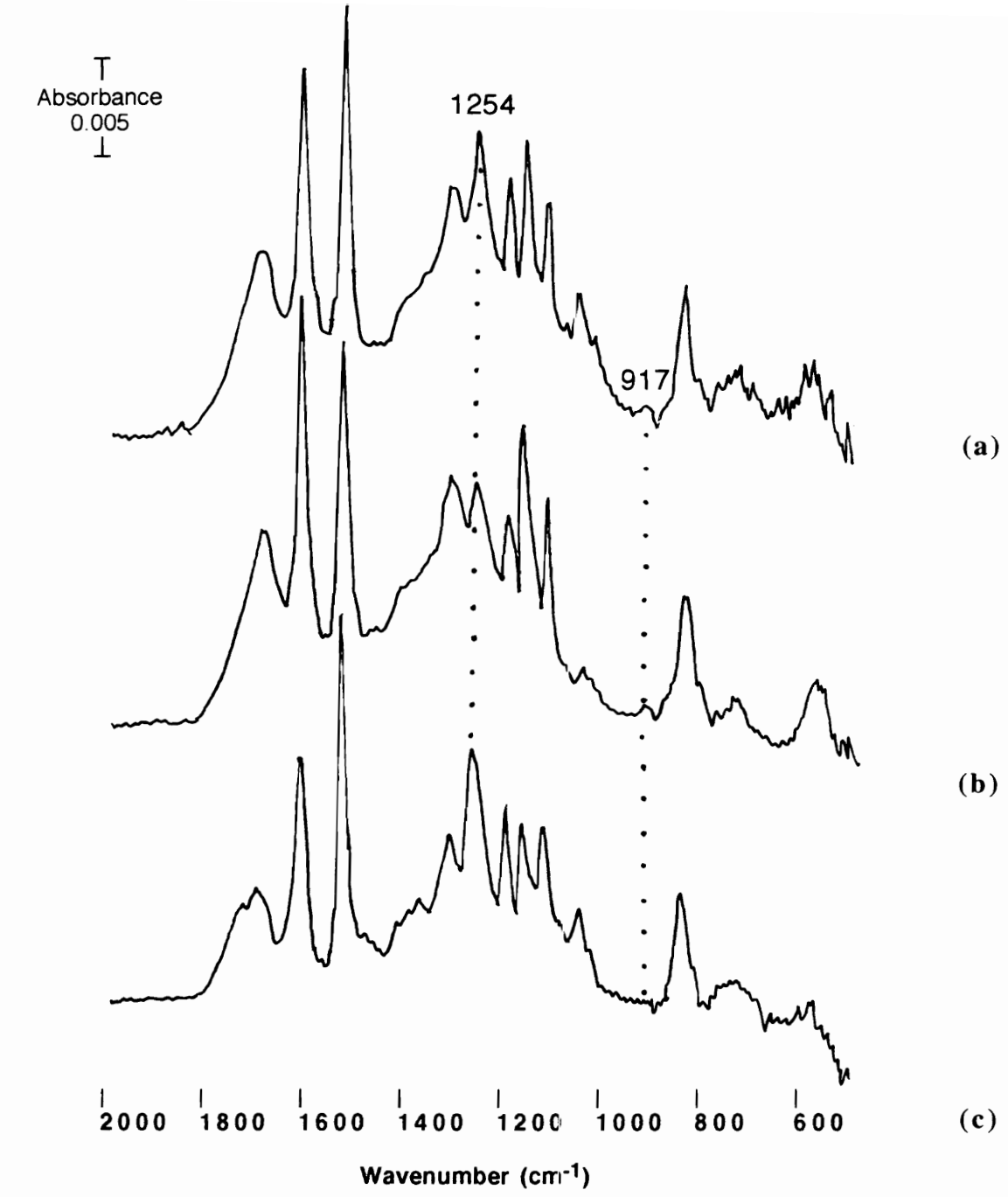

Figure 8.7: IR-RAS spectra of MY 720/HT 976 films following EPON® 830 immersion and solvent rinse. (a) unmodified film (b) oxygen plasma-treated film (c) oxygen plasma-treated film, immersed in EPON® 830 immediately after plasma treatment.

treated MY 720/HT 976 substrate *prior* to immersion in the EPON® 830 bath. This was an additional step which added 30-45 minutes between the plasma treatment and liquid epoxy exposure. Instead, the plasma-treated MY 720/HT 976 surfaces were *immediately* submerged into the EPON® 830 bath following plasma treatment. The IR-RAS spectrum of this surface is seen in Figure 8.7(c). The peak at 1254 cm^{-1} is evident, again confirming that adsorption of the EPON® 830 has indeed taken place. However, in this instance, *no peak* is seen at 917 cm^{-1}, indicating that the epoxide rings have indeed undergone a ring-opening reaction. This result is evidence of some type of interaction between the plasma-treated surface and the liquid epoxy resin. Webster and Wightman also reported epoxy adsorption and polymerization on the surface of oxygen and ammonia plasma-treated poly(phenylene sulfide) [8].

The fact that reaction is observed only when the elapsed time between plasma treatment and epoxy immersion is very short again points to the instability of the plasma-treated surface, as discussed in detail in Chapter VII. The surface is very likely quite reactive immediately following plasma exposure but quickly becomes deactivated upon exposure to the atmosphere. This would be a reasonable explanation for the decrease in bond strength with increasing storage time.

The types of reactions which are possible between the plasma-treated surface and the epoxide ring in the EPON® 830 resin are numerous. The results of XPS and IR-RAS analysis of the oxygen plasma-treated MY 720/HT 976 provide convincing evidence for the presence of hydroxyl, carboxylic acid, ester and ketone functional groups. Work with model compounds has shown that alcohols and phenols may react with glycidal ethers to yield a variety of isomeric products containing hydroxyl groups [10]. These hydroxyl groups are also capable of further reaction with epoxide groups to form polyethers. Carboxylic acid groups have also been observed to react with epoxide rings to form

hydroxy-ester moieties [10]. Alternatively, the plasma-treated substrate may simply be serving as a catalyst for epoxy homopolymerization.

Therefore, the functional groups observed on the oxygen plasma-treated MY 720/HT 976 surfaces are capable of initiating epoxide ring reactions. This type of interfacial reaction may be the basis for the improved hot/wet durability observed in oxygen plasma-treated epoxy composite surfaces discussed in Section 4.2. These results may also explain the minimal loss in bond strength observed following water immersion for the oxygen plasma-treated peel ply laminates, discussed in Section 6.2.

Other researchers have also correlated the presence of interfacial covalent bonds and improved bond durability in hostile environments. Iron/epoxy bonds with excellent water resistance were obtained by using a silane primer, which reportedly formed a interphase impenetrable by water [11]. The use of silanes on titanium surfaces did not greatly improve initial lap shear strengths when bonded with epoxy, but did provide superior strength retention following a 7-day boil in an extracellular liquid [12]. Zisman has also suggested that the presence of interfacial chemical bonds may not necessarily contribute to increased joint strength, but could provide improved heat, water and chemical resistance [13].

8.2 Bismaleimide (BMI) Model Surfaces

8.2.1 IR-RAS Analysis of Components and Cured Film

Prior to the analysis of the plasma-treated surfaces, infrared analysis of the components which make up the model bismaleimide film was carried out. Figure 8.8(a) shows the IR-RAS spectrum of Matrimid® 5292 Part A, a bismaleimide resin. Characteristic imide bands are observed at 1776, 1725 and 693 cm^{-1} [14]. A C-N stretching peak is located at 1399 cm^{-1}, and C-C stretching band is observed at 1516 cm^{-1}.

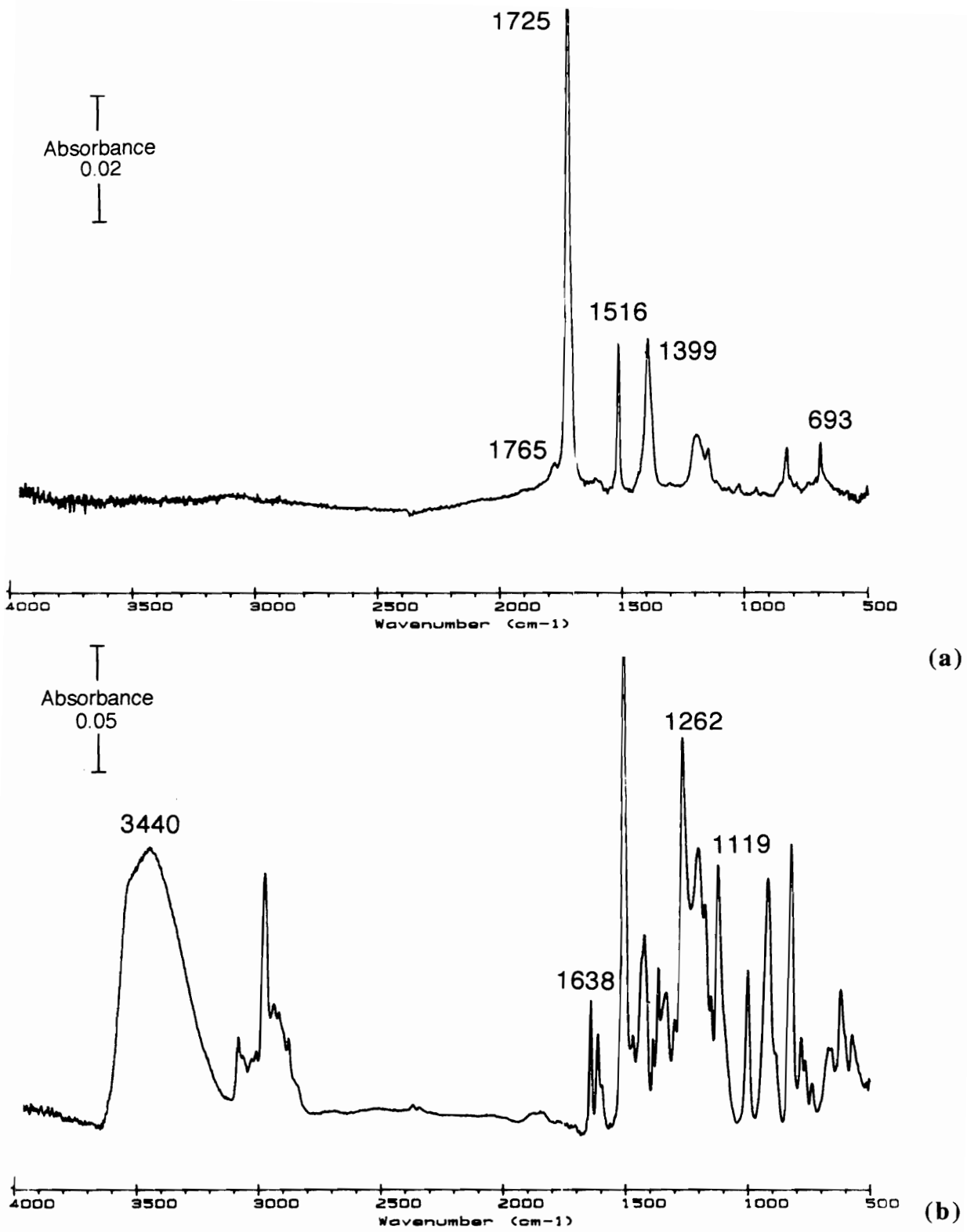

Figure 8.8: (a) IR-RAS spectrum of Matrimid® 5292 bismaleimide resin (Part A), and (b) IR-RAS spectrum of Matrimid® 5292 diallyl phenol (Part B).

The IR-RAS spectrum of Matrimid® 5292 part B, a diallyl bisphenol A comonomer, is shown in Figure 8.8(b). Bands of importance include the aromatic O-H stretching modes at 3440 cm^{-1}, and the corresponding O-H bend located at 1363 cm^{-1}. Bands at 1262, 1172 and 1119 cm^{-1} are characteristic of C-O stretching modes. The band at 1638 cm^{-1} is assigned to the allylic C=C group.

The mechanism for the reaction of Matrimid® 5292 Parts A and B is quite complex and has been studied by only a few researchers. It is known that both the bismaleimide and the diallyl bisphenol A are capable of homopolymerization through their respective double bonds. The diallyl bisphenol A may also react with the bismaleimide double bonds via a Diels-Alder process [15,16].

As seen in the spectrum of the cured Matrimid® 5292 film shown in Figure 8.9, the imide C=O are still present at 1776 and 1725 cm^{-1}. The C=C stretch at 1638 cm^{-1} is no longer observed, indicating that a crosslinking reaction has occurred through the allylic double bonds. An unidentified doublet at 1198 and 1149 cm^{-1} in the spectrum of Matrimid® 5292 Part A has also disappeared, giving rise to a shoulder at 1273 cm^{-1} and a peak at 1189 cm^{-1} in the spectrum of the cured film.

8.2.2 Oxygen Plasma Treatment of Cured Films

XPS and IR-RAS were again used to study the changes which occur in the surface chemistry of oxygen plasma-treated Matrimid® 5292 thin films. Table 8.2 shows the theoretical atomic concentration of a formulation composed of 100 pbw of Part A and 85 pbw Part B, compared to the measured XPS atomic concentrations of a cured, unmodified Matrimid® 5292 film and a cured film treated in oxygen plasma. Good agreement is observed between the theoretical and actual atomic concentrations for the unmodified surface. The small amount of excess oxygen which is found on the unmodified film

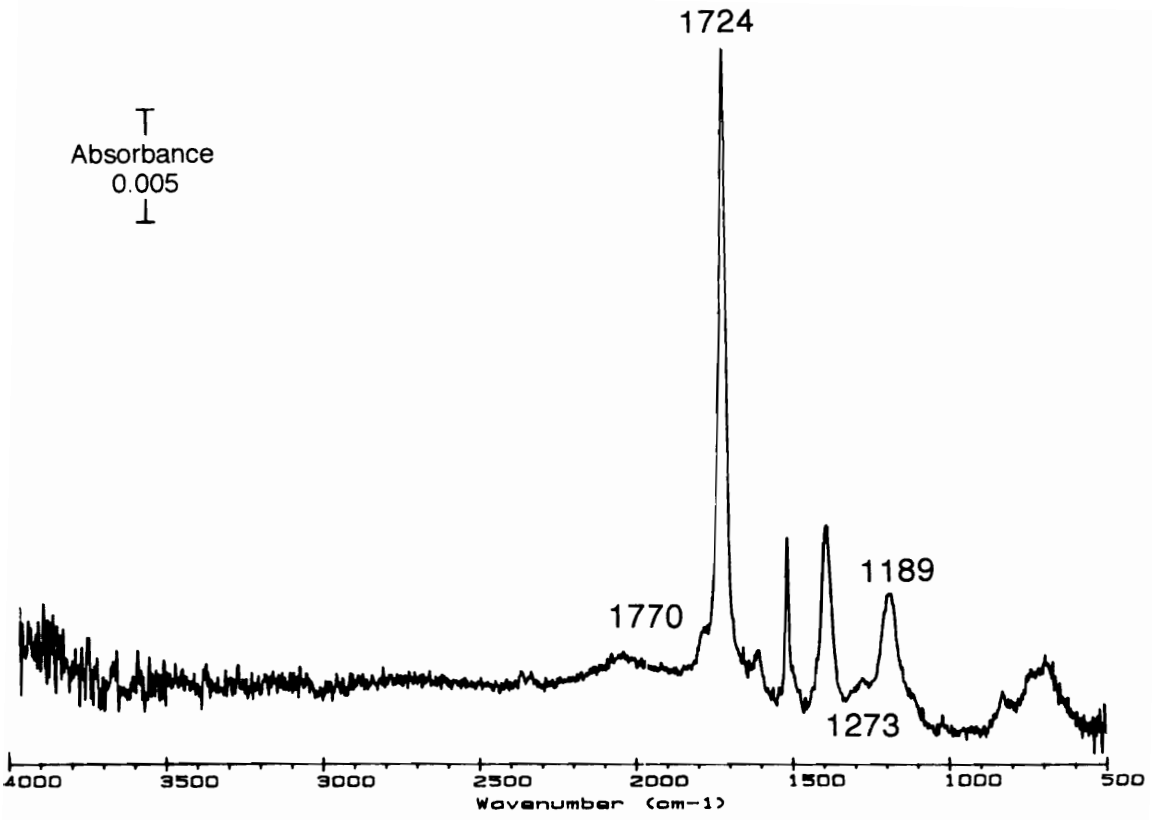

Figure 8.9: IR-RAS spectrum of a cured Matrimid® 5292 film.

Table 8.2: Theoretical and XPS atomic compositions of unmodified and oxygen plasma-treated Matrimid® 5292 films.

	Surface Composition (atomic %)		
	Theoretical	**Unmodified**	**Oxygen Plasma**
Carbon	84	83	63
Oxygen	12	14	32
Nitrogen	4	3	5

surfaces may originate from residual solvent used to spin-coat the films. Following oxygen plasma exposure, the oxygen atomic concentration is seen to significantly increase.

Curve-fitting of the carbon 1s photopeaks was carried out and is depicted in Figure 8.10. In the unmodified surface of Figure 8.10(a), peaks at 284.6, 285.8 and 288.2 eV can be fitted to the main peak envelope. These peaks are identified as C-C/C-H hydrocarbon species, C-O/C-N and imide C=O functionality, respectively [2,17].

Figure 8.10(b) shows the curve-fitted carbon 1s photopeaks for the oxygen plasma-treated surface. The original peaks at 285.8 and 288.2 eV are seen to be increased in intensity following plasma exposure. New peaks are observed at 286.9, 289.7 and 292.7 eV. The species corresponding to the peaks at 286.9 and 289.7 eV may be identified as C-O and O-C=O, respectively. The peak at 292.7 eV is most likely a shake-up satellite. No significant changes were observed in the shape or location of the oxygen 1s or nitrogen 1s photopeaks.

Infrared analysis of the plasma-modified BMI surface served to complement the molecular information obtained from curve-fitting the XPS photopeaks. Figure 8.11 shows the IR-RAS difference spectrum for the oxygen plasma-treated bismaleimide surface. Peaks are observed in the difference spectrum at 1745, 1400 and 1206 cm^{-1}. The peak at 1745 cm^{-1} can be assigned to C=O stretching in ester or carboxylic acid species [5]. This assignment is consistent with the appearance of the XPS peak at 289.7 eV after plasma treatment. The peak at 1205 cm^{-1} is identified as a C-O stretch [4], which corresponds with the increased intensity of the XPS photopeak at 285.8 eV. The peak at 1400 cm^{-1} can be tentatively assigned to either a ketonic methyl or methylene C-H bend or an O-H bend [6]. It is again seen that the XPS and IR-RAS results are in agreement with each other in terms of the surface functional groups identified following oxygen plasma exposure.

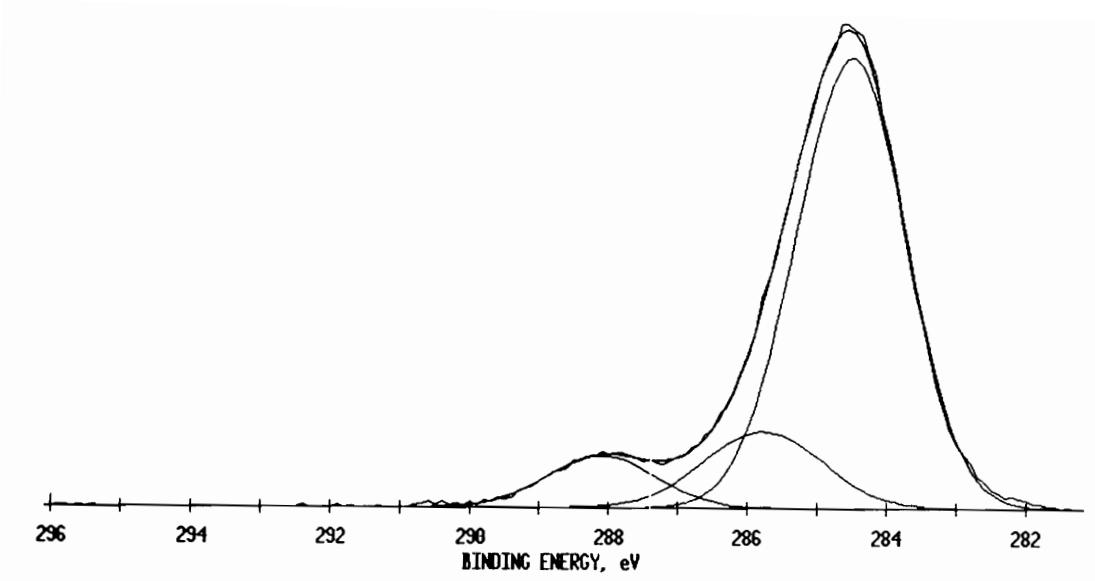

(a)

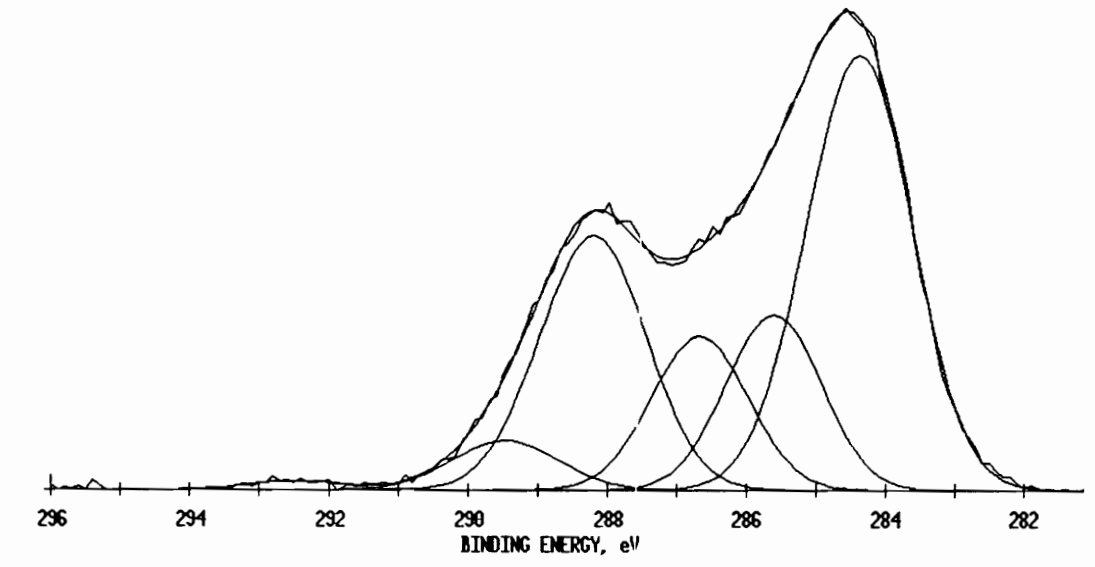

(b)

Figure 8.10: Curve-fitted XPS carbon 1s photopeak for (a) unmodified, and (b) oxygen plasma-treated Matrimid® 5292 films.

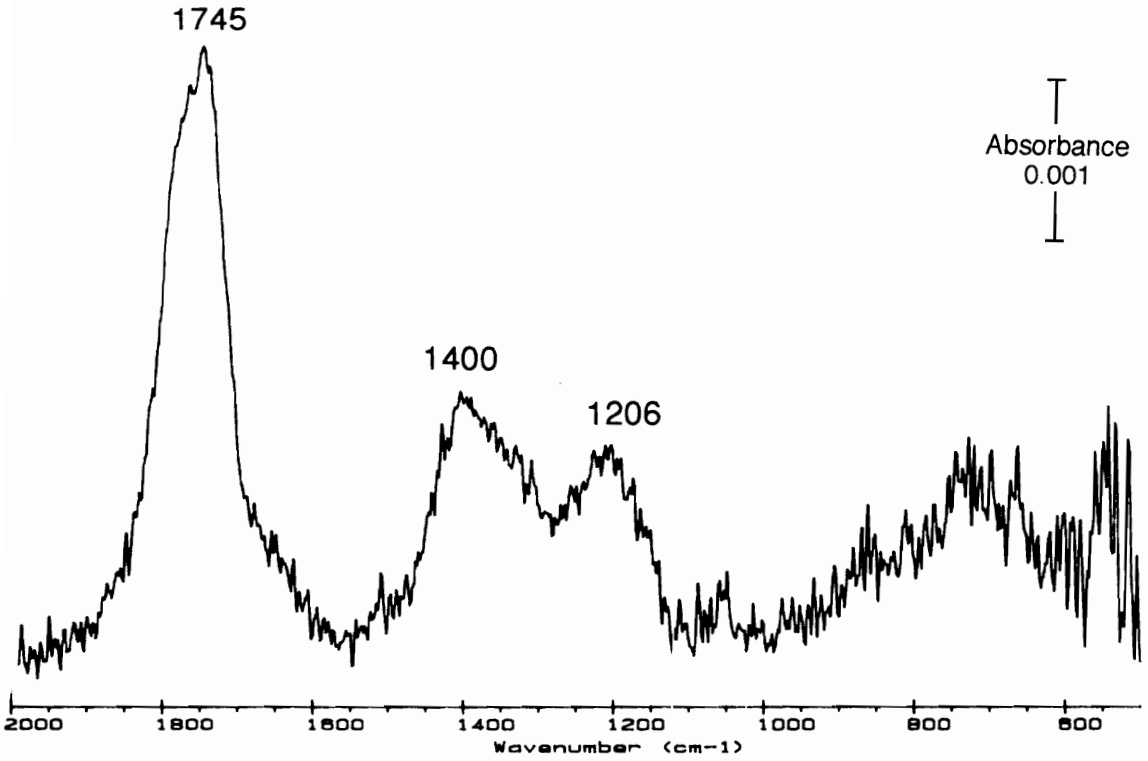

Figure 8.11: IR-RAS difference spectrum of oxygen plasma-modified Matrimid® 5292.

8.2.3 EPON® 830 Adsorption Studies

To study potential interactions of the plasma-treated surface with adhesives, the plasma-treated Matrimid® 5292 surfaces were immersed in liquid EPON® 830 after a 30 second, 50 watt oxygen plasma treatment, as described earlier in Section 8.1.3 for the epoxy model surfaces. Again, it was hypothesized that, following solvent rinsing of the immersed surfaces to remove physisorbed EPON® 830, a thin layer of more tightly bound or chemisorbed material would remain behind.

Figure 8.12(a) shows the IR-RAS spectrum of a non-plasma-treated Matrimid® 5292 film following epoxy immersion and solvent rinsing. When compared to the original spectrum of Matrimid® 5292, a number of changes are evident. New peaks are observed at 1254 and 920 cm^{-1}, corresponding to EPON® 830 C-O-C stretching as well as epoxide ring vibrations. New peaks were observed at 1048 and 1022 cm^{-1}, tentatively identied as C-O stretches, and 1300 cm^{-1}, assigned to an O-H bend. There are also increases in the intensities of the original peaks at 1607 and 1514 cm^{-1}.

These changes observed in the Matrimid® 5292 spectrum following immersion in an epoxy bath indicate that adsorption of EPON® 830 onto the surface of the Matrimid® 5292 film has taken place. However, the presence of the epoxide ring vibration at 920 cm^{-1} indicates that no reaction has occurred between the Matrimid® 5292 surface and the EPON® 830, because the epoxide rings remain unopened and intact.

When the procedure is repeated using an oxygen plasma-treated Matrimid® 5292 substrate, the IR-RAS spectrum shown in Figure 8.12(b) results. This spectrum is virtually identical to the one shown in Figure 8.12(a) for the nonplasma-treated surface. Once again, the presence of the epoxy ring vibration at 920 cm^{-1} originating from the EPON® 830 indicates that no reaction has occurred between the surface and the neat epoxy resin. However, the intensities of the C-O stretch and O-H deformation peaks at 1048,

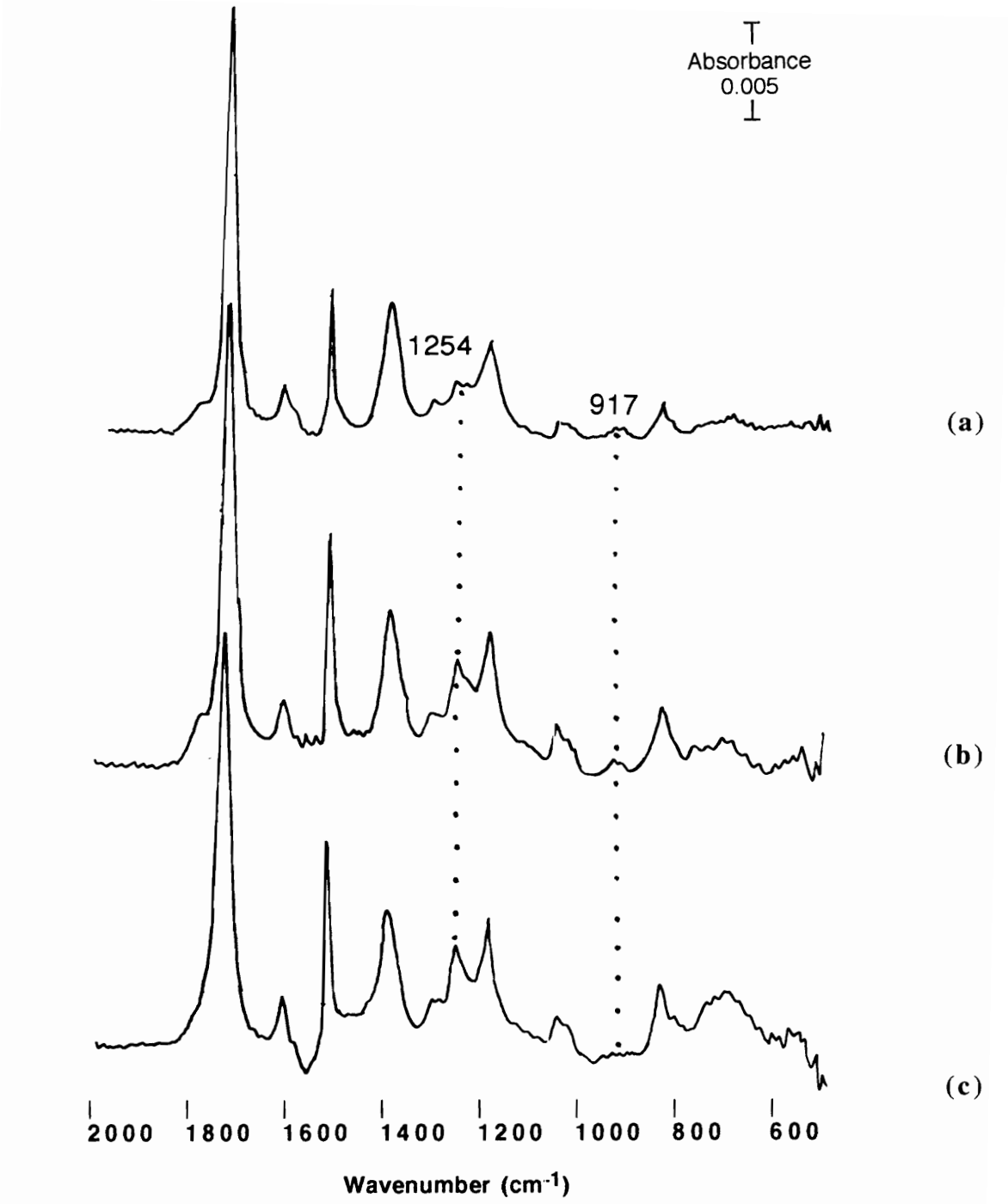

Figure 8.12: IR-RAS spectra of Matrimid® 5292 films following EPON® 830 immersion and solvent rinse. (a) unmodified film (b) oxygen plasma-treated film (c) oxygen plasma-treated film, immersed in EPON® 830 immediately after plasma treatment.

1022 and 1300 cm^{-1} are increased relative to the nonplasma-treated surface. This could indicate that some degree of epoxy ring-opening has taken place.

As was also done with the epoxy model surfaces, the plasma-treated Matrimid® 5292 surfaces were then *immediately* submerged into the EPON® 830 bath following plasma treatment. The IR-RAS spectrum shown in Figure 8.12(c) reveals the results. The peak at 1254 cm^{-1} is evident, again confirming that adsorption of the EPON® 830 has indeed taken place. However, in this instance, *no peak* is seen at 920 cm^{-1}, indicating that the epoxide rings have indeed undergone ring-opening. This result is once again evidence that some type of specific chemical interaction took place between the plasma-treated surface and the liquid epoxy resin.

8.3 Conclusions

As analyzed by XPS, oxygen plasma-treated epoxy and BMI films exhibited behavior similar to that of the oxygen plasma-treated composites discussed in Chapters IV and V. For both materials, increases in the concentration of oxygen-containing functional groups were observed following plasma treatment. IR-RAS analysis of the plasma-treated surfaces revealed the presence of oxygen-containing functional groups such as carbonyl and hydroxyl. These results are consistent with the findings of XPS.

Adsorption of the liquid DGEBA epoxy resin, EPON® 830, was seen to take place on thin films representing both a model epoxy and a model bismaleimide surface. Infrared bands characteristic of the liquid epoxy were observed in the spectra of nonplasma-modified and oxygen plasma-modified substrates after immersion and solvent rinsing. However, epoxy ring-opening reactions, as evidenced by the disappearance of the epoxy ring vibration at 917-920 cm^{-1}, were only observed in the case of oxygen plasma-treated substrates immersed immediately into the liquid epoxy bath after plasma treatment.

Evidence of adsorption was observed on the nonplasma-treated surfaces as well as on plasma-treated surfaces exposed to the liquid epoxy 30-45 minutes after plasma treatment. However, the presence of the epoxy ring vibration ruled out any specific interactions between the substrate and EPON® 830.

These results provide explanations for the data obtained in Chapters VI and VII, related to functionalized peel ply surfaces and plasma aging. Direct evidence for covalent interaction between a reactive, plasma-modified surface and a liquid epoxy resin can be correlated with the improved hot/wet bond durability exhibited by oxygen plasma-treated substrates. However, the fact that this interaction is only observed when a minimal of time elapses between plasma treatment and initial contact with the adhesive resin emphasizes the short-lived reactivity of the plasma-treated surface.

8.4 References

1. H. Lee and K. Neville, *Handbook of Epoxy Resins* (McGraw-Hill, New York, 1967).
2. D. Briggs in *Practical Surface Analysis by Auger and X-ray Photoelectron Spectroscopy*, D. Briggs and M.P. Seah, eds., p. 359 (John Wiley and Sons, London, 1983).
3. G. Beamson and D. Briggs, *High Resolution XPS of Organic Polymers* (John Wiley and Sons, Chichester, 1992).
4. C.D. Wagner, W.M. Riggs, L.E. Davis, J.F. Moulder and G.E. Muilenberg, *Handbook of Photoelectron Spectroscopy* (Perkin-Elmer Corporation, Eden Prairie, 1979).
5. R.M. Silverstein, G. C. Bassler and T. C. Morrill, *Spectrometric Identification of Organic Compounds*, 4th ed., chap. 3 (John Wiley and Sons, New York, 1981).
6. C.J. Pouchert, *The Aldrich Library of Infrared Spectra*, edition III (Aldrich Chemical Company, Milwaukee, 1981).

7. D.S. Dunn and D.J. McClure, *J. Vac. Sci. Technol.*, **A5**(4), 1327 (1987).
8. H.F. Webster and J.P. Wightman, *J. Adhesion Sci. Technol.*, **5**(1), 93 (1991).
9. J.W. Chin and J.P. Wightman, *J. Adhesion*, **36**, 25 (1991).
10. L. Schecter and J. Wynstra, *Ind. Eng. Chem.*, **48**(1), 86 (1956).
11. M. Gettings, F.S. Baker and A.J. Kinloch, *J. Appl. Polym. Sci.*, **21**, 2375 (1977).
12. A.J. Coury, A.H. Jezne and P.T. Callahan in *Proc. Symp. Adhesion Aspects Polymeric Coatings*, K. Mittal, ed. (Plenum Press, New York, 1983).
13. W.A. Zisman, *Ind. Eng. Chem.*, **55**(10), 19 (1963).
14. I.K. Varma, G.M. Fohlen and J.A. Parker, *J. Macromol. Sci. - Chem.*, **A19**(2), 209 (1983).
15. J. Mijovic and B. Schafran, *SAMPE J.*, **26**(3), 51 (1990).
16. R.J. Morgan, R. Jurek and D.E. Larive, *Proceedings of the ACS Division of Polymeric Materials: Science and Engineering*, **63**, 681 (1990).
17. H.J. Leary and D.S. Campbell, *Surf. Interface Anal.*, **1**(3), 75 (1979).

Chapter IX: Summary

Surface pretreatment was carried out on toughened epoxy and toughened bismaleimide composites to facilitate adhesive bonding. MEK wipe, peel ply, grit blasting and plasma treatments were utilized to modify the chemistry and topography of the surface so that interactions between the surface and the adhesive could be optimized. The effect of composite surface properties following pretreatment on both joint strength and durability was of interest.

Changes in the surface properties of the pretreated composites were analyzed by XPS, ISS, contact angle analysis, profilometry and scanning electron microscopy. Surface chemistry and topography was affected in different ways by each pretreatment. Fluoropolymer residues originating from composite processing were removed by oxygen plasma and grit blasting, and prevented from depositing altogether by the use of peel ply. MEK wiping was not effective in removing the fluoropolymer contamination. Removal of the fluoropolymer transformed a low energy surface poorly wetted by water and epoxy resins, into a more wettable, higher energy surface. Oxygen plasma alone was capable of incorporating additional oxygen into the composite surfaces, in the form of hydroxyl, carbonyl and carboxylate functionality. This surface polar functionality increased the surface energy of the plasma-treated surface above that of the surface tension of water.

Surface energies of the composite surfaces were determined by both the Zisman and Kaelble approaches after being first corrected for roughness effects. Reasonable and consistent surface energy values were found for the pretreated composite surfaces; however, the discrepancy between the values obtained from the Zisman and Kaelble procedures became larger as the roughness of the surface increased.

A high degree of surface roughness was observed for the peel ply and grit-blasted surfaces, whereas the MEK-wiped and oxygen plasma-treated surfaces were not modified

significantly in terms of topography. The weave imprint from the peel ply fabric was visible on the peel ply surface, forming a pattern of channels and grooves. The penetration of molten polystyrene into the peel ply-imprinted surfaces illustrated that the exaggerated surface profile of the peel ply surface was not detrimental to adhesive wetting and spreading. Grit blasting effectively removed the topmost layer of resin from the composite surfaces and uncovered the underlying carbon fibers, which also sustained some damage.

Lap shear test results revealed the bond strengths of the MEK-wiped samples to be low, a consequence of fluorine contamination on the surface. Peel ply and oxygen plasma treatments improved the initial lap shear strengths significantly; grit blasting was not as consistent in improving bond strengths. In the case of the bismaleimide composites, grit blasting decreased the lap shear strength relative to the MEK-wiped controls, under all testing conditions. No obvious differences were observed in failure modes between the unconditioned and environmentally conditioned samples, a result which may imply that strength-controlling factors in adhesive bonds are not necessarily interfacial in nature.

Wedge testing also revealed the oxygen plasma and peel ply specimens to be the most durable in 75°C water; grit blasting and MEK wiping did not produce stable wedge joints in this environment. In a dry 75°C environment, very little crack growth was observed for all pretreatments, whereas in boiling water, all of the joints exhibited significant crack extension. Aircraft de-icing fluid caused crack growth to occur only for the MEK-wiped bismaleimide wedge specimens.

The effect of surface functionality on composite bond strength was studied by treating the peel ply surfaces in various ways to obtain surfaces with differing chemistries while maintaining the same topography. Treatment of the surface with a fluorinated mold-release agent created a low energy, non-wettable surface which in turn led to low lap shear strengths and poor hot/wet durability. The original peel ply surface was more easily wetted by epoxy resins and also showed a large improvement in lap shear strength relative to the

fluorinated surface. Modification of the peel ply surface with an oxygen plasma did not provide any additional lap shear strength beyond the level of the original peel ply surface, but prevented significant drops in bond strength in a hot/wet environment. This result could be due to some type of interfacial reaction between the plasma-treated surface and the adhesive resin to create a more moisture-resistance interphase. Thus, while the oxygen plasma treatment did not produce any apparent benefit in improving initial bond strengths, improvements in hot/wet durability may be realized by this surface pretreatment.

The stability of an oxygen plasma-treated surface was studied by assessing the changes in XPS atomic concentrations, wettability by water and liquid epoxy resins, and single lap shear strength as a function of elapsed time following plasma treatment. Oxygen concentration in the surface decreased steadily over a period of 17 weeks, during which time the water contact angle increased, showing a change in the polar nature of the surface. However, very little change was observed in the contact angle of a liquid epoxy. A decrease in bond strength as a function of time following plasma treatment was evident, relative to samples bonded immediately after plasma exposure.

XPS and IR-RAS analysis of model epoxy and bismaleimide films treated with oxygen plasma and exposed to a liquid epoxy bath revealed some insights into interfacial reactions. It was found that while adsorption of epoxy occurs on both plasma and nonplasma-treated surfaces, interfacial reaction as evidenced by the disappearance of epoxide ring functionality in the liquid epoxy occurred only with the plasma-treated surface. In addition, it was observed that these interactions were only possible when contact was made between the plasma-treated surface and the epoxy resin immediately after plasma modification. This very narrow window available for reaction points to the inherent instability of the plasma-treated surface. These results provide explanations for phenomena associated with plasma-induced surface functionality and the aging of plasma-treated surfaces.

fluorinated surface. Modification of the peel ply surface with an oxygen plasma did not provide any additional lap shear strength beyond the level of the original peel ply surface, but prevented significant drops in bond strength in a hot/wet environment. This result could be due to some type of interfacial reaction between the plasma-treated surface and the adhesive resin to create a more moisture-resistance interphase. Thus, while the oxygen plasma treatment did not produce any apparent benefit in improving initial bond strengths, improvements in hot/wet durability may be realized by this surface pretreatment.

The stability of an oxygen plasma-treated surface was studied by assessing the changes in XPS atomic concentrations, wettability by water and liquid epoxy resins, and single lap shear strength as a function of elapsed time following plasma treatment. Oxygen concentration in the surface decreased steadily over a period of 17 weeks, during which time the water contact angle increased, showing a change in the polar nature of the surface. However, very little change was observed in the contact angle of a liquid epoxy. A decrease in bond strength as a function of time following plasma treatment was evident, relative to samples bonded immediately after plasma exposure.

XPS and IR-RAS analysis of model epoxy and bismaleimide films treated with oxygen plasma and exposed to a liquid epoxy bath revealed some insights into interfacial reactions. It was found that while adsorption of epoxy occurs on both plasma and nonplasma-treated surfaces, interfacial reaction as evidenced by the disappearance of epoxide ring functionality in the liquid epoxy occurred only with the plasma-treated surface. In addition, it was observed that these interactions were only possible when contact was made between the plasma-treated surface and the epoxy resin immediately after plasma modification. This very narrow window available for reaction points to the inherent instability of the plasma-treated surface. These results provide explanations for phenomena associated with plasma-induced surface functionality and the aging of plasma-treated surfaces.